U.S. Department
of Transportation
Federal Railroad
Administration

Office of Research,
Development and Technology
Washington, DC 20590

Modeling and Analysis of Phase Change in a DOT-113 Tank Car Surrogate Filled with Liquid Nitrogen

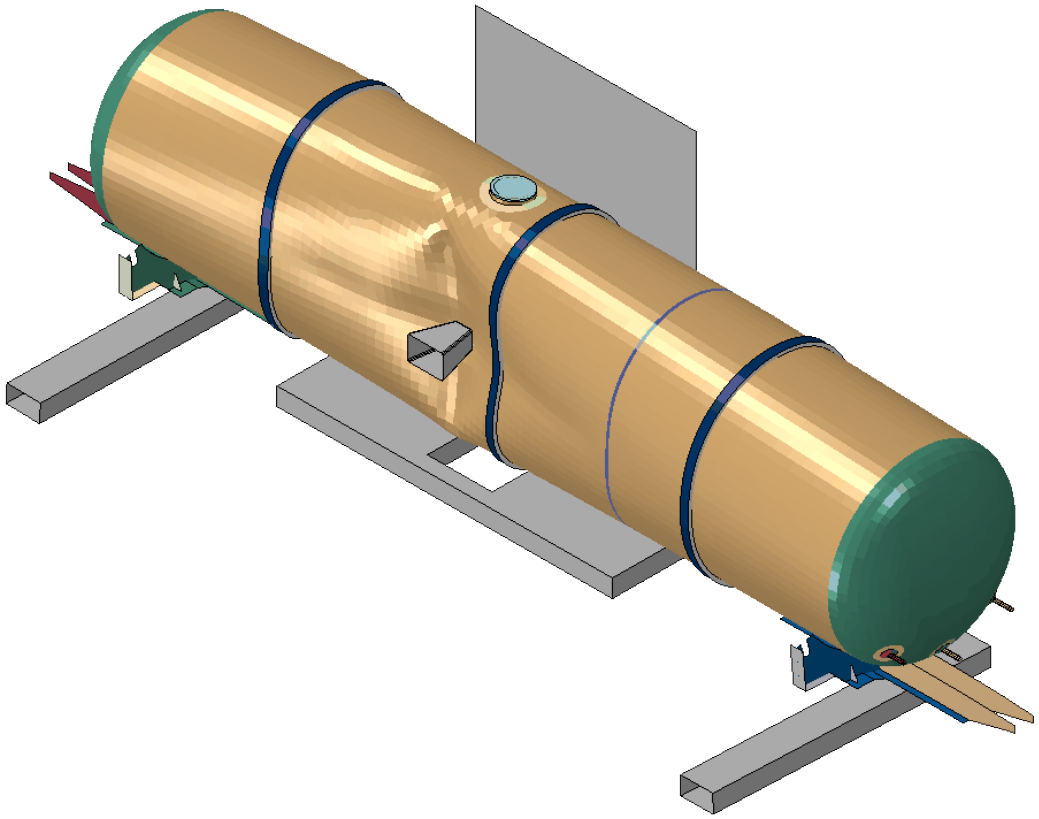

DOT/FRA/ORD-24-12

Final Report | February 2024

REPORT DOCUMENTATION PAGE

Form Approved
OMB No. 0704-0188

1. REPORT DATE *(DD-MM-YYYY)*	2. REPORT TYPE	3. DATES COVERED *(From - To)*
	Technical Report	5/11/2021 to 5/10/2022

4. TITLE AND SUBTITLE
Modeling and Analysis of Phase Change in a DOT-113 Tank Car Surrogate Filled with Liquid Nitrogen

5a. CONTRACT NUMBER

5b. GRANT NUMBER

5c. PROGRAM ELEMENT NUMBER

6. AUTHOR(S)
Michael Carolan – ORCiD: 0000-0002-8758-5739
Shaun Eshraghi – ORCiD: 0000-0002-8152-0838
Aswani Krishnamurthy – ORCiD: 0000-0003-3116-7797

5d. PROJECT NUMBER
RR28A520

5e. TASK NUMBER

5f. WORK UNIT NUMBER

7. PERFORMING ORGANIZATION NAME(S) AND ADDRESS(ES)
Volpe, the National Transportation Systems Center
55 Broadway
Cambridge, MA 02142

8. PERFORMING ORGANIZATION REPORT NUMBER

9. SPONSORING/MONITORING AGENCY NAME(S) AND ADDRESS(ES)
U.S. Department of Transportation
Federal Railroad Administration
Office of Railroad Policy and Development
Office of Research, Development, and Technology
Washington, DC 20590

10. SPONSOR/MONITOR'S ACRONYM(S)

11. SPONSOR/MONITOR'S REPORT NUMBER(S)
DOT/FRA/ORD-24-12

12. DISTRIBUTION/AVAILABILITY STATEMENT
This document is available to the public through the FRA website.

13. SUPPLEMENTARY NOTES
COR: Francisco González, III

14. ABSTRACT

As part of a series of impact tests, the Federal Railroad Administration (FRA) sponsored a research team from Transportation Technology Center, working with Volpe National Transportation Systems Center (Volpe), to analyze the side impact puncture performance of a surrogate DOT-113 tank car filled with cryogenic liquid nitrogen (LN2). This was the third test in a planned series of four tests on DOT-113 tank cars and surrogates. Researchers performed pre-test analyses of the DOT-113 surrogate filled with LN2 (Test 12), and the research team conducted the impact test on July 24, 2021. The surrogate tank car was impacted by a 297,200-lb ram car fitted with a 12 x 12-inch impactor traveling at 18.3 mph. The impact resulted in a significant amount of deformation but did not puncture the tank car. After the test, the team updated the pre-test finite element (FE) model to represent the measured speed of the ram car but observed some discrepancies between the test measurements and simulation results. The testing and modeling effort is described in detail in a separate FRA Technical Report; this report is focused on a phase change discrepancy noted during Test 12.

15. SUBJECT TERMS
Impact test, DOT-113 tank car, tank car performance, transportation safety, liquefied natural gas, LNG, liquid nitrogen, LN2, finite element analysis, FEA, hazardous materials, rolling stock, cryogenic, phase change, thermodynamics

16. SECURITY CLASSIFICATION OF:			17. LIMITATION OF ABSTRACT	18. NUMBER OF PAGES	19a. NAME OF RESPONSIBLE PERSON
a. REPORT	b. ABSTRACT	c. THIS PAGE			Francisco González, III
Unclassified	Unclassified	Unclassified		142	19b. TELEPHONE NUMBER *(Include area code)* 202-493-6076

Standard Form 298 (Rev. 8/98)
Prescribed by ANSI Std. Z39.18

METRIC/ENGLISH CONVERSION FACTORS

ENGLISH TO METRIC

LENGTH (APPROXIMATE)

1 inch (in)	=	2.5 centimeters (cm)
1 foot (ft)	=	30 centimeters (cm)
1 yard (yd)	=	0.9 meter (m)
1 mile (mi)	=	1.6 kilometers (km)

AREA (APPROXIMATE)

1 square inch (sq in, in^2)	=	6.5 square centimeters (cm^2)
1 square foot (sq ft, ft^2)	=	0.09 square meter (m^2)
1 square yard (sq yd, yd^2)	=	0.8 square meter (m^2)
1 square mile (sq mi, mi^2)	=	2.6 square kilometers (km^2)
1 acre = 0.4 hectare (he)	=	4,000 square meters (m^2)

MASS - WEIGHT (APPROXIMATE)

1 ounce (oz)	=	28 grams (gm)
1 pound (lb)	=	0.45 kilogram (kg)
1 short ton = 2,000 pounds (lb)	=	0.9 tonne (t)

VOLUME (APPROXIMATE)

1 teaspoon (tsp)	=	5 milliliters (ml)
1 tablespoon (tbsp)	=	15 milliliters (ml)
1 fluid ounce (fl oz)	=	30 milliliters (ml)
1 cup (c)	=	0.24 liter (l)
1 pint (pt)	=	0.47 liter (l)
1 quart (qt)	=	0.96 liter (l)
1 gallon (gal)	=	3.8 liters (l)
1 cubic foot (cu ft, ft^3)	=	0.03 cubic meter (m^3)
1 cubic yard (cu yd, yd^3)	=	0.76 cubic meter (m^3)

TEMPERATURE (EXACT)

[(x-32)(5/9)] °F = y °C

METRIC TO ENGLISH

LENGTH (APPROXIMATE)

1 millimeter (mm)	=	0.04 inch (in)
1 centimeter (cm)	=	0.4 inch (in)
1 meter (m)	=	3.3 feet (ft)
1 meter (m)	=	1.1 yards (yd)
1 kilometer (km)	=	0.6 mile (mi)

AREA (APPROXIMATE)

1 square centimeter (cm^2)	=	0.16 square inch (sq in, in^2)
1 square meter (m^2)	=	1.2 square yards (sq yd, yd^2)
1 square kilometer (km^2)	=	0.4 square mile (sq mi, mi^2)
10,000 square meters (m^2)	=	1 hectare (ha) = 2.5 acres

MASS - WEIGHT (APPROXIMATE)

1 gram (gm)	=	0.036 ounce (oz)
1 kilogram (kg)	=	2.2 pounds (lb)
1 tonne (t)	=	1,000 kilograms (kg)
	=	1.1 short tons

VOLUME (APPROXIMATE)

1 milliliter (ml)	=	0.03 fluid ounce (fl oz)
1 liter (l)	=	2.1 pints (pt)
1 liter (l)	=	1.06 quarts (qt)
1 liter (l)	=	0.26 gallon (gal)
1 cubic meter (m^3)	=	36 cubic feet (cu ft, ft^3)
1 cubic meter (m^3)	=	1.3 cubic yards (cu yd, yd^3)

TEMPERATURE (EXACT)

[(9/5) y + 32] °C = x °F

QUICK INCH - CENTIMETER LENGTH CONVERSION

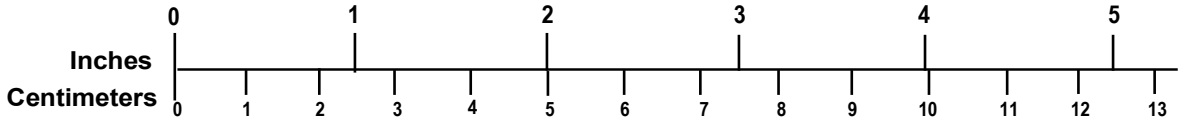

QUICK FAHRENHEIT - CELSIUS TEMPERATURE CONVERSIO

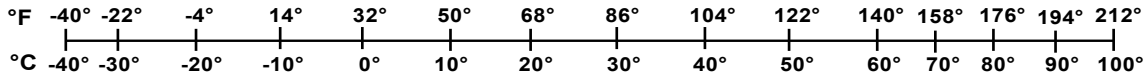

For more exact and or other conversion factors, see NIST Miscellaneous Publication 286, Units of Weights and Measures. Price $2.50 SD Catalog No. C13 10286

Updated 6/17/98

Acknowledgements

The authors of this report gratefully acknowledge the cooperation and assistance of Hector Villarreal and Devangkumar Patel of Taylor-Wharton Americas for providing engineering drawings and design information for the DOT-113 tank car surrogate used in the modeling described in this report.

Additionally, inputs from Francisco González, III of the Federal Railroad Administration were valuable in developing the modeling described in this report and the companion testing program.

Calculations performed by Dr. Phani Raj in Appendix E of this report were helpful as a check on the FE model results incorporating vapor-to-liquid phase change. The authors are grateful for Dr. Raj's technical assistance during the full-scale testing and modeling of tank cars filled with cryogenic liquids.

Contents

Illustrations

Tables

Executive Summary

As part of a series of impact tests, the Federal Railroad Administration (FRA) sponsored a research team from Transportation Technology Center, working with Volpe National Transportation Systems Center (Volpe), to analyze the side impact puncture performance of a surrogate DOT-113 tank car filled with cryogenic liquid nitrogen (LN2). This was the third test in a planned series of four tests on DOT-113 tank cars and surrogates, as shown in Table 1.

Table 1. Planned DOT-113 Side Impact Test Series

Test #	Date	Test Article	Lading	Report
10	Nov. 2019	Legacy DOT-113	Water	[1]
11	June 2020	Surrogate DOT-113	Water	[2]
12	July 2021	Surrogate DOT-113	LN2	[3]
13	May 2022	New DOT-113	LN2	TBD

Researchers performed pre-test analyses of the DOT-113 surrogate filled with LN2 (Test 12), and the research team conducted the impact test on July 24, 2021. The surrogate tank car was impacted by a 297,200-lb ram car fitted with a 12 x 12-inch impactor traveling at 18.3 mph. The impact resulted in a significant amount of deformation but did not puncture the tank car. After the test, the team updated the pre-test finite element (FE) model to represent the measured speed of the ram car but observed some discrepancies between the test measurements and simulation results. The testing and modeling effort is described in detail in a separate FRA Technical Report [3]; this report is focused on a phase change discrepancy noted during Test 12.

Review of the test data from Test 12 revealed that the pressure within the tank was lower after impact (i.e., 26 psig) than before impact (i.e., 30 psig). The volume of the tank was reduced through deformation during the impact, and no venting of LN2 or gaseous nitrogen (GN2) occurred. The team considered two physical explanations for this decrease in pressure accompanied by a decrease in tank volume: 1) a decrease in GN2 temperature caused by mixing with colder LN2 during the impact, or 2) condensation (i.e., a phase change) of GN2 into LN2 caused by pressurization as the inner tank deformed. This report documents the technical challenges and modeling approaches used between Tests 12 and 13 to explain the phase change in a tank car filled with cryogenic LN2.

The team modified the post-test model from Test 12 to simplify several features that were not deemed critical to this study. This non-puncture[1] FE model was updated using the initial conditions from Test 12. Two different approaches for accounting for GN2 to LN2 condensation were independently developed using techniques native to Abaqus FE software:

1. **Tabulated EOS** - a material model using a tabulated equation of state (EOS) featuring a sharp change in the pressure versus density relationship, paired with a Lagrangian mesh

[1] Non-Puncture FE models do not have the capability to puncture. This is in contrast with puncture-capable FE models that can tear the inner and outer tanks through ductile material damage progression and element deletion.

2. **Fluid Exchange** - a pneumatic cavity using the ideal gas law and a prescribed pressure versus flow rate "vent" allowing GN2 to escape the cavity to atmosphere once the saturation pressure is reached

The team also developed a third approach, which did not use FE analysis, using the Test 12 data, a laser scan of the inner tank, and the thermodynamic properties of GN2 and LN2 to estimate the amount of GN2 that condensed into LN2 during the test. This third approach was treated as a "check" case for comparison against the amount of GN2 that was estimated to undergo phase change by the two approaches implemented within the FE model.

1. Introduction

As part of a series of impact tests, the Federal Railroad Administration (FRA) sponsored a research team from Transportation Technology Center, working with Volpe National Transportation Systems Center (Volpe), to analyze the side impact puncture performance of a surrogate DOT-113 tank car filled with cryogenic liquid nitrogen (LN2). The test was performed in July 2021. Before performing any further testing, the research team performed a series of analyses to examine the modeling techniques and effects of an apparent vapor to liquid phase change that occurred during the impact event. This report documents the technical challenges and modeling approaches used in the test to explain the phase change in a tank car filled with cryogenic LN2.

1.1 Background

In the past decade, significant research has been conducted to analyze and improve the impact behavior and puncture resistance of railroad tank cars. Ultimately, the results of this research will be used by federal regulatory agencies (i.e., FRA and the Pipeline and Hazardous Materials Safety Administration (PHMSA) in the United States) to establish performance-based testing requirements and to develop methods to evaluate the crashworthiness and structural integrity of different tank car designs when subjected to a standardized shell impact scenario. A performance-based requirement for tank car head impact protection has already been defined within the current regulations [4], and an optional performance-based requirement for tank car shell impact resistance is applicable to DOT-117P tank cars [5].

To support FRA's ongoing research program, full-scale tests are necessary to provide the technical information to validate modeling efforts and to inform regulatory activities. These tests evaluate the crashworthiness performance of tank cars used in the transportation of hazardous materials, including designs that comply with current regulations as well as innovative new designs that may improve puncture resistance.

A DOT-113 tank car is a specialized tank car that is designed to transport cryogenic liquids[2]. A cryogenic liquid is defined as "a refrigerated liquefied gas having a boiling point colder than -90˚C (-130˚F) at 101.3 kPa (14.7 psia) absolute"[3]. DOT-113 tank cars are "tank-within-a-tank" cars, where the inner tank is in contact with the cryogenic material and resists the pressure exerted by the lading, while an outer tank surrounds the inner tank, with insulation between them, and carries the in-train forces. The article used in this test is referred to as a "surrogate" DOT-113 tank car and was constructed specifically for use in this shell impact test. The surrogate included design features representative of a specification DOT-113 tank car, including typical materials of construction for the inner and outer vessels, typical diameters for the inner and outer vessel shells, typical thicknesses for the inner and outer vessels, and typical pressure relief valve (PRV) arrangements. The tanks in the DOT-113 surrogate tank car were full diameter but were shorter in length than an actual DOT-113. The surrogate did not include

[2] Subpart F – Specification for Cryogenic Liquid Tank Car Tanks and Seamless Steel Tanks (Classes DOT-113 and 107A) https://www.govinfo.gov/content/pkg/CFR-2018-title49-vol3/pdf/CFR-2018-title49-vol3-part179-subpartF.pdf

[3] 49 CFR 173.115(g)

features required of tank cars that would not influence the puncture response during a shell impact (e.g., couplers, trucks, brake piping, or safety appliances). The terms "surrogate" and "tank car surrogate" are used interchangeably throughout this report to describe the test article. Further details on the design of the DOT-113 surrogate are included in the full test report [3].

DOT-113 tank cars include several unique design features that are not found on non-pressure (e.g., DOT-117) or pressure (e.g., DOT-105) tank cars because of the specific properties of cryogenic materials. Since the inner tank of a DOT-113 tank car will be exposed to cryogenic temperatures, it must be constructed of either ASTM A240 Type 304 or Type 304L stainless steel [7], as those grades of steel maintain desirable properties at cryogenic temperatures. Since the inner vessel and lading must be kept at cryogenic temperatures during transit, the inner vessel must be surrounded by highly effective insulation. This insulation may take the form of expanded perlite (i.e., a granular, lightweight, natural mineral) or multiple layers of "super" insulating materials (i.e., multi-layer insulation, or (MLI)). Additionally, a vacuum is typically used in conjunction with either perlite or MLI to further reduce heat transfer into the inner vessel. The specification defines a maximum rate of heat transfer that is permissible through the insulation system, and the inner vessel and insulation must be surrounded by an external tank to contain the insulation, maintain the vacuum, and carry the in-train forces.

Hazardous Materials Regulations (HMR) permit the transportation of several cryogenic liquids via DOT-113 tank cars, including argon and ethylene. Methane, refrigerated liquid (more commonly referred to as LNG), was not authorized for transportation via DOT-113 tank car prior to 2020. PHMSA and FRA published a Notice of Proposed Rulemaking (NPRM) in October 2019,[4] permitting LNG to be transported in DOT-113 tank cars. However, after Test 12, PHMSA and FRA published a second NPRM in November 2021,[5] suspending the transportation of LNG in DOT-113 tank cars until further research could be conducted. The Final Rule suspending transportation of LNG by rail was published in September 2023[6].

Because the existing fleet of DOT-113 tank cars is small compared to the overall tank car fleet and limited accident data exist regarding the performance of these cars in derailments or collisions, a series of full-scale shell impact tests was conducted to provide technical information on the tank car's puncture resistance. The first test in this series (Test 10) was performed in November 2019 [1], and the second test (Test 11) was performed in June 2020 [2]. After the second test, a series of finite element (FE) analyses was conducted to transition from testing and modeling a tank car filled with water to one filled with LN2 [6]. The third test in this series (Test 12) was performed in July 2021 [3].

---

[4] Federal Register/Vol 84, No. 206/Thursday, October 24, 2019.
https://www.regulations.gov/document?D=PHMSA-2018-0025-0002

[5] Federal Register/Vol 86, No. 213/Monday, November 8, 2021.
https://www.regulations.gov/document/PHMSA-2021-0058-0002

[6] Federal Register/Vol 88, No. 169/Friday, September 1, 2023.
https://www.federalregister.gov/documents/2023/09/01/2023-18569/hazardous-materials-suspension-of-hmr-amendments-authorizing-transportation-of-liquefied-natural-gas

1.2 Objectives

The overall objective of the modeling program was to develop FE models capable of estimating the impact response and puncture behavior of the outer and inner vessels of a DOT-113 tank car under cryogenic conditions. The modeling described in this report focused on incorporating the effects of gaseous nitrogen (GN2) vapor condensation on the impact response of a DOT-113 tank car surrogate. The team focused on improving the capability of the post-test FE model to accurately represent a phase change because they anticipated that a phase change would likely occur during the final side impact test of a modern DOT-113 tank car, which would likely affect the puncture resistance of the tank car.

1.3 Overall Approach

FRA has previously conducted side impact tests on DOT-105, DOT-111, DOT-112, DOT-117, and DOT-113 tank cars. These tests were all accompanied by companion FE analyses and covered a wide range of tank car designs (e.g., capacity, shell diameter, shell thickness, vintage, manufacturer, outage level, outage pressure, etc.) The ultimate goal of the tank car shell impact testing and modeling program is to understand how a particular tank car performs under a standardized impact scenario that is representative of typical service conditions. Typical service conditions for a DOT-113 tank car include carrying a cryogenic commodity within the inner vessel. The team used full-scale and laboratory testing with companion FE modeling to understand how the tank car behaves under impact conditions and the potential for performance improvement through design changes. Both the testing and modeling featured increasing complexity to ultimately represent a DOT-113 tank car under LNG service conditions subjected to a shell impact that punctures both inner and outer vessels. The approach included tests and corresponding analyses to examine the influence of different materials/thicknesses used for the tank shell, examine the effect(s) of modeling both the lading and the inner vessel steel using properties at cryogenic conditions, and ultimately modeling a DOT-113 tank car under "representative" conditions expected for LNG service.

Observations, lessons learned, and data collected during the first two impact tests of a DOT-113 tank car and tank car surrogate were used as a starting point for the technically challenging task of modeling a DOT-113 surrogate filled with LN2. The major differences between this third test and the previous two tests in this series was the use of LN2 and the temperature of the lading and inner tank. A further design complexity was the consideration of puncturing one or both tanks.

Researchers collaborated with FRA and PHMSA to determine the targeted outage, pressure, and temperature of the DOT-113 surrogate filled with LN2. After the targeted initial conditions were determined, the team conducted pre-test modeling to quantify the level of uncertainty in the speed necessary to cause puncture of the DOT-113 surrogate. The pre-test model results were used to determine a targeted impact speed for each test.

1.4 Scope

This report includes discussion of the development and execution of the FE models used in this test program, including developing a tabulated EOS material model for nitrogen, examining various mesh techniques to implement the tabulated EOS material, developing a "fluid exchange" model for phase change, and calibrating the volumetric flow rate for the fluid exchange. This report also includes a comparison between the amount of GN2 estimated to

undergo phase change from each FE implementation compared with a calculation made using Test 12 data.

Researchers compared several analyses with the test results to assess whether including the effects of GN2 condensation improve the test-model agreement compared to the pre-test FE models. Further details on the Test 12 procedure, results, pre-test model development, and model comparison are contained within the Test 12 report [3].

1.5 Organization of the Report

Section 2 summarizes the results of Test 12 and describes the initial post-test model used to investigate the likelihood of vapor to liquid condensation during the test.

Section 3 summarizes several equation of state (EOS) material models available in the FE modeling software. This section also describes the development of a tabulated EOS representing nitrogen vapor-to-liquid condensation in the post-test FE model.

Section 4 describes how the results of the Tabulated EOS model were used to calibrate a fluid exchange implemented within a pneumatic cavity approach to modeling the outage in Test 12.

Section 5 presents the results of FE models run using the Tabulated EOS model and the Fluid Exchange model and comparisons of the results obtained using these two different approaches.

Section 6 contains concluding remarks.

Appendix A describes the non-puncture FE model of the DOT-113 surrogate filled with LN2 discussed in the report.

Appendix B contains the results of the non-puncture FE model run using the Tabulated EOS model at various assumed conditions.

Appendix C contains comparisons between the results of the non-puncture FE model run using the Tabulated EOS model and the Fluid Exchange model at various assumed conditions.

Appendix D describes the process used to estimate the post-test inner tank volume from the Test 12 DOT-113 surrogate.

Appendix E provides a mathematical model to calculate the rise in pressure in the outage (i.e., vapor) volume space of a cryogenic tank car when the volume of the inner tank is compressed during a side impact.

2. Test 12 Results and Initial Post-test Models

This section includes a summary of the results of Test 12 supporting the hypothesis that GN2 condensed into LN2 during the test. A complete discussion of the results of Test 12 are found in the full test report [3].

This section also includes a summary of the Test 12 post-test FE model used to investigate the two different implementation techniques for phase change. Several FE results using the Test 12 FE model, but not incorporating phase change effects, are included in this section to demonstrate the discrepancies that led the team to incorporate phase change effects into further post-test models.

2.1 Test 12 Results

Test 12 featured a 297,200-lb impactor equipped with a 12 x 12-inch impactor impacting the shell of the tank car at 18.3 mph. As a result of the impact, the inner and outer tanks deformed but neither tank punctured. No GN2 or LN2 released from the tank through any punctures, piping, or the PRV. Initially, the tank was filled to approximately 95 percent of its volume with LN2 (i.e., a 5 percent outage). As discussed in the Test 12 report [3], vapor venting prior to the time of the test resulted in an estimated filling level of 91 percent (i.e., a 9 percent outage) at the time of the test. The initial liquid and outage conditions for Test 12 are summarized in Table 2.

Table 2. Summary of Initial Liquid and Outage Conditions in Test

Parameter	Value from Test
Commodity in Tank	LN2
Commodity Temperature	~ -305°F (~86 K)
Initial Tank Volume	17,900 gal
Outage Volume	~9%
Initial Outage Pressure	30 psig

The instrumentation recorded data for 30 seconds after initial contact was made by the impactor on the tank shell. At the end of this period, the internal pressure within the tank had settled to approximately 26 psig, 4 psi lower than the initial pressure. The post-test volume of the inner tank was estimated to be 17,300 gallons using a post-test LiDAR scan of the inner tank (discussed in Appendix D). A tank that did not vent any material but experienced a reduction in volume would be expected to have a post-test pressure higher than the initial pressure, since the vapor would be compressed into a smaller volume. One explanation for the measured drop in pressure was that some amount of GN2 had condensed into LN2 during the test, leaving the remaining GN2 at a lower pressure after the tank recovered its elastic energy. The phase change behavior during this test was highly complex. During the impact, the volume of the tank was decreased through deformation. The LN2 would have sloshed through the GN2, potentially decreasing the outage temperature at the same time deformation was increasing pressure. Both a temperature drop and a pressure increase on the GN2 would tend to result in condensation. After the impactor was brought to a stop, the tanks would recover their elastic energy and with that, recover some volume. An increase in tank volume would tend to reduce the internal pressure, potentially resulting in some LN2 vaporizing back into GN2.

2.2 Initial Post-test Phase Change Modeling

In previously conducted tank car tests using air at atmospheric or elevated pressure and ambient temperature, the gas in the outage could be correctly assumed to remain a gas for the duration of the impact event. This assumption simplified modeling the outage in those tests, as the ideal gas law was applicable without additional considerations. For Test 12, the gaseous N2 in the outage was initially at a pressure of 30 psig. At Pueblo, CO's elevation (approximately 4,700 feet above sea level [8]), this corresponded to an absolute pressure of 42.3 psia [9]. At this pressure, the N2's saturation temperature was approximately 87.6 K [10]. An increase in pressure also results in an increase in the saturation temperature (see the saturation curve in Figure 5). If the pressure of the gas were increased such that the temperature was now below the saturation temperature at the new pressure, the gas could experience a phase change by condensing into a liquid. A vapor-to-liquid phase change could also occur if the pressure of the gas remained the same but the temperature of the gas dropped below the saturation temperature.

A simple solution would be to keep the gas at a temperature that is much higher than the saturation temperature at the initial pressure of 42.3 psia. An elevated temperature of the gas would require a more substantial decrease in temperature or increase in pressure to cross the saturation curve. However, it is not necessarily possible to maintain equilibrium between GN2 and LN2 with such a large difference in temperature, as the LN2 must be kept *below* the saturation temperature at a given pressure to remain in the liquid state.

Prior to Test 12, a modeling study was conducted to examine adapting existing modeling techniques used for water and air-filled tank cars to GN2 and LN2 [6]. The conclusions made in this modeling study were then incorporated into the Test 12 pre-test models, which are documented in the Test 12 report [2]. The Test 12 report also documents the initial post-test modeling that was conducted using test conditions which led to the determination that additional modeling techniques for capturing the effects of GN2-LN2 condensation were needed. The post-test models from Test 12 are briefly summarized below.

The Test 12 pre- and post-test models were run using two limiting behaviors assumed for the GN2 in the outage. Assuming that GN2 is initially at its saturation temperature and that its temperature remains constant, the process of compressing the gas should be isobaric (i.e., occurring at a constant pressure). On the other hand, if the gas were above its saturation temperature it would not undergo a phase change unless the pressure increased above the saturation pressure at the gas's temperature. If the GN2 remained at a constant temperature while being compressed, the process would be isothermal. Figure 1 contains the force-displacement responses from Test 12 and the post-test models that used an isothermal or isobaric assumption for the GN2.

These modeling efforts provided the upper and lower bound estimates of the response during the test. The isobaric model featured lower forces and a higher maximum impactor travel than the Test 12 data, while the isothermal model featured higher forces and a slightly lower maximum impactor travel than the Test 12 data. These outcomes implied that the actual behavior in Test 12 was somewhere between these two extremes.

While not being conclusive, these model results support the hypothesis that some of the GN2 in Test 12 condensed into LN2 during the test. If the GN2 were initially at a temperature above its saturation temperature at the initial pressure, then some increase in pressure would be possible as the impact occurred. This behavior is consistent with the isothermal response. However, the

isothermal model overpredicted the force measured during the test. If the pressure increased during the test but then reached the saturation pressure of the GN2, continued pressure increase would be prevented while the phase change occurred. In other words, the GN2 would initially behave more like the isothermal approximation, but once reaching the saturation pressure would begin to behave more like the isobaric approximation.

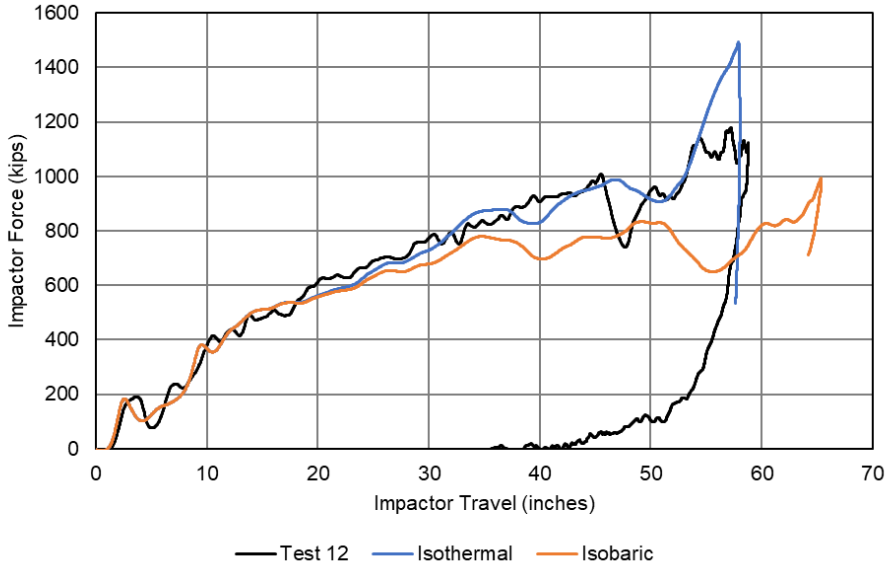

Figure 1. Force-displacement Responses from the Isothermal and Isobaric Post-test Models Compared to Test Result (Image from [2])

As a test of this hypothesis, a simplified Fluid Exchange model was developed and incorporated into the Test 12 post-test FE model. The purpose of this first investigation was simply to explore whether modeling this supposed isothermal/isobaric behavior could lead to closer test-model agreement. As the Test 12 FE model used a pneumatic cavity for the GN2, a volumetric flow rate versus pressure behavior was developed to simulate GN2 being "lost" due to phase change. This initial model was calibrated to have zero flow rate out of the cavity at pressures below 70 psia, and a prescribed volumetric flow rate versus pressure if pressure exceeded 70 psia. The value of 70 psia was chosen based on review of the Test 12 pressure data and the isothermal FE model and cannot be considered model validation. As seen in Figure 2, the post-test model incorporating volumetric flow as a stand-in for phase change was in better agreement with both the maximum force and maximum impactor travel measured during Test 12.

Based on the improved correlation between the Test 12 measurements and the results of this first attempt at representing phase change within the FE model, the team undertook a further effort at developing a phase change material model for GN2 at a temperature above its saturation temperature. Since phase change occurred during Test 12, and the next planned test would use substantially similar conditions (e.g., LN2, outage volume, initial pressure), researchers reasonably concluded that phase change could also be expected to occur in Test 13. The pre-test models developed for Test 13 should therefore account for phase change using defensible modeling techniques that did not depend on using test measurements to calibrate the model response.

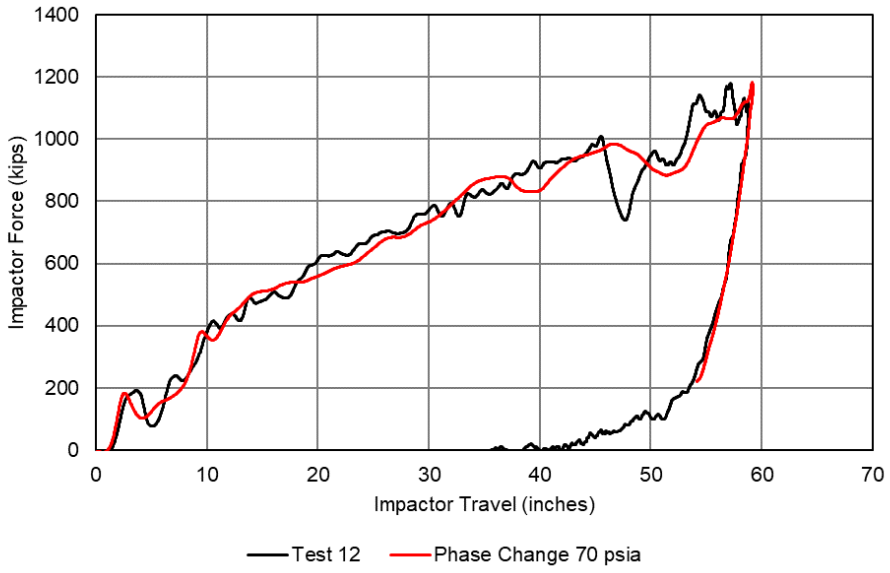

Figure 2. Force-displacement Response from Post-test Model Saturated at 70 psia (57.7 psig) Compared to Test Result (image from [2])

3. Development of a Tabulated EOS for N2 Condensation

The FE models developed in support of Test 12 all included a representation of the LN2 partially filling the tank and the pressurized GN2 in the outage space. The results indicated that some amount of GN2 likely condensed into LN2 during the test. Since the follow-up test (Test 13) would also use a DOT-113 tank filled with pressurized LN2 and GN2, the team needed to develop a modeling technique that could predict the onset of phase change, which was expected to limit the pressure rise that could occur within the tank, and in turn would affect the forces developed between the impactor and the tank car and ultimately puncture.

The team first examined the EOS implementations available within the Abaqus software. The Abaqus documentation states that EOS models "determine the pressure (positive in compression) as a function of the density, ρ, and the specific energy (the internal energy per unit mass), E_m" [9]. A second approach used the results of models run using the EOS implementation to calibrate a volumetric leakage rate. This then could be incorporated into a pneumatic cavity representing the outage using a fluid exchange between the cavity and atmosphere.

The team used a non-puncture version of the Test 12 FE model (shown in Figure 3 with mesh and constraints visible), which is a simplified version of the model developed for Test 12 (based on a working draft of the CAD model from the manufacturer). The stub sills on this model were reversed (i.e., the tapered end should be located inboard of the bolster), but this inconsistency was not expected to have a significant effect on the fluid response within the tank. The Test 12 FE model was modified to remove unnecessary details, including the ability to puncture. The DOT-113 surrogate in Test 12 did not puncture, so a non-puncture model should be capable of reproducing the test results without a loss of confidence. The FE model used in the development of the phase change GN2 material model is described in Appendix A.

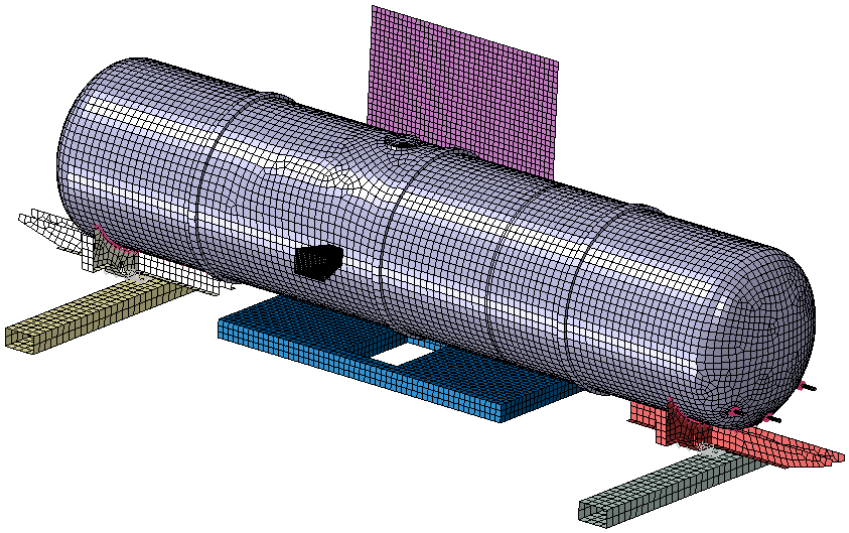

Figure 3. Non-puncture Test 12 Model

Two different approaches to modeling the GN2 were studied. In the first approach, a GN2 material model was developed and applied to a mesh of Lagrangian, tetrahedral elements filling the outage. The resulting meshes for LN2 (bottom) and GN2 (top) used in that portion of the

study are shown in Figure 4. A tied constraint connecting the bottom of the GN2 with the top of the LN2 is also visible in this figure.

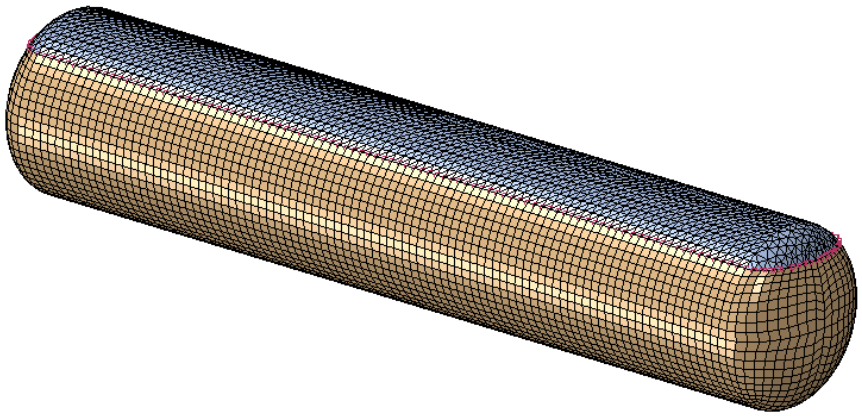

Figure 4. Lagrangian Meshes for Lading and Outage

In a second approach to modeling GN2, the team replaced the GN2 material model and Lagrangian mesh with a pneumatic cavity. The cavity was assigned a prescribed leakage rate using a fluid exchange between the cavity and atmosphere that was calibrated based on the saturation properties of the GN2 at the chosen temperature and the results of the corresponding EOS model. The team continued to model the LN2 using a Lagrangian mesh and the same material model used in the GN2 material model. This second approach is described in Section 4.

3.1 Approach to Modeling Phase Change

A phase change is a complicated thermodynamic process. Implementing a numerical (e.g., FE) model of a phase change is an additional complication, as there are limitations to any commercially available software package. The goal was not to faithfully reproduce and account for all of the potential thermodynamic processes that governed phase change, but to develop a material model that accounted for the *effects* of the GN2 to LN2 condensation that was believed to occur during Test 12. Researchers employed a set of guidelines to aid in developing the techniques used to simulate phase change:

1) The techniques would be implemented in the Abaqus/Explicit [9] FE solver, as that was the solver used with the original Test 12 FE model.
2) The techniques only needed to represent condensation between vapor and liquid, as that was the phase change of interest during the test. Liquid to vapor evaporation or any phase change involving the solid state were outside the test scope.
3) The techniques should not assume that the vapor was initially saturated.
4) The techniques should be implemented using built-in features of the Abaqus FE software without the need to develop any user subroutines.
5) The techniques should not require complete redevelopment of the existing Test 12 FE models.
6) The techniques should not result in a substantial increase in model runtime compared to existing Test 12 FE models.

7) The techniques should be capable of representing phase change under a variety of unknown initial conditions, such as varied initial pressure and temperature.

8) The techniques should be adaptable to cryogenic liquids beyond just LN2. Test 12 used LN2 as its lading but future modeling was anticipated using other cryogenic liquids.

Figure 5 shows the saturation curve for N2 using data from the National Institute of Standards and Technology (NIST) [10]. The vertical axis shows the saturation pressure and the horizontal axis shows the saturation temperature. LN2 can only exist at pressure/temperature combinations on or above the saturation curve (e.g., at high pressures or low temperatures) and GN2 can only exist at pressure/temperature combinations on or below the saturation curve (e.g., at low pressures or high temperatures). Liquid and vapor can exist simultaneously for combinations of pressure and temperature on the saturation curve.

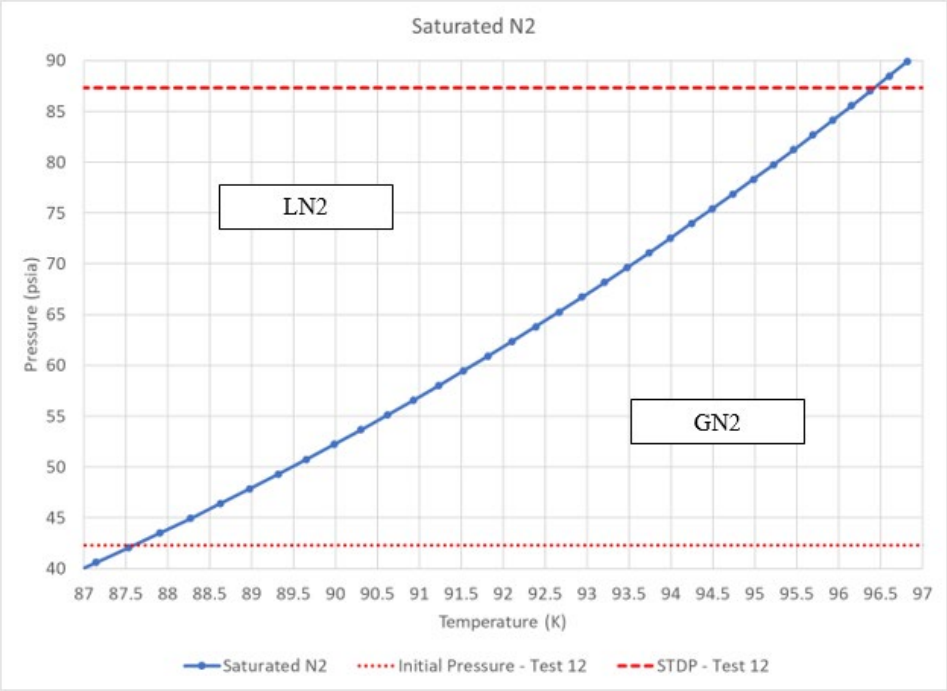

Figure 5. Saturation Curve for N2 with Pressures of Interest Noted

Figure 5 also shows two horizontal dashed lines indicating two relevant pressures from Test 12. The initial pressure of the inner tank of the tank car was consistently measured by several pressure transducers and mechanical gauges as 30 psig, or 42.3 psia [2]. While the exact temperature of the vapor in the outage was not measured during the test, knowing the initial pressure of 42.3 psia limits the possible temperatures at which GN2 could have existed. As shown on Figure 5, a pressure of 42.3 psia corresponds to a saturation temperature of approximately 87.6 K. For GN2 to exist at a pressure of 42.3 psia, its temperature must be no lower than 87.6 K. This property sets a lower limit to the temperature range of interest for any material model capturing GN2 phase change under Test 12 conditions.

An upper limit to the temperature range of interest can be estimated from the design of the tank itself. The tank used in Test 12 included a PRV with a start-to-discharge pressure (STDP) of 75 psig, (i.e., 87.3 psia at Pueblo, CO's elevation). If the pressure of the GN2 reached 87.3 psia during the test, the tank would begin to vent as designed. This PRV also effectively limits the

pressure range over which phase change is likely. Any attempt to pressurize the GN2 above the STDP results in activation of the PRV. N2's saturation temperature is approximately 96.4 K at the STDP of the PRV used in Test 12. While GN2 can and does exist at temperatures above 96.4 K, it was not necessary to develop a phase change EOS model for any greater temperatures assumed for Test 12. If the saturation temperature were above 96.4 K the PRV would activate and reduce pressure in the tank before the saturation pressure could be reached[7].

Density versus pressure relationships for N2 at fixed temperatures (i.e., isotherms) between 88 K and 100 K are shown in Figure 6. These relationships were developed using data from the NIST [10] converted into the unit system used in the Test 12 FE model. The dashed vertical lines represent the saturation pressure at a given temperature. Densities below the dashed line correspond to GN2 and the higher densities correspond to LN2. At 98 K and 100 K, the Test 12 tank car would be expected to begin to vent at a lower pressure than the pressure needed to initiate phase change. These temperatures were included in this study to examine the sensitivity of the model's response to a range of assumed initial temperatures.

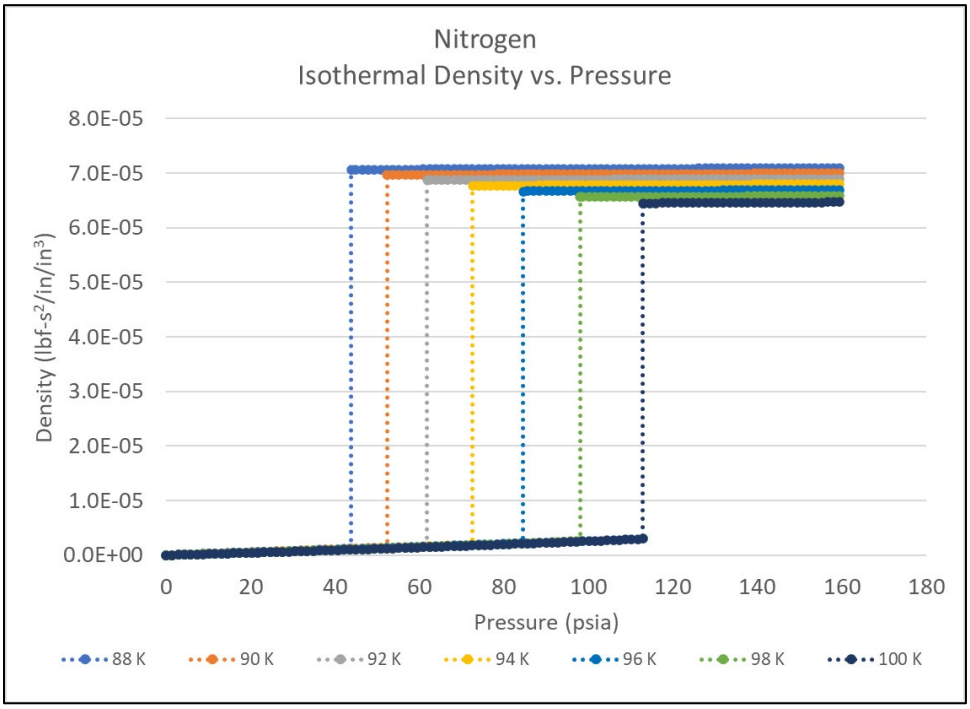

Figure 6. Isothermal Density Versus Pressure for Nitrogen (Data from NIST [10])

Researchers believed the sudden change in N2 density at the saturation pressure was an essential feature of a phase change implementation in Abaqus. For a given temperature, pressures below the saturation pressure would result in the gas behaving like a real gas. As the pressure increased, the GN2's density would increase gradually. If the saturation pressure was reached, any further attempt to compress the GN2 would cause an abrupt increase in density. In a numerical implementation, this sudden increase in density would be achieved by a sudden reduction in element volume, while the mass of a Lagrangian element typically remains constant throughout

[7] In theory, a very rapid buildup of pressure that exceeds the PRV's flow rate could occur. In this case, pressure within the tank could exceed the STDP of the PRV despite the PRV actively venting.

an analysis. Notably, in the liquid phase the density of N2 remains nearly constant with increasing pressure, confirming that LN2 can be treated as an incompressible liquid.

As stated earlier in this section, the EOS material models available in the Abaqus software relate pressure to density and internal energy. The team determined that an EOS model was a logical starting point to simulate the abrupt density change associated with phase change.

3.2 Gas Modeling in Abaqus: Ideal Gas EOS

An ideal gas is a theoretical gas containing molecules moving randomly that are not subject to inter-particle forces. The ideal gas model has two assumptions:

(1) intermolecular forces (e.g., van der Waals forces[8]) are neglected, and;

(2) the volume occupied by a gas molecule is neglected.

The ideal gas model is typically not applicable at very low temperatures or high pressures where the molecular size and intermolecular forces can affect the random motion of molecules. The very low temperature limitation is relevant to cryogenic systems, as the vapor outage above a cryogenic liquid is typically at a temperature where a gas does not follow the ideal gas law. The authors presented a discussion on thermodynamic systems and ideal gases in a report documenting modeling studies performed to transition between Test 11, using water, and Test 12, using LN2 within the DOT-113 surrogate tank [6].

The symbols used in the ideal gas equations discussed in this section are defined in Table 3.

Table 3. Symbols used in Ideal Gas EOS

Symbol	Parameter
p	Pressure
p_A	Ambient pressure
ρ	Current density
R	Specific gas constant
R_u	Universal gas constant
MW	Molecular weight
c_v	Constant volume specific heat
T	Current temperature
T^Z	Absolute zero temperature
T_0	Initial temperature
E_m	Internal energy per unit mass
E_{m0}	Initial internal energy per unit mass
V	Volume
n	Number of moles
Z	Compressibility factor

[8] van der Waals forces are weak intermolecular forces that are dependent on the distance between atoms or molecules. These forces arise from the interactions between uncharged atoms/molecules.

The ideal gas law is an EOS given in terms of absolute pressure (p), volume (V), number of moles (n), universal gas constant (R_u), and absolute temperature (T). To consider attractive forces between the molecules of a real gas, a compressibility factor (Z) can be incorporated to describe the deviation, as shown in Equation 1.

Equation 1. Ideal Gas Law (a) and Definition of Compressibility Factor (b)

$$pV = nR_uT \quad (a)$$

$$pV = ZnR_uT \quad (b)$$

The compressibility factor is dependent on temperature and molar volume (V_m) or pressure. When the compressibility factor is less than 1, attractive forces dominate the interaction. When the compressibility factor is greater than 1, repulsive forces dominate the interaction. At cryogenic temperatures, the compressibility factor is typically less than 1 because van der Waals forces result in a significant attractive force. This attractive force causes a gas to behave more like a liquid.

The Abaqus software includes an ideal gas EOS material model. This EOS follows the relationship shown in Equation 2 [9]. The specific form of the ideal gas law in Abaqus differs slightly from Equation 1(a) in that the volume (V) of the gas is not an explicit term, being incorporated into the density (ρ) of the gas. The form of the ideal gas EOS used by Abaqus also requires the specific gas constant (R) rather than the universal gas constant (R_u). Additionally, the Abaqus form allows the user to specify the ambient pressure (p_A) and absolute zero temperature (T^Z) being used in the model's unit system. Finally, the form of the ideal gas EOS in Abaqus does not allow for compressibility (Z) to be defined.

Equation 2. Ideal Gas EOS in Abaqus

$$p + p_A = \rho R(T - T^Z)$$

If p_A is assumed to be zero (i.e., absolute pressure values are used to define the ideal gas) and a temperature scale with a T^Z of zero is used, then Equation 2 simplifies to Equation 3.

Equation 3. Simplified Ideal Gas EOS in Abaqus

$$p = \rho RT$$

The value of R is found according to Equation 4. Note that the value of R is dependent on the gas for which the ideal gas EOS is being developed.

Equation 4. Specific Gas Constant used in Abaqus

$$R = \frac{R_u}{MW}$$

Equation 5 shows the equation Abaqus uses to calculate the specific energy (i.e., internal energy per unit mass, E_m) of an ideal gas. E_m depends only on the temperature of the ideal gas and the value(s) of c_v as a function of temperature. Neither pressure nor density appear in this relationship. The initial value of E_{m0} is calculated in a similar way, according to Equation 6.

Equation 5. Internal Energy per Unit Mass of an Ideal Gas in Abaqus

$$E_m = E_{m0} + \int_{T_0 - T^Z}^{T - T^Z} c_v(T)\, dT$$

Equation 6. Initial Internal Energy per Unit Mass of an Ideal Gas in Abaqus

$$E_{m0} = \int_{0}^{T_0 - T^Z} c_v(T)\, dT$$

There are two limitations to the Ideal Gas EOS implementation within Abaqus that hinders its suitability to modeling the GN2 in Test 12. First, the Abaqus implementation does not allow the use of a compressibility factor *Z*, as shown in Equation 1. This limitation may or may not be significant, as the difference between an ideal gas law and real gas law was investigated in the pre-test modeling before Test 12 [6]. The more significant limitation is that once the saturation pressure is reached the pressure-density relationship is entirely different than the relationship described by the ideal gas law.

3.3 Liquid Modeling in Abaqus: Us-Up EOS

The Linear Us-Up Hugoniot EOS (Us-Up EOS) is another EOS implementation available in Abaqus. This material model has been used to model bulk liquid responses in previous tank car impact simulations [9]. The Us-Up EOS has been successfully used to model impacts to tank cars filled with clay slurry [11], water [12], and LN2 [2]. This EOS follows Equation 7. The symbols in this equation are defined in Table 4.

Table 4. Symbols used in Us-Up EOS

Symbol	Parameter
p	Pressure
ρ_0	Reference density
ρ	Current density
c_0	Reference speed of sound
η	Nominal volumetric compressive strain
Γ_0	Material constant
s	Coefficient relating shock and particle velocities
E_m	Internal Energy per Unit Mass

Equation 7. Us-Up EOS in Abaqus

$$p = \frac{\rho_0 c_0^2 \eta}{(1 - s\eta)^2} \cdot \left(1 - \frac{\Gamma_0 \eta}{2}\right) + \Gamma_0 \rho_0 E_m$$

The nominal volumetric compressive strain, η, is a relationship between the current density (ρ) and reference (initial) density (ρ_0) defined according to Equation 8.

Equation 8. Nominal Volumetric Compressive Strain

$$\eta = 1 - \frac{\rho_0}{\rho}$$

Previous finite element simulations of tank car impacts using the Us-Up EOS for water (i.e., an incompressible liquid) have achieved a high level of agreement with measured test results assuming the parameters Γ_0 and s are both equal to 0. Using this assumption and substituting Equation 8, Equation 7 becomes Equation 9 and dependance on E_m is eliminated. Thus, the pressure-density relationship of a liquid that follows this behavior depends only on the reference density and reference speed of sound.

Equation 9. Simplified Us-Up Equation Used in Tank Car Impact Models for Incompressible Liquids

$$p = \rho_0 \cdot c_0^2 \cdot (1 - \frac{\rho_0}{\rho})$$

While the Us-Up EOS has been shown to provide suitable performance when modeling incompressible liquids, this EOS does not appear suitable for modeling vapor-to-liquid condensation. Specifically, the abrupt change in density associated with vapor reaching its saturation pressure would not be adequately captured by the Us-Up EOS in the form used to model incompressible liquids.

3.4 Gas-to-Liquid Modeling in Abaqus: Tabulated EOS

The Abaqus software includes the ability to define an EOS as a series of entries on a table, referred to as a *Tabulated EOS* [9]. The Abaqus documentation includes the statement that "[t]he tabulated [EOS] provides flexibility in modeling the hydrodynamic response of materials that exhibit sharp transitions in the pressure-density relationship, such as those induced by phase transformations" [9]. The Tabulated EOS used in Abaqus takes the form shown in Equation 10 using the symbols defined in Table 5.

Equation 10. Tabulated EOS in Abaqus

$$p = f_1(\varepsilon_{vol}) + \rho_0 \cdot f_2(\varepsilon_{vol}) \cdot E_m$$

Table 5. Symbols used in Tabulated EOS

Symbol	Parameter
p	Pressure
ρ_0	Reference density
ρ	Current density
$f_1(\varepsilon_{vol})$	User-defined function 1
$f_2(\varepsilon_{vol})$	User-defined function 2
ε_{vol}	Logarithmic volumetric strain
E_m	Internal energy per unit mass
E_{m0}	Initial internal energy per unit mass

The logarithmic volumetric compressive strain, ε_{vol}, is defined according to Equation 11 as the natural logarithm of the ratio between reference (initial) density (ρ_0) and current density (ρ).

Equation 11. Logarithmic Volumetric Compressive Strain

$$\varepsilon_{vol} = \ln\left(\frac{\rho_0}{\rho}\right)$$

The tabulated EOS can be used to define a broad variety of materials. In the Tabulated EOS approach, the user defines the values of f_1 and f_2 at a given value of logarithmic volumetric strain (ε_{vol}). Since ε_{vol} is user-defined in the table and varies with current density, the user has control over the range of densities over which the EOS should be defined. For each value of ε_{vol} the software calculates the resulting pressure within the material and the internal energy per unit mass (E_m). The reference density (ρ_0) and initial value for E_m (E_{m0}) are also defined by the user. Additional entries for f_1 and f_2 can be provided for a series of different ε_{vol} values, building a table of user-defined functions for different densities.

The user is left to determine a series of f_1 and f_2 values based on the pressure-density-energy relationship of the material the EOS represents. It is important to note that the values for the user-defined functions f_1 and f_2 cannot be defined arbitrarily. The Abaqus software requires data to be input according to certain rules:

1. A value of ε_{vol} = 0 (i.e., when the current density is the initial density) must appear in the tabular entries.
2. At ε_{vol} = 0, f_1 =*0*.
3. The values for f_1 must be defined in monotonic, increasing order.
4. Values for f_2 may increase, decrease, or remain the same for different values of ε_{vol}.
5. The software will regularize ε_{vol} if ε_{vol} was defined using a non-constant difference ($\Delta\varepsilon_{vol}$) between consecutive values of ε_{vol}.

The Tabulated EOS was chosen as the most suitable approach for capturing the nonlinear pressure-density relationship associated with vapor condensing into liquid. The constants f_1 and f_2 were developed for the vapor and liquid phases and a third, "pseudo-phase" between vapor and liquid.

3.4.1 Tabulated EOS for Liquid Phase

Comparing the forms of the simplified Us-Up EOS shown in Equation 9 and the Tabulated EOS shown in Equation 10, it is apparent that using rearrangement, the Us-Up behavior of a liquid can be defined instead using the Tabulated EOS. Specifically, the simplified Us-Up EOS for an incompressible liquid has no dependence on E_m, as Γ_0 is set equal to zero. If the Tabulated EOS for an incompressible liquid is also assumed to have no dependance on E_m, f_2 is assumed to be zero for all values of ε_{vol} corresponding to liquid densities, and Equation 10 simplifies to Equation 12.

Equation 12. Simplified Tabulated EOS Assuming no Internal Energy Dependence

$$p = f_1(\varepsilon_{vol})$$

Using a Tabulated EOS to model a liquid with a density and pressure relationship that doesn't depend on E_m simplifies to setting f_1 equal to the desired pressure at a series of values of ε_{vol}. For many liquids, including LN2, the saturation pressure and corresponding density for the liquid can readily be obtained from literature at the temperature(s) of interest.

3.4.2 Tabulated EOS for Gas Phase

In theory, the pressure-density relationship of a vapor condensing to a liquid state can be approximated using the Tabulated EOS contained within Abaqus. However, there are several simplifying assumptions that are either implicitly contained within this approach, or that will explicitly be made.

The first major assumption is that it is acceptable to neglect the latent heat associated with the phase change. During a vapor-to-liquid phase change, heat is released by the vapor as it condenses to a liquid. The amount of heat released during the phase change is the difference between the internal energy of the liquid state and the vapor state. This heat is referred to as the latent heat of condensation, and is equal in quantity but opposite in magnitude to the latent heat of vaporization (i.e., the heat that must be added to a liquid to cause it to vaporize).

While the Abaqus software does include a *LATENT HEAT keyword, this keyword is only meaningful in analyses run using a coupled temperature-displacement analysis procedure. Due to neglecting latent heat, the tabulated EOS model is expected to undergo phase changes more readily than a real substance. Additionally, without accounting for latent heat, the Tabulated EOS material could rapidly switch back-and-forth between vapor and liquid states if the pressure was close to the saturation pressure. This is particularly relevant to the tank car impact models, as the pressure within the tank car reaches a peak value and then begins to decrease if the impactor rebounds from the tank. In a physical test, any GN2 that condensed to LN2 would need adequate latent heat to be removed during that phase change. If the pressure subsequently dropped (such as could occur when the tank recovered its elastic strain energy) and the LN2 was now above its saturation temperature, liquid-to-vapor evaporation could occur. In a physical system, additional heat would need to be taken up by the LN2 to overcome its latent heat of vaporization. In the model, this phase change will occur without any latent heat being added to or removed from the N2.

The second assumption is that the phase change material model can be assumed to be isothermal. Equation 10 does not contain a term for temperature, so a Tabulated EOS material will remain at the same temperature throughout the simulation. A previous study concluded that modeling the outage as isothermal resulted in better agreement with the test data than modeling the outage as adiabatic [6]. Thus, the Tabulated EOS model should also be assumed to be isothermal.

The Tabulated EOS is implemented by a user defining a series of values f_1 *and* f_2 that vary with volumetric strain (see Equation 10). The constant f_2 is multiplied by the initial density (ρ_0) and the internal energy per unit mass (E_m). Recall that for an ideal gas E_m depends only on the current temperature of the gas (Equation 5). For an isothermal condition the temperature at any point in time will be equal to the initial temperature. Thus, the integral portion of Equation 5 will become zero and the equation will simplify to Equation 13.

Equation 13. Specific Energy of an Isothermal Ideal Gas

$$E_m = E_{m0}$$

By assuming the vapor in the outage behaves isothermally, the term f_2 in Equation 10 is now multiplied by both the *initial* density (ρ_0) and the *initial* specific energy (E_{m0}), neither of which will vary with time. Thus, f_1 and f_2 are the only terms that differ with respect to ε_{vol} as shown in Equation 14.

Equation 14. Tabulated EOS in Abaqus for Assumed Isothermal Gas

$$p = f_1(\varepsilon_{vol}) + \rho_0 \cdot f_2(\varepsilon_{vol}) \cdot E_{m0}$$

This constant E_m assumption was used to develop the first version of the Tabulated EOS. However, after reviewing the results of simulations run using this Tabulated EOS, it was apparent that E_m of the Tabulated EOS material was changing during the simulation. Further investigation revealed that the E_m being used by the Tabulated EOS material model included the contribution of pressure-volume (*P-V*) work being done by or on the Tabulated EOS material.

An approximate relationship for E_m was developed to be used in determining f_1 and f_2, according to Equation 15. E_m is equal to the initial specific energy (E_{m0}) minus the work done by the gas. The work done by the gas is the integral of pressure with respect to *specific volume* from the initial specific volume (v_0) to the current specific volume (v). Specific volume is the reciprocal of density. The negative sign indicates that a decrease in specific volume (i.e., an increase in vapor density) corresponds to work being done *on* the vapor by external forces, while an increase in specific volume corresponds to work being done *by* the vapor.

Equation 15. Specific Energy Incorporating Specific *P-V* Work

$$E_m = E_{m0} - \int_{v_0}^{v} P\, dv$$

The post-test 12 model was run using both Tabulated EOS assumptions for E_m. To distinguish between them, the two models are referred to as having either "constant E_m" for the Tabulated EOS developed assuming E_m was equal to E_{m0}, or "variable E_m" for the Tabulated EOS developed using Equation 15. Only the results from models run using the constant E_m Tabulated EOS are presented in the body of this report. Results from both the constant and variable E_m approaches were shown to be in close agreement with one another, and are presented in Appendix B.

3.4.3 Tabulated EOS for Interphase Transition

A third pseudo-phase of the Tabulated EOS material model corresponded to the densities that were higher than the saturated vapor density but lower than the saturated liquid density. This "transition" phase is not a physical state of matter. Rather, it is a consequence of the Tabulated EOS model using a regularized ε_{vol} that is a function of the current density. If the incremental change in density used to define $\Delta\varepsilon_{vol}$ was based on the change in density between saturated vapor and saturated liquid, the large increment would result in very few tabular entries to describe the GN2 and LN2 phases away from the saturation pressure. If a very small $\Delta\varepsilon_{vol}$ is used to capture the GN2 and LN2 behaviors away from saturation conditions, ε_{vol} values corresponding to densities between saturated vapor and saturated liquid will be included in the Tabulated EOS. While they are nonphysical, these transition densities still must have f_1 and f_2 functions assigned to them, consistent with the Abaqus Tabulated EOS conventions. An element that is calculated to have a density above that of saturated vapor and below that of saturated liquid may be thought of as containing a mixture of both GN2 and LN2, such that the *average* density within that element is between the saturation densities of the two true states of matter.

For simplicity, the transition phase was assumed to follow the same form as the liquid phase. That is, f_2 was assumed to be zero in the transition phase. As previously shown in Equation 12, this resulted in the pressure being equal to the f_1 function at a given ε_{vol}. The assumption that the transition phase's pressure versus density relationship is independent of the specific energy may warrant further investigation in a future study.

3.5 Development of Tabulated EOS Material Models for N2

This section describes the process used to develop the Tabulated EOS material models that were incorporated into the Test 12 post-test FE model. A different Tabulated EOS material input card was developed at 88 K, 90 K, 92 K, 94 K, 96 K, 98 K, and 100 K. The overall process of developing each material model was the same. A Visual Basic for Applications (VBA) macro was developed in Microsoft Excel to automate the process of generating the Tabulated EOS material models for N2 at each temperature.

For a given Tabulated EOS model, the user must define the isothermal temperature, ρ_0 (42.3 psia for Test 12), ρ_0 (obtained from NIST [10]), E_{m0} (obtained from NIST [10]), and $\Delta\varepsilon_{vol}$ (0.0001 for the Tabulated N2 EOS) to be used for the material model. The influence of the chosen $\Delta\varepsilon_{vol}$ on the resulting Tabulated EOS and simulation of Test 12 is discussed in Appendix B. The user must also decide on the range of densities and pressures over which the EOS must be defined, as this will affect the maximum and minimum values of ε_{vol}.

The liquid phase Tabulated EOS is straightforward to develop, as f_2 is assumed to be zero and f_1 then equals the pressure at a given density. The value of ε_{vol} corresponding to the saturated density of LN2 is calculated according to Equation 16. For any value of ε_{vol} smaller (i.e., more negative) than $\varepsilon_{vol}^{satLN2}$ the liquid form of the Tabulated EOS (Equation 12) should be used to calculate f_1.

Equation 16. Calculation of ε_{vol} for Saturated LN2

$$\varepsilon_{vol}^{satLN2} = \ln\left(\frac{\rho_0}{\rho^{satLN2}}\right)$$

The pressure versus density relationship for the vapor phase at a given temperature could be obtained either from the ideal gas equation or from literature. Data from literature for GN2 at temperatures from 88 K to 100 K were obtained from NIST [10], since at these temperatures GN2 was not assumed to be an ideal gas. Values for f_1 and f_2 were first calculated for the initial conditions of the vapor. Recall that the initial state corresponds to an ε_{vol} of zero, and that $f_1(0)$ must also be zero. The Tabulated EOS shown in Equation 10 becomes Equation 17 for the initial gas state.

Equation 17. Tabulated EOS for Initial Gas State

$$p_0 = 0 + \rho_0 \cdot f_2(0) \cdot E_{m0}$$

The initial pressure (p_0), initial density (ρ_0), and initial specific energy (E_{m0}) of the gas are all user-defined properties that must be self-consistent with one another. The value of $f_2(0)$ can then be found according to Equation 18.

Equation 18. Function f_2 for Initial Gas State

$$f_2(0) = \frac{p_0}{\rho_0 \cdot E_{m0}}$$

For a given isotherm, an increase in GN2 pressure also increases the density above its initial value (see Figure 6). For gas densities above the initial density, ε_{vol} will be negative, and for gas densities below the initial density, ε_{vol} will be positive. For the gas phase portion of the Tabulated EOS to be capable of modeling either an increase or a decrease in gas pressure, the range of densities used to develop the EOS must include values both above and below the initial density. This means that ε_{vol} will range from a negative value to a positive value, passing through zero (i.e., the initial state) along the way.

Whether the value of ε_{vol} was positive or negative, the same approaches to defining f_1 and f_2 were used in this project. The value of ε_{vol} corresponding to the saturated density of GN2 was calculated according to Equation 19. For any value of ε_{vol} that is greater than $\varepsilon_{vol}^{satGN2}$ the N2 will be in the vapor state and the calculations below should be used to determine f_1 and f_2.

Equation 19. Calculation of ε_{vol} for Saturated GN2

$$\varepsilon_{vol}^{satGN2} = \ln\left(\frac{\rho_0}{\rho^{satGN2}}\right)$$

For any nonzero value of ε_{vol} in the vapor state, both f_1 and f_2 are unknown. While f_1 must be monotonically increasing with increasing values of ε_{vol}, f_2 is not bound by the same constraint. The value of f_2 at ε_{vol} = 0 was determined by Equation 18. Additionally, f_2 is assumed to be zero in the transition pseudo-phase. The transition pseudo-phase begins at the first tabular entry for ε_{vol} that is smaller (i.e., more negative) than $\varepsilon_{vol}^{satGN2}$. As a means of avoiding an abrupt change in f_2 between vapor and transition, researchers decided to linearly ramp f_2 down to zero between the initial state and the transition state. Similarly, the value of f_2 was linearly ramped upward at the same slope for values of ε_{vol} that were greater than the initial value of ε_{vol}. Since f_2 is not subject to the same constraints as f_1, there may be additional approaches to varying f_2 that also produce satisfactory Tabulated EOS results.

Rearranging Equation 10 to solve for f_1 at a given value of ε_{vol} in the vapor phase produces Equation 20. Beginning at ε_{vol}=0 and incrementing by $\Delta\varepsilon_{vol}$, the corresponding density of GN2 is found using Equation 11. The corresponding pressure of GN2 having this density was obtained through literature [10] and substituted into Equation 20. The initial density of GN2 is determined by the initial pressure and temperature and can also be obtained from literature. The value of f_2 was interpolated as previously described. Finally, E_m at the current ε_{vol}, pressure, and density was found by Equation 15. This leaves f_1 at the current ε_{vol} as the only unknown in Equation 20.

Equation 20. Calculation of f_1 for Vapor Phase

$$f_1(\varepsilon_{vol}) = p - (\rho_0 \cdot f_2(\varepsilon_{vol}) \cdot E_m)$$

Finally, for values of ε_{vol} between $\varepsilon_{vol}^{satGN2}$ and $\varepsilon_{vol}^{satLN2}$ the N2 is in the transition pseudo-phase. As discussed previously, for simplicity the pressure of N2 in the transition pseudo-phase was assumed to depend only on f_1. The vapor and liquid states exist simultaneously at the saturation pressure. Because the Tabulated EOS uses a regularly spaced discretization for ε_{vol}, the EOS will always feature some pressure difference between the tabular entries for the maximum vapor density and the minimum liquid density. As the number of tabular entries increases, the magnitude of this pressure difference decreases but increases the number of tabular points that must be defined in the transition phase. A linear interpolation for the density-pressure

relationship between the tabular entry for the maximum vapor density and the minimum liquid density was used to define the values of f_1 in the transition pseudo-phase.

Table 6 contains a summary of the five different ranges of values for ε_{vol} that could occur. A positive value for ε_{vol} only occurs if the current state is a vapor having a smaller density than the initial density. This condition would only occur if the vapor were at a pressure below the initial pressure. An ε_{vol} of zero corresponds to the initial vapor state. For all subsequent states, the value of ε_{vol} will be negative. If the value of ε_{vol} is negative but greater than $\varepsilon_{vol}^{satGN2}$, the N2 is still a vapor but at a pressure above the initial pressure. If the value of ε_{vol} is between $\varepsilon_{vol}^{satGN2}$ and $\varepsilon_{vol}^{satLN2}$ the N2 is in the transition pseudo-phase between a vapor and a liquid. Finally, when ε_{vol} is smaller (i.e., a more negative number) than $\varepsilon_{vol}^{satLN2}$ the N2 is in the liquid state.

Table 6. Summary of ε_{vol} and Current States for Five Regions of Tabulated EOS

ε_{vol}	ε_{vol} Sign	Relative Density	Description of Current State
$\varepsilon_{vol} > 0$	+	$\rho < \rho_0$	Vapor at a pressure below ρ_0
0	N/A	$\rho = \rho_0$	Initial vapor state
$\varepsilon_{vol}^{satGN2} \leq \varepsilon_{vol} < 0$	-	$\rho_0 < \rho \leq \rho^{satGN2}$	Vapor at a pressure above p_0, at or below ρ^{sat}.
$\varepsilon_{vol}^{satLN2} < \varepsilon_{vol} < \varepsilon_{vol}^{satGN2}$	-	$\rho^{satGN2} < \rho < \rho^{satLN2}$	Transition pseudo-phase between saturated vapor and saturated liquid.
$\varepsilon_{vol} \leq \varepsilon_{vol}^{satLN2}$	-	$\rho \geq \rho^{satLN2}$	Liquid at pressure above at or above ρ^{sat}.

The resulting family of Tabulated EOS for the temperatures between 88 K and 100 K (in 2 K increments) resulted in several thousand tabular entries per EOS. The density versus pressure relationships that were manually (i.e., outside of Abaqus) calculated for the Tabulated EOS (assuming a constant value for E_m) are plotted in Figure 7 alongside the reference density-pressure relationships used to develop the Tabulated EOS.

The density versus pressure relationships that were manually calculated for the Tabulated EOS (assuming a variable value for E_m) are plotted in Figure 8 alongside the reference density-pressure relationships used to develop the Tabulated EOS. The density-pressure relationships for a given isotherm are similar whether the value for E_m is assumed to be constant or variable. However, as discussed in Appendix A.3, the tabulated values used to obtain these relationships are different. Additionally, the Tabulated EOS developed using a variable E_m is limited to a smaller range of pressures due to assumptions made in how function f_2 varied.

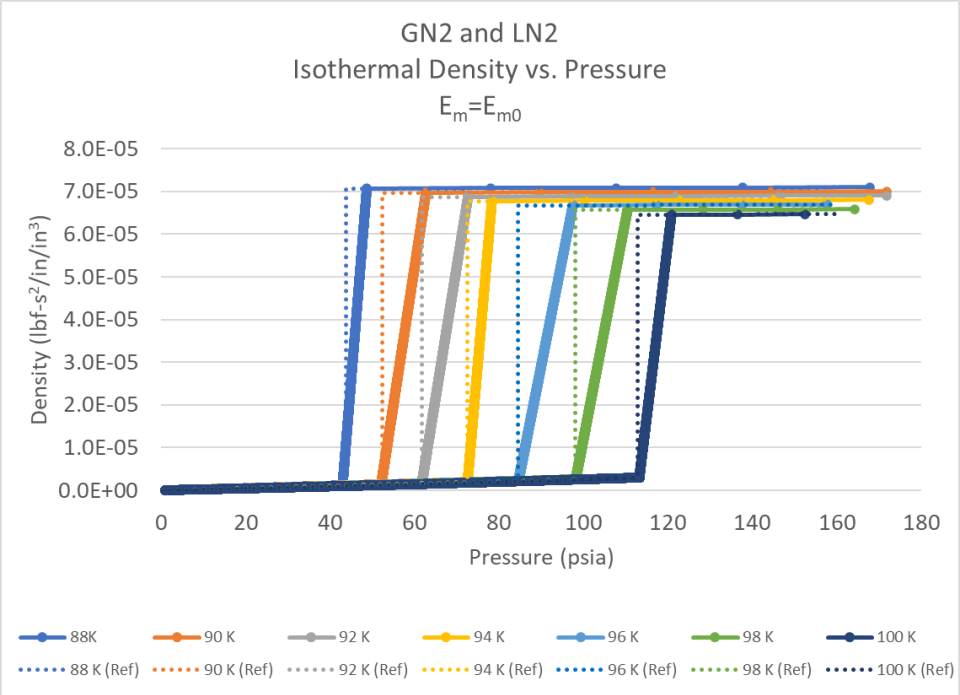

Figure 7. Density-Pressure Relationships Calculated Using EOS Models with Constant E_m (Solid Lines with Markers) and Using NIST Data [10] (Dashed Lines)

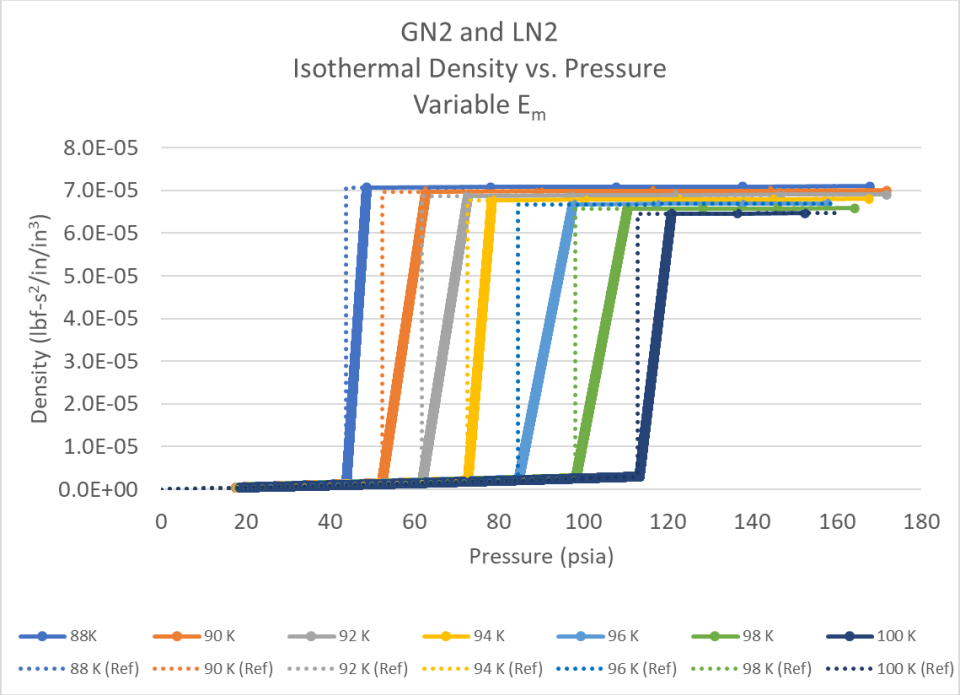

Figure 8. Density-Pressure Relationships Calculated Using EOS Models with Variable E_m (Solid Lines with Markers) and Using NIST Data [10] (Dashed Lines)

4. Development of a Fluid Exchange for N2 Condensation

In pre- and post-test side impact models of the DOT-113 surrogate filled with LN2 (Test 12) [3], the team used a pneumatic cavity in Abaqus/Explicit to represent the pressure-volume relationship of the GN2 in the outage. In the pre-test models, researchers limited the pneumatic cavity to have either 1) no phase change and a pressure-density relationship according to the ideal gas relationship with a constant temperature (i.e., isothermal) or 2) only phase change and no pressure rise (i.e., isobaric). This approach was taken to bound the possible test outcomes given numerous uncertainties in the temperature and pressure of the lading before filling. The two bounding cases from the pre-test model succeeded in bounding the test outcome (see Figure 1).

After Test 12, the team added a fluid exchange to the pneumatic cavity in Abaqus to allow pressure rise to a certain point (i.e., the saturation pressure) and then mass from the pneumatic cavity was allowed to exit to atmosphere as a surrogate for a vapor-to-liquid phase change. While the mass from the vapor should flow into the liquid, the team determined that the mass of vapor condensing to liquid was insignificant compared to the total mass of liquid inside the tank. Based on review of the test results, researchers calibrated a fluid exchange starting at 70 psia which gave good agreement with the test results (see Figure 2). The volumetric flow rate versus pressure definition used in the post-test model is shown in Figure 9.

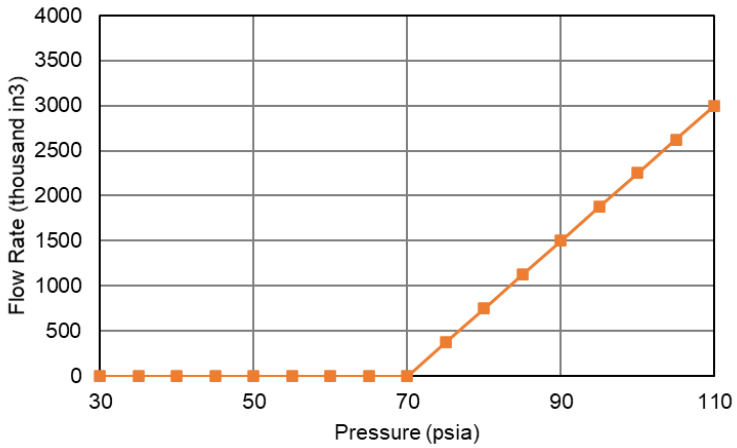

Figure 9. Fluid Exchange Property from Post-test 12 Model of DOT-113 Surrogate Filled with LN2

The team calibrated the fluid exchange definition to match the behavior observed in the test and demonstrate that pressure rise followed by condensation could explain the force-displacement and pressure-time results observed after the test. Note that this approach does not conserve mass in the outage as the process is non-reversible (i.e., fluid does not flow back into the cavity after the pressure drops). However, it was determined that this was acceptable for simulating an impact test as puncture of the tank car was not likely to occur after the compressed volume of the inner tank began to recover.

After developing a non-puncture model with a Lagrangian Tabulated EOS representation of the outage (Section 3), the team updated the fluid exchange definition based on the results of the Lagrangian Tabulated EOS model. There were several advantages to using a simple pneumatic cavity versus a Lagrangian Tabulated EOS model, including faster model runtime and better

model stability. To calibrate fluid exchange definitions for the pneumatic cavity from the Lagrangian Tabulated EOS results, the team post-processed density, volume, and pressure from each element in the outage of the Tabulated EOS model at 88 K, 90 K, 92 K, 94 K, 96 K, 98 K, and 100 K. Researchers used element density and volume to compute the total mass of GN2 versus LN2 in the outage at each time point, as shown in Appendix B9.

The team then computed the mass rate of change of GN2 to LN2, then converted the mass rate of change to volumetric flow rate for the fluid exchange definition by dividing the mass flow rate by the saturation density of GN2 at the model temperature. Finally, the team plotted the volumetric flow rate against the average element pressure in the outage and fit a simple piecewise bi- or tri-linear curve through the results. Figure 10 shows an exemplar fit of a piecewise linear curve over the Tabulated EOS model result at 94 K.

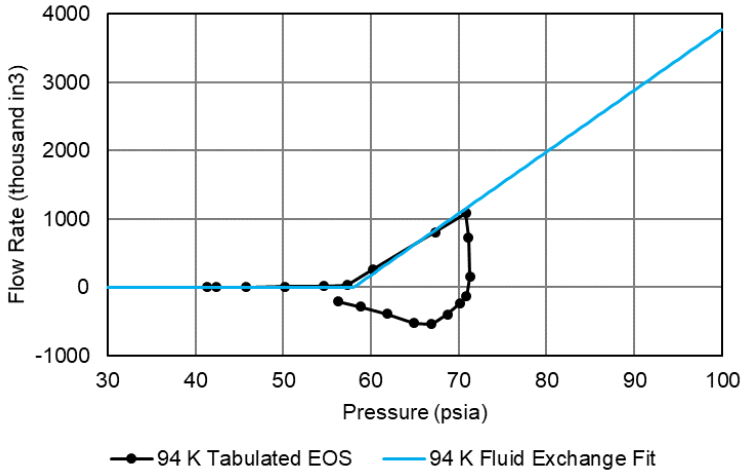

Figure 10. Fluid Exchange Piecewise Linear Fit over Tabulated EOS Results at 94 K

Figure 11 shows the resulting piecewise linear fluid exchange definitions for each temperature obtained using the same procedure. The team used the volumetric flow rate versus pressure behaviors shown in Figure 11 to simulate GN2 to LN2 condensation at various GN2 temperatures in the FE model results reported in Section 5.2.

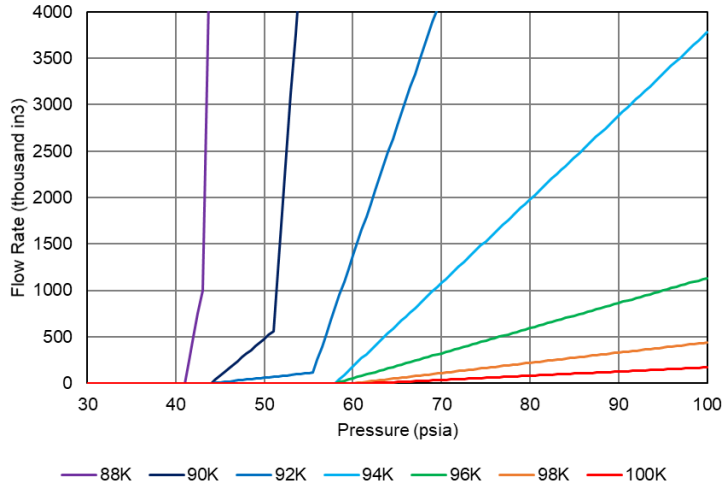

Figure 11. Volumetric Flow Rate Versus Pressure for Various Temperatures, Pneumatic Cavity with Fluid Exchange Model

5. Phase Change Model Results

A series of FE models were run using the Test 12 impact conditions. The models used the same tank geometry, steel material properties, initial pressures, and initial filling volumes. One model used a Lagrangian mesh for the LN2 and GN2 with the constant and variable E_m Tabulated EOS material models applied to the GN2. The other model used a pneumatic cavity for the GN2 with a prescribed pressure-leakage rate (i.e., fluid exchange) relationship simulating phase change. As the initial temperature of the GN2 was not known for Test 12, each model was run over the same range of temperatures, as discussed in Section 3.

5.1 Tabulated EOS Model Results

This section presents FEA results from the Tabulated EOS model with constant E_m. The complete set of Tabulated EOS model results, including variable E_m, are provided in Appendix B. The impactor force versus time responses at each temperature modeled using the Tabulated EOS material models are shown in Figure 12 for constant E_m and in Figure B1 for variable E_m. These figures also show the average force-time response measured in Test 12. In general, the shapes of the force-time responses are all like one another. As the assumed initial GN2 temperature increases, the peak force estimated by the model also increases.

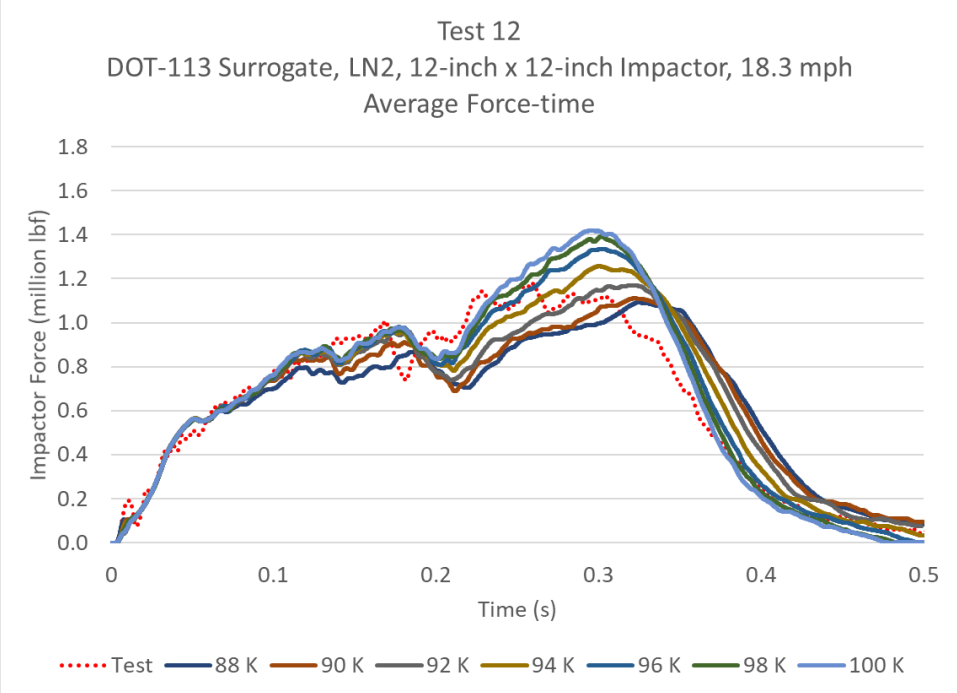

Figure 12. Impactor Force Versus Time for EOS Material Models at Various Temperatures (Constant E_m)

In Test 12, pressure measurements were made via pressure transducers installed in several pipes external to the tank. As discussed in the Test 12 report [3], this approach led to some challenges in interpreting the pressure results after the test. Each transducer measured a unique pressure-time history, apparently affected by its location within a pipe and that pipe's point of communication with the inner tank. Therefore, it was difficult to generalize the average pressure-

time history of the bulk GN2 since each transducer measured unique local behavior. The transducer names and descriptions of their locations are shown in Table 7.

Table 7. Summary of Pressure Transducers in Test 12 (from [2])

Location	Channel Name
Manway	P-MH1
Manway	P-MH2
Line to PRV	P-PRV
Top Fill Line	P-V5
Low Pressure Isolation Valve	P-V14
High Pressure Isolation Valve	P-V15

The pressure-time histories of the FE models using the different Tabulated EOS material models were obtained in two different ways. In one approach, the total contact force and contact area on the top surface of the LN2 was requested as history output data. The average contact pressure on the top surface of the liquid was calculated by dividing the force by the area. Figure 13 contains a plot of the pressure-time history of each pressure transducer in Test 12 alongside the average pressure-time history obtained from the free surface approach for constant E_m. Figure B2 contains the same plot for variable E_m.

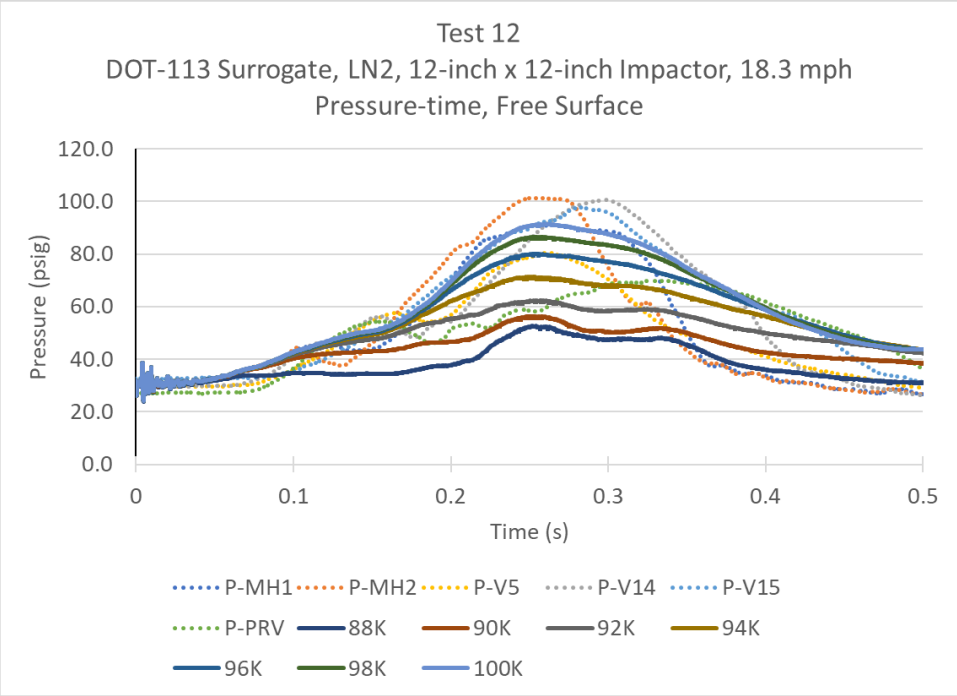

Figure 13. Pressure-time Histories Averaged over Surface of LN2 in Communication with GN2 for EOS Material Models at Various Temperatures (Constant E_m)

In the second approach, the pressure in each GN2 element's integration point was extracted at each frame of field output. The average pressure across the total volume of GN2 was calculated. Figure 13 contains a plot of the pressure-time history of each pressure transducer in Test 12 alongside the average pressure-time history obtained from the bulk average approach. Figure B3 contains the same plot for variable E_m.

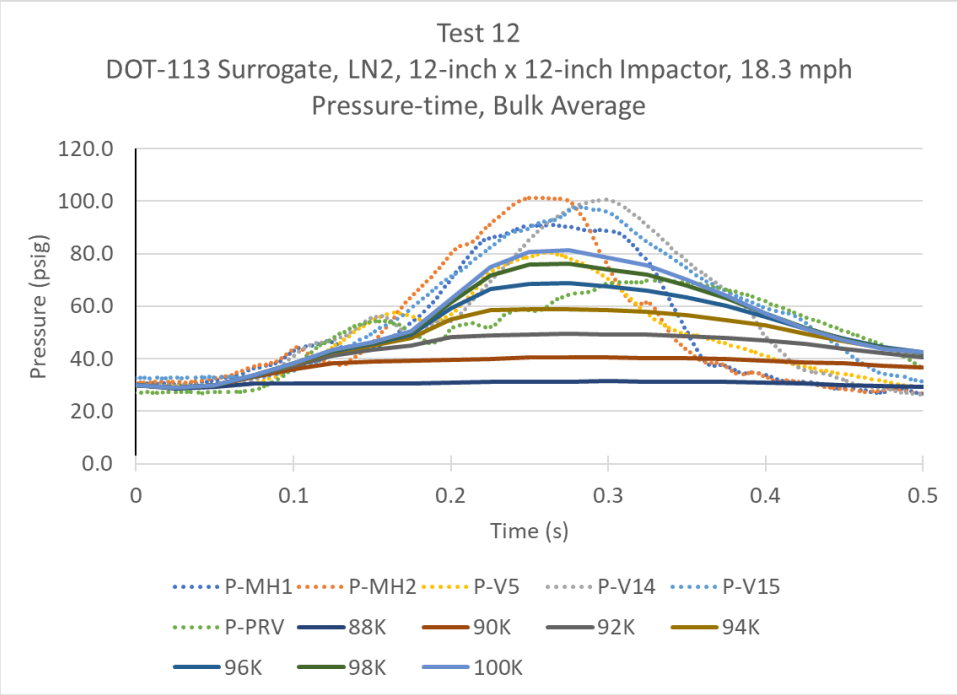

Figure 14. Bulk Pressure-time Histories Averaged over Entire Outage, for EOS Material Models at Various Temperatures, Constant E_m

Regardless of the approach used to average the outage pressure in the FE models, the general trend remained the same. As the assumed initial temperature of the GN2 increased the peak pressure within the outage also increased.

The FE model of the Test 12 surrogate that used the Tabulated EOS material model also featured a non-functional pneumatic cavity defined over the entire interior surface of the inner tank. This cavity was made nonfunctional by prescribing zero initial pressure at its reference point. The cavity was used as a convenient method of tracking the volume of the tank during the impact, without contributing to the model's structural response. The resulting tank volume versus time histories from the model run using each Tabulated EOS material model are shown in Figure 15[9] for constant E_m. Figure B4 shows the same plot for variable E_m. The dashed line represents the inner tank's nominal 17,900 gallon initial volume. The initial volume of the cavity was slightly greater, likely due to the discretization error associated with the tank's mesh.

The overall shapes of the volume-time responses were similar regardless of the assumed initial temperature of GN2 modeled. The tank volume decreased as the impact occurred. The volume reached a minimum, then began to increase again. Comparing the results of Figure 15 with the force-time history in Figure 12, the minimum tank volume corresponded with the approximate time the peak force was reached. As the tank recovered its elastic energy and the compressed GN2 expanded (Figure 13 and Figure 14) its volume increases until reaching a steady value between the initial value and the minimum value.

[9]The FE models described in this section were initially run for 0.5 seconds of impact time. Since the tank volume had not reached a steady state by this time, the models were re-run for 1.0 second. Except for Figure 15 the results in this section were obtained from the models run to 0.5 seconds.

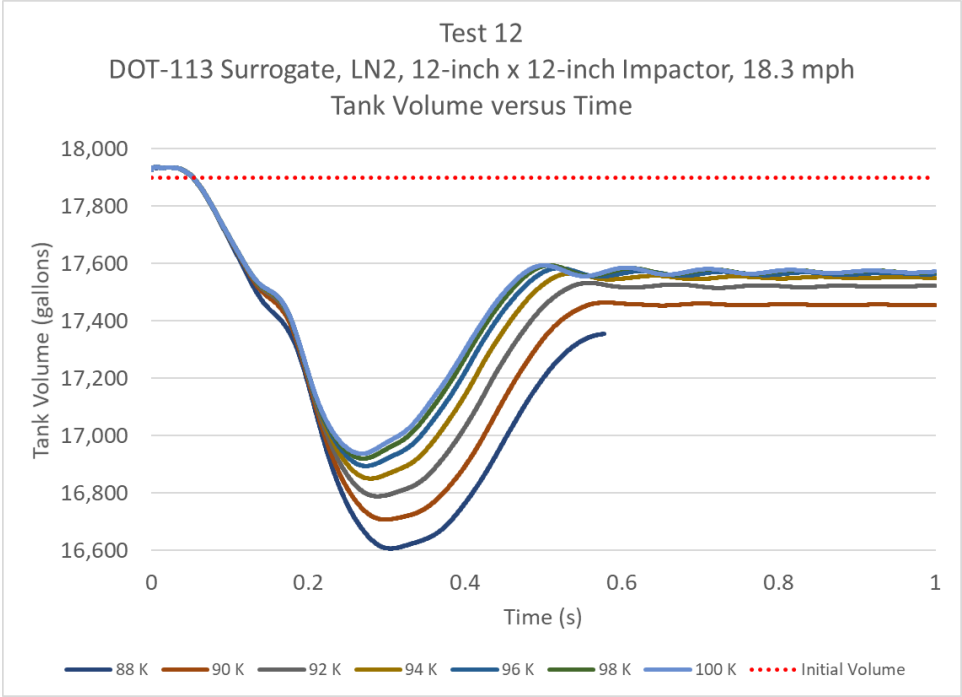

Figure 15. Inner Tank Volume-time Histories for EOS Material Models at Various Temperatures, Constant E_m

Table B1 contains a summary of the reduction in tank volume for each assumed GN2 temperature simulated using the Tabulated EOS material models. The final tank volume is the last data point in each simulation. For each temperature except 88 K, the simulation was run until 1 second. The 88 K model terminated at approximately 0.58 seconds, the time at which the final tank volume measurement was recorded. The reduction in volume is expressed both as a volume difference in gallons and a percent difference. For each calculation of reduction in volume, the initial tank volume calculated in the FE model was used, rather than the nominal 17,900 gallons. Over the range of temperatures simulated, the inner tank experienced a reduction in volume of between 2.0 and 3.2 percent.

Figure 16 contains a plot of the impactor force versus impactor travel for each of the assumed temperatures simulated using a constant E_m Tabulated EOS material model, alongside the average Test 12 data. Figure B5 contains the same plot for variable E_m. As the assumed temperature of the GN2 was lowered, the maximum indentation of the tank increased. As discussed previously, the maximum impact force also decreased as the assumed initial temperature was decreased.

The FE model at each assumed initial temperature was post-processed to examine the amount of GN2 that underwent phase change during the simulation. Pressure, density, and volume field output results were extracted from each element in the outage at each frame of the simulation. It was not practical to request history output at a higher frequency for each element in the outage due to the large number of elements in the outage mesh.

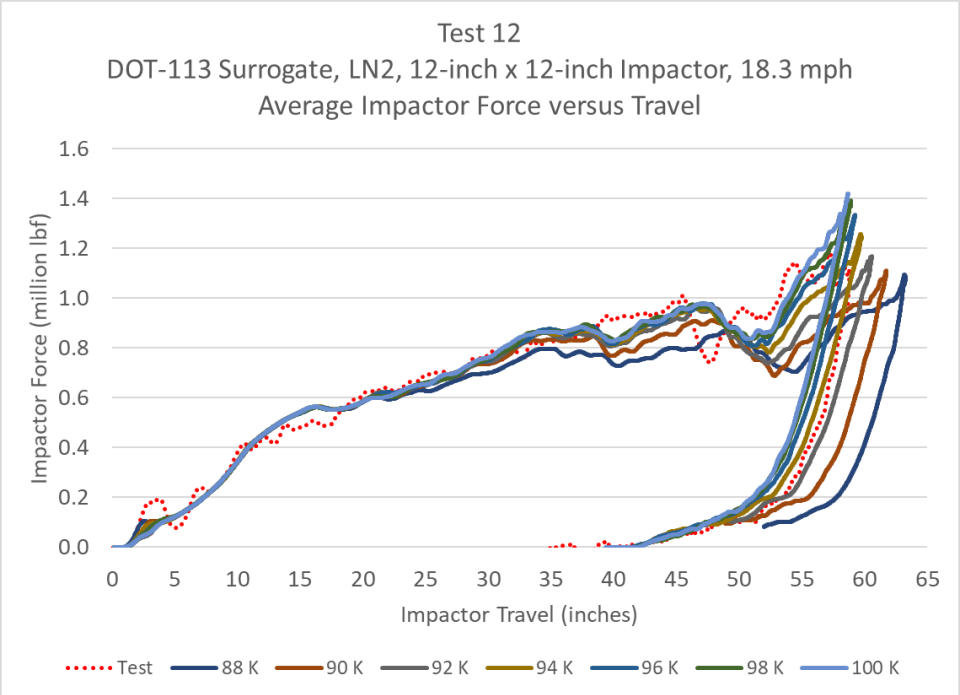

Figure 16. Impactor Force Versus Impactor Travel for Tabulated EOS Material Models at Various Temperatures, Constant E_m

For each simulation, each outage element could be categorized into one of three pseudo-phases based on its density (see Table 8). If an element's density was at or below the saturation density of vapor at the assumed temperature, the element was filled with GN2. If the element's density was at or above the saturation density of liquid, the element was filled with LN2. If the element's density was above the saturated vapor density but below the saturated liquid density, additional postprocessing was needed to determine the volume of LN2 and GN2 within such an element.

Table 8. Categories of Density and Outage Element Material Phases for Post-processing EOS Material Models

Outage Element Density	Outage Element Material Phase
$\rho \leq \rho_{sat}^{vap}$	GN2
$\rho_{sat}^{vap} < \rho < \rho_{sat}^{liq}$	GN2 and LN2 (*Transition)*
$\rho \geq \rho_{sat}^{liq}$	LN2

In a physical material, the *transition* pseudo-phase does not exist. The N2 is either LN2 or GN2, with a corresponding density. However, due to the modeling simplifications and the need for the Tabulated EOS to have a continuous series of volumetric strains (discussed further in Appendix A.3), it was possible for elements in the FE model to develop a density that fell between the maximum density of a vapor and the minimum density of a liquid at the chosen temperature. These elements were identified as being in the *transition* pseudo-phase. A physical explanation for this density would be to assume that the volume of N2 within a *transition* element was a

mixture of both GN2 and LN2. This could occur in a physical system if the density of some volume were averaged over a region of the N2 that included both vapor and liquid. Because the outage was modeled using a coarse Lagrangian mesh, it was logical that some elements would exist where the initial GN2 had begun to condense to LN2 but had not yet completed the phase change. Elements in the *transition* pseudo-phase were post-processed according to the process described in Appendix B.9 to determine the amount of N2 in the GN2 and LN2 states within those elements.

Plots showing the mass percentage of LN2 and GN2 within the outage at each temperature for the Tabulated EOS are shown in Figure 17 using the constant E_m assumption and in Figure B6 using the variable E_m assumption. For either assumption the trends are the same, with lower initial temperatures exhibiting a larger mass percentage of LN2 condensation than higher initial temperatures. In these figures, solid lines denote the mass percentage of liquid in the outage and dashed lines denote the mass percentage of vapor in the outage. Initially, the outage is entirely composed of vapor. For a given assumed initial temperature, the mass percentage of liquid and vapor at each time equals one hundred percent, as no material was allowed to leave the tank in the simulations run using the Tabulated EOS material models.

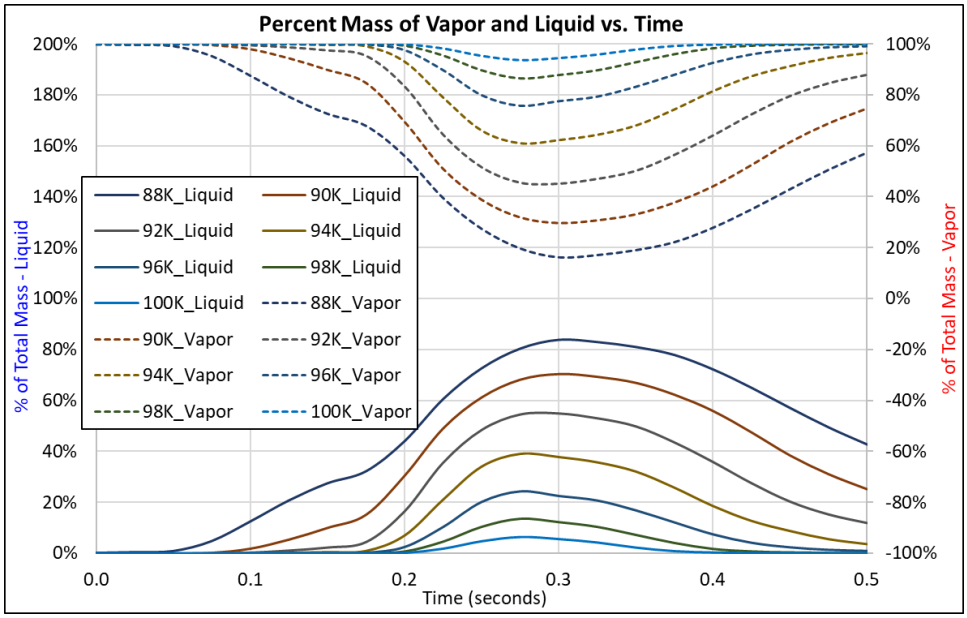

Figure 17. Percentage by Mass of Vapor and Liquid in Outage Versus Time, Tabulated EOS Material Models at Various Temperatures, Constant E_m

Table 9 contains a summary of the maximum amount of LN2 to condense and minimum amount of GN2 by mass percent at each temperature using the constant E_m assumption. Table B3 contains the same data from the models run using the variable E_m assumption.

Table 10 contains a summary of several peak test measurements and the corresponding values from simulations of EOS material models run at different assumed initial temperatures using the constant E_m assumption. Table B4 contains similar results for the models developed using the variable E_m assumption. All these results are obtained from the force-displacement responses of Test 12 and the FE models, as the force-displacement response is a good indicator of the global level of agreement between the impact test and companion FE model.

Table 9. Peak GN2 and LN2 Amounts in Outage, Constant E_m

Temperature (K)	Maximum Amount of LN2 (% of Outage Mass)	Minimum Amount of GN2 (% of Outage Mass)
88	83.8%	16.2%
90	70.3%	29.7%
92	55.0%	45.0%
94	39.1%	60.9%
96	24.2%	75.8%
98	13.4%	86.6%
100	6.5%	93.5%

Table 10. Selected Results from Test Measurements and FE Results, EOS Material Models at Various Temperatures, Constant E_m

		Test	88 K	90 K	92 K	94 K	96 K	98 K	100 K
First Peak Force	kips	1,008.4	883.6	910.2	959.6	958.6	979.7	1,011.5	1,010.4
Displacement at First Peak Force	in	45.5	49.6	47.8	46.5	47.5	47.1	54.3	54.0
Global Peak Force	kips	1,179.5	1,094.2	1,110.1	1,168.4	1,256.2	1,334.7	1,392.0	1,418.6
Displacement at Global Peak Force	in	57.2	63.2	61.7	60.6	59.7	59.2	58.9	58.7
Maximum Displacement	in	58.8	63.3	61.7	60.6	59.8	59.2	58.9	58.7

Table 11 contains the percent difference between the results shown in Table 10 from the FE simulations run at different temperatures using a constant E_m assumption and the corresponding test measurement. Table B5 contains the same percent difference comparison but for the data shown in Table B4 using a variable E_m assumption. The *average absolute error* shown in this table is the average of the absolute values of the percent differences of the individual measurements. This *average absolute error* is meant as a single measure of the overall quality of the agreement between the test measurements and the FE results at the examined temperatures. Based on this *average absolute error*, the highest overall level of agreement was obtained using an outage temperature of 92 K. The results are similar whether the constant E_m or variable E_m (see Appendix B.1) assumption was used to develop the Tabulated EOS.

Table 11. Percent Difference Between Selected Results from Test Measurements and FE Results, EOS Material Models at Various Temperatures, Constant E_m

	88 K	90 K	92 K	94 K	96 K	98 K	100 K
First Peak Force	-12.4%	-9.7%	-4.8%	-4.9%	-2.8%	0.3%	0.2%
Displacement at First Peak Force	9.0%	5.1%	2.1%	4.3%	3.5%	19.2%	18.6%
Global Peak Force	-7.2%	-5.9%	-0.9%	6.5%	13.2%	18.0%	20.3%
Displacement at Global Peak Force	10.4%	7.9%	5.9%	4.3%	3.5%	2.9%	2.6%
Maximum Displacement	7.6%	5.0%	3.1%	1.7%	0.7%	0.2%	-0.2%
Average Absolute Error	**9.3%**	**6.7%**	**3.4%**	**4.3%**	**4.8%**	**8.1%**	**8.4%**

5.2 Fluid Exchange Model Results

The impactor force versus impactor travel responses for the Fluid Exchange model at each temperature are shown in Figure 18. This figure also shows the average force-travel response measured in Test 12. In general, the force-travel responses are all alike. As the assumed initial GN2 temperature increased, the peak force estimated by the model also increased while the amount of indentation decreased.

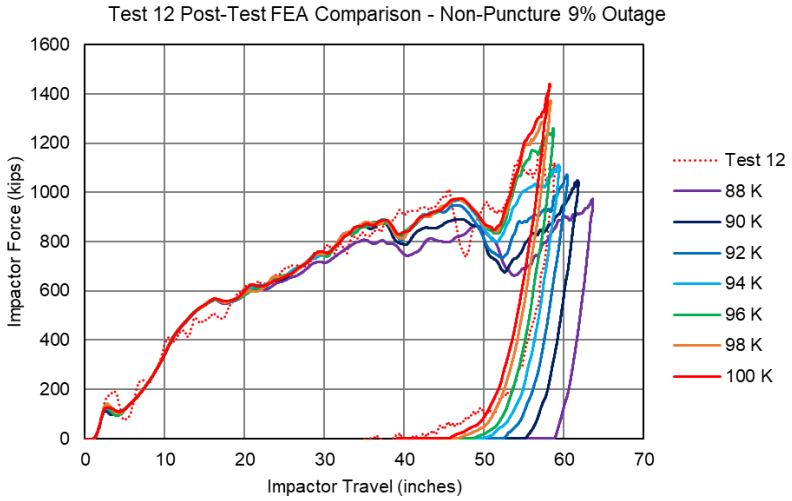

Figure 18. Impactor Force Versus Impactor Travel for Fluid Exchange Models at Various Temperatures

Figure 19 contains a plot of the average pressure-time history in Test 12 alongside the average pressure-time history from each Fluid Exchange model. The pneumatic cavity modeling technique results in a single average pressure over the entire volume of the cavity at each time increment. As the assumed initial temperature of the GN2 increased the peak pressure within the outage also increased. The final pressure also tended to be lower with lower initial temperatures, as more of the GN2 left the cavity and "condensed" into LN2 as the initial temperature was decreased.

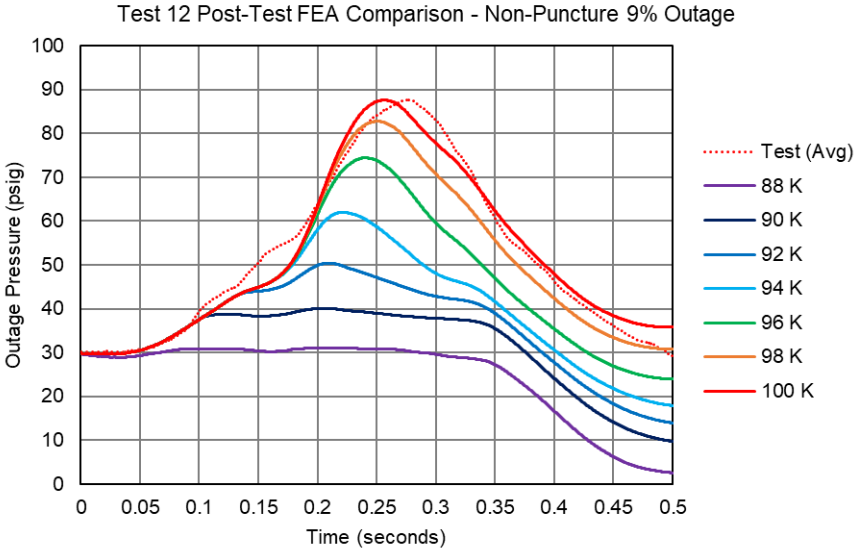

Figure 19. Pressure-time Histories for Fluid Exchange Models at Various Temperatures

The resulting tank volume versus time histories from the model run using each Fluid Exchange model are shown in Figure 20. The dashed line represents the nominal 17,900 gallon initial volume.

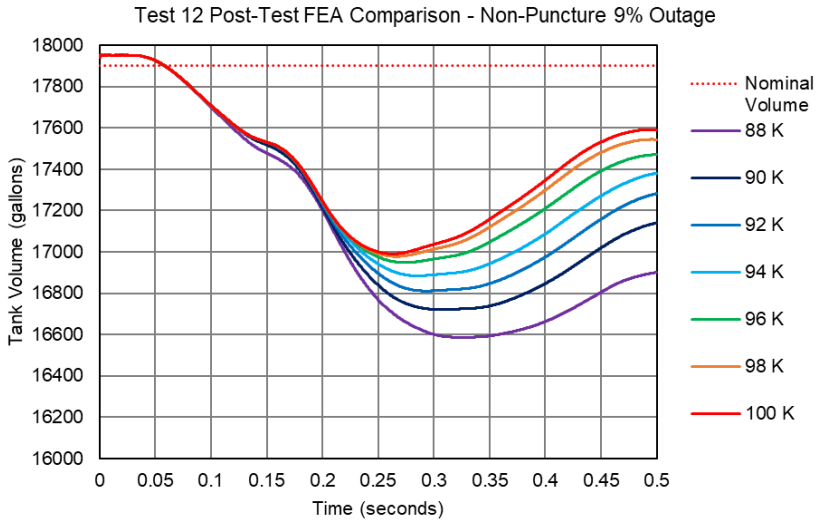

Figure 20. Inner Tank Volume-time Histories for Fluid Exchange Models at Various Temperatures

Regardless of the assumed initial temperature of GN2 modeled, the overall shapes of the volume-time responses were similar. The tank volume decreased as the impact occurred. The volume reached a minimum, then began to increase again. The minimum tank volume corresponded with the approximate time the peak force was reached. As the tank recovered its elastic energy and the compressed GN2 expanded, its volume increased until reaching a steady value between the initial and the minimum value.

Table 9 contains a summary of the amount of LN2 to be condensed by mass percent at each temperature. Results are reported at two different times. The first column of mass data was obtained at the time when the maximum pressure was reached in the cavity. The second column was the maximum amount of condensed LN2 that occurred during the simulation. Both sets of values were obtained by requesting the mass of GN2 in the pneumatic cavity (CMASS) as a function of time for each simulation. The mass of "condensed" LN2 was set equal to the difference between the initial mass of GN2 in the cavity and the mass at any subsequent point in time during the simulation. The percentage of LN2 is the value of this mass divided by the initial mass of GN2 in the cavity.

Table 12. Peak GN2 and LN2 Amounts in Outage, Fluid Exchange Models

Temperature (K)	Amount of Condensed LN2 at Peak Pressure (% of Initial GN2 Mass)	Maximum Amount of Condensed LN2 (% of Initial GN2 Mass)
88	51.2%	89.5%
90	39.3%	75.8%
92	27.7%	65.1%
94	21.3%	55.1%
96	17.1%	40.8%
98	10.0%	24.3%
100	4.7%	11.9%

The results in Table 12 demonstrate that the amount of LN2 to condense out of GN2 decreased as the initial temperature increased. Additionally, a substantial amount of LN2 was condensed from GN2 after the maximum pressure occurred in the simulation due to the fluid exchange being irreversible. In contrast, the Tabulated EOS model was reversible and the total mass of LN2 decreased as the pressure subsided from its peak value.

Table 13 contains a summary of several peak test measurements and the corresponding values from the Fluid Exchange models run at different assumed initial temperatures. All of these results are obtained from the force-displacement responses of Test 12 and the FE models, as the force-displacement response is a good indicator of the global level of agreement between the impact test and companion FE model.

Table 13. Selected Results from Test Measurements and FE Results, Fluid Exchange Models at Various Temperatures

		Test	88 K	90 K	92 K	94 K	96 K	98 K	100 K
First Peak Force	kips	1008.4	863.2	891.2	946.6	969.0	971.0	975.0	974.5
Displacement at First Peak Force	in	45.5	48.9	46.6	46.4	46.9	46.8	46.5	47.0
Global Peak Force	kips	1179.5	974.0	1049.2	1073.2	1112.7	1260.7	1372.4	1441.0
Displacement at Global Peak Force	in	57.2	63.6	61.7	60.3	59.4	58.7	58.4	58.2
Maximum Displacement	in	58.8	63.6	61.8	60.5	59.4	58.7	58.4	58.2

Table 14 contains the percent difference between the results shown in Table 13 from the FE simulations run at different temperatures and the corresponding test measurement. Based on the *average absolute error*, the highest overall level of agreement was obtained using an outage temperature of 96 K, with 94 K showing only slightly higher average absolute error.

Table 14. Percent Difference between Selected Results from Test Measurements and FE Results, Fluid Exchange Models at Various Temperatures

	88 K	90 K	92 K	94 K	96 K	98 K	100 K
First Peak Force	-14.4%	-11.6%	-6.1%	-3.9%	-3.7%	-3.3%	-3.4%
Displacement at First Peak Force	7.5%	2.3%	2.0%	3.1%	2.8%	2.2%	3.3%
Global Peak Force	-17.4%	-11.0%	-9.0%	-5.7%	6.9%	16.4%	22.2%
Displacement at Global Peak Force	11.1%	7.9%	5.5%	3.8%	2.5%	2.0%	1.8%
Maximum Displacement	8.2%	5.1%	2.8%	1.1%	-0.2%	-0.7%	-0.9%
Average Absolute Error	11.7%	7.6%	5.1%	3.5%	3.2%	4.9%	6.3%

5.3 Comparison of Model Results

A complete set of comparison plots between the Tabulated EOS models (both constant and variable E_m), Pneumatic Cavity with Fluid Exchange model, and Test 12 results is provided in Appendix C. This section includes comparisons of individual results for assumed initial temperatures of 92 K and 96 K. A temperature of 92 K showed the highest level of agreement between the Tabulated EOS models and Test 12 while a temperature of 96 K showed the highest level of agreement between the Fluid Exchange model and Test 12.

Figure 21 shows the force-time histories of the three FE models and Test 12 at 92 K on the left and 96 K on the right. At either temperature, the two models using the Tabulated EOS produced nearly identical results to one another. Additionally, the Fluid Exchange approach agreed with both Tabulated EOS results during the initial portion of the impact. After approximately 0.2 seconds at 92 K or 0.24 seconds at 96 K, the pneumatic cavity with fluid exchange model exhibited a softer response than the Tabulated EOS models. At either temperature, the pneumatic cavity with fluid exchange approach to modeling produced a lower global peak force than the Tabulated EOS models.

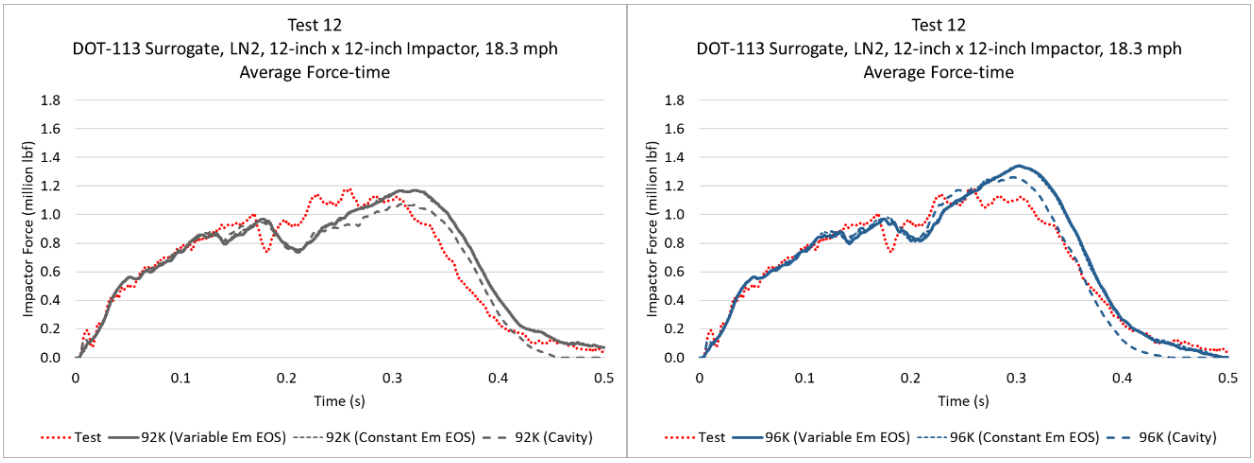

Figure 21. Comparison of Force Versus Time Results, 92 K (left) & 96 K (right)

Figure 22 contains similar plots of impactor force versus travel at 92 K on the left and 96 K on the right. At either temperature, the Tabulated EOS models produced a lower maximum impactor travel than the pneumatic cavity with fluid exchange approach to modeling.

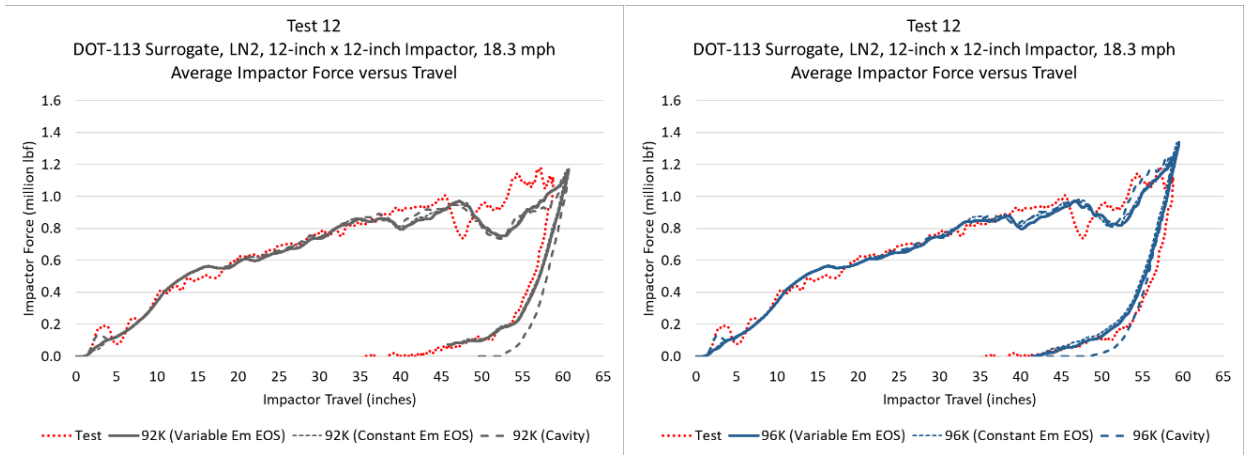

Figure 22. Comparison of Force Versus Impactor Travel Results, 92 K (left) & 96 K (right)

Figure 23 contains plots of average outage pressure versus time at 92 K on the left and 96 K on the right. The peak values of outage pressure is similar in all three models. The Fluid Exchange model produced a quicker drop in pressure following the peak compared to the Tabulated EOS models.

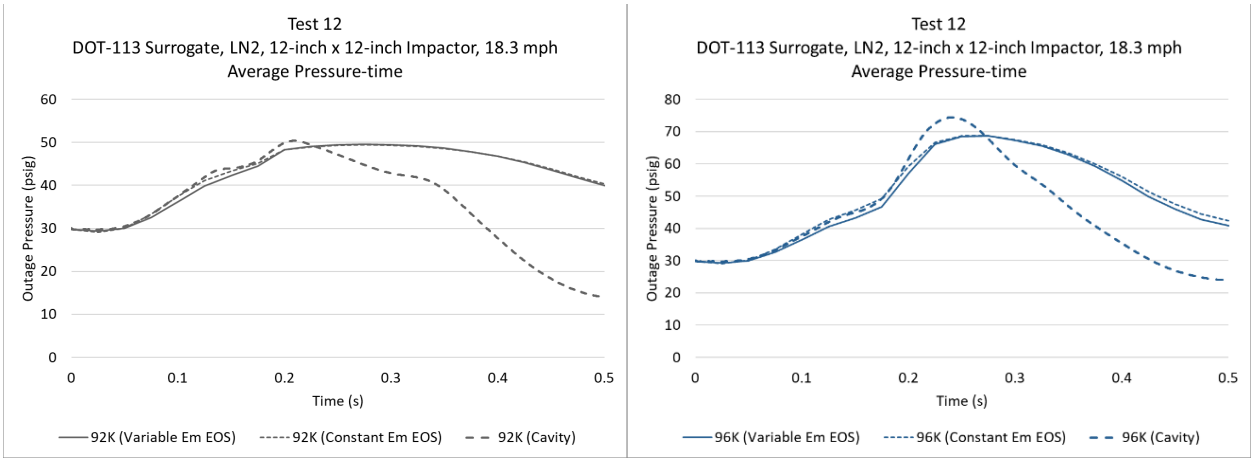

Figure 23. Comparison of Outage Pressure Versus Time Results, 92 K (left) & 96 K (right)

Figure 24 contains plots of tank volume versus time at 92 K on the left and 96 K on the right. The minimum value of outage volume is similar in all three models for a given temperature. The Fluid Exchange model produced a slower volume recovery compared to the Tabulated EOS models.

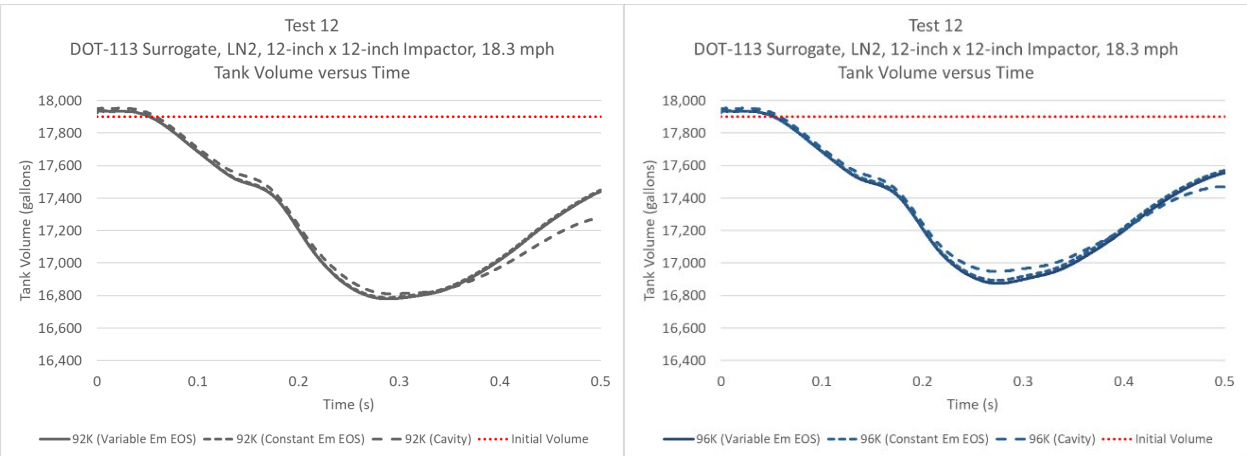

Figure 24. Comparison of Tank Volume Versus Time Results, 92 K (left) & 96 K (right)

Figure 25 contains a plot of the minimum volume of the inner tank during each impact simulation from all three models run at each temperature. All the models exhibited the same trend, where increasing temperatures exhibited a larger minimum volume. The three modeling techniques also showed reasonable agreement with one another at all temperatures.

Figure 26 contains a similar plot of the final tank volume following each simulated impact. The final volume at a given temperature was similar between the two EOS models, but the pneumatic cavity with fluid exchange model exhibited a lower final volume. The difference between final volumes between the Tabulated EOS models and the Fluid Exchange model was generally larger than the difference between the minimum volumes in the different models.

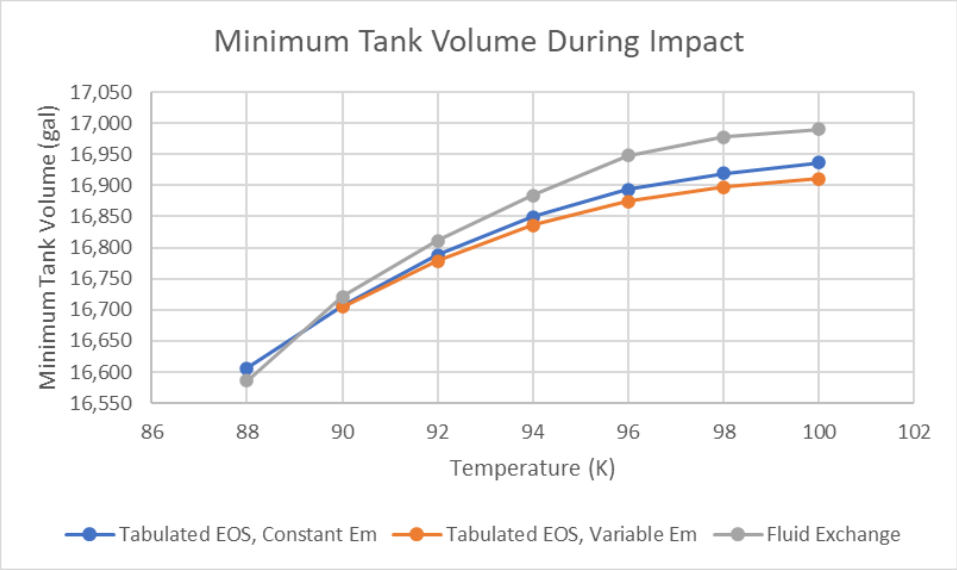

Figure 25. Minimum Tank Volume from Each FE Model at Various Temperatures

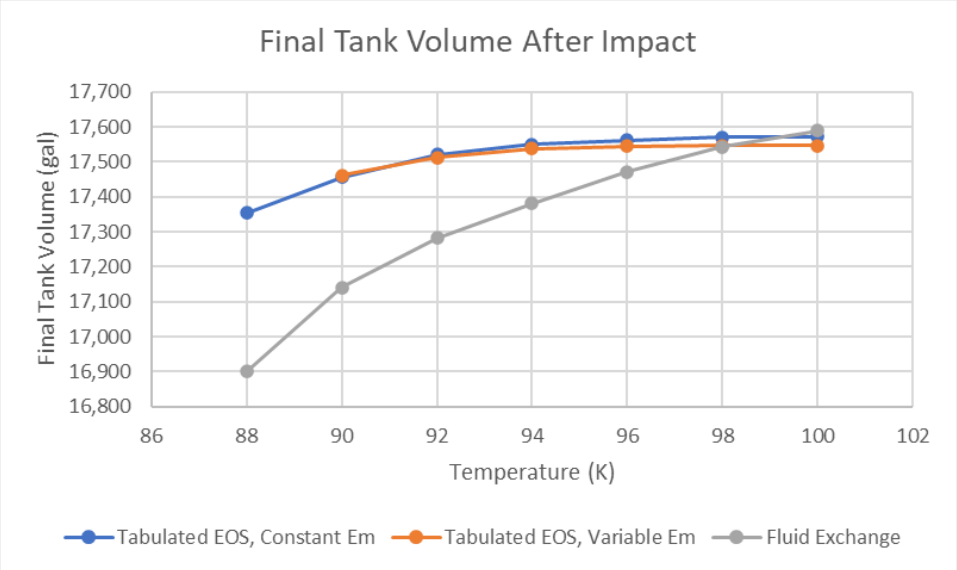

Figure 26. Final Tank Volume from Each FE Model at Various Temperatures

This difference could be explained by the reversibility of each modeling technique. In the Tabulated EOS approach, the LN2 created from condensing GN2 could re-vaporize as the pressure reduced within the tank following the impact. As the LN2 re-vaporized, the tank would recover more of its volume. In the Fluid Exchange approach, any GN2 that underwent "phase change" was in fact vented from the inner tank. This material was no longer in the tank and could therefore not contribute to the tank's volume recovery during impact. In this respect, the Tabulated EOS could be thought to represent a phase change model that was completely reversible, as no latent heat needs to be supplied or removed for a phase change to occur. The Fluid Exchange with volumetric leakage could be thought of as an irreversible phase change, where phase change could only happen in one direction.

Table 15 contains a summary of the minimum and final tank volumes from the two Tabulated EOS models and the Fluid Exchange model at each assumed initial temperature. These data were used to produce Figure 25 and Figure 26.

Table 15. Summary of Minimum and Final Tank Volumes in FE Models

	Tabulated EOS, Constant E_m	Tabulated EOS, Variable E_m	Fluid Exchange	Tabulated EOS, Constant E_m	Tabulated EOS, Variable E_m	Fluid Exchange
Assumed GN2 Temperature	Minimum Tank Volume	Minimum Tank Volume	Minimum Tank Volume	Final Tank Volume	Final Tank Volume	Final Tank Volume
K	gal	gal	gal	gal	gal	gal
88	16,606	-	16,586	17,354	-	16,901
90	16,707	16,705	16,721	17,455	17,462	17,141
92	16,788	16,779	16,811	17,521	17,512	17,282
94	16,850	16,836	16,884	17,549	17,537	17,380
96	16,894	16,874	16,948	17,562	17,545	17,471
98	16,920	16,898	16,977	17,570	17,547	17,544
100	16,936	16,911	16,990	17,572	17,547	17,589

As the assumed initial temperature of the GN2 decreased, the peak reduction in tank volume (i.e., the minimum volume reached during the impact) became larger. Additionally, as the GN2 was assumed to be colder there was less volume recovered following the peak. Colder N2 has a lower saturation pressure than warm N2. The colder GN2 will undergo phase change at a lower pressure than the warmer GN2, meaning that there is less P-V work done to compress cold vapor before phase change occurs. This behavior may explain the decreased final tank volume at the colder assumed GN2 temperatures. Without stored energy from compressing the GN2 prior to phase change, the tank's volume recovery is only due to recovery of the elastic energy within the steel walls of the tank.

As discussed in Appendix C, the post-test volume of the inner tank was estimated to be approximately 17,300 gallons based on a LiDAR scan. This scan was made well after the tank car had been drained of LN2, meaning the volume was measured after the tank had thermally expanded back to ambient temperature. This rough volume is in the vicinity of the final tank volumes obtained from the models. The method of estimating volume from the LiDAR scan was approximate at best, owing to the numerous mesh gaps.

Additionally, the lack of a latent heat component in the Tabulated EOS models meant post-impact LN2 to GN2 vaporization could occur more readily in the model than in the test. If the LN2 that was condensed from GN2 re-vaporized after the impactor came to a stop, the tank in the model would have more pressure pushing the indentation back out. The final volume of the tank would then be larger in the model than in the test, where condensed LN2 would need additional heat to re-vaporize.

Table 16 contains a summary of the peak amount of LN2 to condense from the outage in each model. The amount of LN2 is expressed as a mass percentage of the total outage mass. The Tabulated EOS models with constant and variable E_m are alike at each temperature. The Fluid Exchange model produced a similar trend, but a larger mass percentage of LN2 condensed at

each temperature, compared to the Tabulated EOS models. As a point of reference, the simplified non-FE calculations in Appendix E estimated that 56.5 percent of the initial GN2 in the outage condensed into LN2 during Test 12. This value is consistent with the estimated peak amount of LN2 to condense from the Tabulated EOS models at 92 K, or with the Fluid Exchange model at 94 K.

Table 16. Summary of Peak Amount of LN2 Condensation in FE Models

	Tabulated EOS, Constant E_m	Tabulated EOS, Variable E_m	Fluid Exchange
Assumed GN2 Temperature	**Peak Amount of Condensed LN2**	**Peak Amount of Condensed LN2**	**Peak Amount of Condensed LN2**
K	**% of Outage Mass**	**% of Outage Mass**	**% of Outage Mass**
88	83.8%	-	89.5%
90	70.3%	70.5%	75.8%
92	55.0%	55.6%	65.1%
94	39.1%	40.2%	55.1%
96	24.2%	25.4%	40.8%
98	13.4%	14.2%	24.3%
100	6.5%	6.8%	11.9%

The results in Table 16 demonstrate a significant range of condensed LN2 over a 12 K variation in assumed initial GN2 temperature. At the lower temperature estimate of 88 K, nearly all the GN2 was predicted to condense into LN2. At the upper estimate of 100 K, the vast majority of the GN2 (by mass) was expected to remain in its gaseous state. This set of results indicates the sensitivity of the condensation to the initial temperature of the GN2 within the tank.

6. Conclusion

This report documents efforts to analyze the side impact puncture performance of a surrogate DOT-113 tank car filled with cryogenic LN2 in anticipation of performing a follow-on impact test under this loading condition. Modeling efforts were focused on investigating two different techniques to represent the apparent phase change of GN2 condensing into LN2 that was inferred from the results of Test 12. The post-test model from Test 12 was simplified to represent a generalized DOT-113 surrogate with the initial conditions from that test. Two approaches for simulating vapor-to-liquid condensation (i.e., Tabulated EOS and Fluid Exchange) were separately developed and implemented into this post-test 12 model. The team investigated the overall effect of each approach.

The team developed a Tabulated EOS material model of nitrogen for use in the Abaqus FE code. Published data on the properties of GN2 and LN2 at different temperatures were used to develop the input values to the Tabulated EOS based on the specific format required by the solver. Two different assumptions on the behavior of the specific energy, E_m, were used to develop the Tabulated EOS. A series of material models were developed based on different assumed bulk temperatures for the GN2 that could have existed in the tank during Test 12. Each material model was applied individually to a non-puncture simulation of the Test 12 surrogate DOT-113 under the impact conditions of Test 12.

The results of these simulations demonstrated: 1) the tabulated EOS material model behaved as expected, simulating an abrupt change in density with increasing pressure; 2) as the assumed initial temperature increased, less GN2 was expected to undergo phase change; 3) the results of simulations run at different assumed temperatures differed from one another due only to GN2 phase change; 4) the tabulated EOS models performed similarly for a given temperature for both assumptions on E_m; 5) a calibrated leakage rate in a pneumatic cavity model also produced reasonable agreement with Test 12 at a lower computational cost; and 6) the peak test-model agreement using the Tabulated EOS approach was attained when the GN2 was assumed to have an initial temperature of 92 – 94 K.

This report also documents the development of a volumetric flow rate versus pressure relationship used in concert with a pneumatic cavity modeling approach to represent the outage for the Fluid Exchange models. The pneumatic cavity approach had been used in both the pre- and post-test modeling of Test 12. A series of volumetric flow rate versus pressure relationships were developed over a range of assumed temperatures for GN2 based on the results of the Tabulated EOS models. For pressures below the saturation pressure at a given assumed temperature, GN2 followed the ideal gas law. Once the average internal pressure of the cavity reached the saturation pressure, GN2 was allowed to leave the cavity to atmosphere. The best test-model agreement between Test 12 and the Fluid Exchange models at different outage temperatures was attained when the outage was assumed to have an initial temperature of 96 K (see Table 14).

The Fluid Exchange approach was more computationally efficient to implement than the Tabulated EOS material model. The Tabulated EOS model required Lagrangian elements to mesh the cavity, with the potential for element distortion causing the simulations to terminate prematurely. Models run using either Tabulated EOS or the Fluid Exchange approaches were in reasonable agreement with one another at a given outage temperature. In general, the Tabulated EOS approach produced a higher impact force than the Fluid Exchange approach at a given

temperature. The Fluid Exchange approach tended to estimate a higher mass of GN2 condensing to LN2 at a given temperature. Both the Fluid Exchange and Tabulated EOS produced masses of condensed LN2 that were consistent with the results of a simplified, non-FE estimation of the mass of LN2 undergoing condensation.

The range of temperatures examined using either the Tabulated EOS approach or the pneumatic cavity with fluid exchange approach was small, from 88 K to 100 K (-301.3 to -279.7 °F). However, the results of the simulations demonstrate that the GN2 temperature can have a significant effect on the amount of GN2 that condenses into LN2. The amount of condensing GN2 and the pressure at which it condenses affects the peak force reached during the simulation. While the models used in this study were not capable of simulating puncture of the inner or outer tank, the models are useful in studying the global force-displacement response of the cryogenic surrogate tank car. Once the models are refined, they can be used in full-scale puncture-capable models.

Considering the number of inter-related variables affecting the response of the surrogate tank car due to the complexity of LN2 and GN2 behaviors and the phase change that can occur due to changes in pressure and/or temperature, this effort captured the measured responses reasonably well. The modeling described in this report is a starting point toward future modeling of fluid-structure interaction of a cryogenic fluid undergoing a condensation phase change. As the technology progresses and FE software that can better represent these kinds of complex behaviors and interactions is developed, the level of correlation can be further improved and further confidence may be developed in FE models representing the behavior of the physical system being simulated. This is important because the same FE model can be used to analyze other operating conditions, different lading, different materials, and different thicknesses and dimensions for the tank car shells.

At the time the phase change modeling study was performed, a future impact test (Test 13) was planned within FRA's testing program. Test 13 was to feature a newly constructed DOT-113 tank car filled with LN2 and pressurized GN2. Based on the results of this study, pre-test models used to plan for Test 13 incorporated GN2 to LN2 condensation. Additionally, Test 13 instrumentation included additional sensors (e.g., thermocouples) to specifically measure the pre-test LN2 and GN2 temperatures to accurately model the initial state of the fluid within the inner tank.

While not examined in this study, the Tabulated EOS material model coupled with a Lagrangian mesh offers the opportunity to spatially vary the temperature within the GN2. While the Tabulated EOS materials are all assumed to be isothermal, several different material models can be assigned to the elements defining the GN2. For example, the bottom of the GN2 could be assigned a lower temperature material model than the top portion if the GN2 was thought to have stratified. While the temperature of each material would remain constant during the simulation and there would be no mixing of material, this approach would result in partial phase change occurring at two different pressures as each material reached its saturation pressure.

Finally, the methods described in this report are not limited to use only with LN2 and GN2. A similar approach could be used to develop Tabulated EOS and/or Fluid Exchange models of other cryogenic liquids of interest if suitable material data were available. The range of temperatures and pressures likely to be encountered in transportation and their relationship to the saturation pressures and temperatures of a different cryogenic liquid would determine whether

phase change behavior should be included in any future models that may use a cryogenic liquid other than LN2.

7. References

[1] Trevithick, S., Carolan, M., Eshraghi, S., & Wilson, N. (2021). Side Impact Test and Analyses of a Legacy DOT-113 Tank Car (Report No. DOT/FRA/ORD-21/28). Federal Railroad Administration.

[2] Wilson, N., Carolan, M., Trevithick, S., & Eshraghi, S. (2021). Side Impact Test and Analyses of a DOT-113 Surrogate Tank Car with Water (Report No. DOT/FRA/ORD-21/35). Federal Railroad Administration.

[3] Belport, S., Carolan, M. E., Trevithick, S., Eshraghi, S., & Krishnamurthy, A. (2022). Side Impact Test and Analyses of a DOT-113 Surrogate Tank Car with Cryogenic Lading (Report No. DOT/FRA/ORD-22/33). Federal Railroad Administration.

[4] Pipeline and Hazardous Materials Safety Administration (2015). Tank-head puncture-resistance systems (§ 179.16). Department of Transportation.

[5] Pipeline and Hazardous Materials Safety Administration (2015). Performance standard requirements (§ 179.202–12). Department of Transportation.

[6] Eshraghi, S., Krishnamurthy, A., & Carolan, M. (2022). Finite Element Analyses of Side Impacts to DOT-113 Surrogate Tank Cars with Water and Liquid Nitrogen (Report No. DOT/FRA/ORD-22/22). Federal Railroad Administration.

[7] ASTM International (2019). *ASTM A240/A240M: Standard Specification for Chromium and Chromium-Nickel Stainless Steel Plate, Sheet, and Strip for Pressure Vessels and for General Applications.* Conshocken, PA.

[8] Colorado Department of Transportation (2022). Pueblo Memorial Airport - Colorado Department of Transportation. Accessed 2022 8 December.

[9] The Engineering Toolbox (2003). Air - Density and Specific Volume vs. Altitude. Accessed 17 March 2020.

[10] National Institute of Standards and Technology (2023). NIST Standard Reference Database Number 69.

[11] Dassault Systèmes Simulia Corporation (2019). *Abaqus 2019*.

[12] Yu, H., Tang, Y. H., Gordon, J., & Jeong, D. Y. (2009). Modeling the Effect of Fluid-Structure Interaction on the Impact Dynamics of Pressurized Tank Cars. *Proceedings of IMECE 2009 - 2009 ASME International Mechanical Engineering Congress and Exposition.* Lake Buena Vista, FL.

[13] Rakoczy, P., Carolan, M., Eshraghi, S., & Gorhum, T. (2019). Side Impact Test and Analyses of a DOT-117 Tank Car (Report No. DOT/FRA/ORD-19/13). Federal Railroad Administration.

[14] The Engineering ToolBox (2004). Universal and Individual Gas Constants. Accessed 12 March 2020.

[15] Livermore Software Technology Corporation (2018). *LS-PrePost 4.6 x64*.

[16] The Engineering ToolBox (2003). Water - Density, Specific Weight and Thermal Expansion Coefficients. Accessed 12 March 2020.

[17] The Engineering ToolBox (2004). Water - Speed of Sound vs. Temperature. Accessed 2 November 2021.

[18] Strobridge, T.R. (1962). The Thermodynamic Properties of Nitrogen from 64 to 300° K, 0.1 to 200 Atmospheres. NBS Technical Note 129, Boulder Laboratories, National Bureau of Standards.

Appendix A.
Description of Non-puncture FE Model

Following Test 12, a non-puncture model of the DOT-113 surrogate tank car was analyzed with a 9 percent N2 outage initially at 30 psig under an 18.3 mph impact condition. The non-puncture model is shown in Figure A1. The model contained all the features of the puncture-capable model used to estimate the speed to cause puncture for Test 12 except that it did not have puncture-capable "solid patch" regions in the outer and inner vessels. The exclusion of very small solid elements allowed the model to run to completion approximately eight times faster. This allowed for a series of models to be run examining two different approaches to simulating condensation of GN2 to LN2 during the impact event.

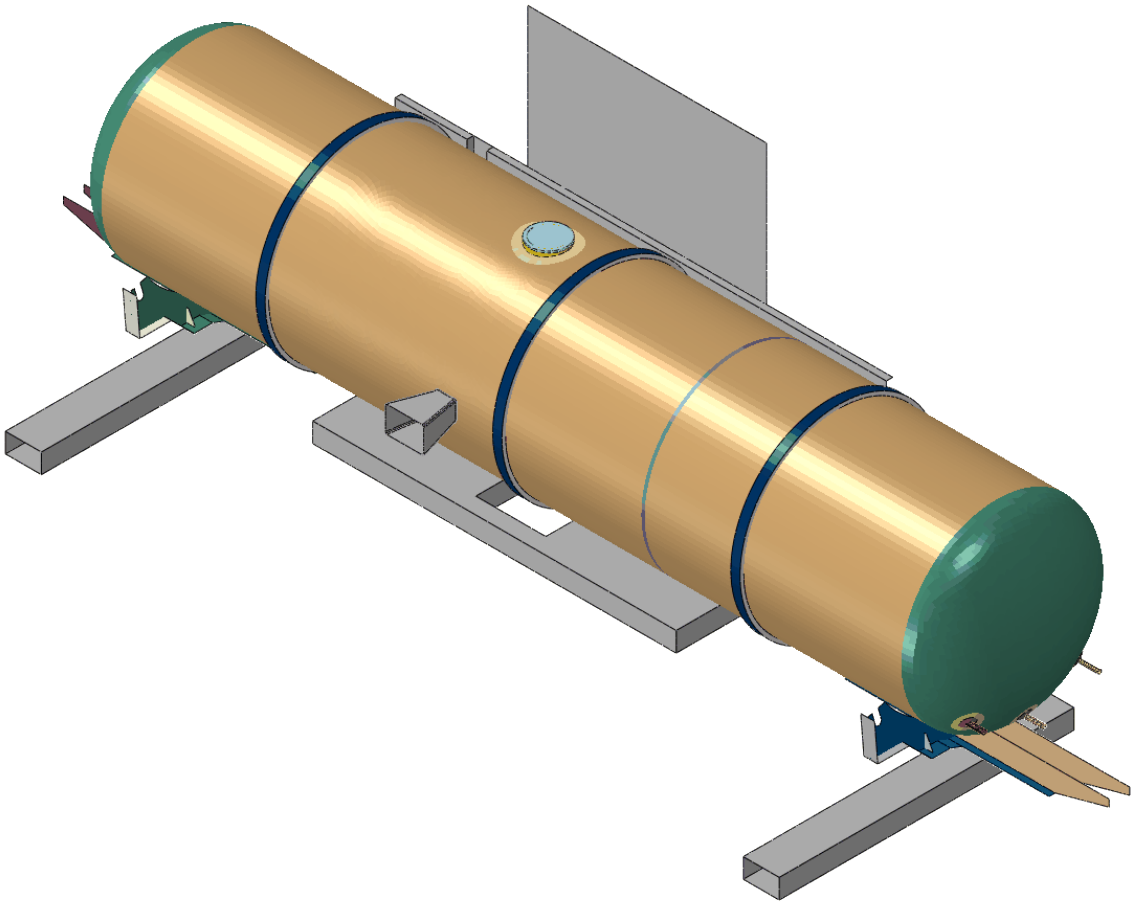

Figure A1. DOT-113 Surrogate Non-puncture FE Model

Figure A2 shows a cut view centered on the longitudinal impact plane of the DOT-113 surrogate non-puncture FE model that used the pneumatic cavity GN2 modeling approach. Figure A3 shows a similar cut view of the FE model that used the Tabulated EOS GN2 modeling approach. Within the inner vessel, the liquid lading (grey) was represented as a Lagrangian EOS and is described in Appendix A.5. The gas phase was represented using either a Lagrangian mesh of elements with a Tabulated EOS material model (Appendix A.3) or a pneumatic cavity with a prescribed leakage (Appendix A.4).

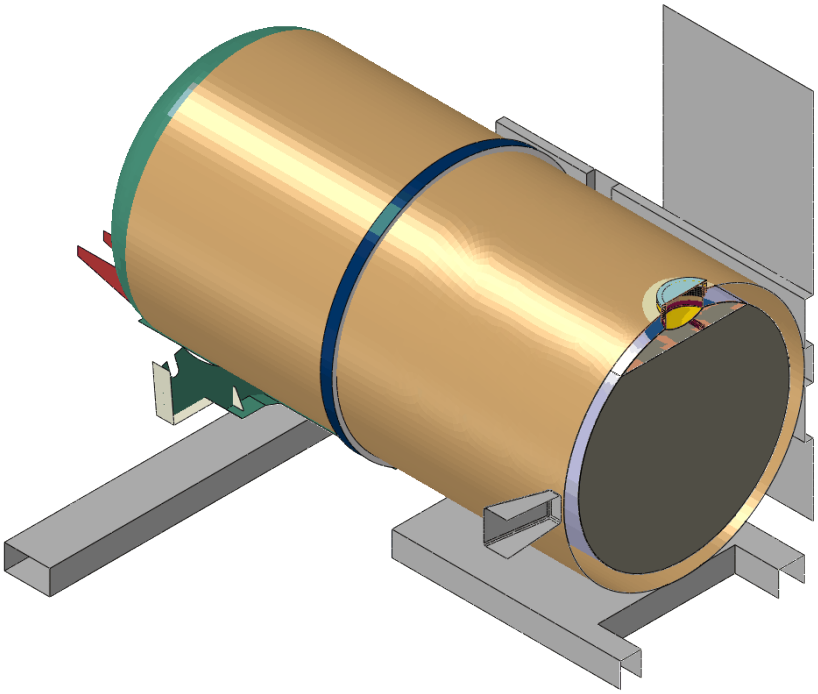

Figure A2. DOT-113 Surrogate Non-puncture FE Model Cut View, Pneumatic Cavity

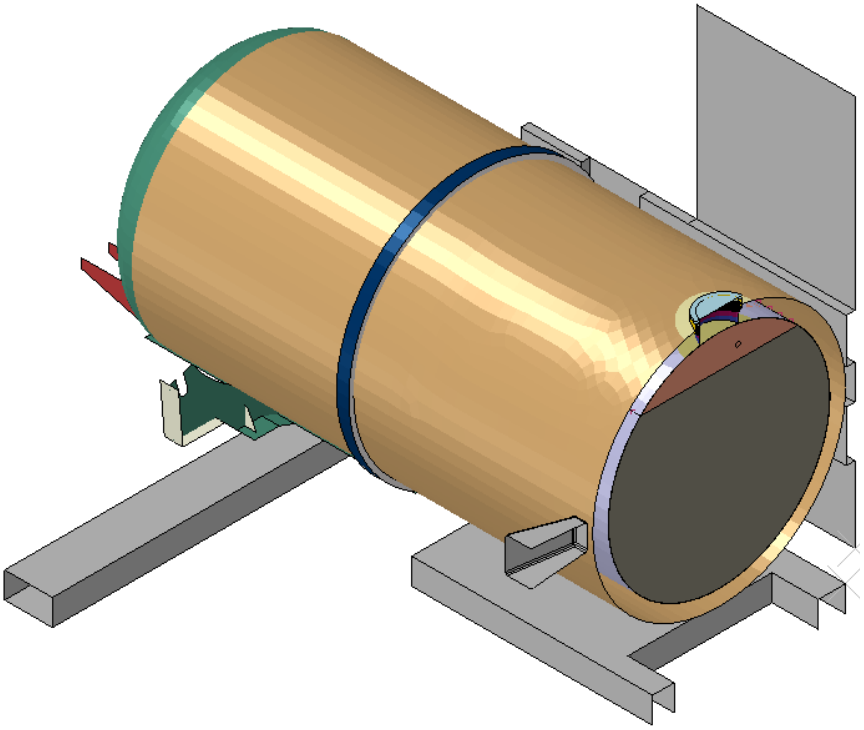

Figure A3. DOT-113 Surrogate Non-puncture FE Model Cut View, Tabulated EOS

A.1. AAR TC128, Grade B Carbon Steel

The AAR TC128-B material model used in this study is the same model documented in FRA Report No. DOT/FRA/ORD-22/22 [6].

A.2. ASTM A240 Type 304 Stainless Steel

The ASTM A240 Type 304 stainless teel material model used in this study is the same model documented in FRA Report No. DOT/FRA/ORD-22/22 [6].

A.3. Gaseous Nitrogen – Tabulated EOS

The gas phase of the lading was modeled as N2 at an initial gauge pressure of 30 psi (42.3 psia), as this was the measured internal pressure for the tank car at the beginning of Test 12. Two different modeling approaches were developed to simulate the effects of GN2 to LN2 condensation on the overall impact response.

In the first approach, a Tabulated EOS material model was developed for GN2 at a fixed initial temperature. A different Tabulated EOS material model was developed at 88 K, 90 K, 92 K, 94 K, 96 K, 98 K, and 100 K, as the exact initial temperature of the GN2 in Test 12 was not known. Two different Tabulated EOS were developed at each temperature. In the first, the specific energy was assumed to remain constant (i.e., E_m=E_{m0}). This is thermodynamically correct for an isothermal gas. Post-processing of these models revealed that the internal energy of the elements was changing as the pressure and volume of the elements changed during the simulation. While this may be a nomenclature inconsistency between thermodynamic "internal energy" and "internal energy" as defined in Abaqus, a second Tabulated EOS was developed based on a simplified calculation of E_m varying with pressure and volume.

Developing a series of Tabulated EOS material models over a range of practical temperatures also allowed the researchers to examine the sensitivity of the model's response to the initial temperature. Each Tabulated EOS material model was then applied to a Lagrangian mesh of C3D4 elements representing the GN2. A tied constraint was defined between the bottom surface of the GN2 and the top surface of the LN2, preventing the two fluid species from separating. A summary of the mesh and the GN2 properties that remained constant for each Tabulated EOS material model is shown in Table A1.

Table A1. Summary of Properties for GN2, Tabulated EOS Material Models

Parameter	Value
Initial Pressure	42.3 psia
Dynamic Viscosity	9.21 x 10^{-10} psi·s
Mesh Implementation	5-inch Linear Tetrahedral (C3D4) Elements
Number of Elements	22,096
Distortion Control	Yes, length ratio = 0.125

As discussed in Section 3.5, a Tabulated EOS material model requires the user to define values for two functions, f_1 and f_2, at user-defined values of logarithmic volumetric compressive strain

(ε_{vol}). The logarithmic volumetric compressive strain is itself a function of the current density of the material (Equation 11).

The Tabulated EOS relationships for N2 defined for this study relied on data from NIST [10]. Each material model was defined at a user-prescribed temperature between 88 and 100 K with a fixed increment of logarithmic volumetric compressive strain ($\Delta\varepsilon_{vol}$) of 0.001. In addition to using *EOS, type=tabulated, the material model at each temperature also included definitions of *Density and *Viscosity. Additionally, initial pressure (ρ_0) and initial internal energy per unit mass (E_{m0}) were assigned to the outage mesh as initial conditions.

Table C1 contains the initial values of vapor density and viscosity that were directly specified in each material model, as well as the values of c_v and E_{m0} that were used in the calculation of the Tabulated EOS at each temperature. This table also includes the saturated vapor and liquid densities of N2 at each temperature, which were used in the Tabulated EOS calculations. All the values in this table are given in the unit system used in the FE models.

Table C1. Material Properties for EOS Material Models at Various Temperatures

Temperature K	Initial Vapor Density (ρ_0) lbf-s^2/in/in^3	Saturated Vapor Density (ρ_{sat}^{vap}) lbf-s^2/in/in^3	Saturated Liquid Density (ρ_{sat}^{liq}) lbf-s^2/in/in^3	Initial Specific Heat (c_v) in^2/(s^{2}K)	Initial Internal Energy per Unit Mass (E_{m0}) in^2/s^2
88	1.14 x 10^{-6}	1.19 x 10^{-6}	7.07 x 10^{-5}	1.24 x 10^6	9.38 x 10^7
90	1.11 x 10^{-6}	1.41 x 10^{-6}	6.97 x 10^{-5}	1.23 x 10^6	9.65 x 10^7
92	1.08 x 10^{-6}	1.66 x 10^{-6}	6.87 x 10^{-5}	1.22 x 10^6	9.91 x 10^7
94	1.05 x 10^{-6}	1.93 x 10^{-6}	6.78 x 10^{-5}	1.21 x 10^6	1.02 x 10^8
96	1.02 x 10^{-6}	2.24 x 10^{-6}	6.67 x 10^{-5}	1.21 x 10^6	1.04 x 10^8
98	9.96 x 10^{-7}	2.60 x 10^{-6}	6.56 x 10^{-5}	1.20 x 10^6	1.07 x 10^8
100	9.72 x 10^{-7}	2.99 x 10^{-6}	6.45 x 10^{-5}	1.19 x 10^6	1.09 x 10^8

A small value for $\Delta\varepsilon_{vol}$ was necessary to capture the abrupt change in density that occurred due to phase change. While a variable $\Delta\varepsilon_{vol}$ could have been used (with a small value used only for densities around the saturation pressure), the Abaqus software regularizes Tabulated EOS materials by ε_{vol} to use a constant $\Delta\varepsilon_{vol}$ increment. Therefore, the Tabulated EOS material was developed using a constant $\Delta\varepsilon_{vol}$ increment to remove any uncertainties caused by the Abaqus software regularizing the data. As a consequence of using a small value for $\Delta\varepsilon_{vol}$ and a Tabulated EOS material spanning both vapor and liquid phase densities, a very large number of tabulated entries were defined for each material.

The Tabulated EOS material model developed at a temperature of 88 K, a constant value of E_m equal to E_{m0}, and a $\Delta\varepsilon_{vol}$ of 0.001 used 7,588 values for f_1 and f_2. The approximate number of tabulated points varied slightly at each temperature but was approximately the same as this example at 88 K. It was not practical to re-print each Tabulated EOS material model in this appendix.

Figure A4 and Figure A5 contain plots of f_1 and f_2 versus density, respectively, for the constant E_m Tabulated EOS developed at 88 K. The data in each figure has been identified for each of the three pseudo-phases. As can be seen in each of these figures, GN2 corresponds to the lowest densities and LN2 corresponds to the highest densities. In actual N2, the GN2-LN2 transition

features a discontinuity in density, as there is no state of matter between vapor and liquid. However, because the Tabulated EOS material in Abaqus is regularized by ε_{vol}, and ε_{vol} is a function of the current density (see Equation 11), a substantial number of *transition* densities must be defined between the GN2 and LN2 phases.

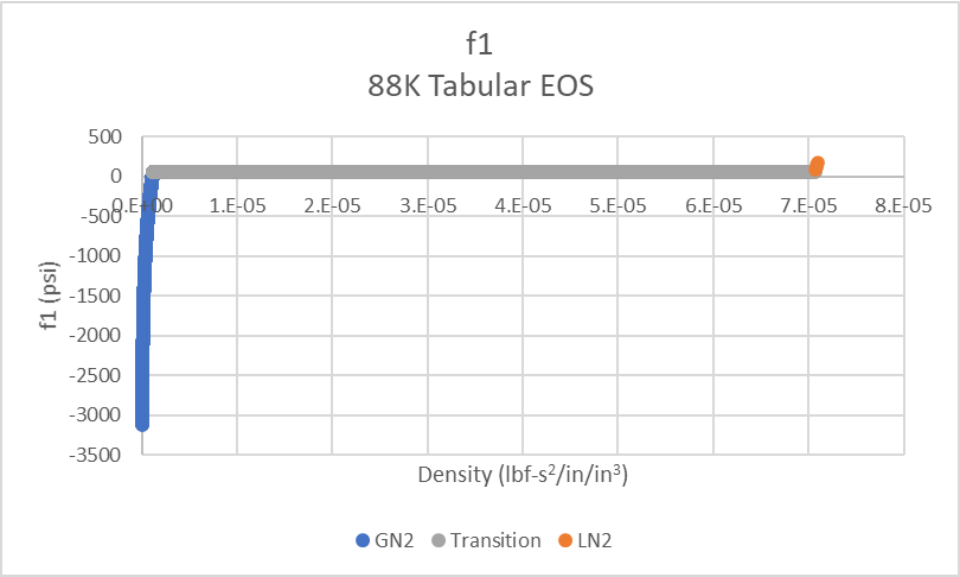

Figure A4. Calculated f_1 Versus Density, 88 K Constant E_m Tabulated EOS Material

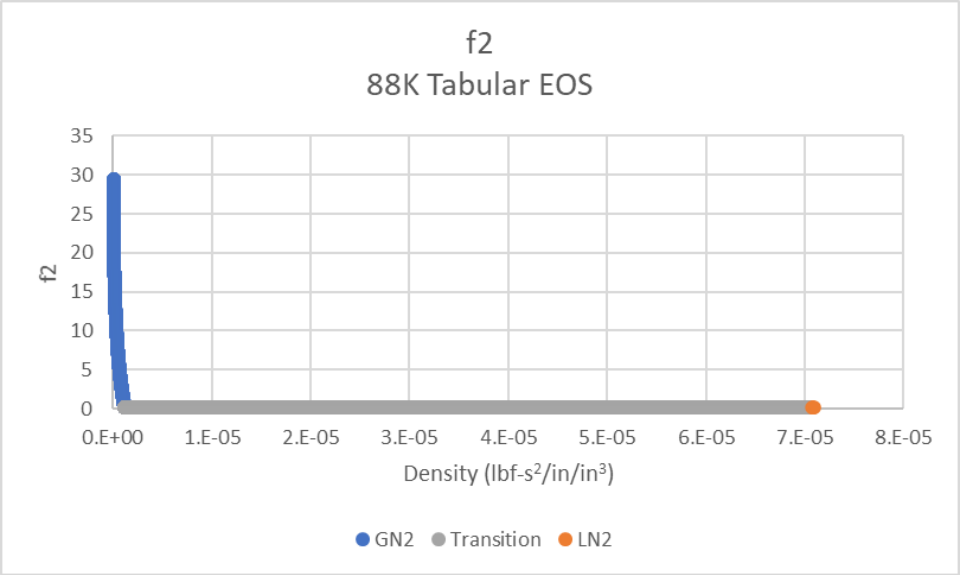

Figure A5. Calculated f_2 Versus Density, 88 K Constant E_m Tabulated EOS Material

While the modeling that is documented within this report used a $\Delta\varepsilon_{vol}$ of 0.001, a different value could be used to approximate a Tabulated EOS material model using the equations above and suitably chosen density (ρ) values. Appendix B.8 contains a comparison of model results using three different values of $\Delta\varepsilon_{vol}$.

A.4. Gaseous Nitrogen – Pneumatic Cavity with Fluid Exchange

In the second approach, a pneumatic cavity modeling technique was implemented within Abaqus, with a *Fluid Exchange* defined between the cavity and atmosphere. This Fluid Exchange featured a calibrated volumetric flow rate versus pressure relationship to mimic the effects of GN2 condensing into LN2. For pressures below a threshold value within the cavity, the GN2 behaved according to the ideal gas law. If the impact caused the pressure to increase to the threshold value, the fluid exchange allowed GN2 to exit the cavity, approximating the reduction in GN2 volume as it condensed into LN2. This approach does not account for the resulting volume increase of LN2 within the tank. This is a limitation of the pneumatic cavity modeling approach but was assumed by the modelers to be an inconsequential approximation.

The pneumatic cavity modeling technique within Abaqus requires a surface to be defined that encloses the cavity. A reference point must also be defined within this cavity to which initial temperature and pressure can be assigned.

The pneumatic cavity approach models the entire cavity with a single uniform pressure and uniform temperature value. The GN2 pressure within the model was allowed to change as the volume of the tank changed due to the impact while the temperature was held constant. The modeling inputs defined for the pneumatic cavity representation of the GN2 phase of the model are summarized in Table A2. This table includes the unit system used in the FE model.

Table A2. Properties for Nitrogen (Pneumatic Cavity)

Property	Value	Reference
Universal Gas Constant (R)	73.583 in-lbf/(mol-K)	[13]
Molecular Weight (MW)	1.60 x 10^{-4} lbf·s^2/(in·mol)	[10]
Constant Temperature	88, 90, 92, 94, 96, 98, or 100 K	
Molar Specific Heat ($c_{p,m}$)	257.59 in-lbf/(mol-K)	[10]
Initial Pressure	42.3 psia (30 psig)	

The molar specific heat capacity at constant pressure ($c_{p,m}$) for GN2 was calculated according to Equation A1.

Equation A1. Calculation of Molar Specific Heat

$$c_{P.m} = c_P \cdot MW$$

A.5. LN2

The DOT-113 surrogate in Test 12 had an initial outage volume of 9 percent and internal pressure of 30 psig. The liquid phase of the lading was modeled as LN2 at a temperature of 86 K. Within Abaqus, the Us-Up EOS model was used to describe the behavior of LN2 and applied to a Lagrangian mesh. The fluid was meshed with 3 inch fully integrated brick (C3D8) elements. The key material properties that must be input to this material model are the material's density, dynamic viscosity, and bulk modulus. The bulk modulus can be calculated from the density and speed of sound as shown in Equation A2 The material properties were obtained from NIST

Standard Reference Database Number 69 [10] at a constant pressure of 42.3 psia and temperature of 86 K.

Equation A2. Calculation of Bulk Modulus

$$K = c^2 \rho$$

Table A3 summarizes the properties of the LN2 included in the DOT-113 surrogate FE model. The same material model was used in the models run using the Tabulated EOS or the pneumatic cavity approaches to modeling the outage. Note that the mesh size was changed between the two modeling approaches to maintain a similar element size between the Lagrangian meshes used for LN2 and GN2. These tables include the unit system used in the FE model.

Table A3. Summary of Properties for LN2

Parameter	Value
Mass Density	7.16 x 10^{-5} lbf·s^2/in^4
Initial Pressure	42.3 psia
Initial Temperature	86 K
Sound Speed	3.00 x 10^4 in/s
Dynamic Viscosity	1.6987 x 10^{-8} psi·s
Bulk Modulus	6.44 x 10^4 psi
Mesh Implementation	3-inch Fully Integrated Brick (C3D8) Elements (Pneumatic Cavity) 5-inch C3D8 Elements (Tabulated EOS)
Distortion Control	Yes, length ratio = 0.1 (default)

A.6. Membrane

An artificial surface was modeled within the inner tank to define the limits of the pneumatic cavity (i.e., outage). Frictionless, hard contact was assigned between the membrane and the inner vessel and lading. Because this surface does not correspond to any physical feature within the tank, modeling techniques were chosen to minimize the increase in either mass or stiffness introduced into the model by the membrane while not negatively impacting the FE model's stability or runtime. A membrane was not included in the models using the Tabulated EOS approach to modeling GN2. The material properties of the membrane are summarized in Table A4. This table includes the U.S. customary units used in the FE model.

Table A4. Material Properties Defined for Membrane Material

Parameter	Value
Density	7.35 x 10^{-6} lbf-s^2/in^4
Modulus of Elasticity	1.0 x 10^4 psi

Appendix B.
Tabulated EOS Model Results

This appendix contains plots of model results and Test 12 data (where appropriate) at each of the temperatures where a Tabulated EOS material model was developed.

Table B1. Summary of Inner Tank Volume Reductions for EOS Material Models at Various Temperatures, Constant E_m

Assumed GN2 Temperature	Final Tank Volume	Reduction in Volume	Reduction in Volume
K	gal	gal	%
88[10]	17,354	570	3.2%
90	17,455	469	2.6%
92	17,521	403	2.2%
94	17,549	375	2.1%
96	17,562	362	2.0%
98	17,570	354	2.0%
100	17,572	352	2.0%

Table B2. Summary of Inner Tank Volume Reductions for EOS Material Models at Various Temperatures, Variable E_m

Assumed GN2 Temperature	Final Tank Volume	Reduction in Volume	Reduction in Volume
K	gal	gal	%
88[11]	-	-	-
90[10]	17,462	462	2.6%
92	17,512	412	2.3%
94	17,537	387	2.2%
96	17,545	379	2.1%
98	17,547	377	2.1%
100	17,547	377	2.1%

[10]The FE model terminated before 1 second of simulation time. The volume at the time of termination is used in this table.

[11]The FE model terminated before reaching a minimum volume, so no results are shown.

B.1 Variable E_m FE Results at All Temperatures

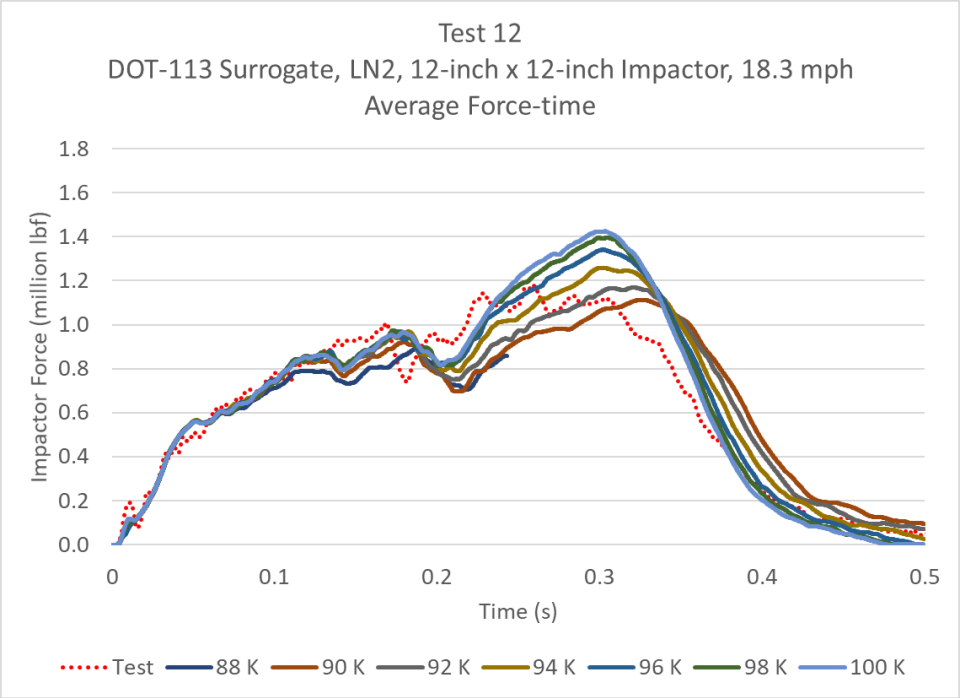

Figure B1. Impactor Force Versus Time for EOS Material Models at Various Temperatures (Variable E_m)

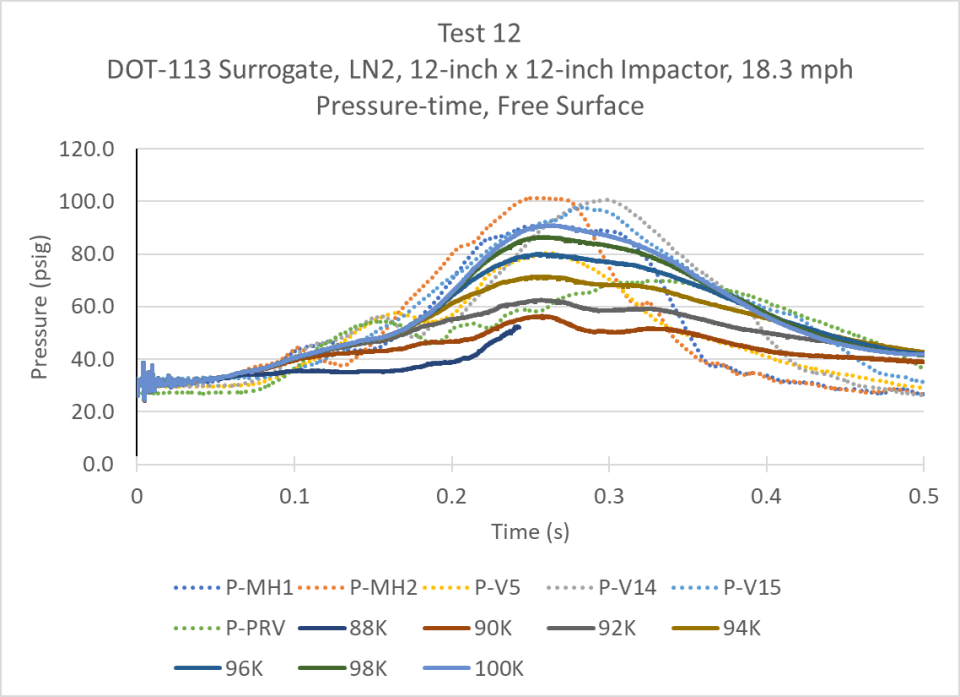

Figure B2. Pressure-time Histories Averaged over Surface of LN2 in Communication with GN2 for EOS Material Models at Various Temperatures (Variable E_m)

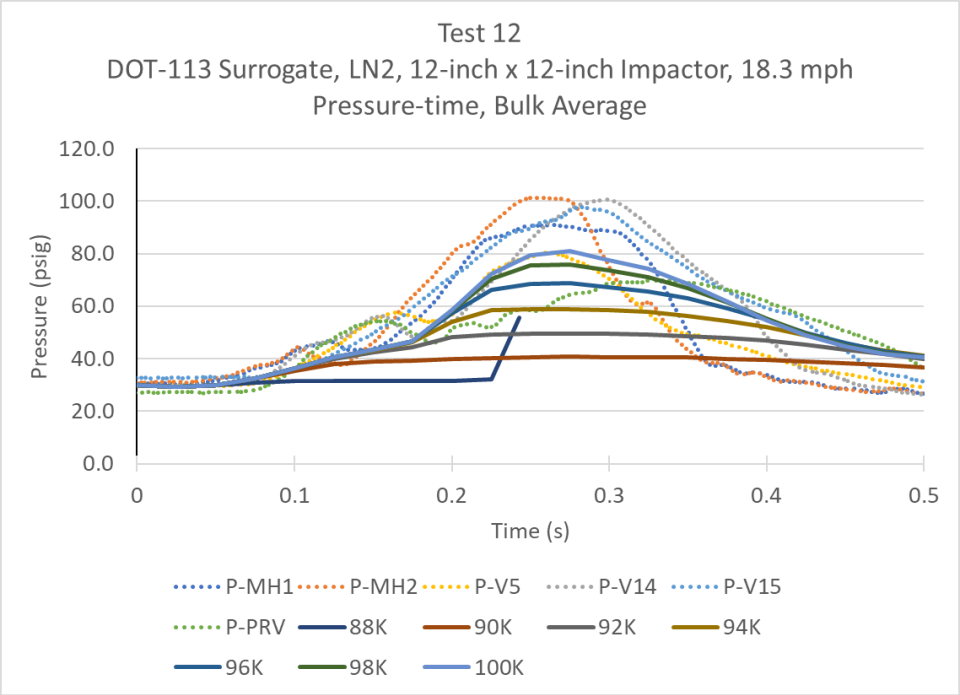

Figure B3. Bulk Pressure-time Histories Averaged over Entire Outage, for EOS Material Models at Various Temperatures, Variable E_m

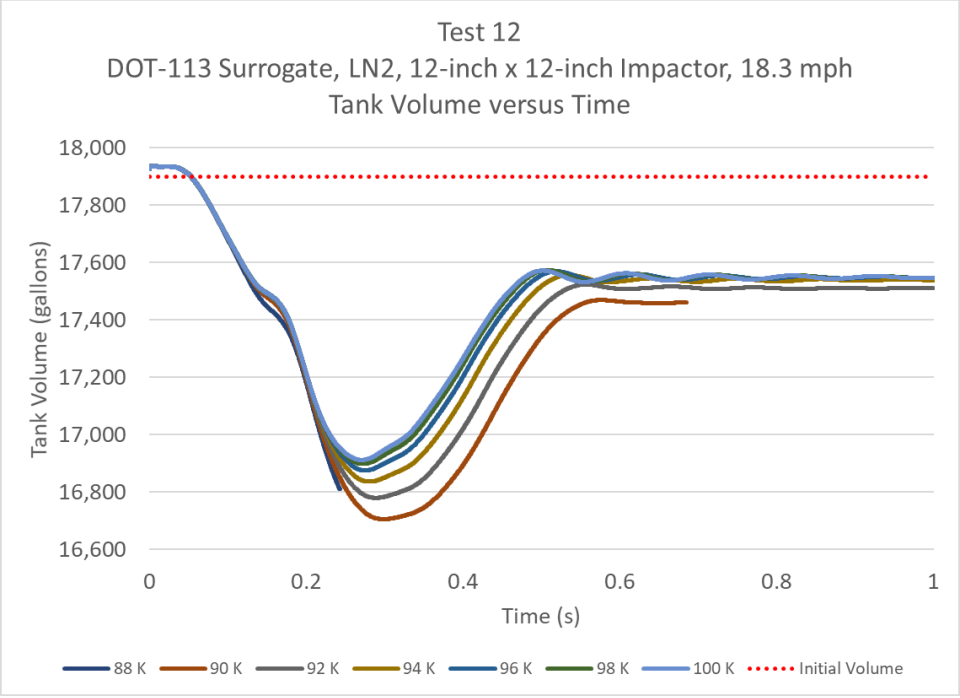

Figure B4. Inner Tank Volume-time Histories for EOS Material Models at Various Temperatures, Variable E_m

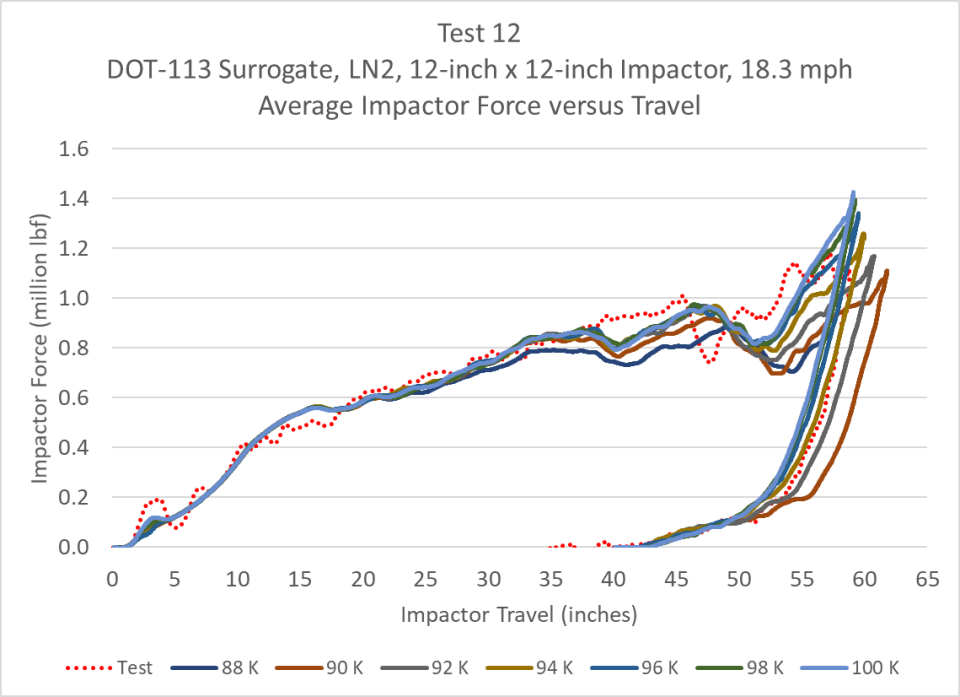

Figure B5. Impactor Force Versus Impactor Travel for Tabulated EOS Material Models at Various Temperatures, Variable E_m

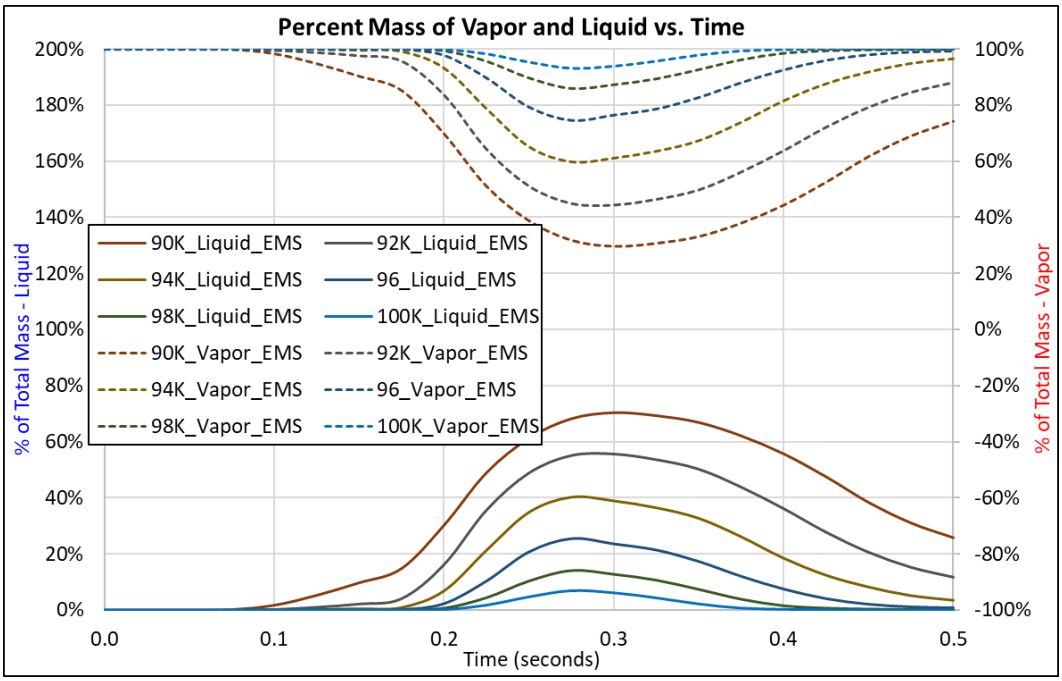

Figure B6. Percentage by Mass of Vapor and Liquid in Outage Versus Time, Tabulated EOS Material Models at Various Temperatures, Variable E_m

Table B3. Peak GN2 and LN2 Amounts in Outage, Variable E_m

Temperature (K)	Maximum Amount of LN2 (% of Outage Mass)	Minimum Amount of GN2 (% of Outage Mass)
88[12]	-NA-	-NA-
90	70.5%	29.5%
92	55.6%	44.4%
94	40.2%	59.8%
96	25.4%	74.6%
98	14.2%	85.8%
100	6.8%	93.2%

Table B4. Selected Results from Test Measurements and FE Results, EOS Material Models at Various Temperatures, Variable E_m

		Test	88 K	90 K	92 K	94 K	96 K	98 K	100 K
First Peak Force	kips	1,008.4	890.0	919.3	969.2	968.6	970.5	973.9	974.9
Displacement at First Peak Force	in	45.5	49.2	47.8	47.2	48.1	46.7	46.4	54.2
Global Peak Force	kips	1,179.5	890.0	1,111.4	1,168.3	1,259.1	1,340.2	1,395.4	1,424.3
Displacement at Global Peak Force	in	57.2	49.2	61.8	60.7	59.9	59.5	59.2	59.1
Maximum Displacement	in	58.8	57.2	61.8	60.8	60.0	59.5	59.3	59.1

Table B5. Percent Difference between Selected Results from Test Measurements and FE Results, EOS Material Models at Various Temperatures, Variable E_m

	88 K	90 K	92 K	94 K	96 K	98 K	100 K
First Peak Force	-11.7%	-8.8%	-3.9%	-3.9%	-3.8%	-3.4%	-3.3%
Displacement at First Peak Force	8.1%	5.0%	3.8%	5.6%	2.6%	2.0%	19.0%
Global Peak Force	-24.5%	-5.8%	-1.0%	6.7%	13.6%	18.3%	20.8%
Displacement at Global Peak Force	-14.0%	8.0%	6.2%	4.7%	4.0%	3.6%	3.3%
Maximum Displacement	-2.7%	5.1%	3.3%	2.0%	1.2%	0.8%	0.6%
Average Absolute Error	**12.2%**	**6.5%**	**3.6%**	**4.6%**	**5.0%**	**5.6%**	**9.4%**

[12] No results available for 88 K because FEA stopped due to an error.

B.1 GN2 at 88 K

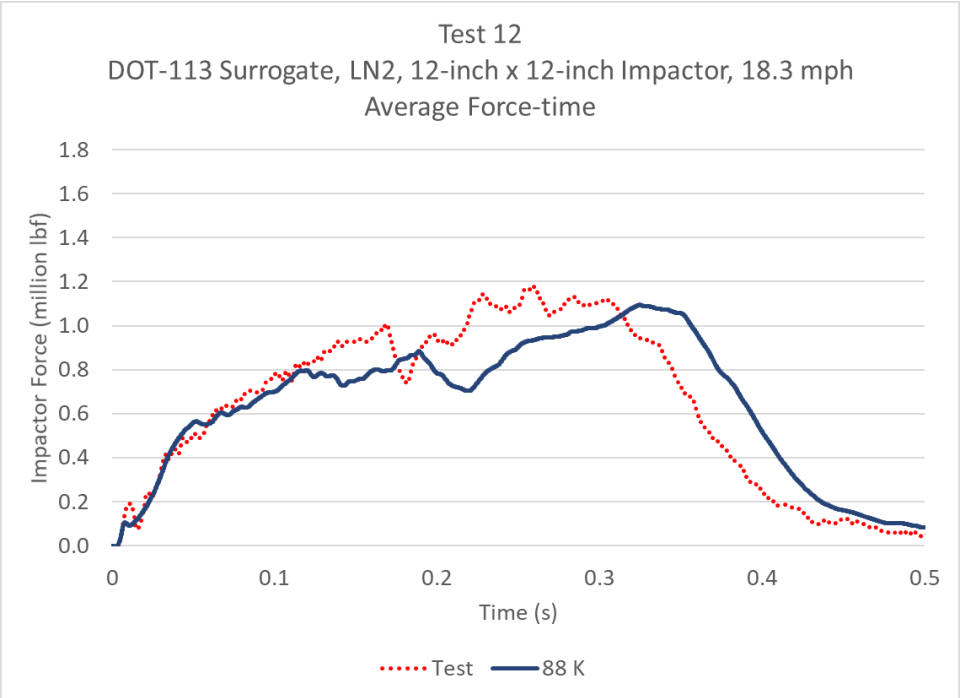

Figure B7. Impactor Force Versus Time for Test and EOS Material Model at 88 K, Constant E_m

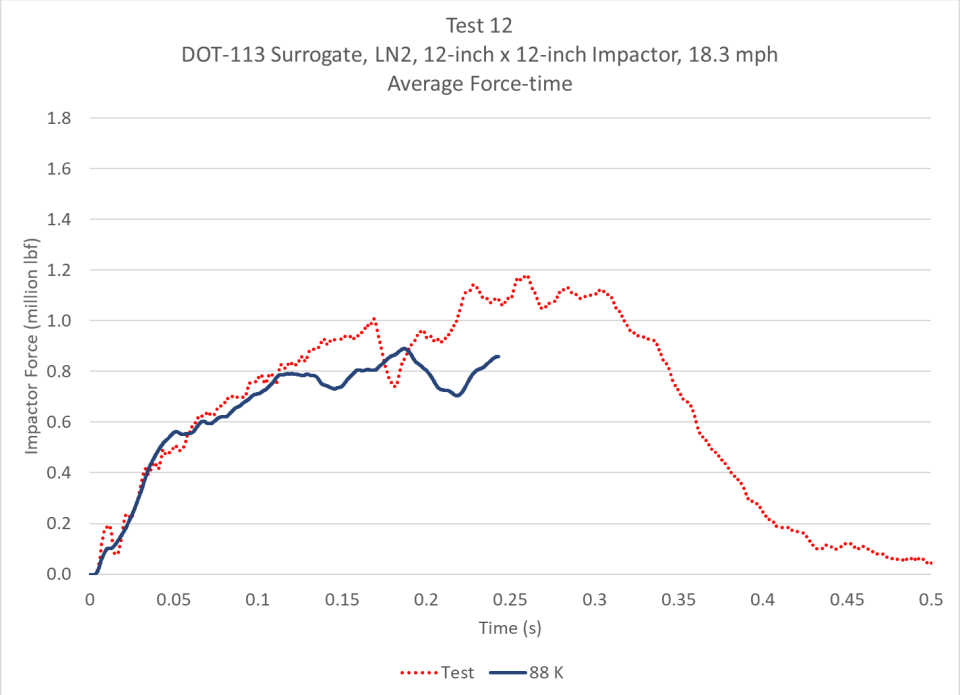

Figure B8. Impactor Force Versus Time for Test and EOS Material Model at 88 K, Variable E_m

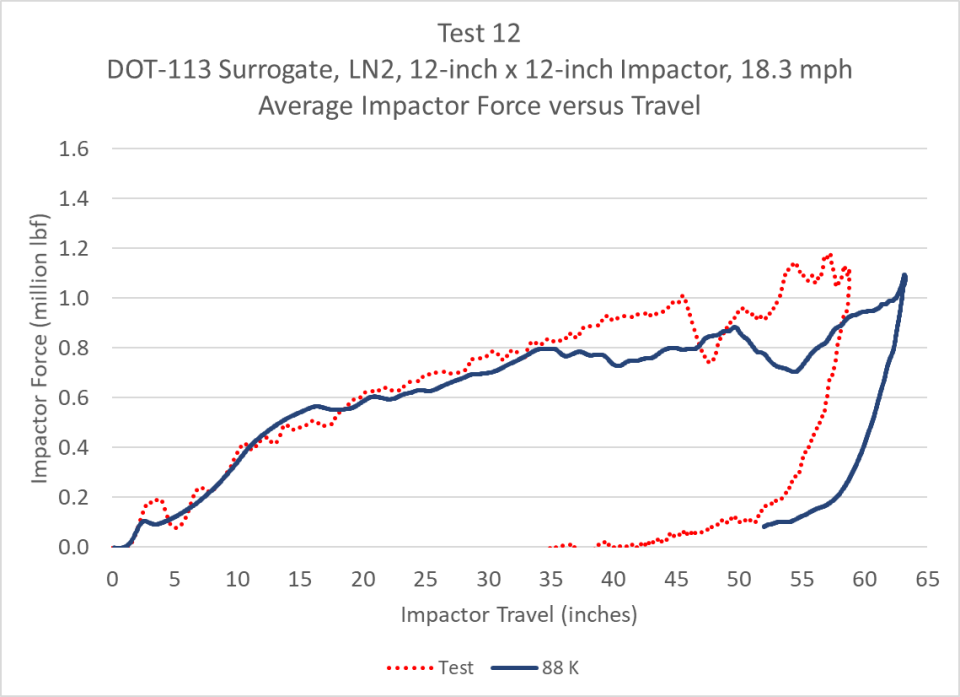

Figure B9. Impactor Force Versus Impactor Travel for Test and EOS Material Model at 88 K, Constant E_m

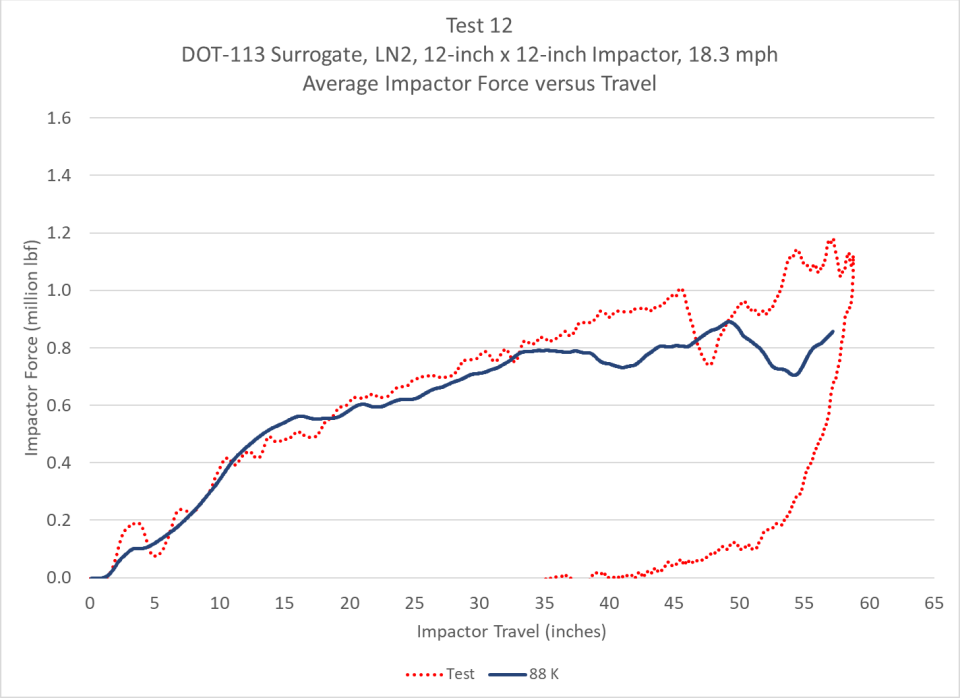

Figure B10. Impactor Force Versus Impactor Travel for Test and EOS Material Model at 88 K, Variable E_m

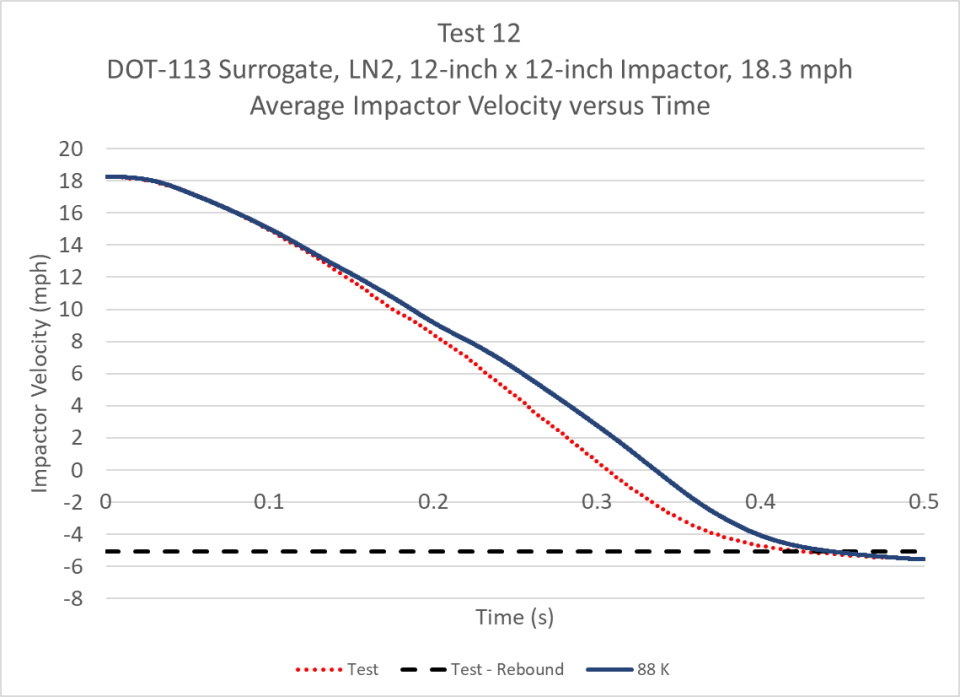

Figure B11. Impactor Velocity Versus Time for Test and EOS Material Model at 88 K, Constant E_m

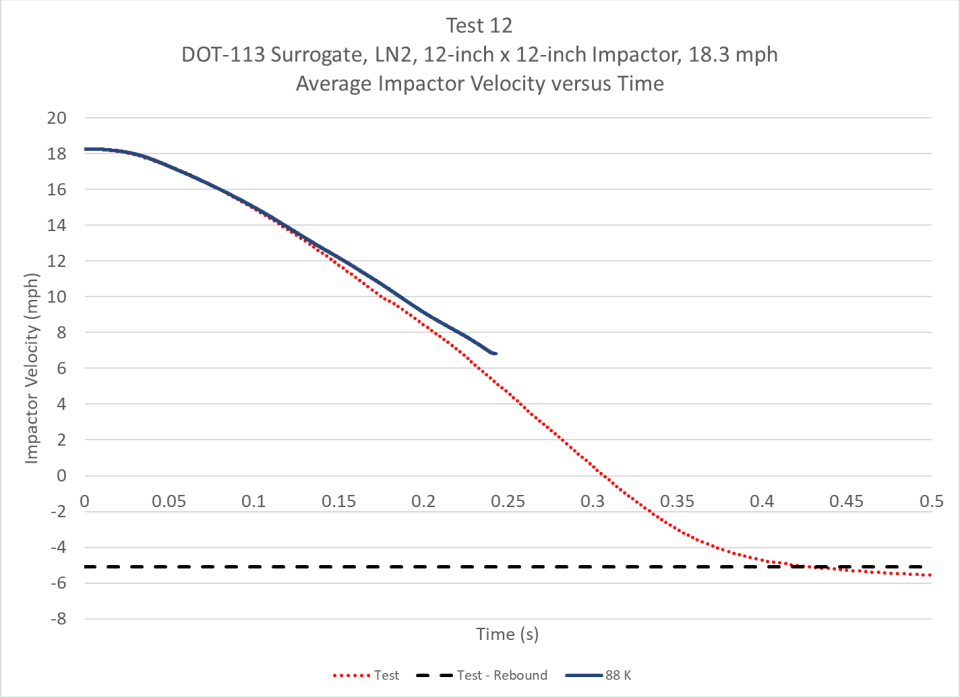

Figure B12. Impactor Velocity Versus Time for Test and EOS Material Model at 88 K, Variable E_m

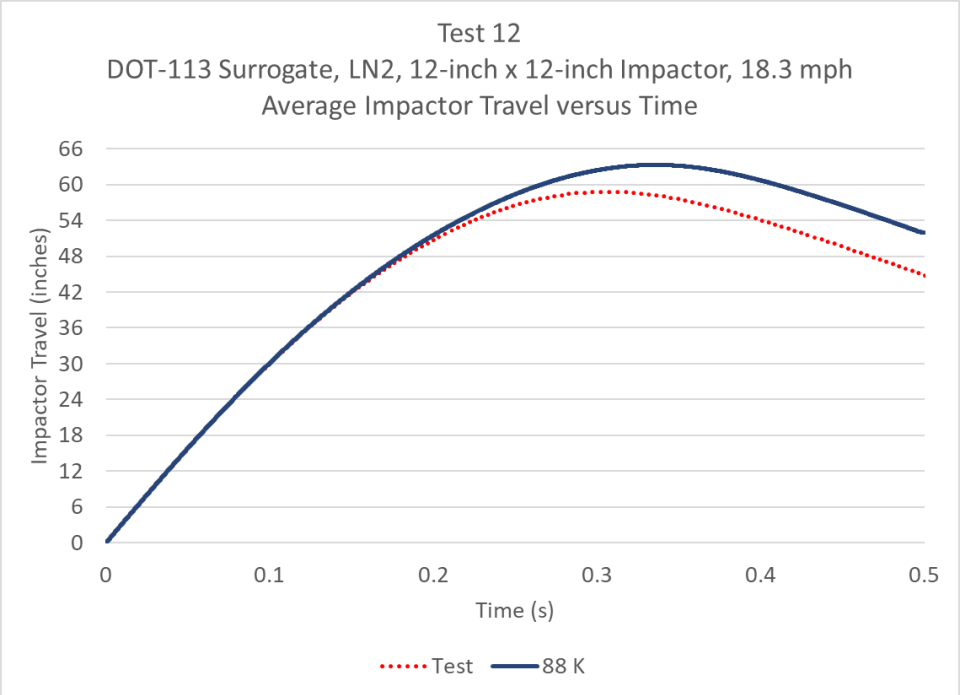

Figure B13. Impactor Displacement Versus Time for Test and EOS Material Model at 88 K, Constant E_m

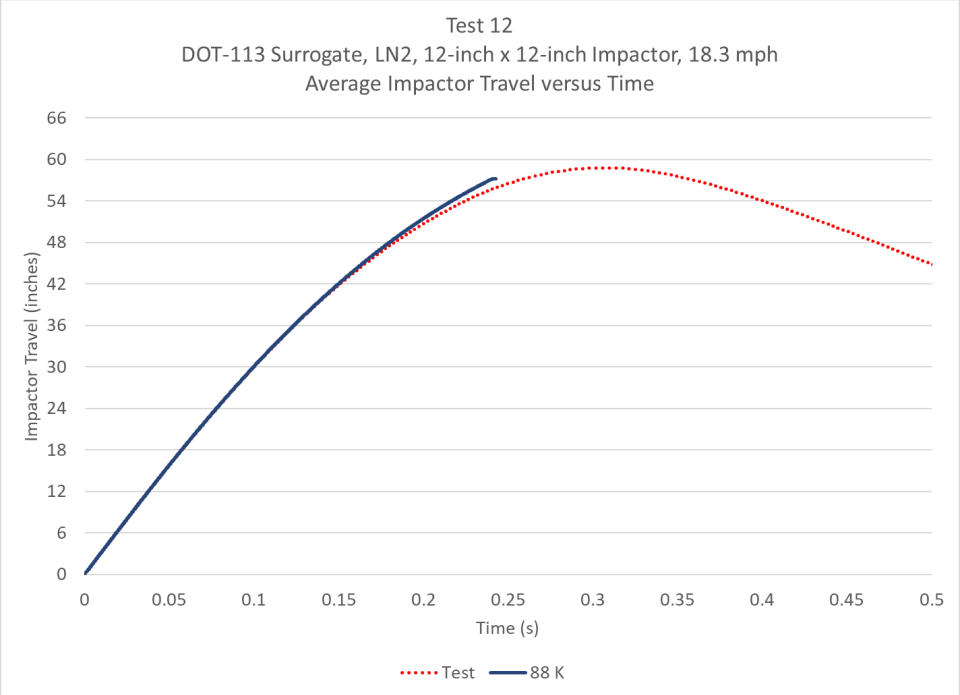

Figure B14. Impactor Displacement Versus Time for Test and EOS Material Model at 88 K, Variable E_m

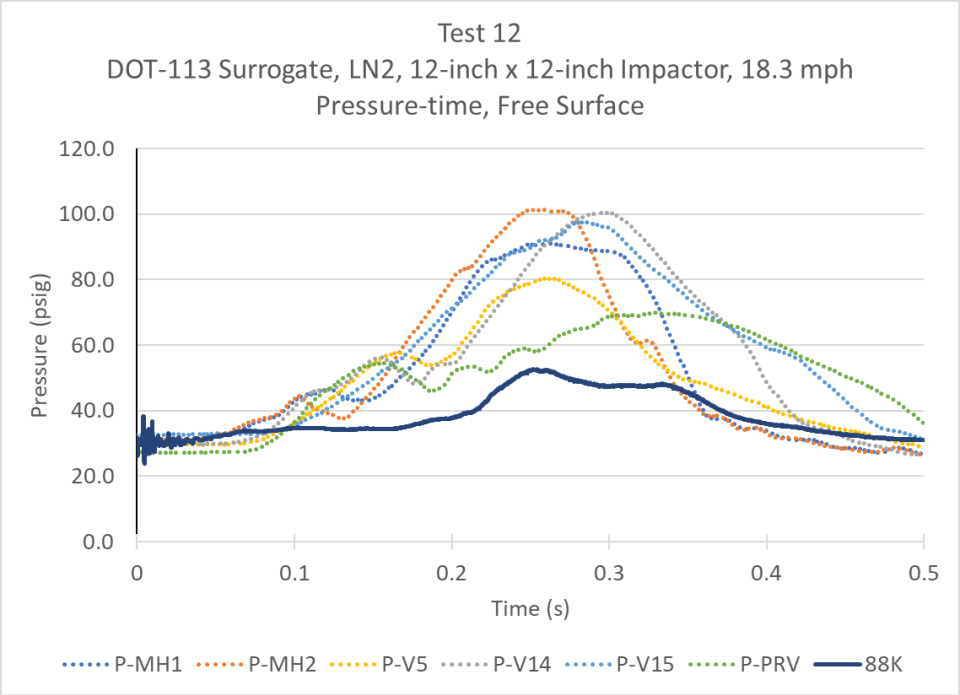

Figure B15. Average Pressure on Bottom Surface of GN2 for EOS Material Model at 88 K and Test Pressure Measurements, Constant E_m

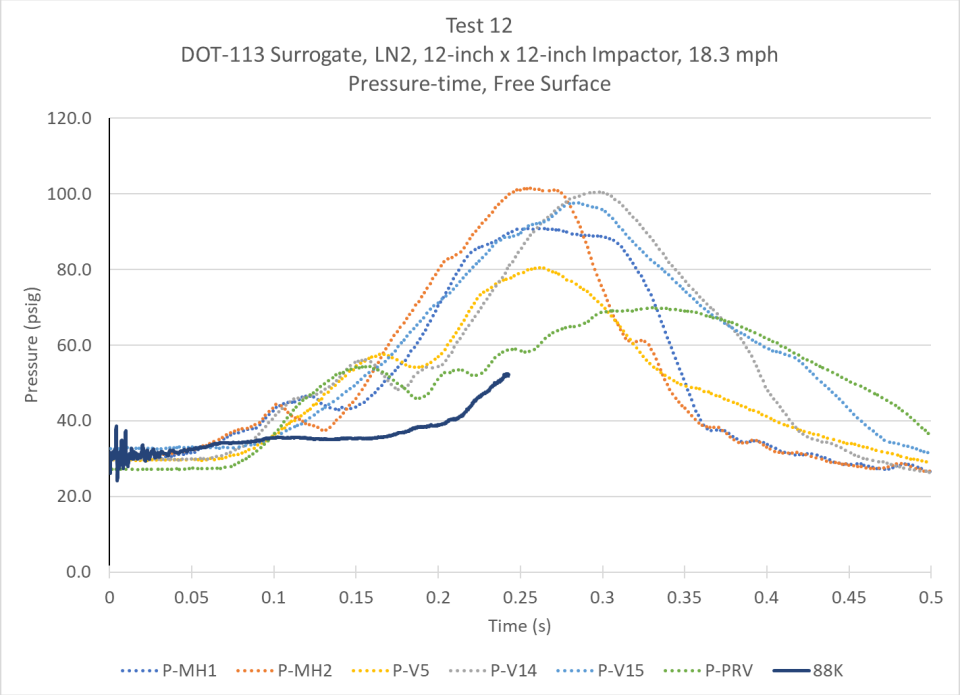

Figure B16. Average Pressure on Bottom Surface of GN2 for EOS Material Model at 88 K and Test Pressure Measurements, Variable E_m

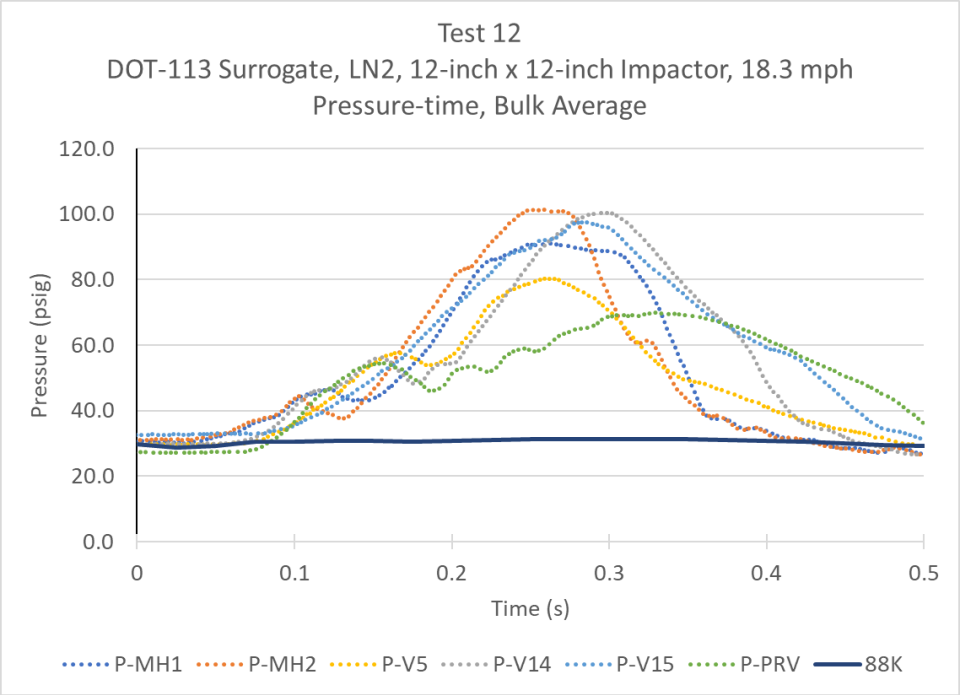

Figure B17. Average Pressure throughout Volume of GN2 for EOS Material Model at 88 K and Test Pressure Measurements, Constant E_m

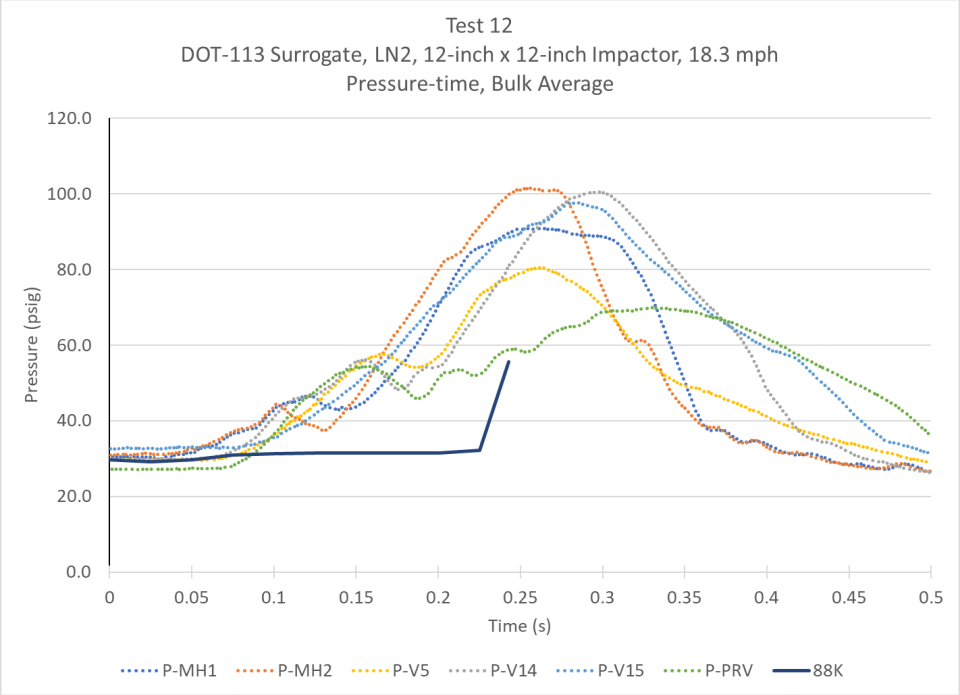

Figure B18. Average Pressure throughout Volume of GN2 for EOS Material Model at 88 K and Test Pressure Measurements, Variable E_m

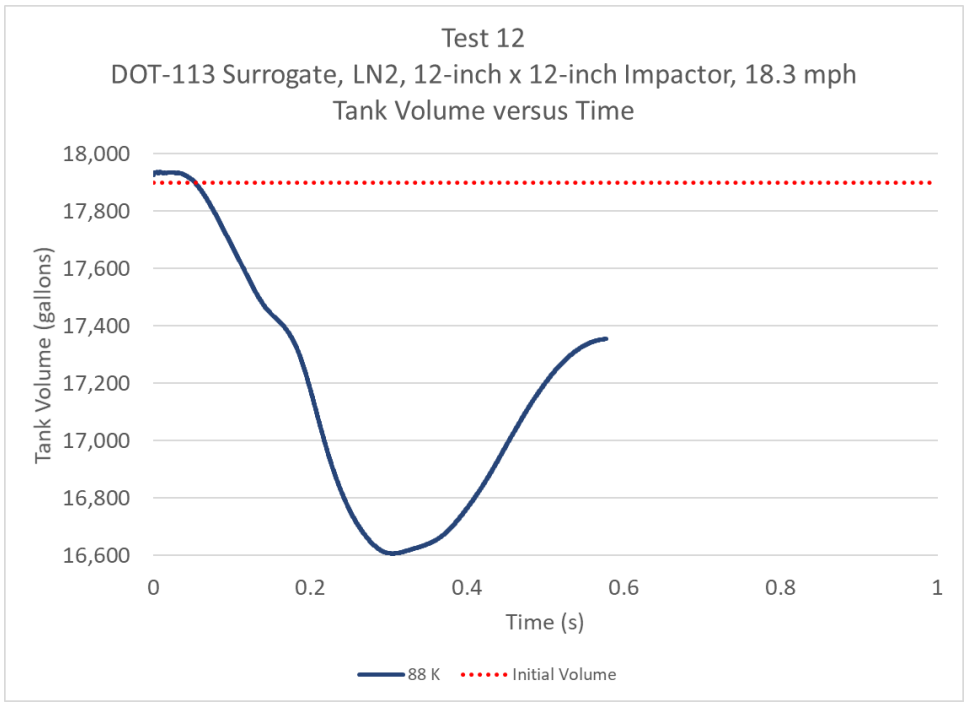

Figure B19. Tank Volume Versus Time for EOS Material Model at 88 K, Constant E_m

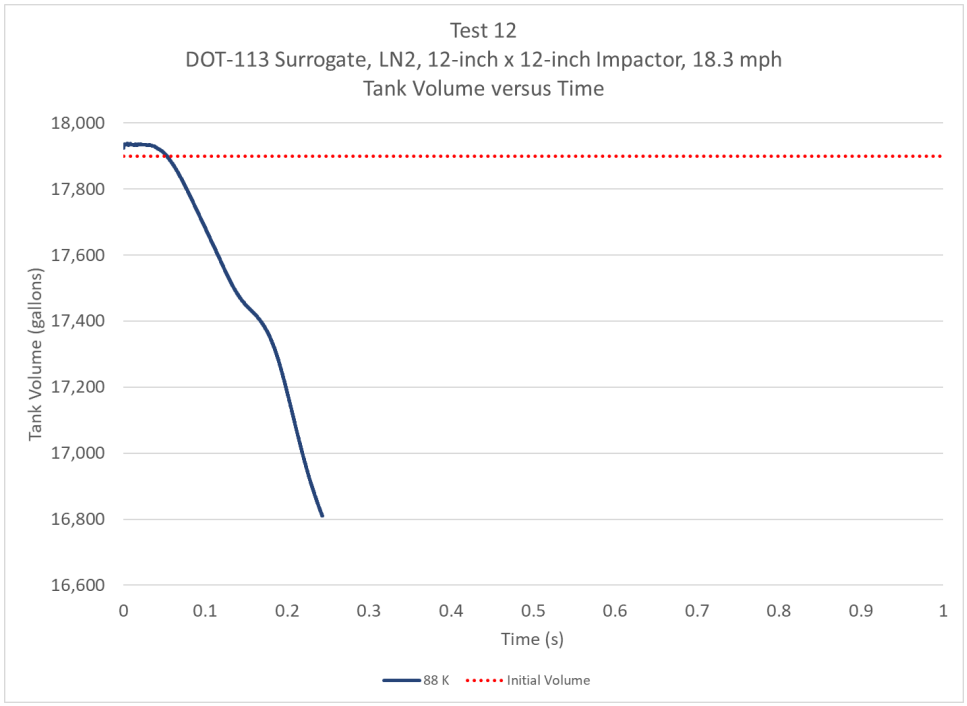

Figure B20. Tank Volume Versus Time for EOS Material Model at 88 K, Variable E_m

B.2 GN2 at 90K

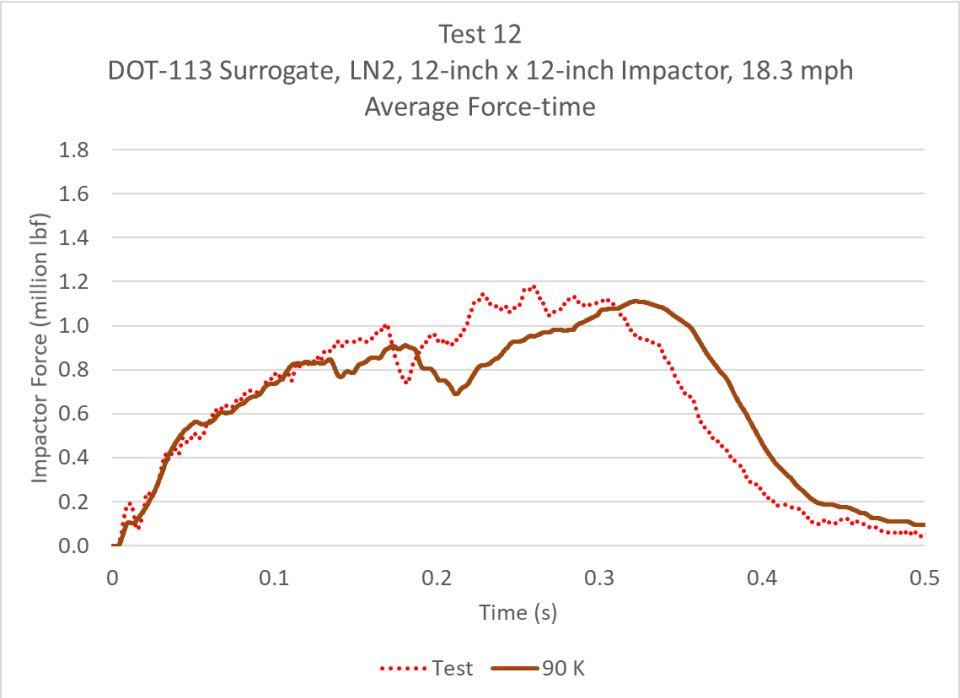

Figure B21. Impactor Force Versus Time for Test and EOS Material Model at 90 K, Constant E_m

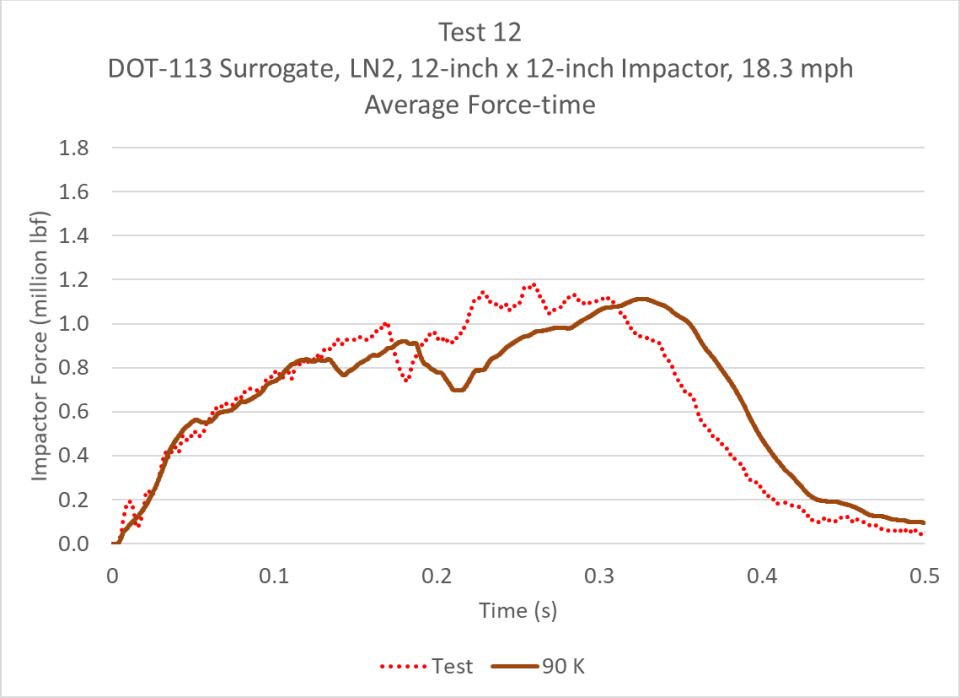

Figure B22. Impactor Force Versus Time for Test and EOS Material Model at 90 K, Variable E_m

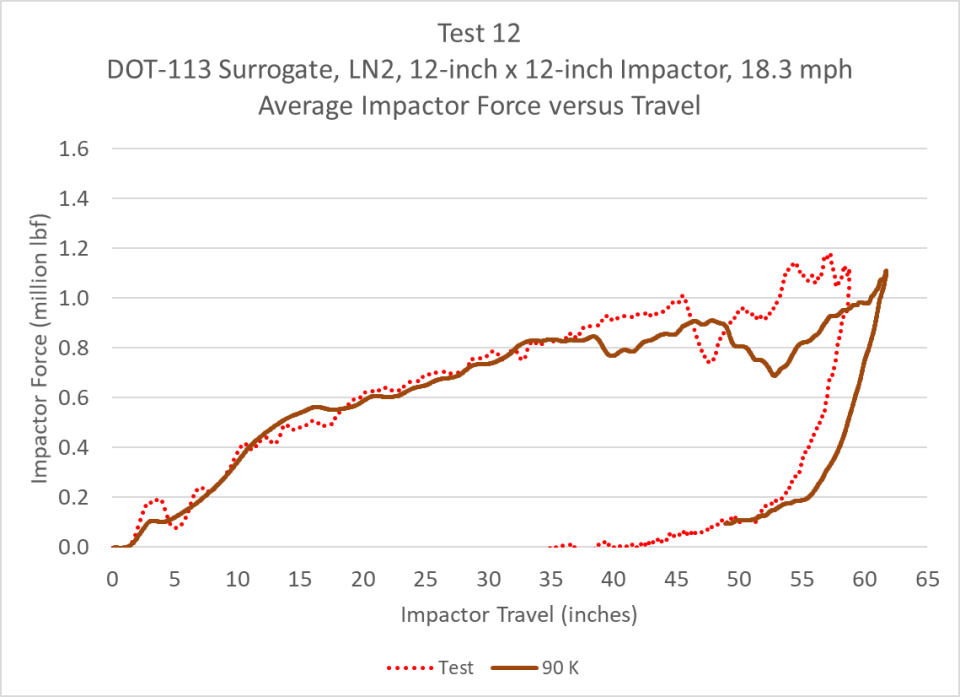

Figure B23. Impactor Force Versus Impactor Travel for Test and EOS Material Model at 90 K, Constant E_m

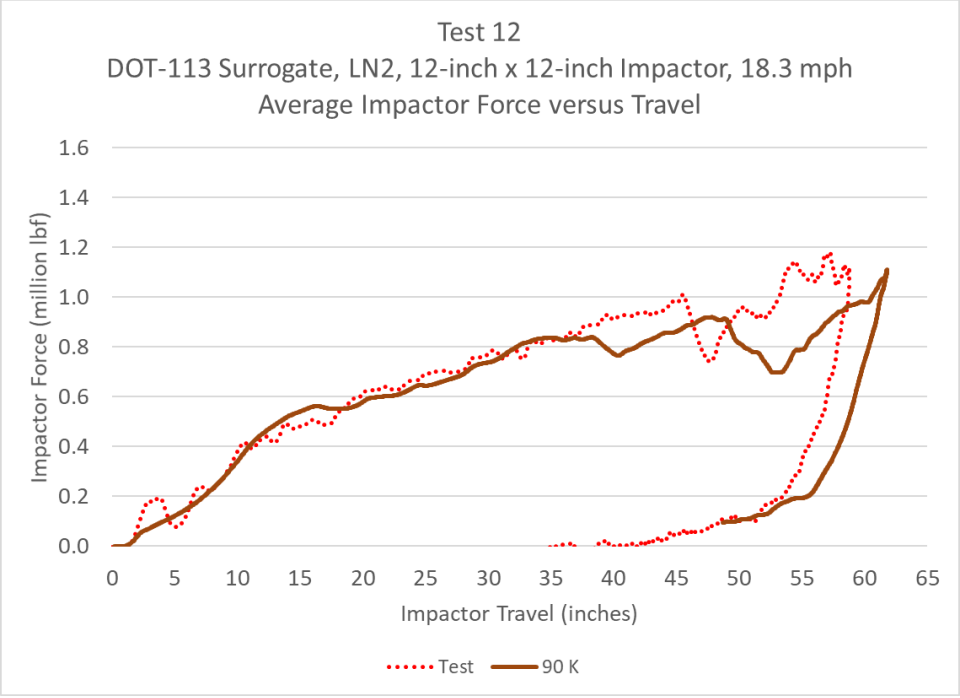

Figure B24. Impactor Force Versus Impactor Travel for Test and EOS Material Model at 90 K, Variable E_m

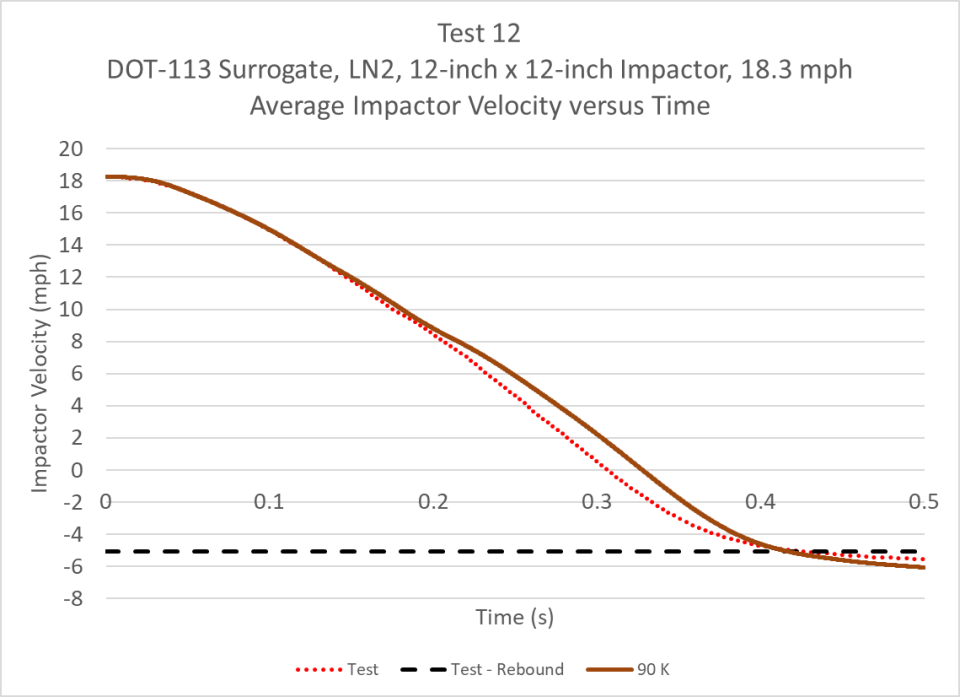

Figure B25. Impactor Velocity Versus Time for Test and EOS Material Model at 90 K, Constant E_m

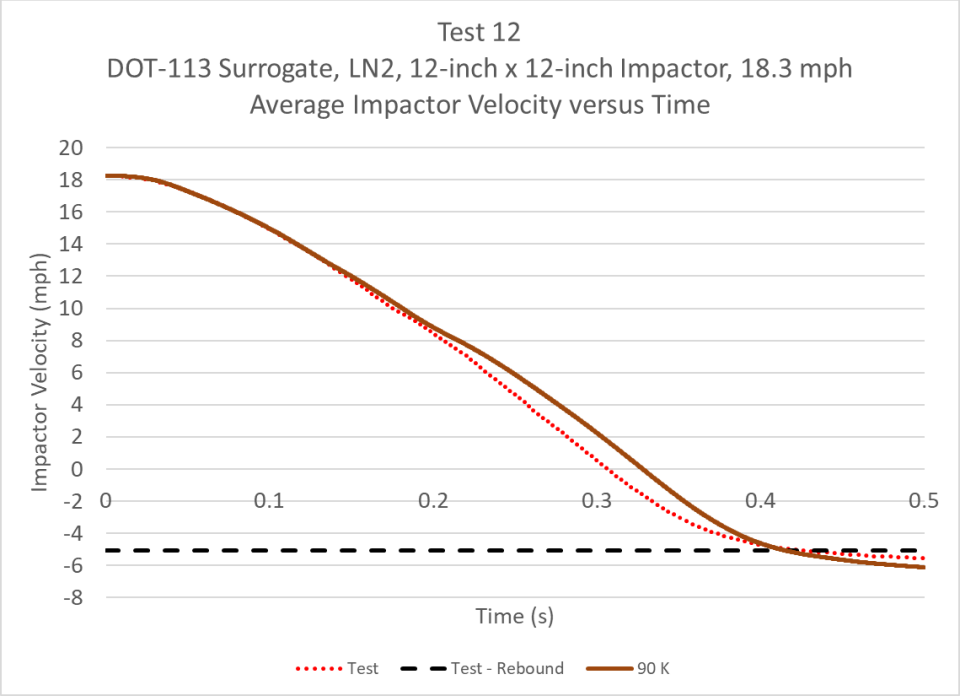

Figure B26. Impactor Velocity Versus Time for Test and EOS Material Model at 90 K, Variable E_m

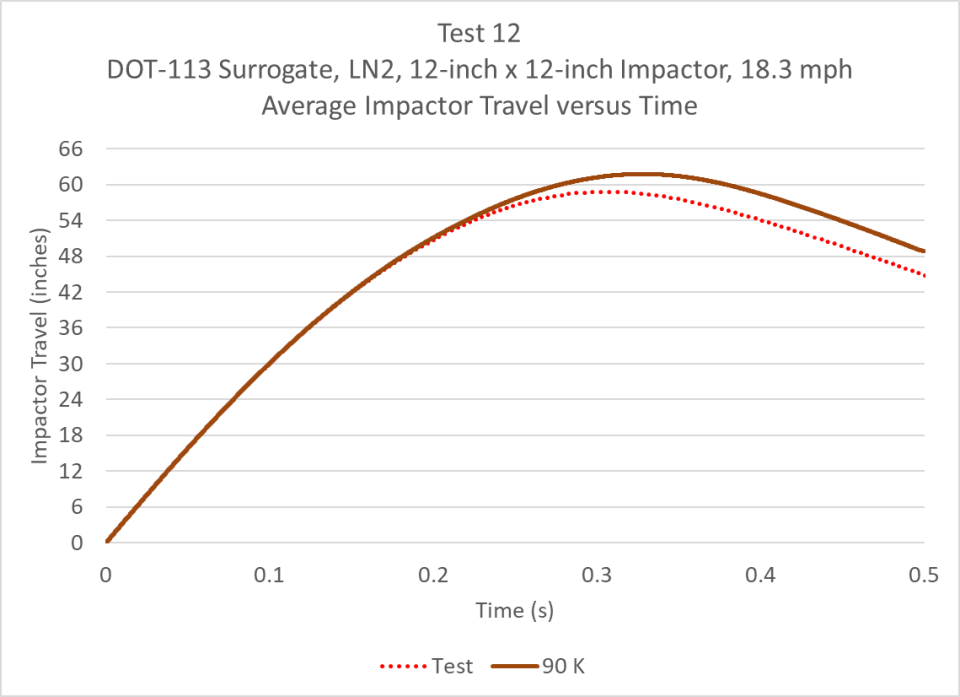

Figure B27. Impactor Displacement Versus Time for Test and EOS Material Model at 90 K, Constant E_m

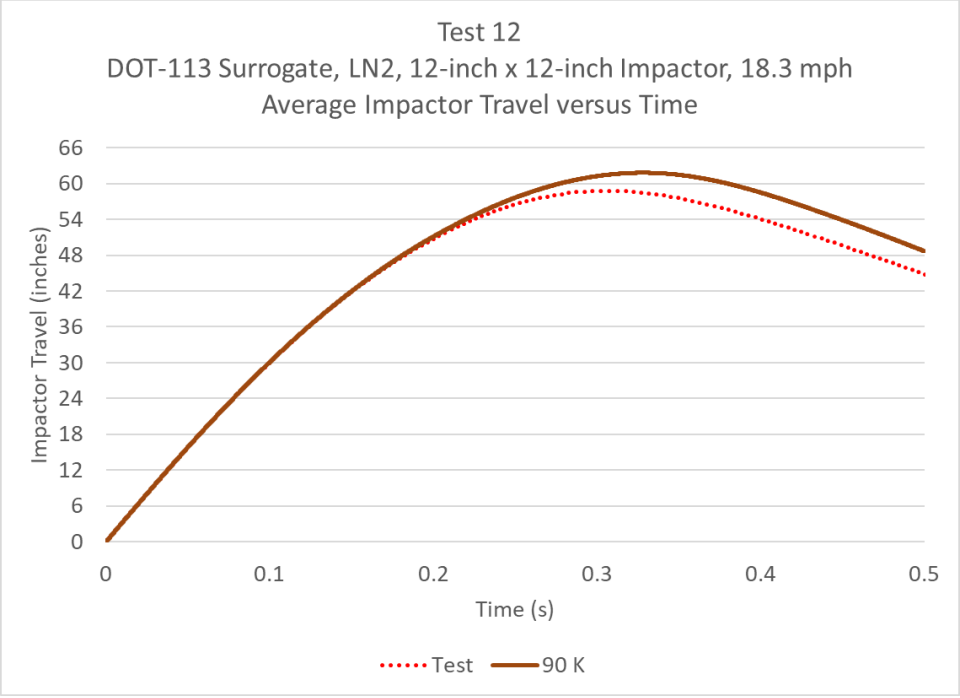

Figure B28. Impactor Displacement Versus Time for Test and EOS Material Model at 90 K, Variable E_m

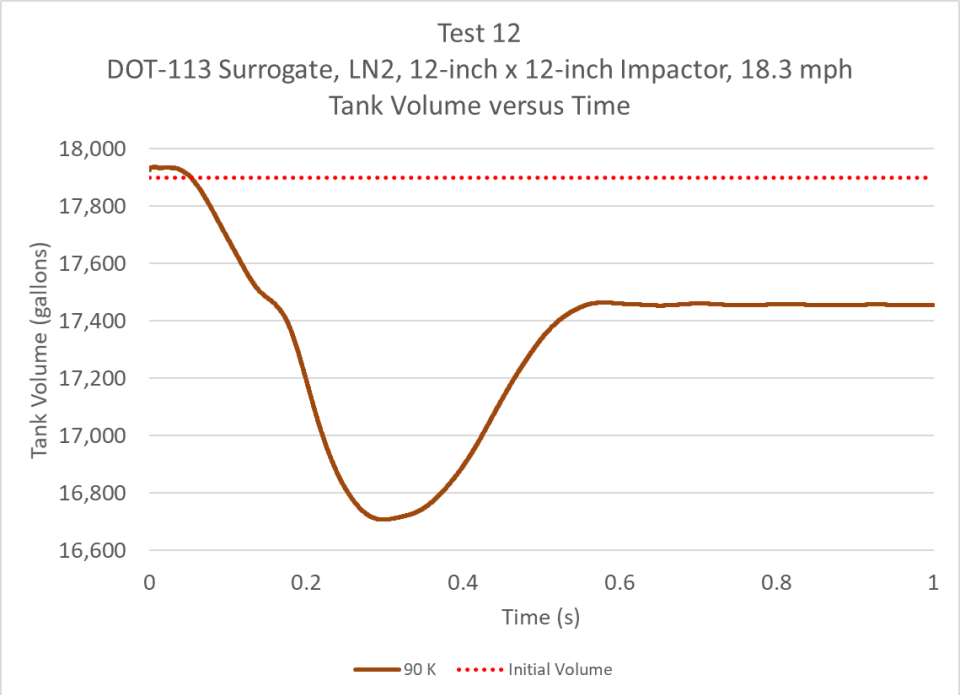

Figure B29. Tank Volume Versus Time for EOS Material Model at 90 K, Constant E_m

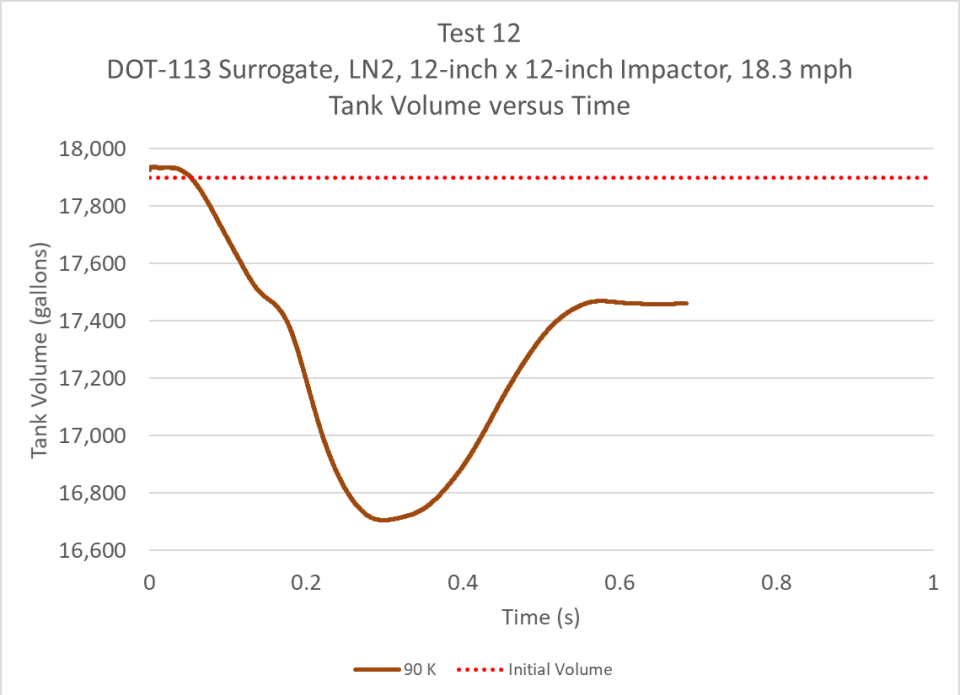

Figure B30. Tank Volume Versus Time for EOS Material Model at 90K, Variable E_m

B.3 GN2 at 92K

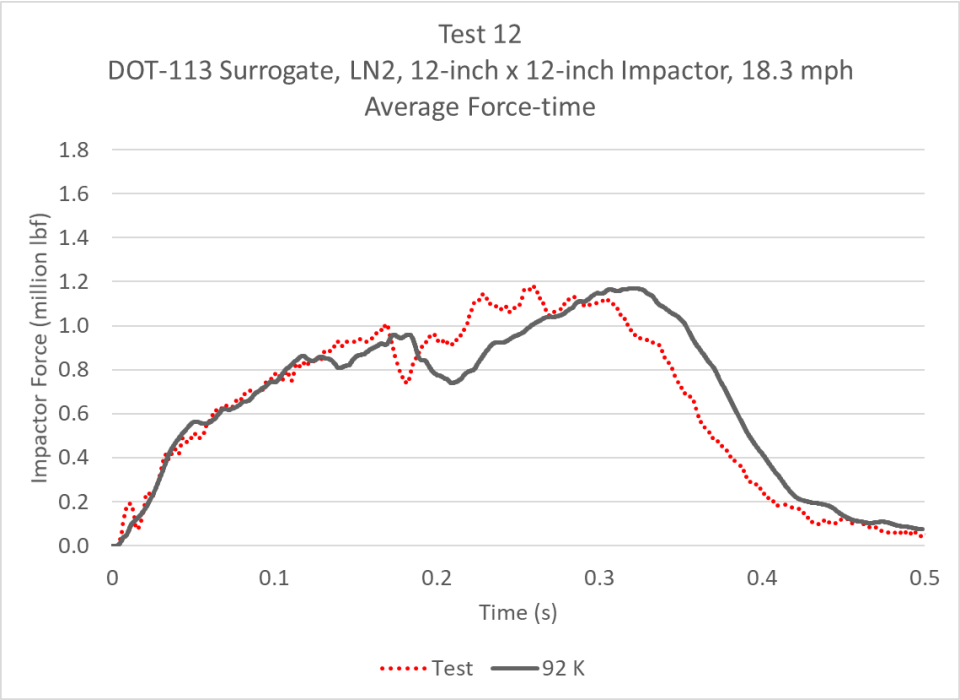

Figure B31. Impactor Force Versus Time for Test and EOS Material Model at 92 K, Constant E_m

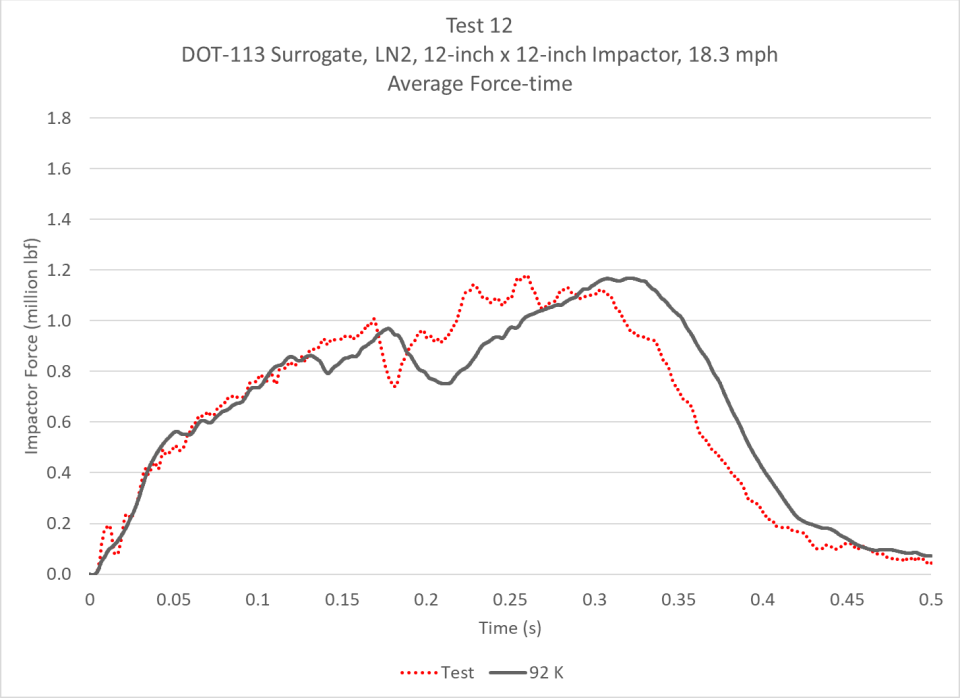

Figure B32. Impactor Force Versus Time for Test and EOS Material Model at 92 K, Variable E_m

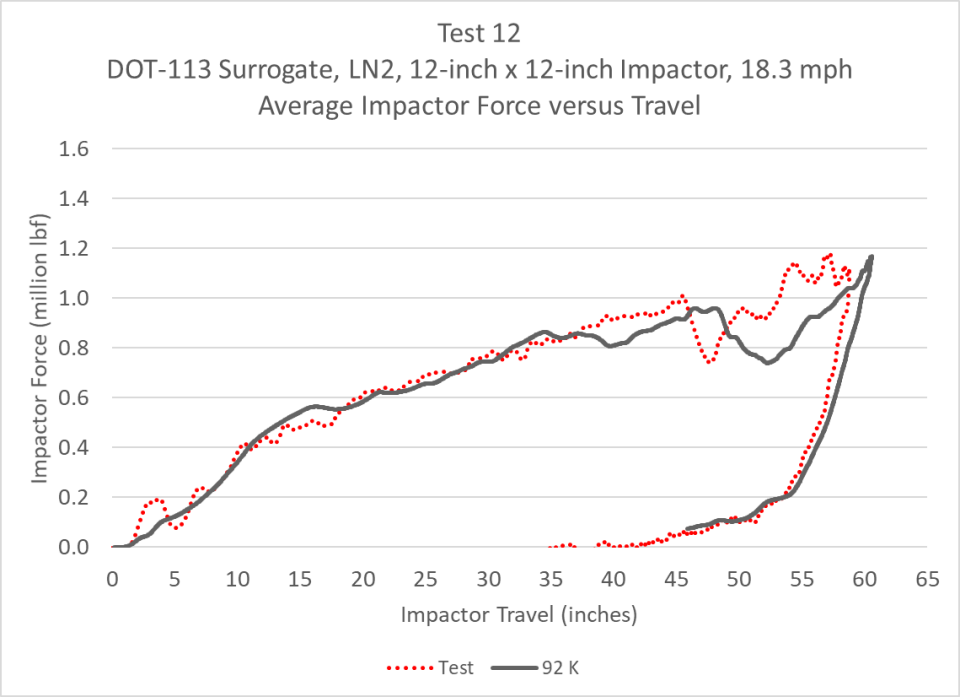

Figure B33. Impactor Force Versus Impactor Travel for Test and EOS Material Model at 92 K, Constant E_m

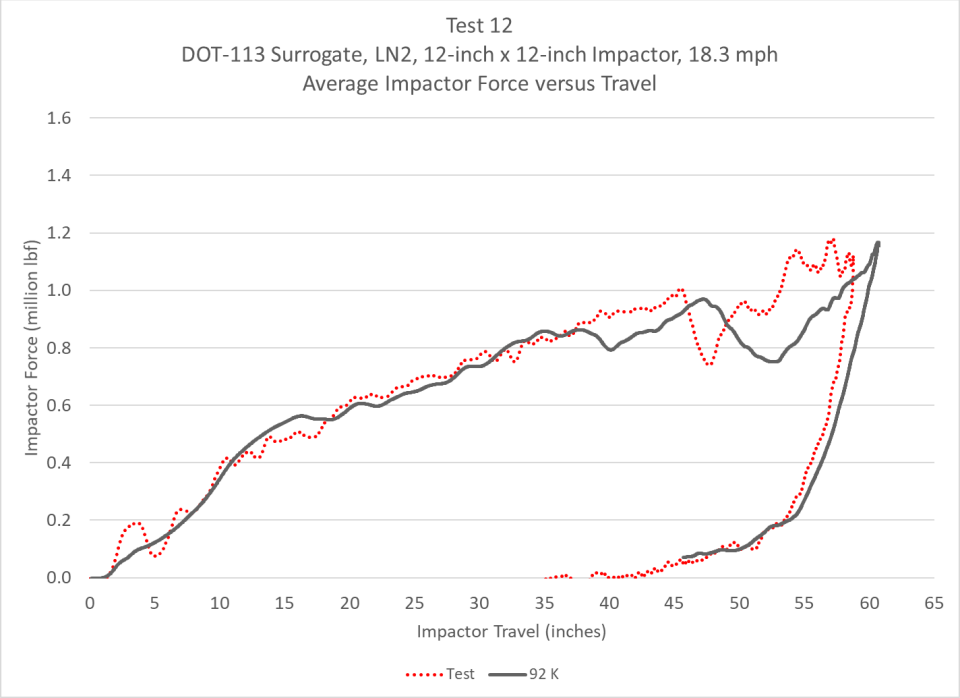

Figure B34. Impactor Force Versus Impactor Travel for Test and EOS Material Model at 92 K, Variable E_m

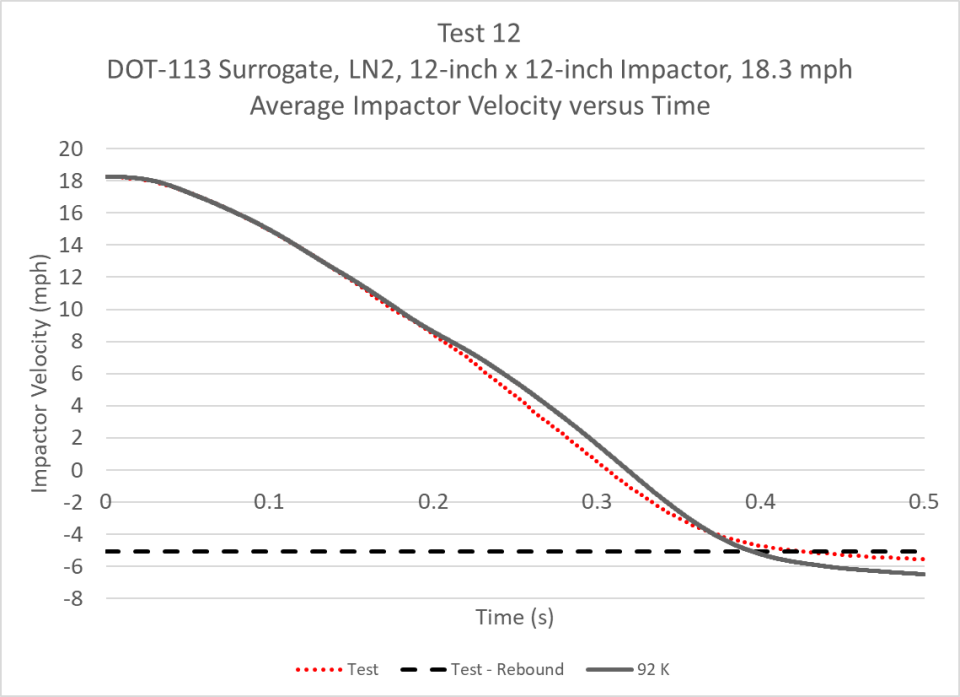

Figure B35. Impactor Velocity Versus Time for Test and EOS Material Model at 92 K, Constant E_m

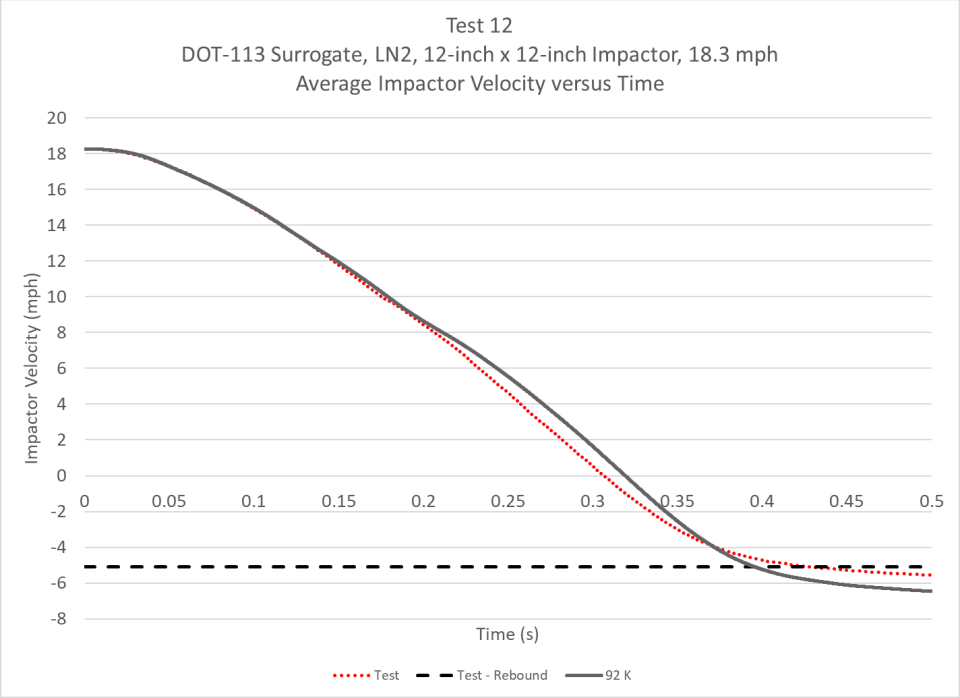

Figure B36. Impactor Velocity Versus Time for Test and EOS Material Model at 92 K, Variable E_m

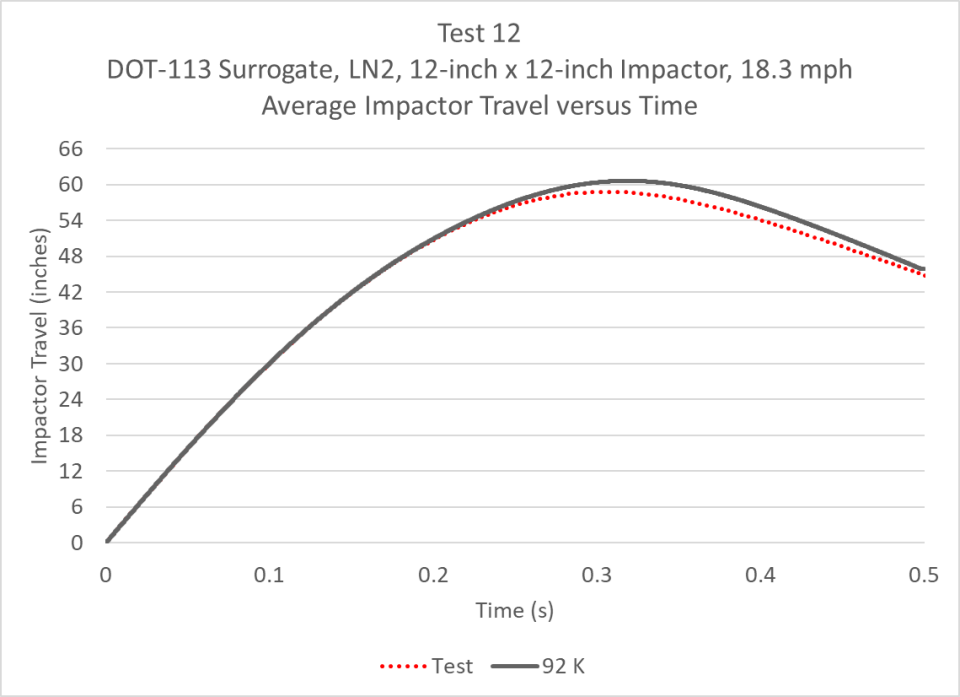

Figure B37. Impactor Displacement Versus Time for Test and EOS Material Model at 92 K, Constant E_m

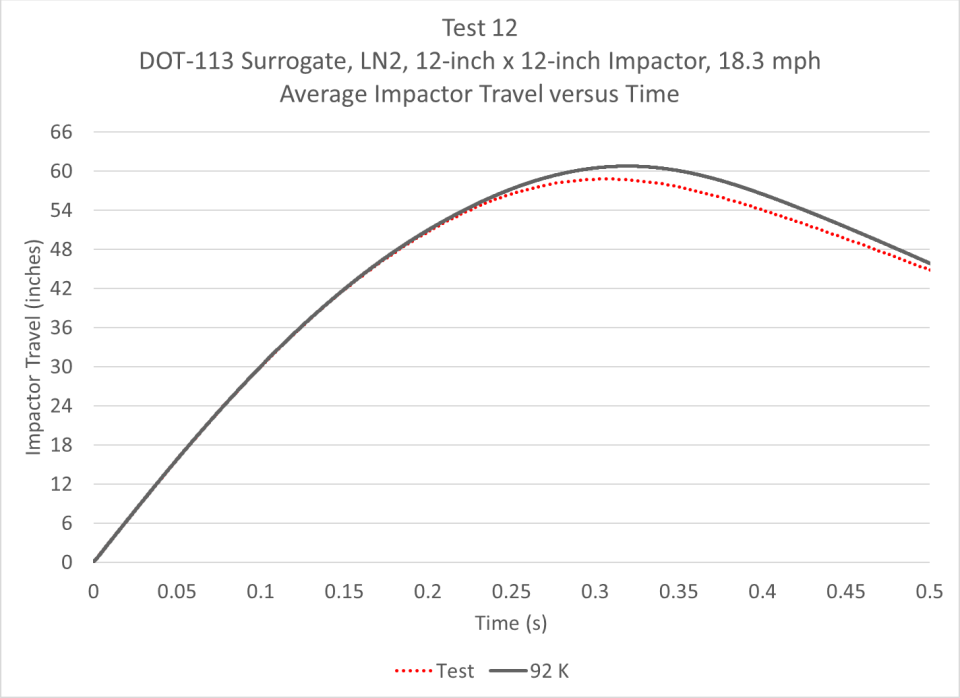

Figure B38. Impactor Displacement Versus Time for Test and EOS Material Model at 92 K, Variable E_m

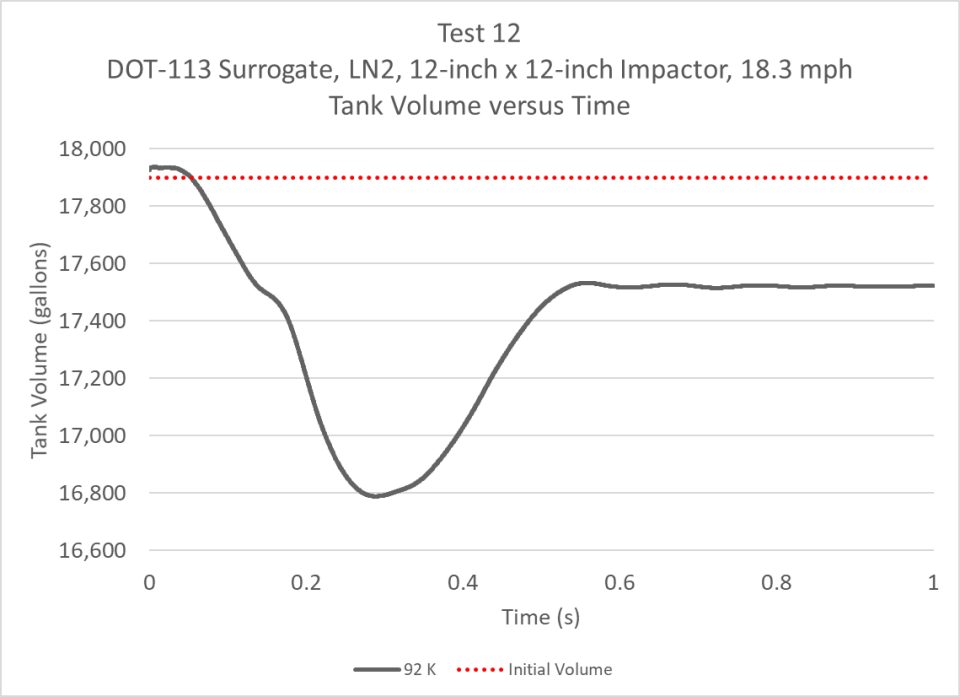

Figure B39. Tank Volume Versus Time for EOS Material Model at 92 K, Constant E_m

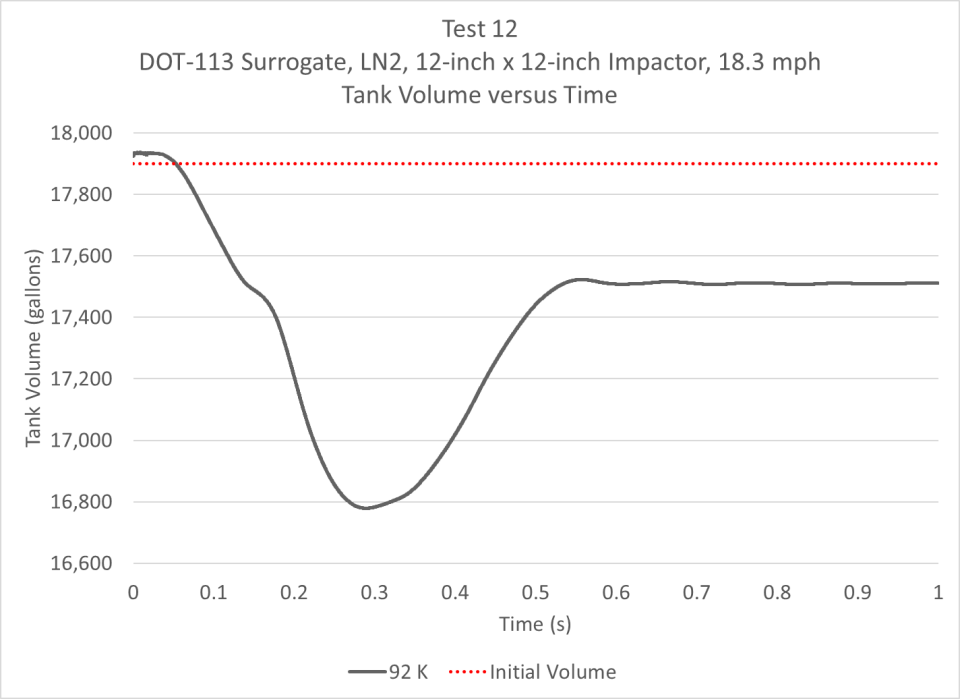

Figure B40. Tank Volume Versus Time for EOS Material Model at 92 K, Variable E_m

B.4 GN2 at 94K

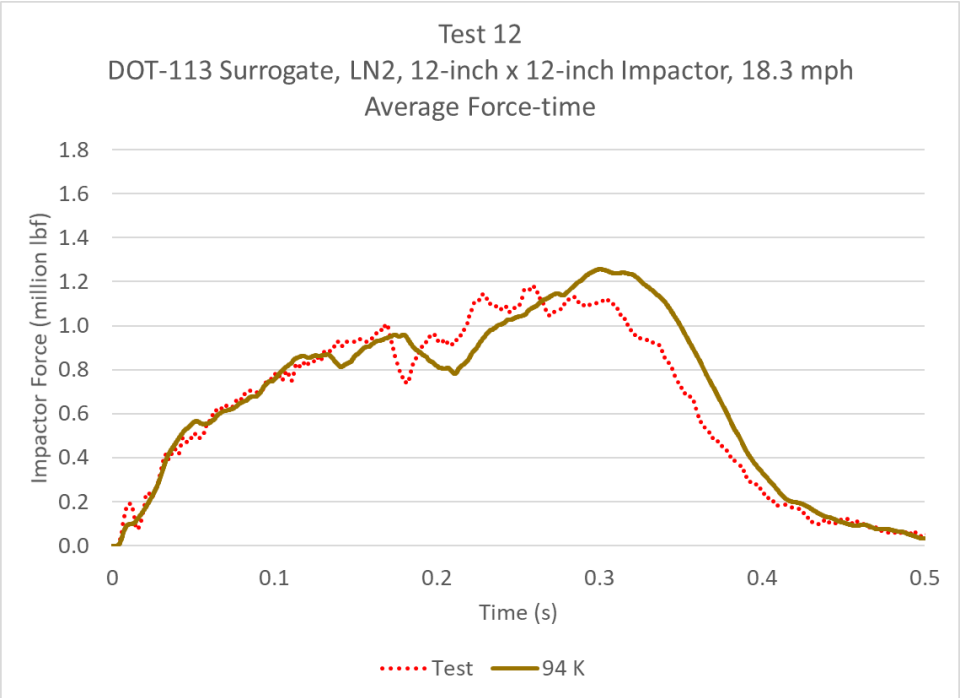

Figure B41. Impactor Force Versus Time for Test and EOS Material Model at 94 K, Constant E_m

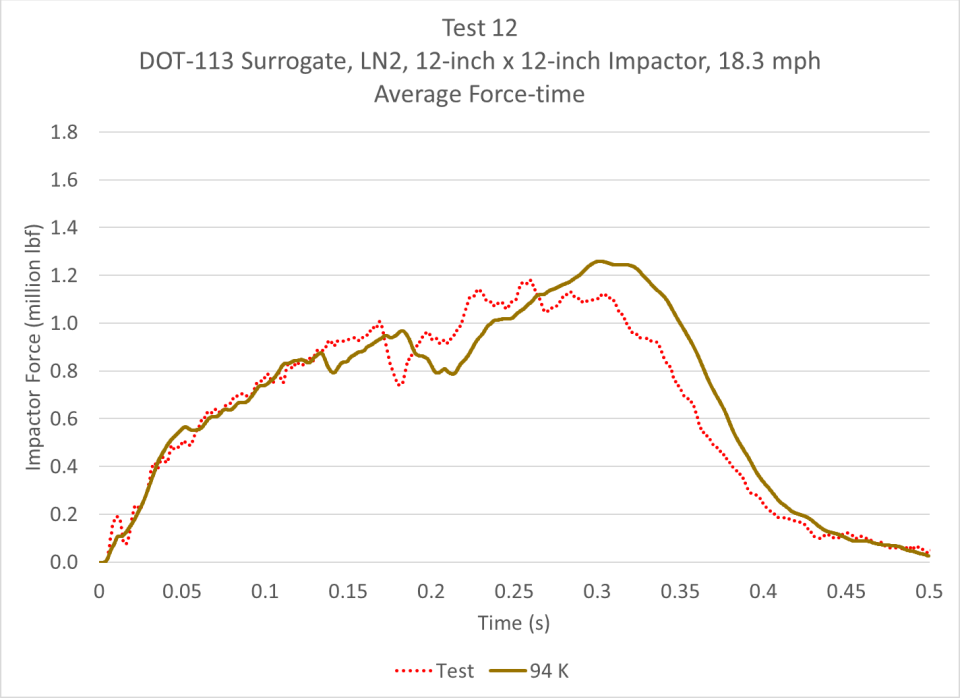

Figure B42. Impactor Force Versus Time for Test and EOS Material Model at 94 K, Variable E_m

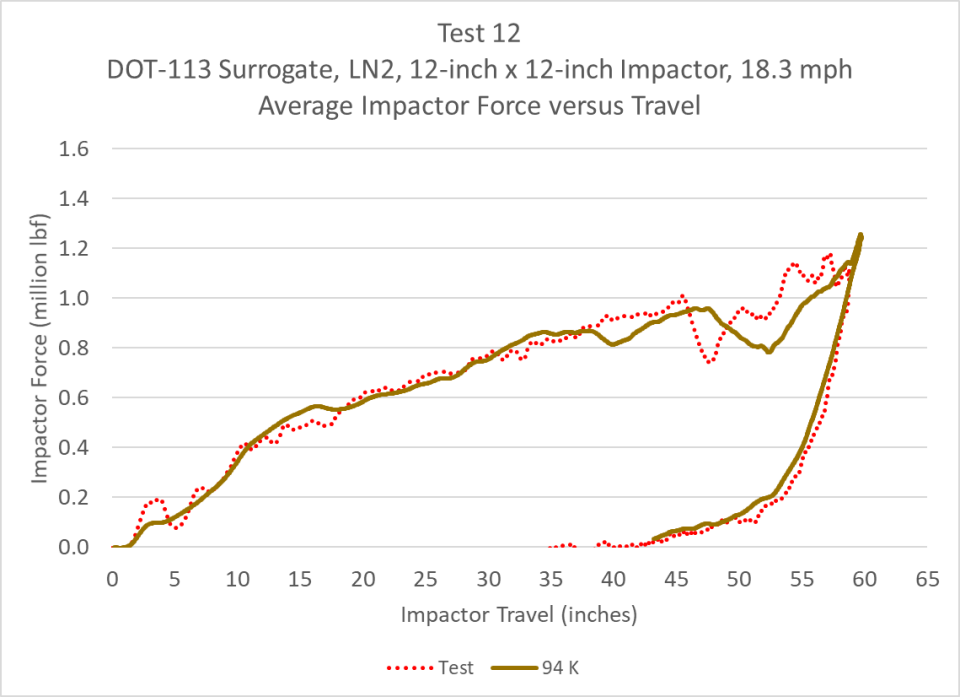

Figure B43. Impactor Force Versus Impactor Travel for Test and EOS Material Model at 94 K, Constant E_m

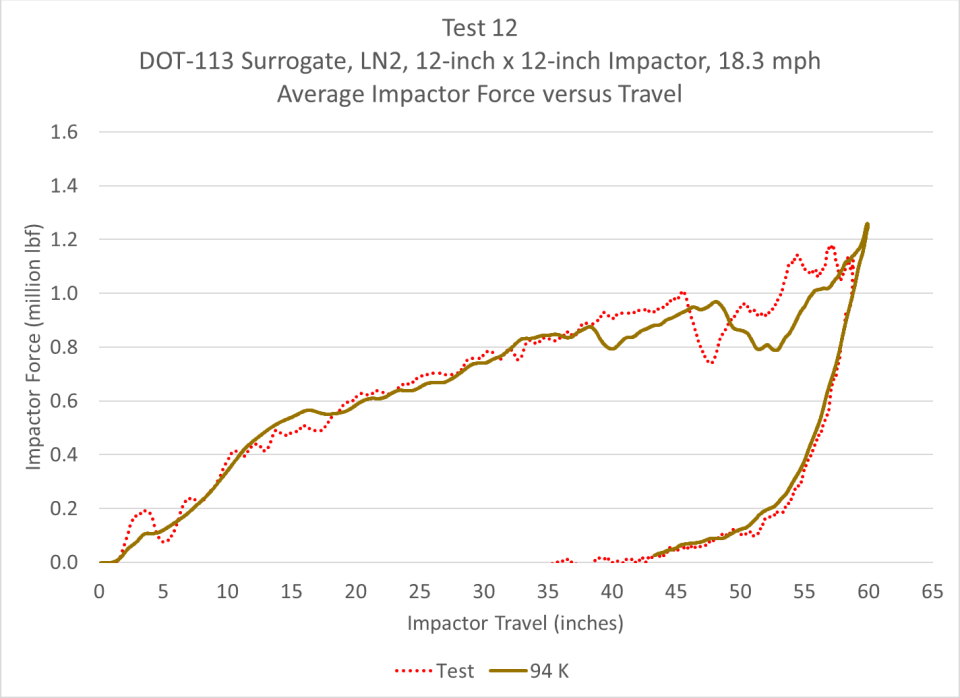

Figure B44. Impactor Force Versus Impactor Travel for Test and EOS Material Model at 94 K, Variable E_m

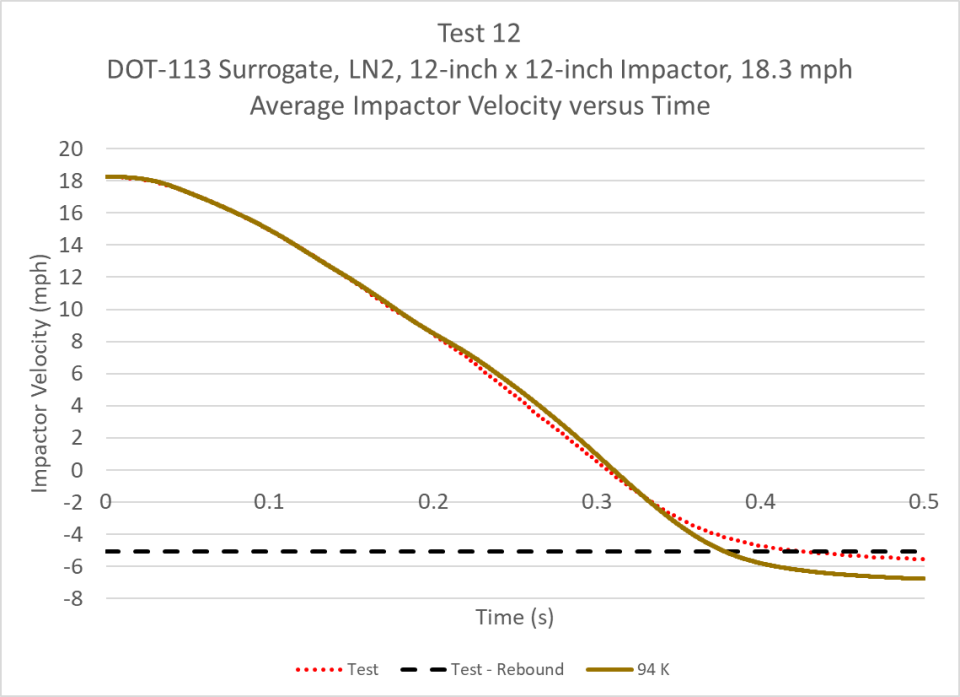

Figure B45. Impactor Velocity Versus Time for Test and EOS Material Model at 94 K, Constant E_m

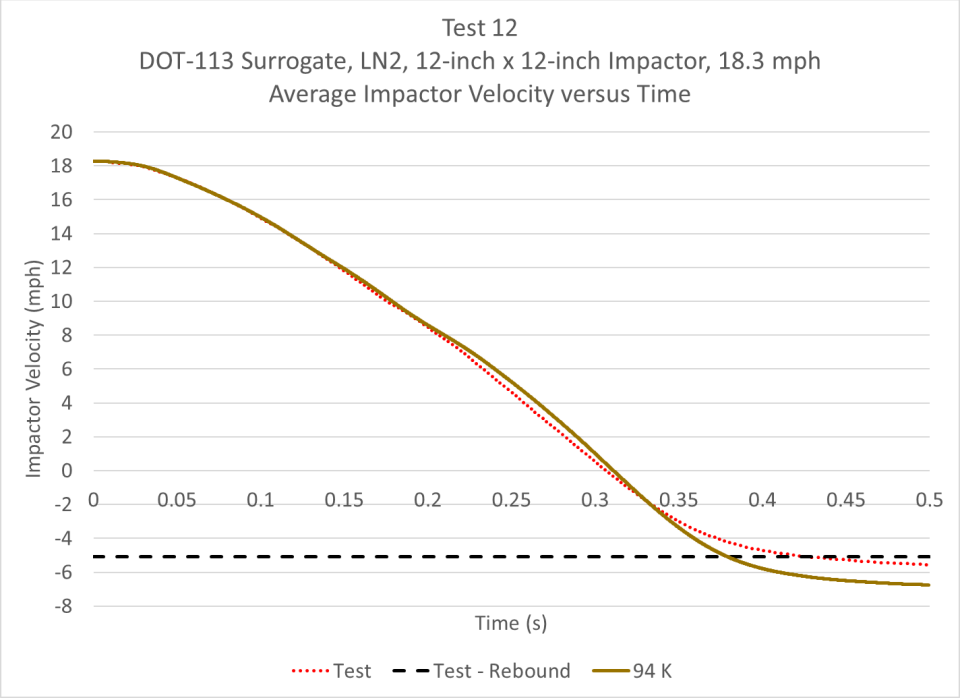

Figure B46. Impactor Velocity Versus Time for Test and EOS Material Model at 94 K, Variable E_m

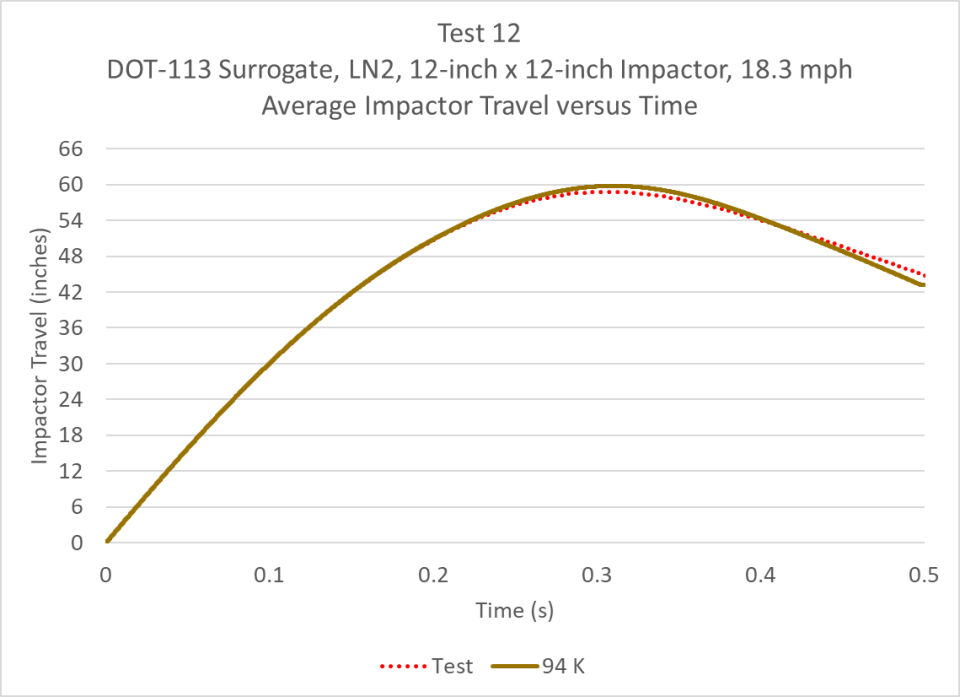

Figure B47. Impactor Displacement Versus Time for Test and EOS Material Model at 94 K, Constant E_m

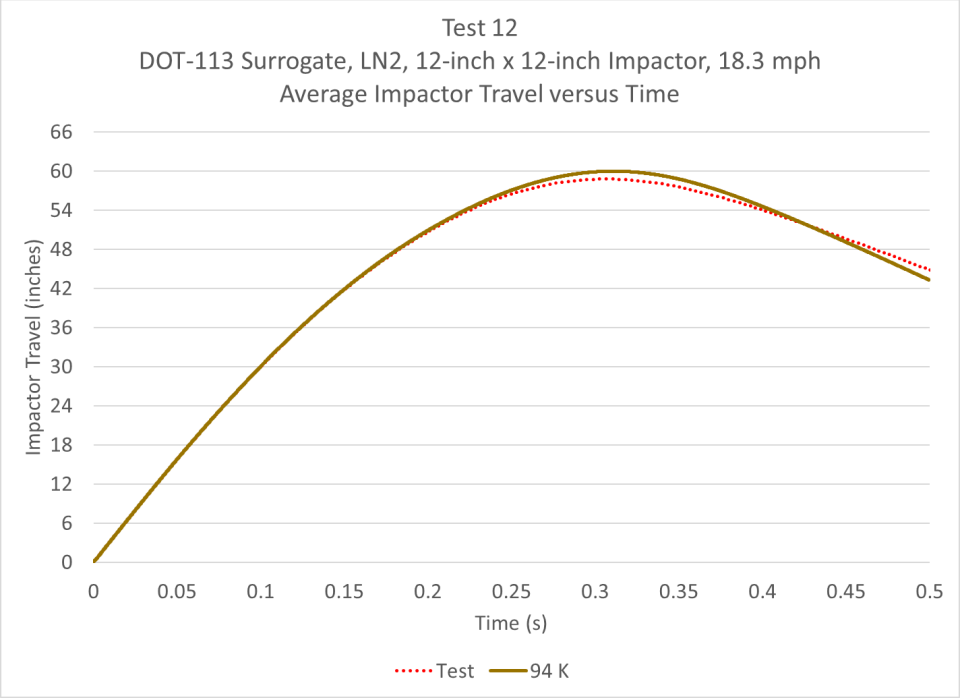

Figure B48. Impactor Displacement Versus Time for Test and EOS Material Model at 94 K, Variable E_m

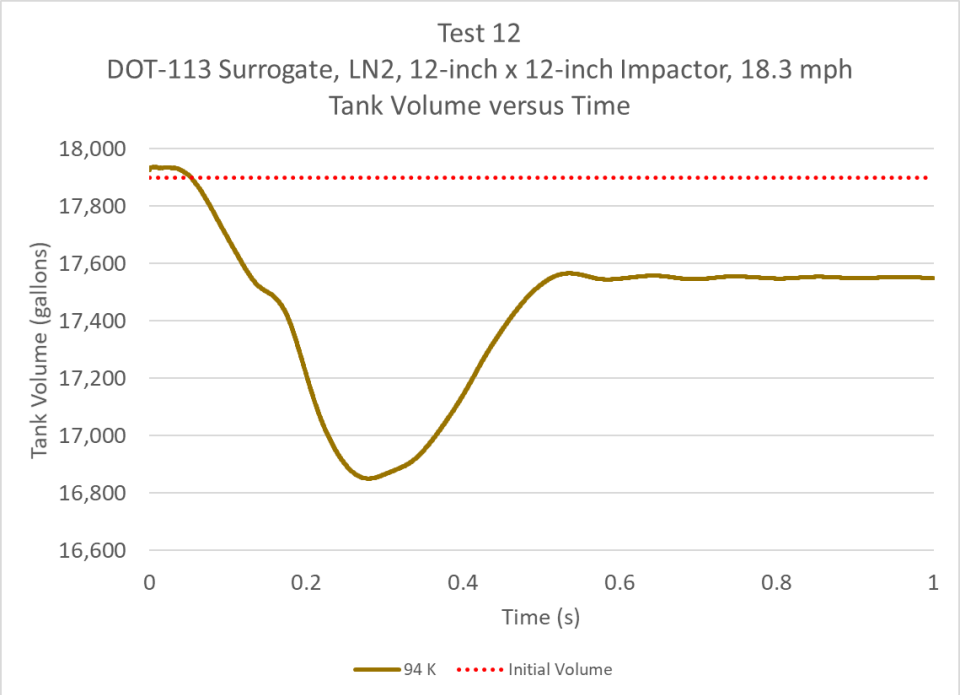

Figure B49. Tank Volume Versus Time for EOS Material Model at 94 K, Constant E_m

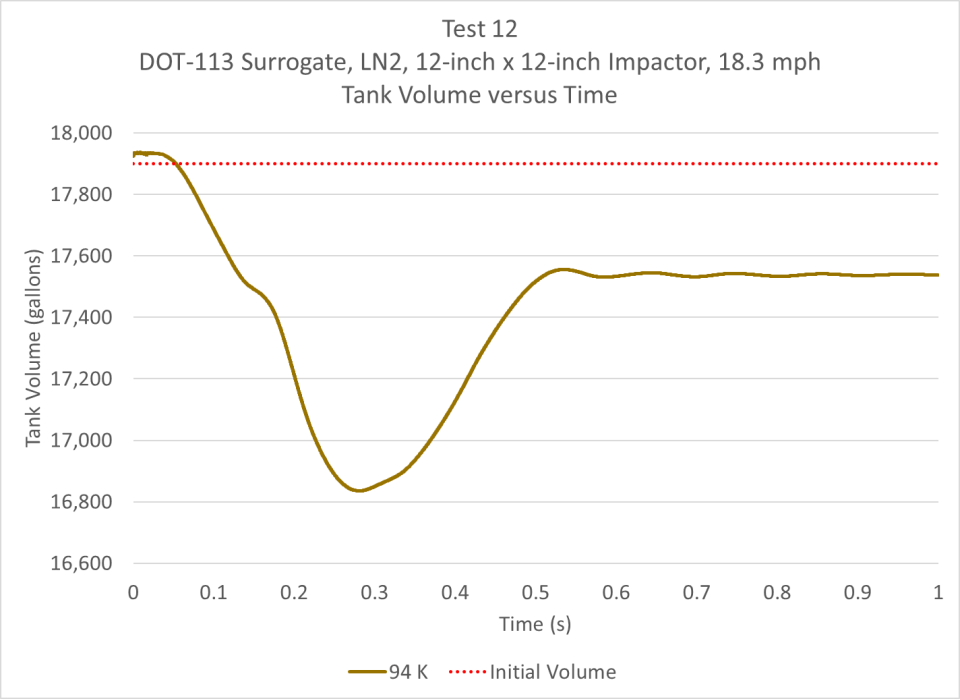

Figure B50. Tank Volume Versus Time for EOS Material Model at 94 K, Variable E_m

B.5 GN2 at 96K

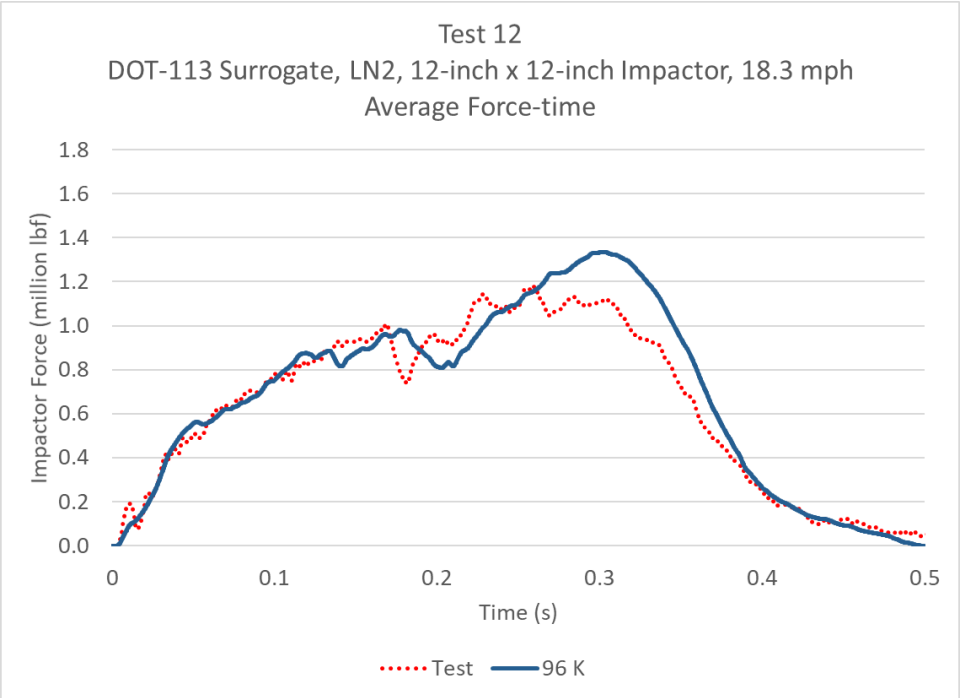

Figure B51. Impactor Force Versus Time for Test and EOS Material Model at 96 K, Constant E_m

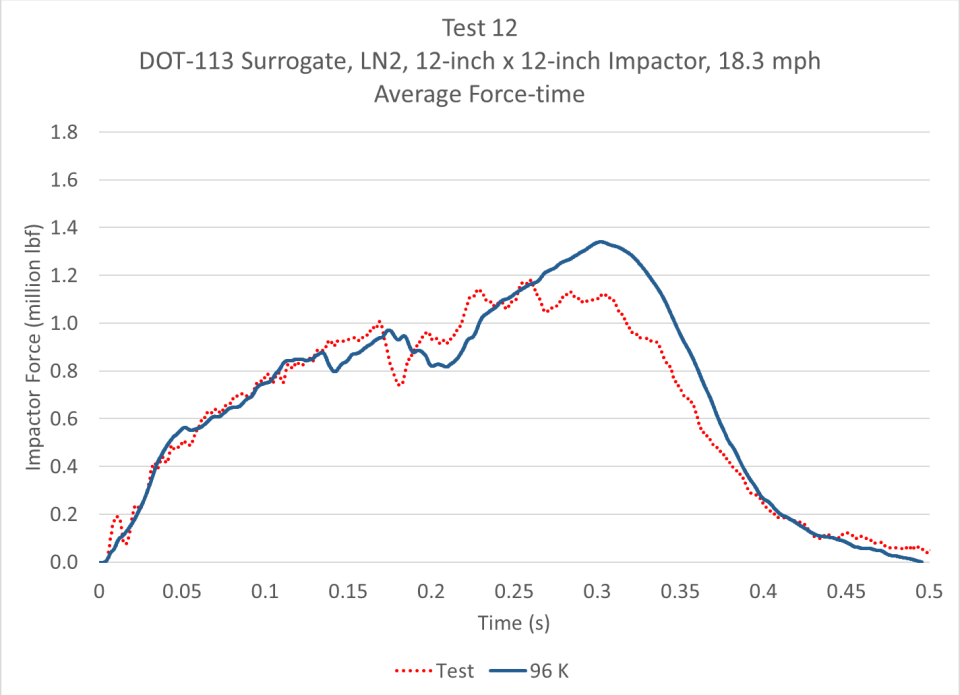

Figure B52. Impactor Force Versus Time for Test and EOS Material Model at 96 K, Variable E_m

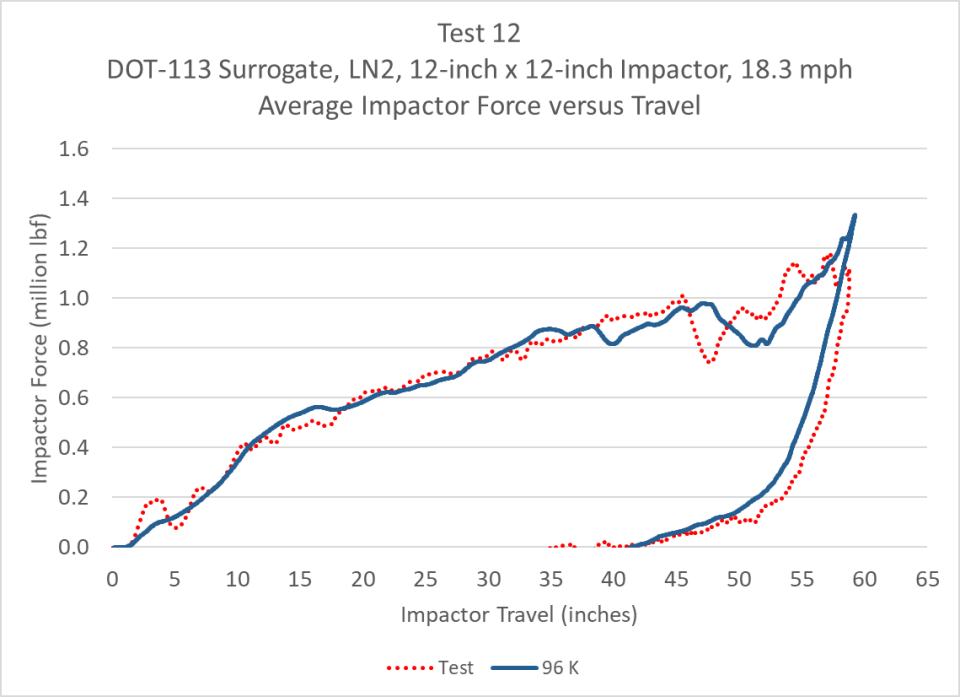

Figure B53. Impactor Force Versus Impactor Travel for Test and EOS Material Model at 96 K, Constant E_m

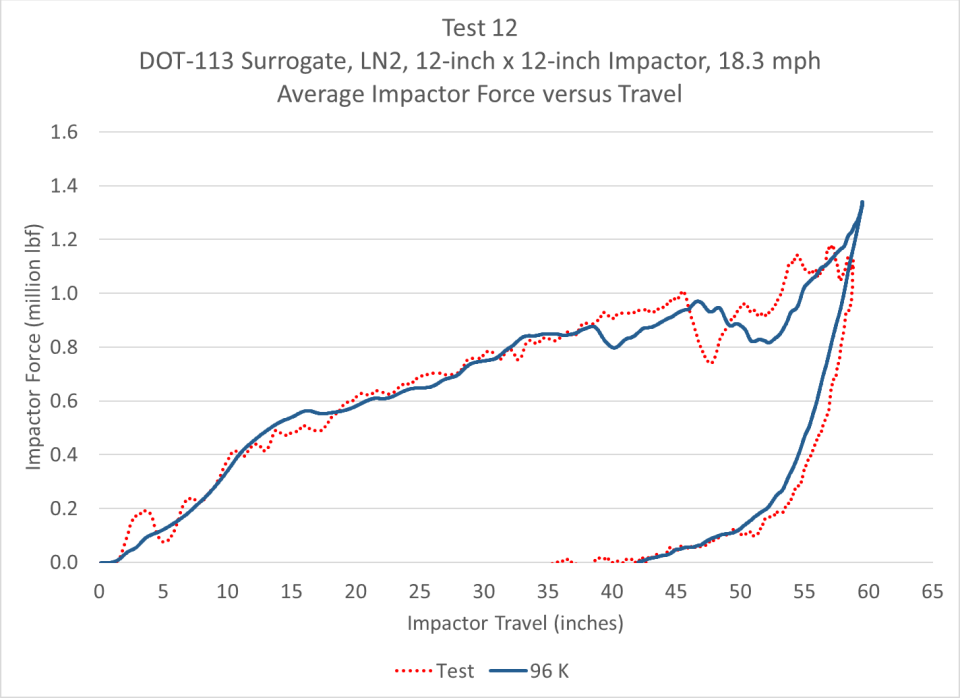

Figure B54. Impactor Force Versus Impactor Travel for Test and EOS Material Model at 96 K, Variable E_m

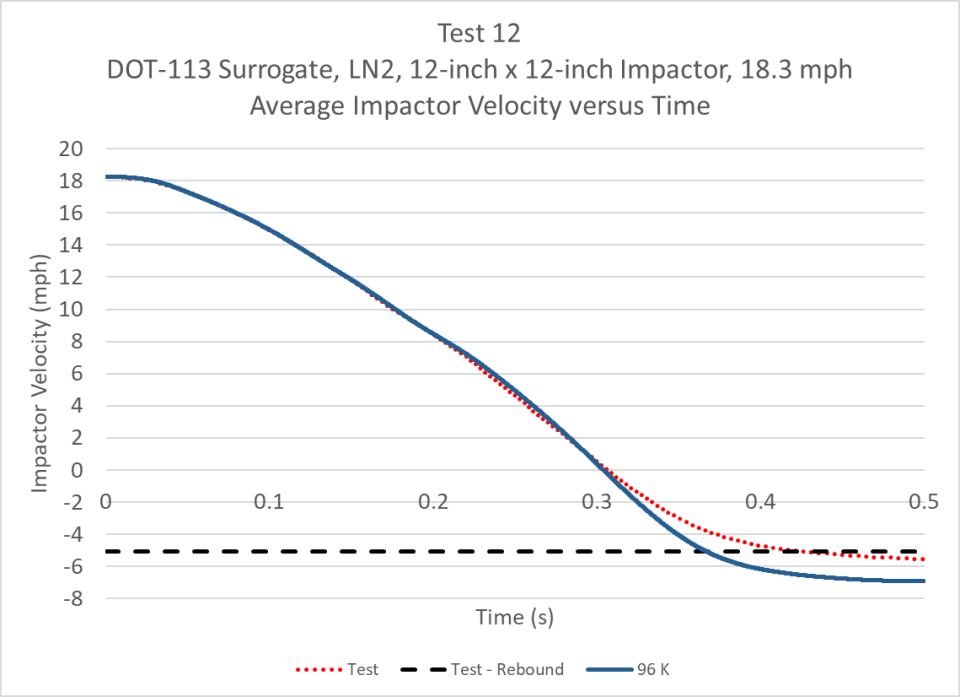

Figure B55. Impactor Velocity Versus Time for Test and EOS Material Model at 96 K, Constant E_m

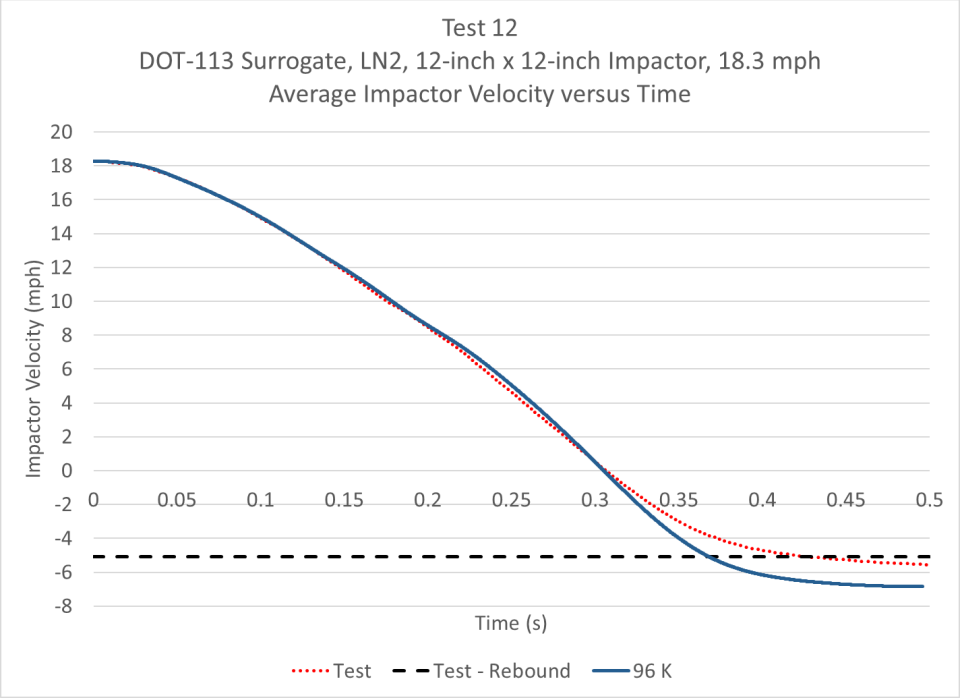

Figure B56. Impactor Velocity Versus Time for Test and EOS Material Model at 96 K, Variable E_m

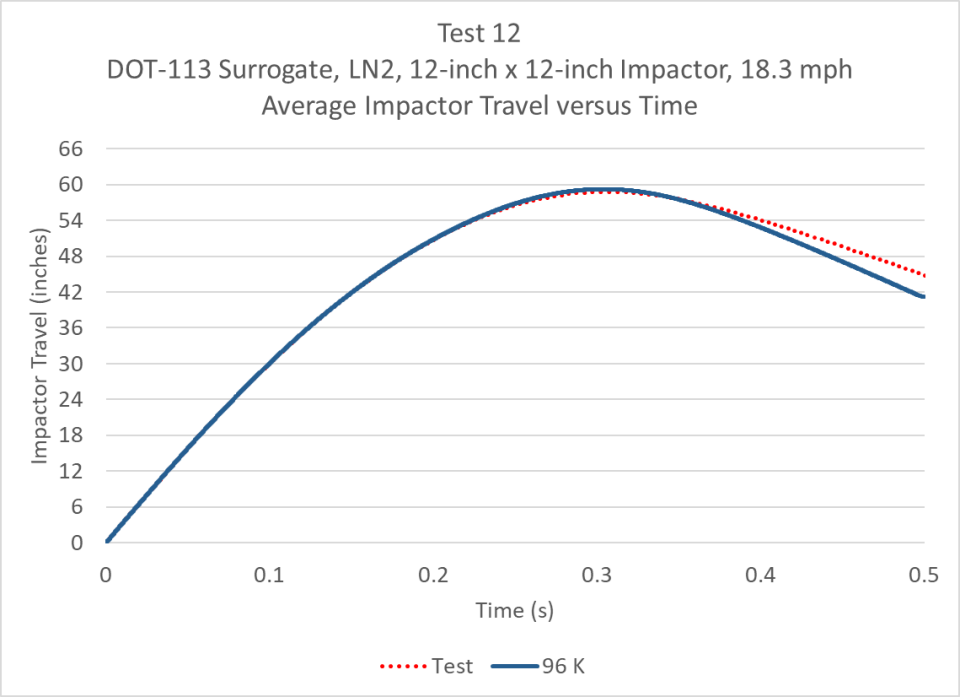

Figure B57. Impactor Displacement Versus Time for Test and EOS Material Model at 96 K, Constant E_m

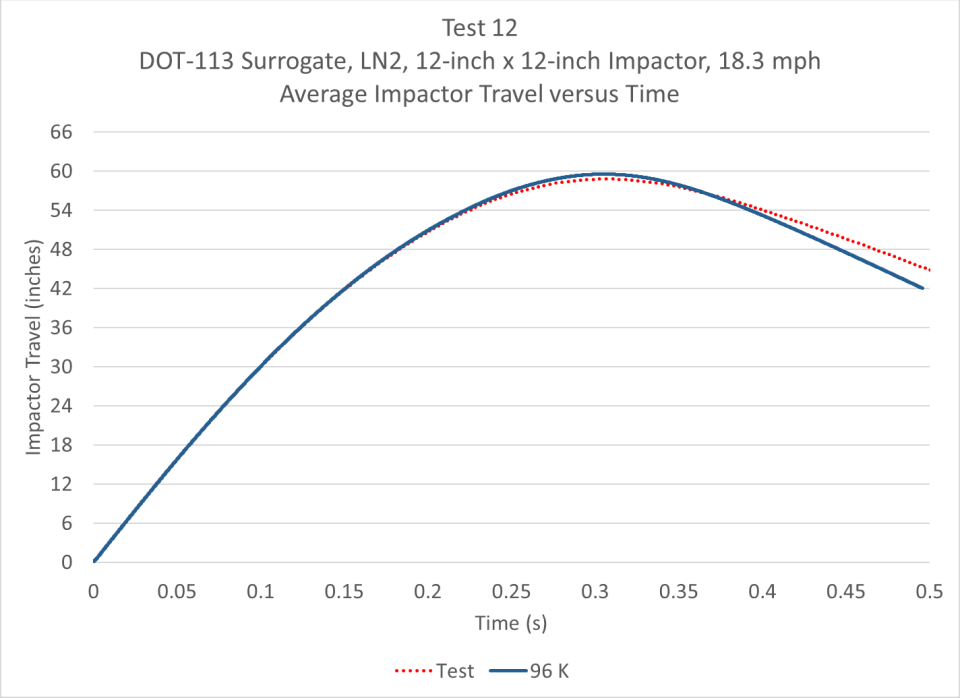

Figure B58. Impactor Displacement Versus Time for Test and EOS Material Model at 96 K, Variable E_m

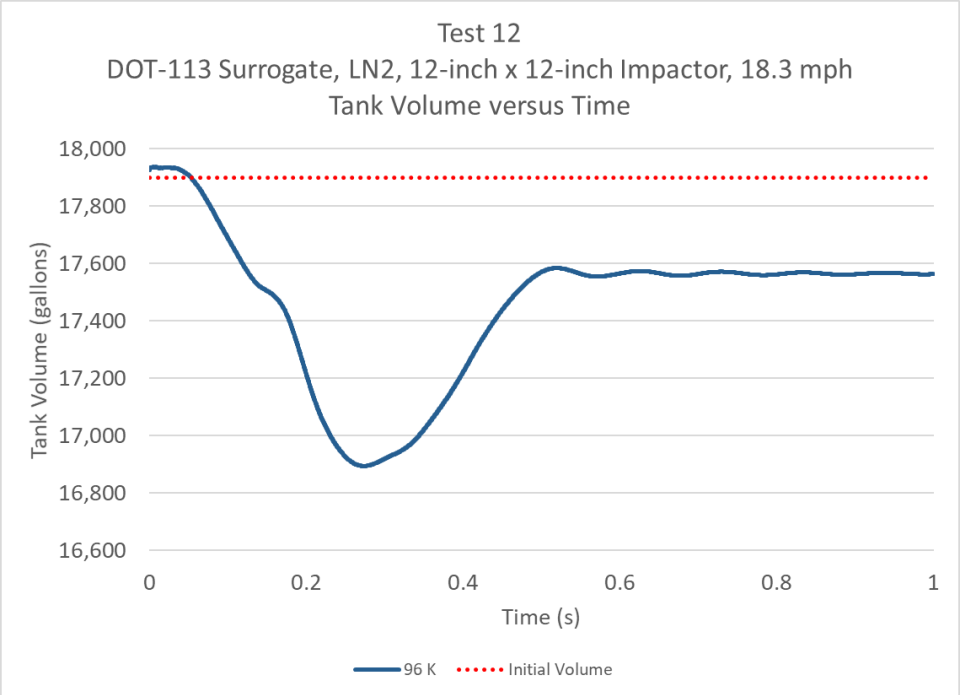

Figure B59. Tank Volume Versus Time for EOS Material Model at 96 K, Constant E_m

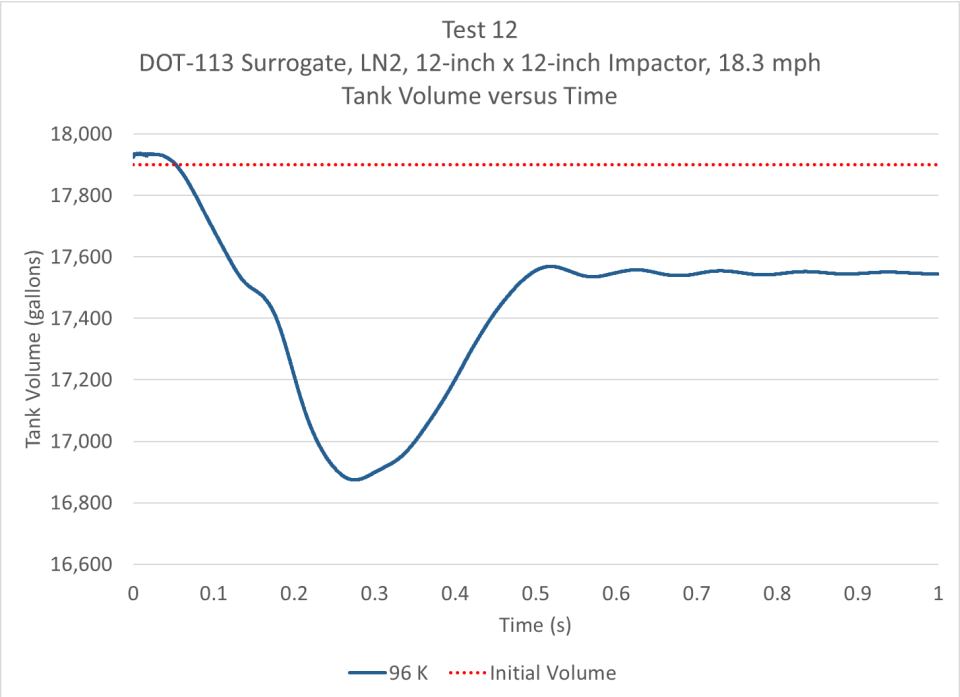

Figure B60. Tank Volume Versus Time for EOS Material Model at 96 K, Variable E_m

B.6 GN2 at 98K

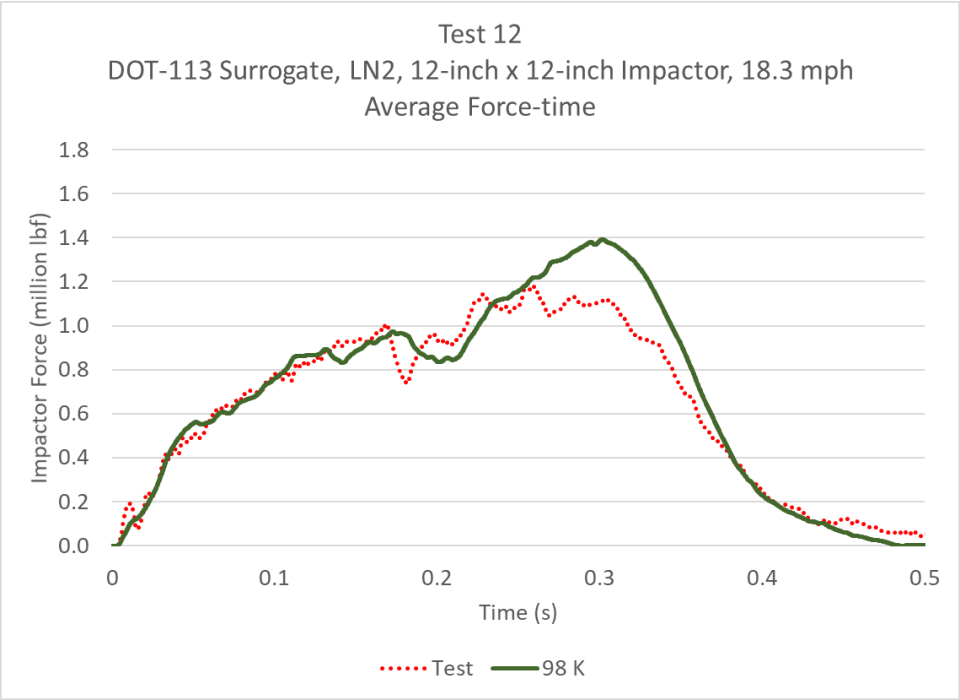

Figure B61. Impactor Force Versus Time for Test and EOS Material Model at 98 K, Constant E_m

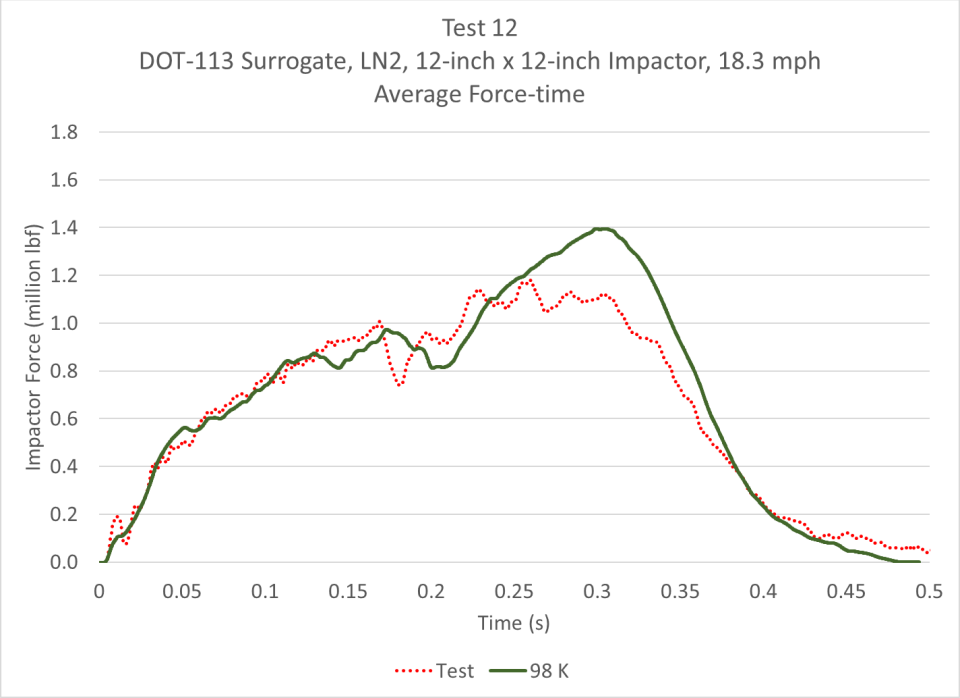

Figure B62. Impactor Force Versus Time for Test and EOS Material Model at 98 K, Variable E_m

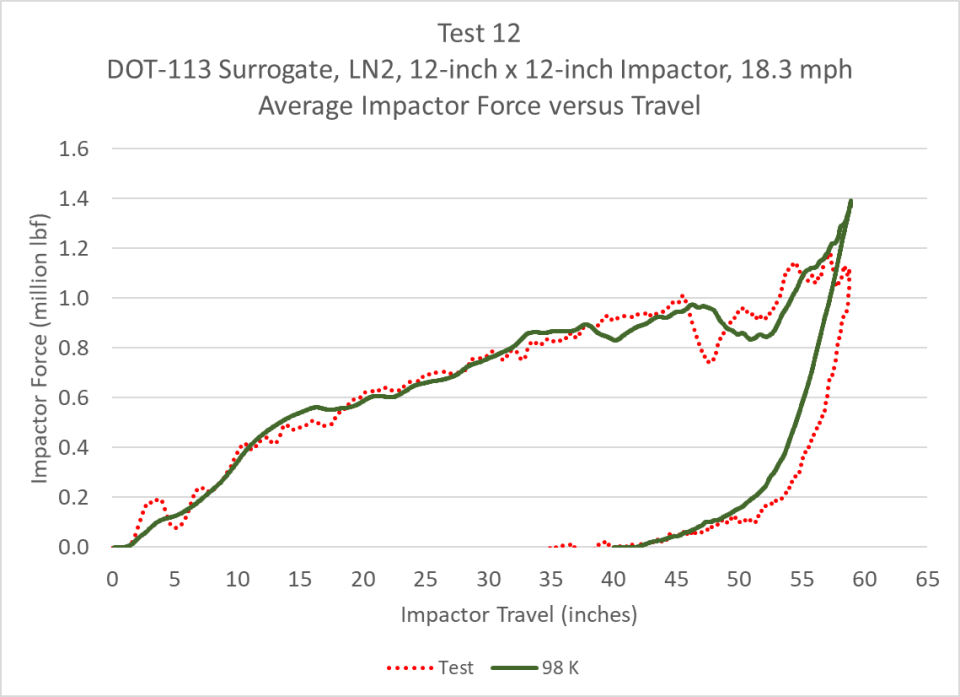

Figure B63. Impactor Force Versus Impactor Travel for Test and EOS Material Model at 98 K, Constant E_m

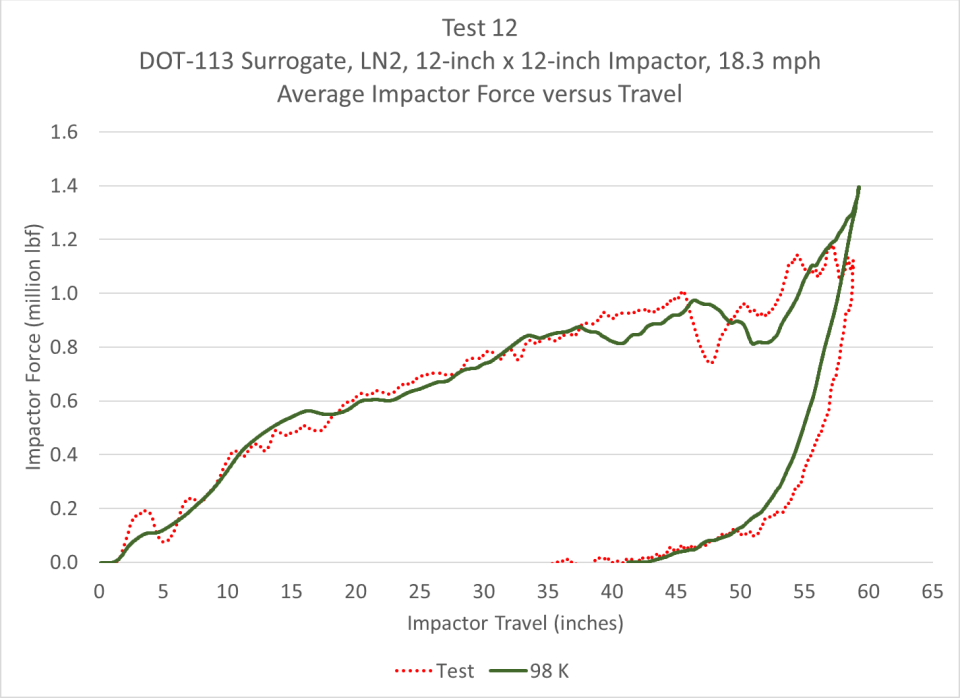

Figure B64. Impactor Force Versus Impactor Travel for Test and EOS Material Model at 98 K, Variable E_m

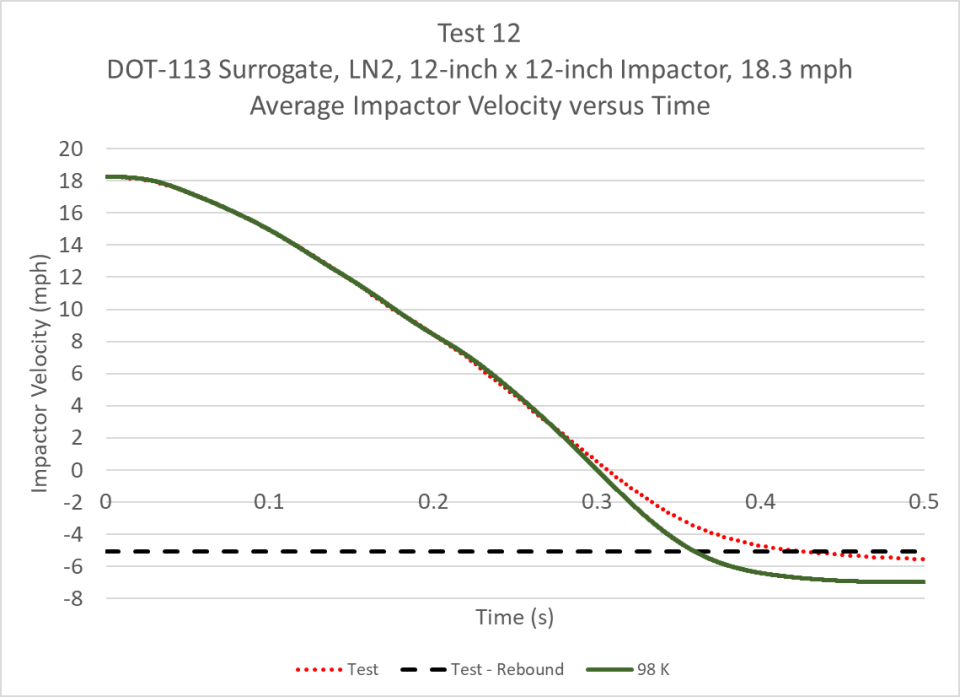

Figure B65. Impactor Velocity Versus Time for Test and EOS Material Model at 98 K, Constant E_m

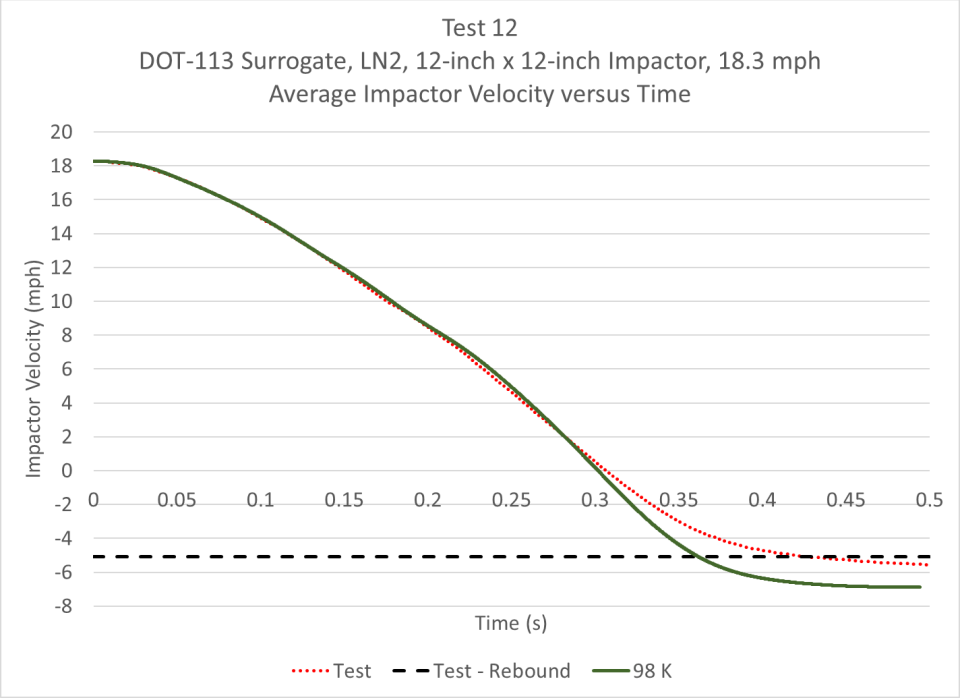

Figure B66. Impactor Velocity Versus Time for Test and EOS Material Model at 98 K, Variable E_m

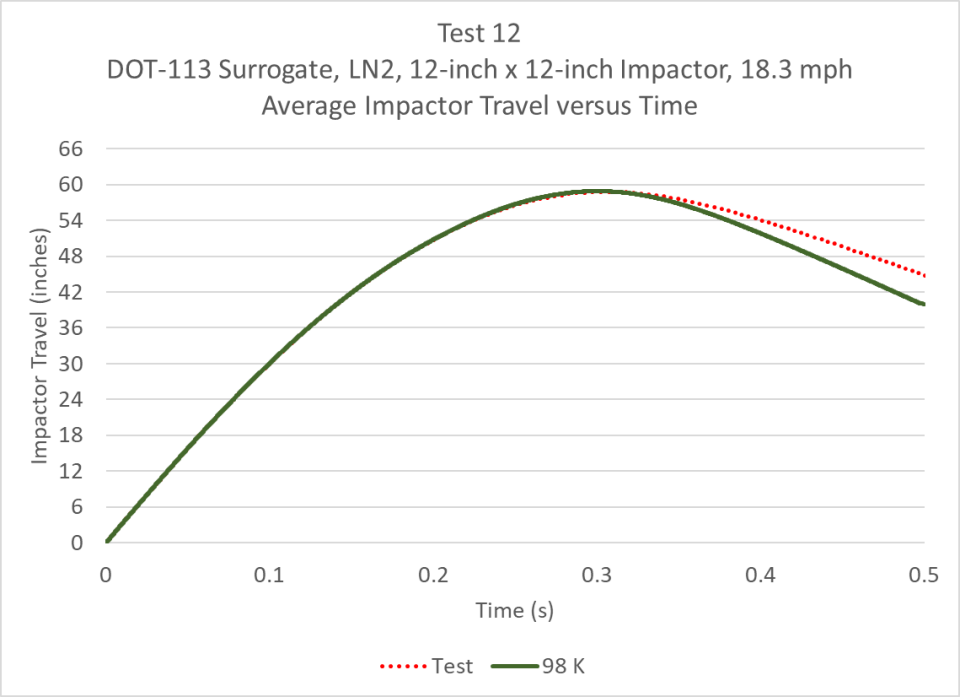

Figure B67. Impactor Displacement Versus Time for Test and EOS Material Model at 98 K, Constant E_m

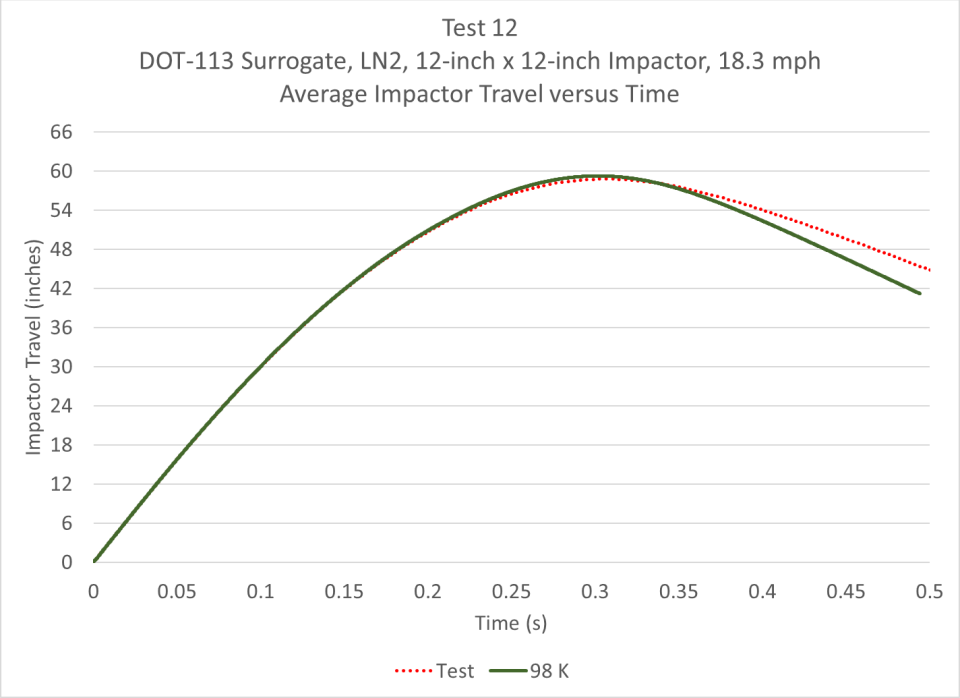

Figure B68. Impactor Displacement Versus Time for Test and EOS Material Model at 98 K, Variable E_m

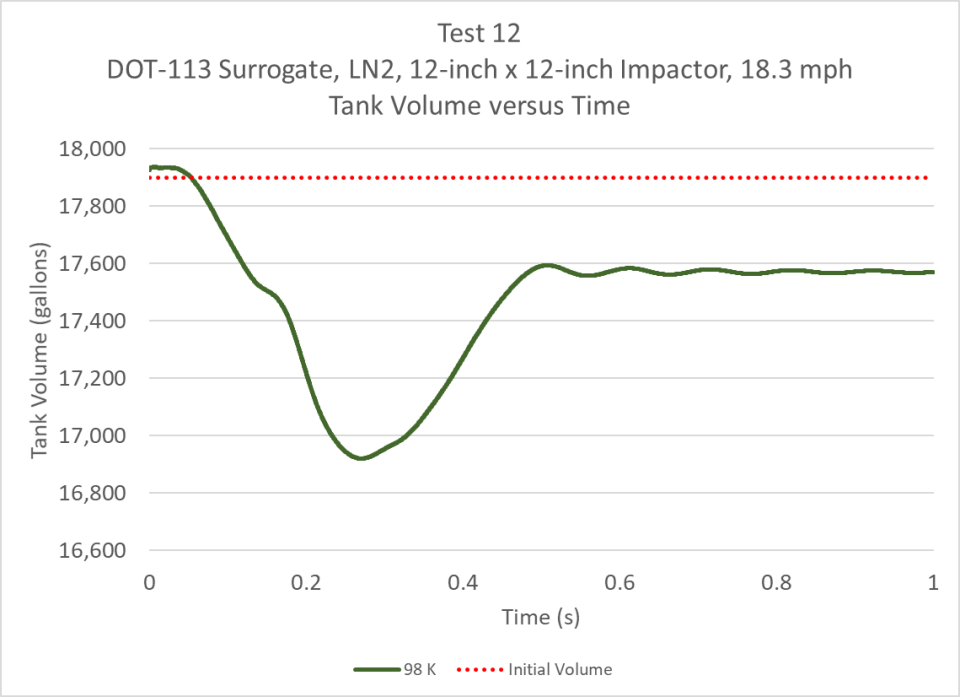

Figure B69. Tank Volume Versus Time for EOS Material Model at 98 K, Constant E_m

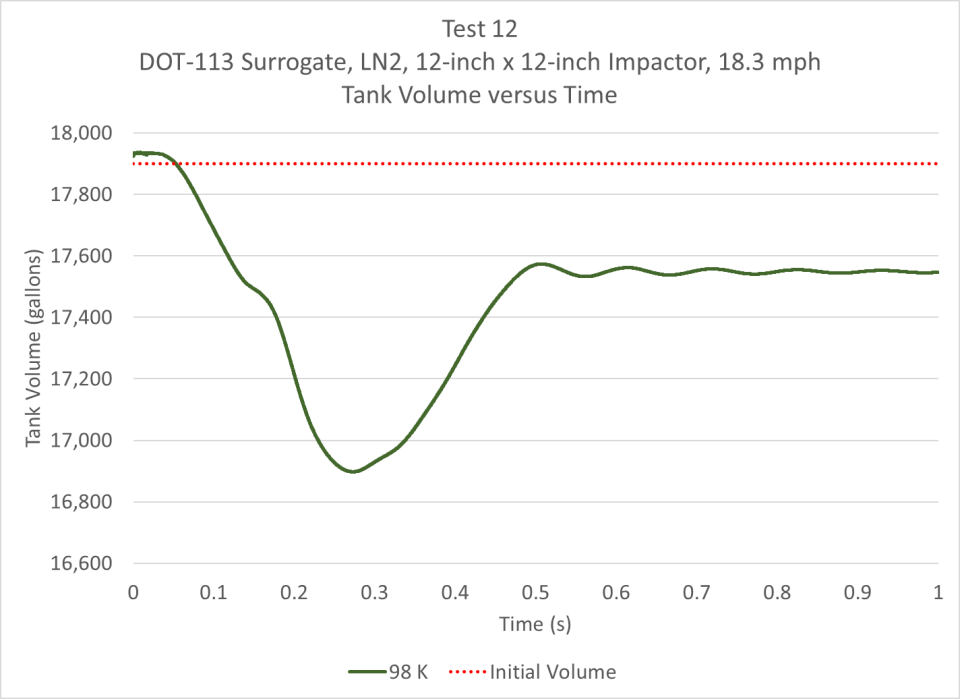

Figure B70. Tank Volume Versus Time for EOS Material Model at 98 K, Variable E_m

B.7 GN2 at 100K

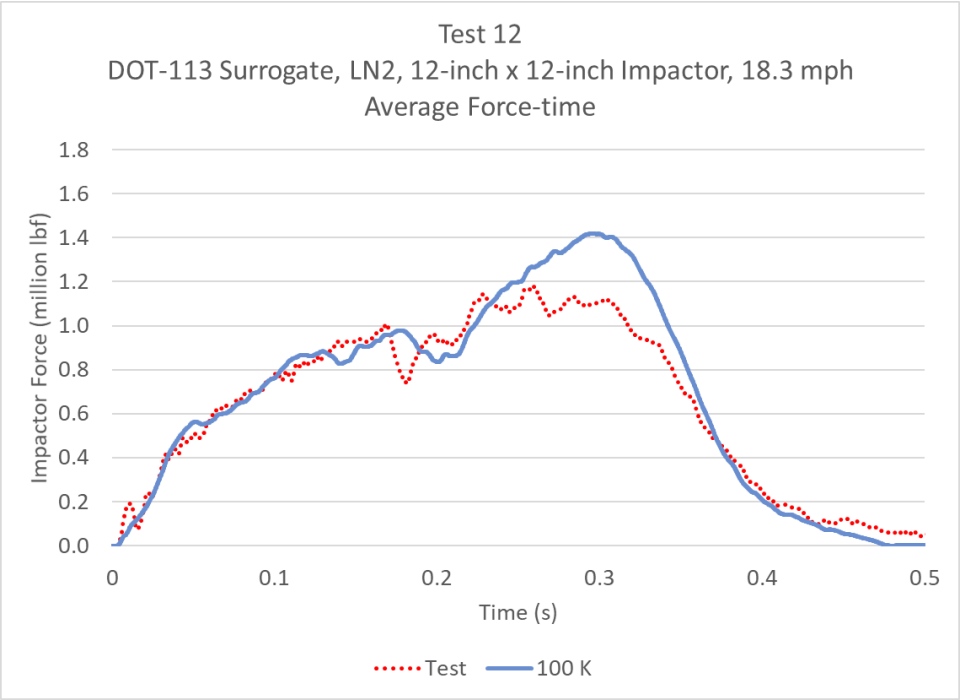

Figure B71. Impactor Force Versus Time for Test and EOS Material Model at 100 K, Constant E_m

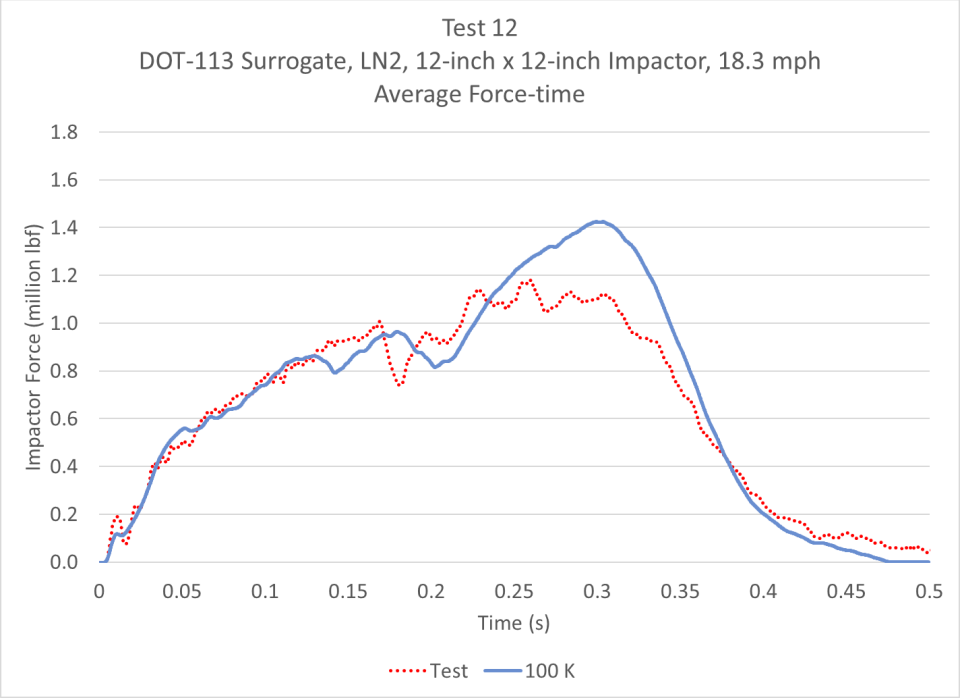

Figure B72. Impactor Force Versus Time for Test and EOS Material Model at 100 K, Variable E_m

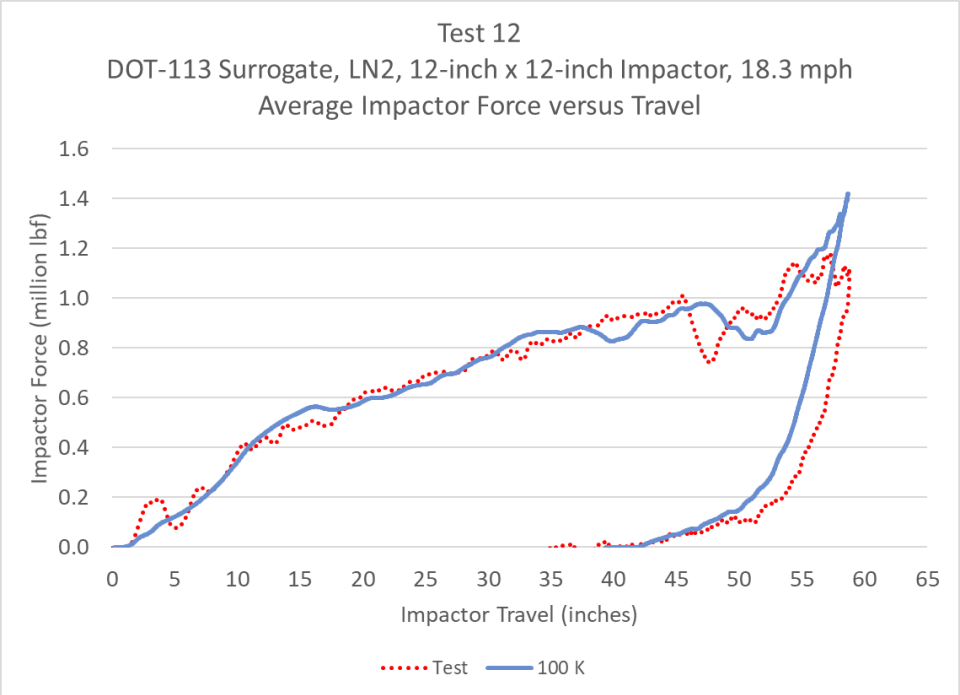

Figure B73. Impactor Force Versus Impactor Travel for Test and EOS Material Model at 100 K, Constant E_m

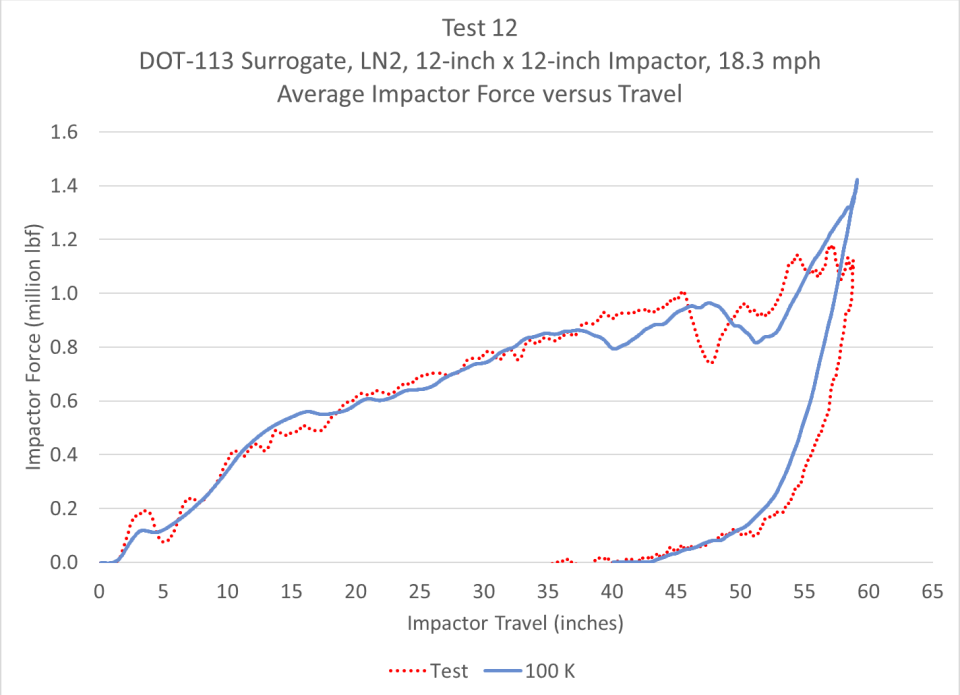

Figure B74. Impactor Force Versus Impactor Travel for Test and EOS Material Model at 100 K, Variable E_m

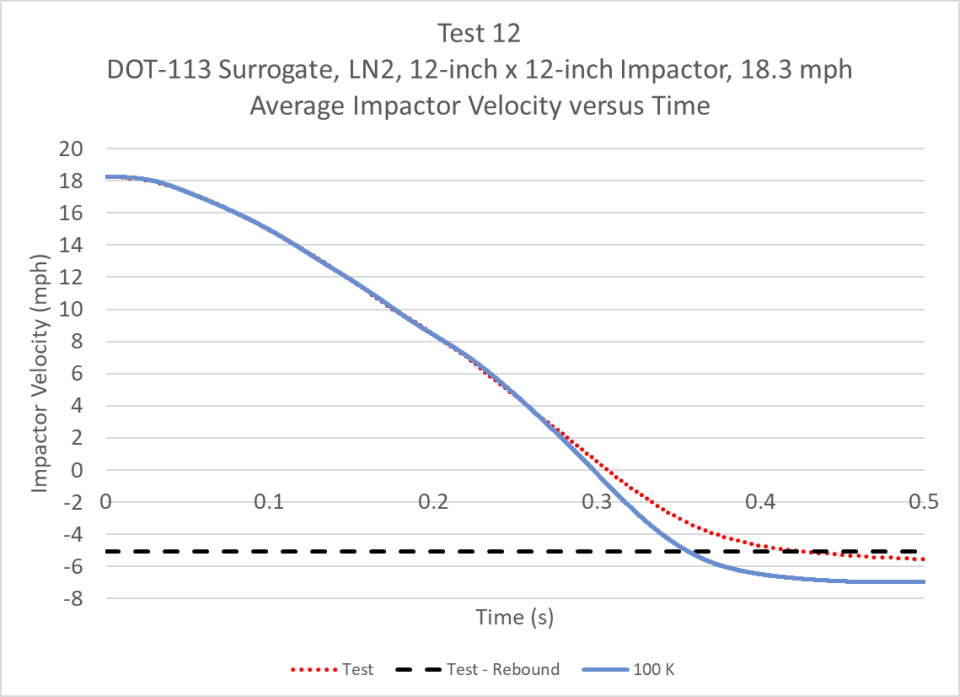

Figure B75. Impactor Velocity Versus Time for Test and EOS Material Model at 100 K, Constant E_m

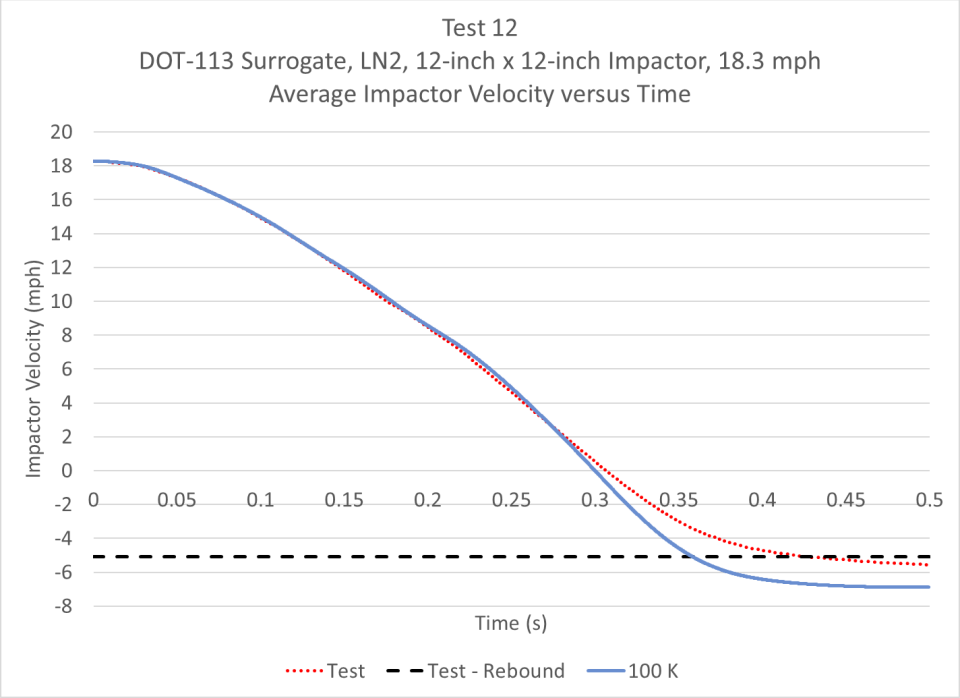

Figure B76. Impactor Velocity Versus Time for Test and EOS Material Model at 100 K, Variable E_m

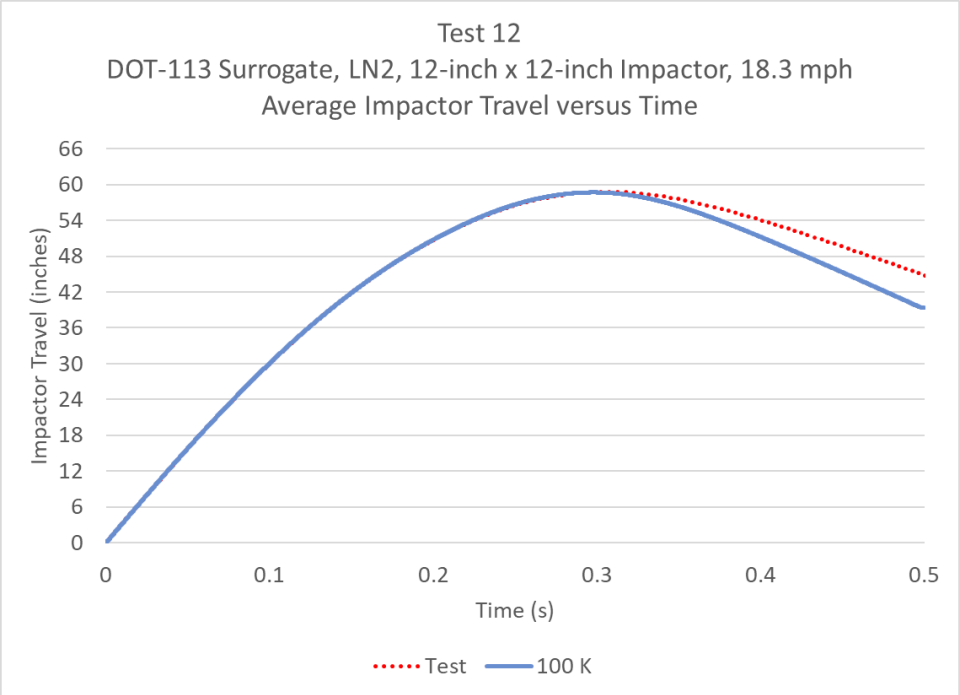

Figure B77. Impactor Displacement Versus Time for Test and EOS Material Model at 100 K, Constant E_m

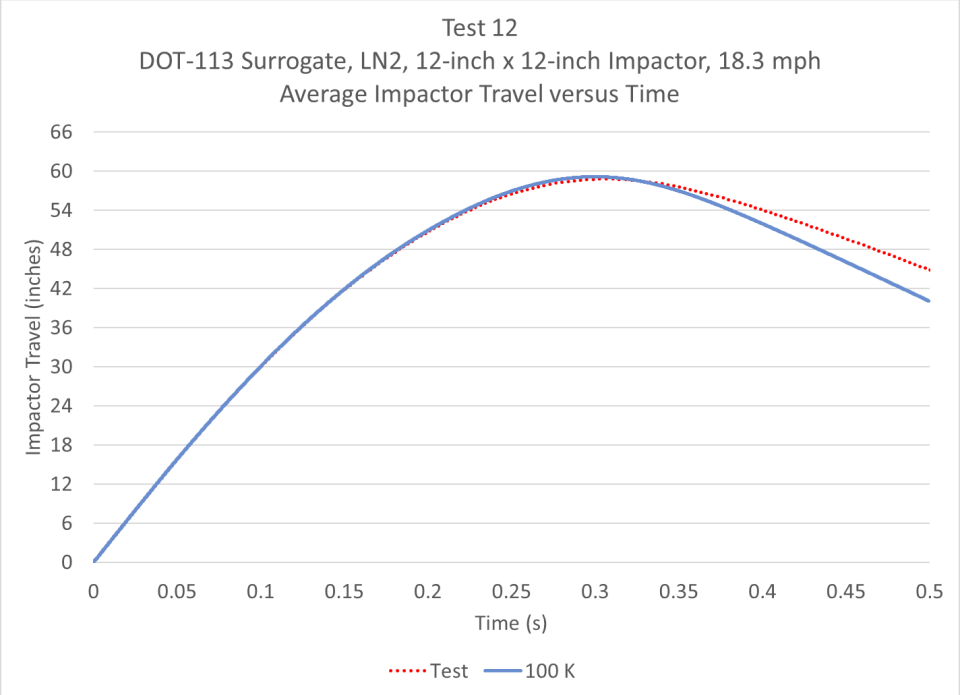

Figure B78. Impactor Displacement Versus Time for Test and EOS Material Model at 100 K, Variable E_m

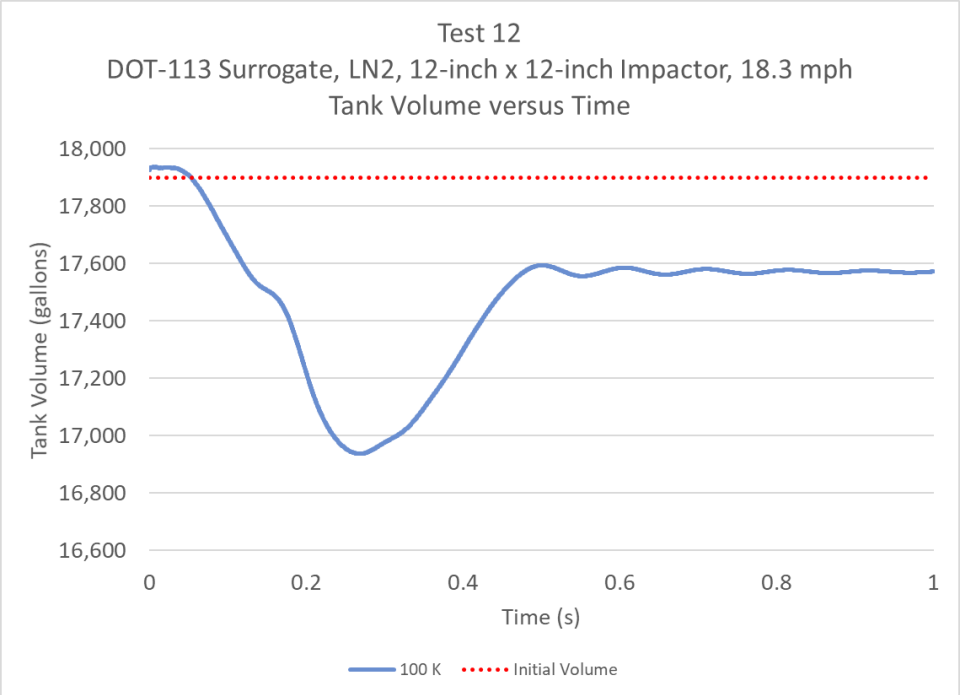

Figure B79. Tank Volume Versus Time for EOS Material Model at 100 K, Constant E_m

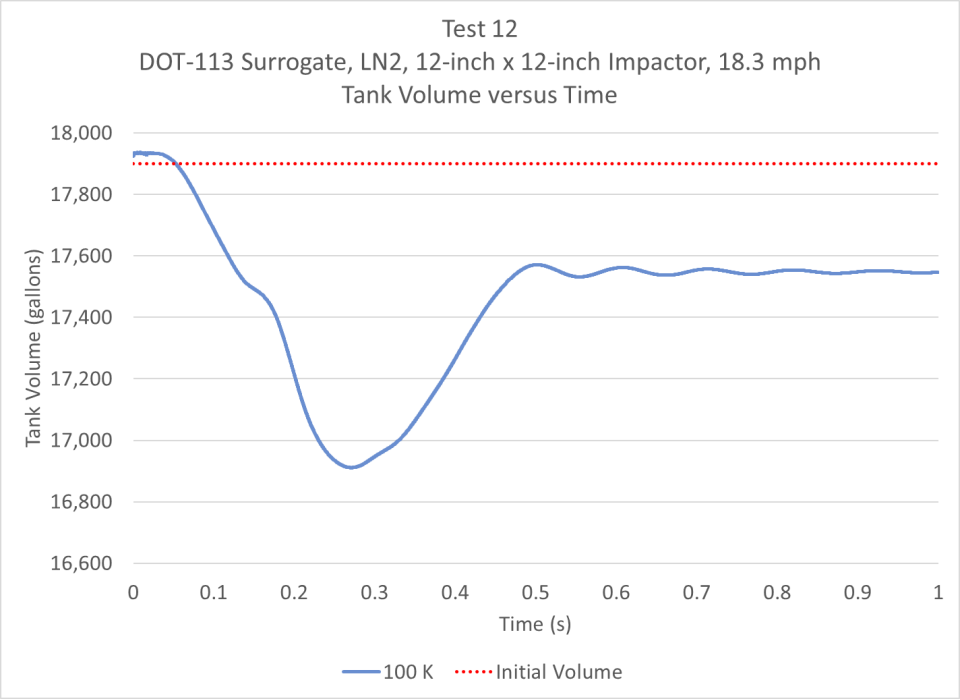

Figure B80. Tank Volume Versus Time for EOS Material Model at 100 K, Variable E_m

B.8 GN2 at 92K, Various $\Delta\varepsilon_{vol}$

Three additional simulations were run as a check on the effects of the user-selected volumetric strain increment ($\Delta\varepsilon_{vol}$) on the results of the model. In each case, a 92 K Tabulated EOS with variable E_m was developed using a different $\Delta\varepsilon_{vol}$. The resulting density-pressure relationships are shown in Figure B81, compared to the reference data [10]. Note that while reference data exists down to a zero pressure – zero density theoretical state, the Tabulated EOS is only defined to approximately 19 psia. The lower pressure limit is a result of the requirement that f_1 be monotonically increasing. Based on the range of f_2 values chosen to develop the Tabulated EOS, the value of f_1 begins to decrease for pressures below 19 psia. While this limitation could be addressed by selecting a new range of f_2 values to ensure f_1 remained monotonically increasing, the limitation was not expected to affect the Test 12 model comparisons since pressures below 19 psia were not expected to be encountered in this impact scenario.

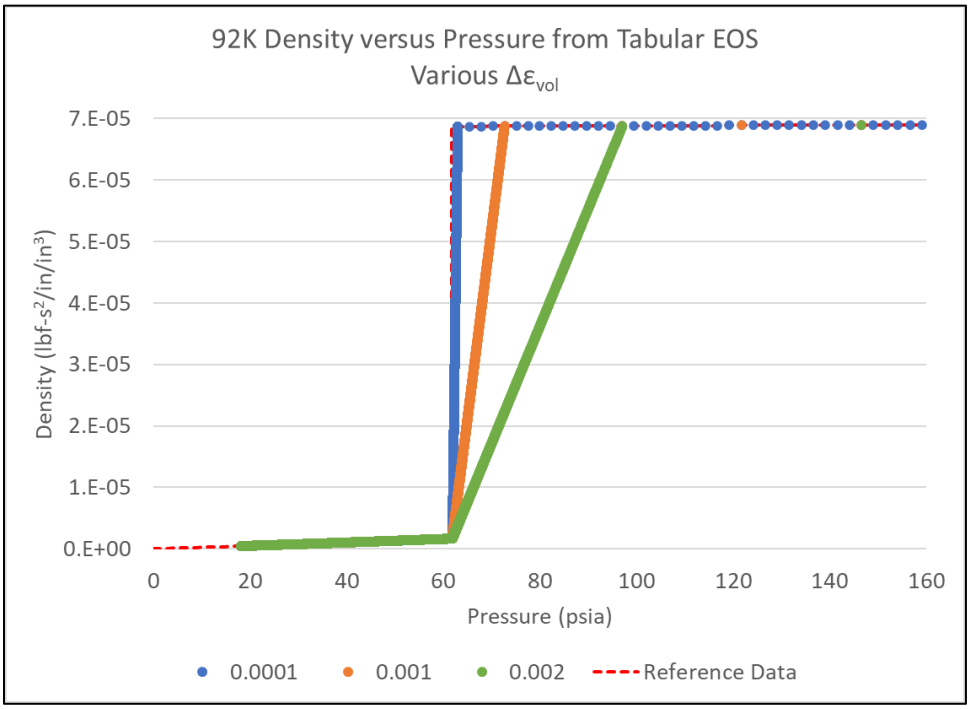

Figure B81. Density Versus Pressure Relationships at 92 K using Various $\Delta\varepsilon_{vol}$

The resulting force-displacement responses from these three models are shown in Figure B82. There are only negligible differences between the three different levels of discretization. Note that the simulation using $\Delta\varepsilon_{vol}$=0.002 terminated prior to the 1.0 second prescribed runtime due to excessive element distortion.

Figure B 83 contains a plot of the bulk average pressure over the entire outage versus time for each of the three simulations. The Tabulated EOS using a $\Delta\varepsilon_{vol}$ of 0.002 shows a sudden increase in pressure just before the simulation self-terminated due to excess element distortion. The more refined Tabulated EOS models show pressure-time responses very similar to one another.

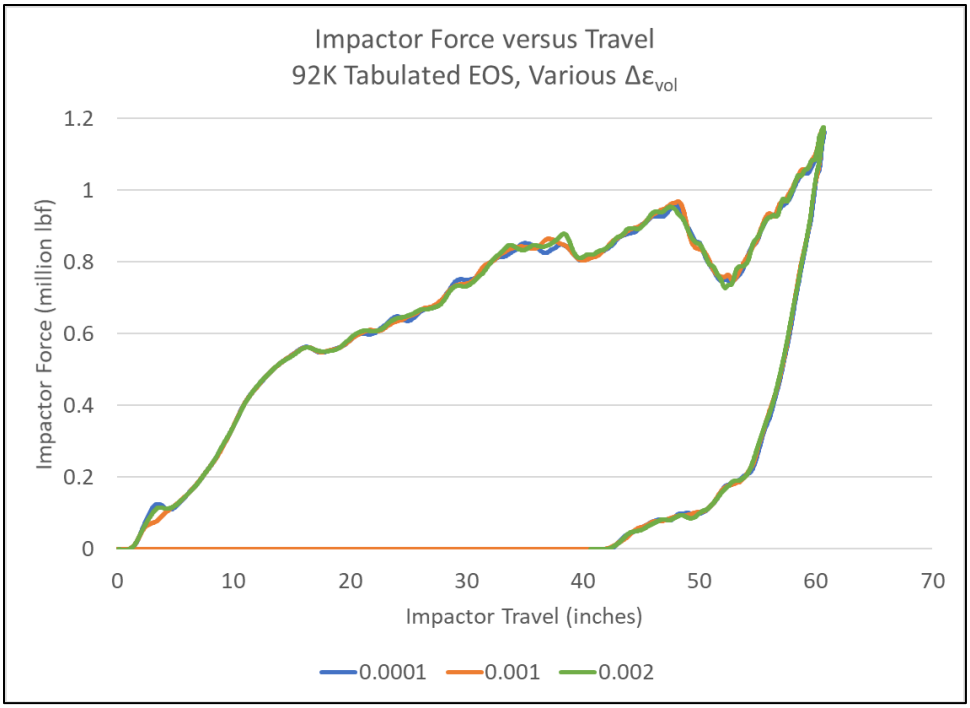

Figure B82. Impactor Force Versus Travel for 92 K Tabulated EOS using Various $\Delta\varepsilon_{vol}$

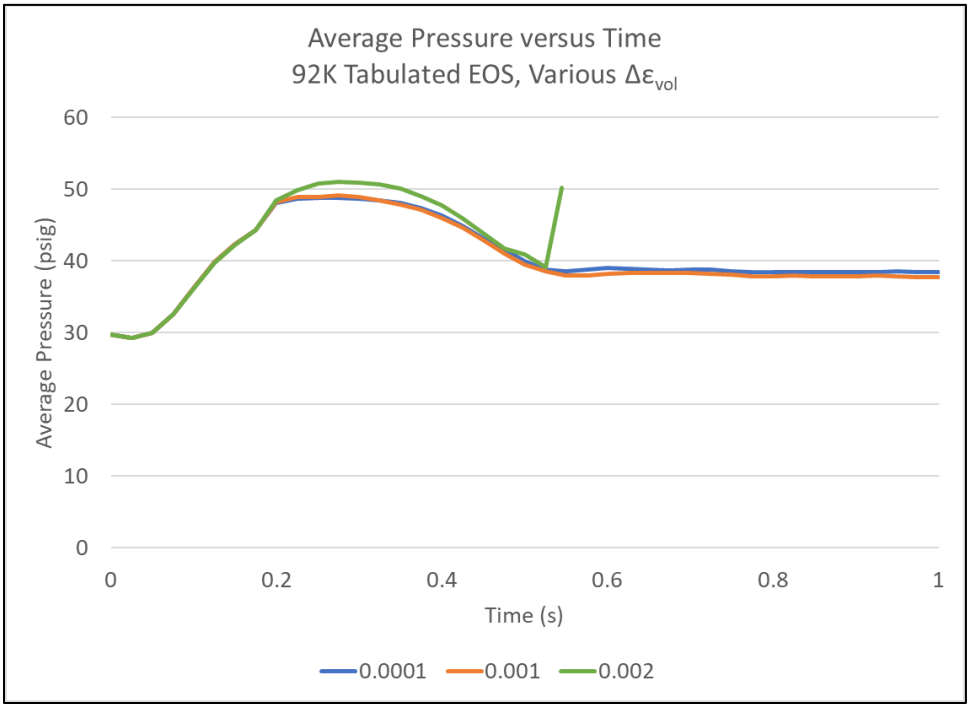

Figure B 83. Bulk Average Outage Pressure Versus Time for 92 K Tabulated EOS using Various $\Delta\varepsilon_{vol}$

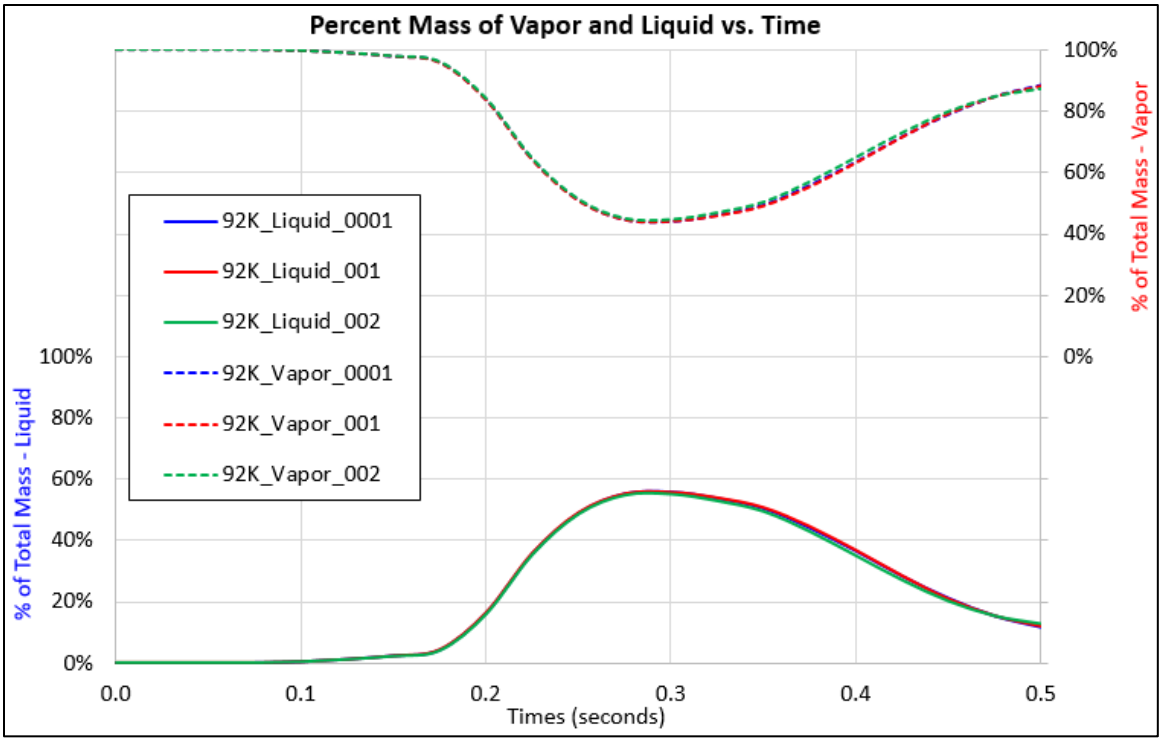

Figure B84. Percentage by Mass of Vapor and Liquid in Outage Versus Time for 92 K Tabulated EOS using Various $\Delta\varepsilon_{vol}$

Figure B85 contains a plot of the density versus pressure relationship from the 92 K Tabulated EOS using $\Delta\varepsilon_{vol}$ = 0.0001 and reference data. Two elements assigned the Tabulated EOS material in the model had the pressure and density results extracted from their respective centroids at each field output frame. One element exhibited a significant decrease in density and the other exhibited a significant increase in density during the simulation. These two results are used as a "spot check" on the density-pressure relationship developed during the simulation compared with the reference relationship and the theoretical relationship that the Tabulated EOS model should be producing. Over the full range of the Tabulated EOS the agreement between the Tabulated EOS and the output from the elements appears to be reasonable.

Figure B86 contains the same data as the previous figure, but with the axis re-scaled to focus on the vapor phase. There is reasonable agreement between the reference data and the element outputs for the vapor phase, even at pressures below the pressure range over which the Tabulated EOS has been defined.

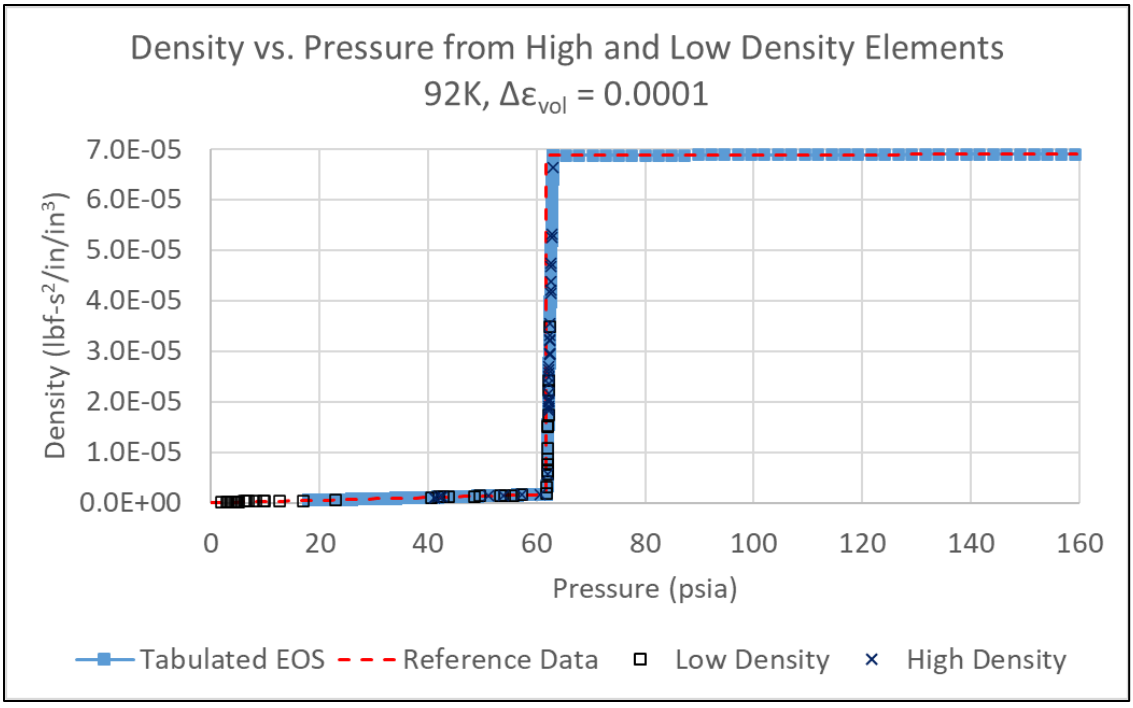

Figure B85. Density Versus Pressure from High- and Low-Density Elements, 92 K Tabulated EOS, $\Delta\varepsilon_{vol}$ = 0.0001

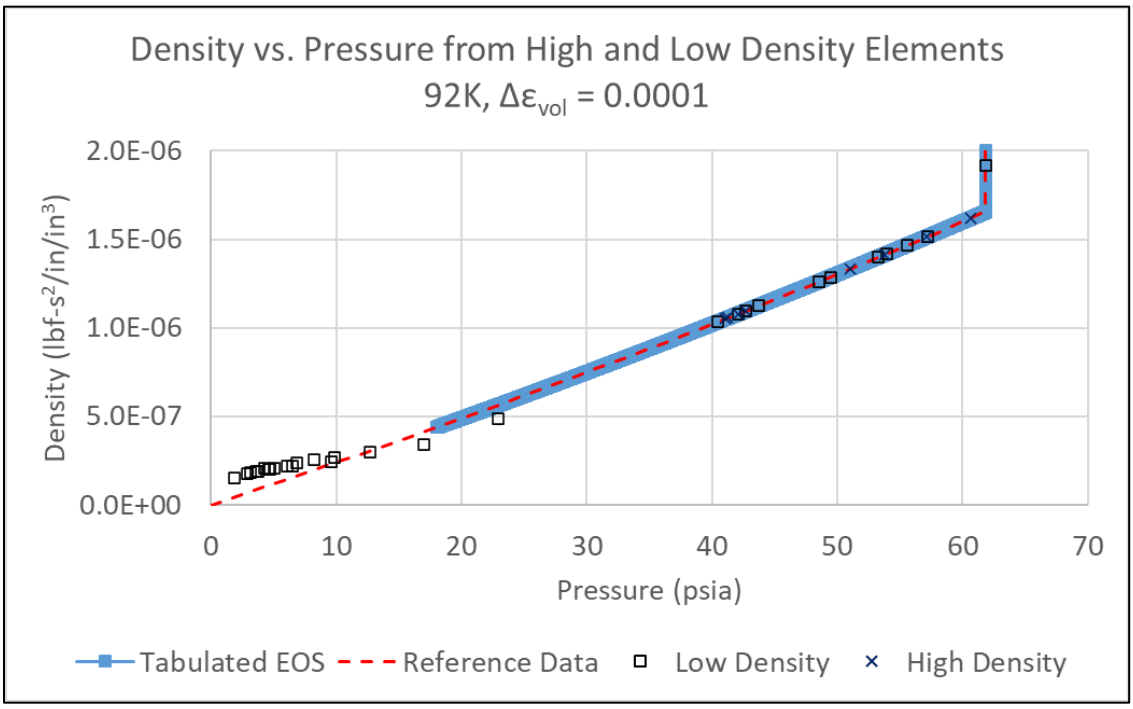

Figure B86. Density Versus Pressure from High- and Low-Density Elements, Vapor Phase, 92 K Tabulated EOS, $\Delta\varepsilon_{vol}$ = 0.0001

Figure B87 contains a similar plot for the model using $\Delta\varepsilon_{vol}$ = 0.001 over the full range of pressures. Figure B88 contains the results for the vapor phase pressures for $\Delta\varepsilon_{vol}$ = 0.001.

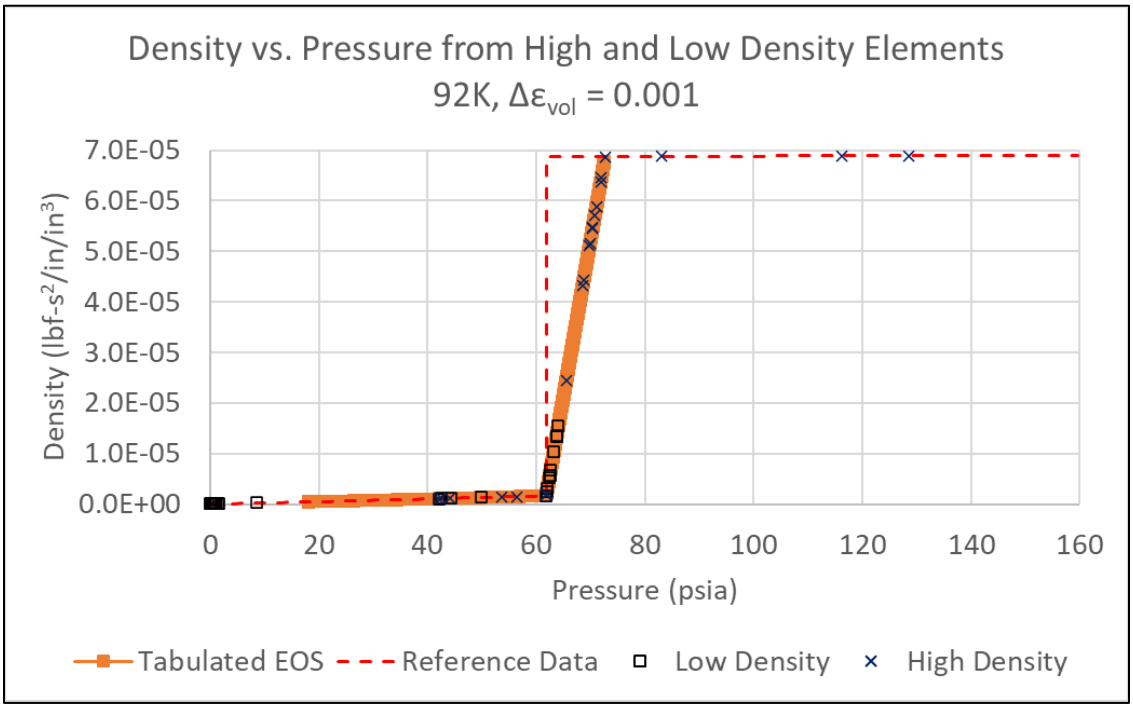

Figure B87. Density Versus Pressure from High- and Low-Density Elements, 92 K Tabulated EOS, $\Delta\varepsilon_{vol}$ = 0.001

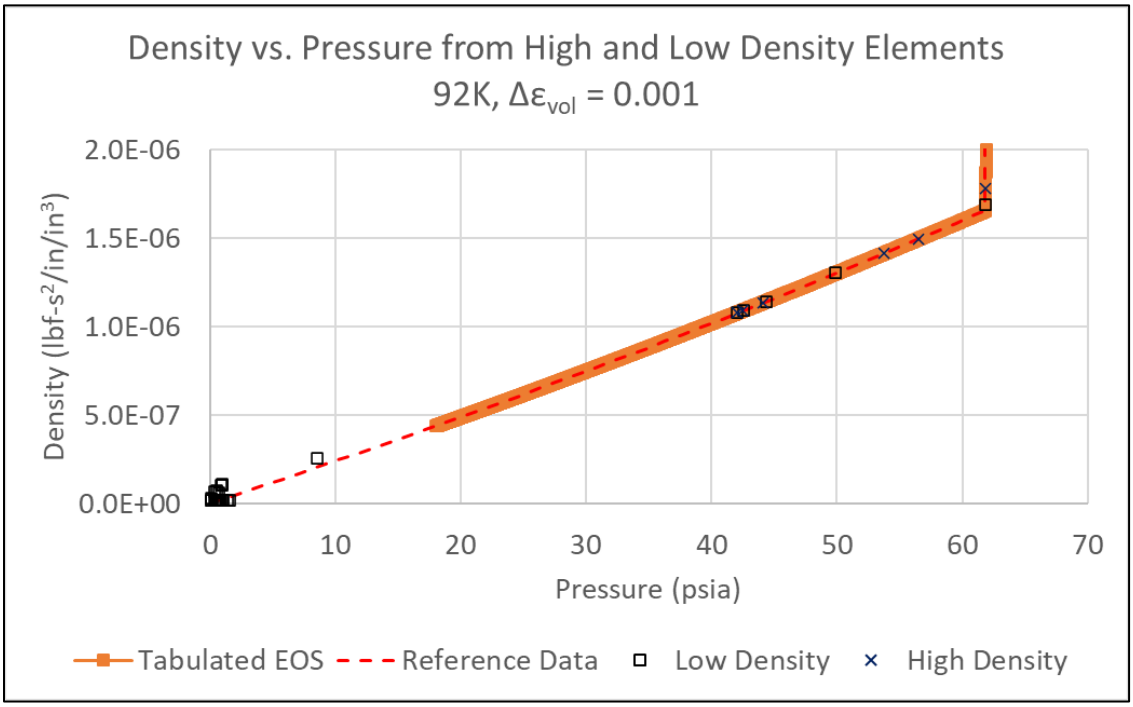

Figure B88. Density Versus Pressure from High- and Low-Density Elements, Vapor Phase, 92 K Tabulated EOS, $\Delta\varepsilon_{vol}$ = 0.001

Figure B89 contains a similar plot for the model using $\Delta\varepsilon_{vol}$ = 0.002 over the full range of pressures. Figure B90 contains the results for the vapor phase pressures for $\Delta\varepsilon_{vol}$ = 0.002.

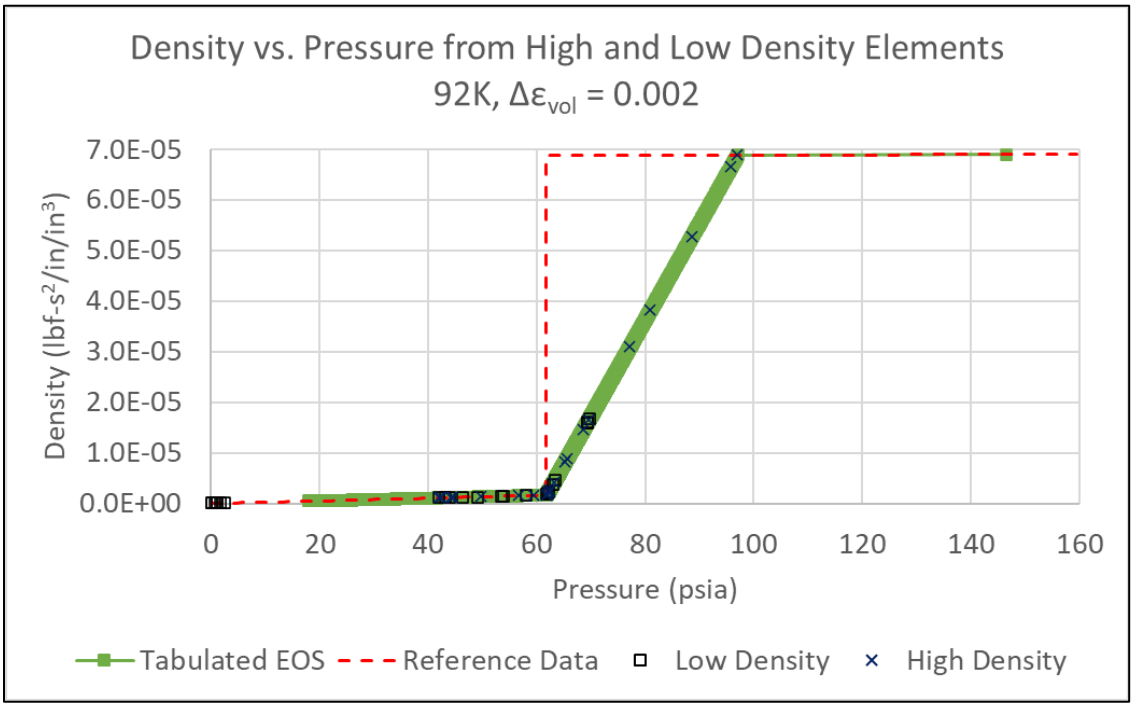

Figure B89. Density Versus Pressure from High- and Low-Density Elements, 92 K Tabulated EOS, $\Delta\varepsilon_{vol}$ = 0.002

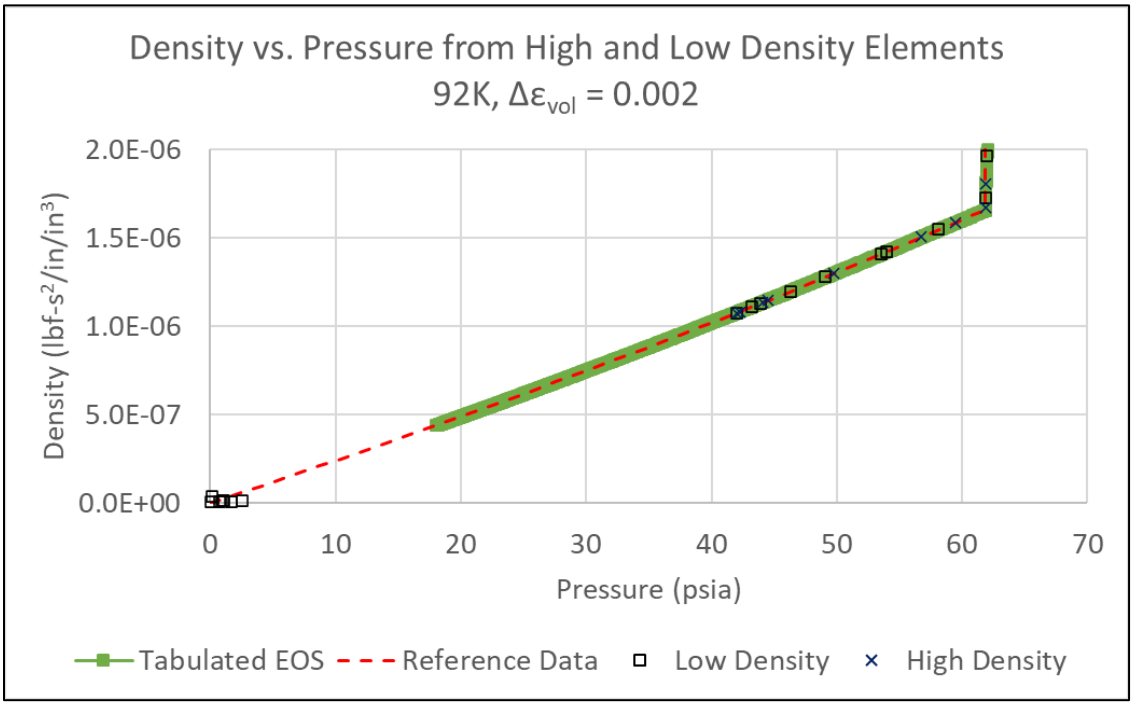

Figure B90. Density Versus Pressure from High- and Low-Density Elements, Vapor Phase, 92 K Tabulated EOS, $\Delta\varepsilon_{vol}$ = 0.002

B.9 Post-processing of Elements Containing GN2 and LN2

Outage elements having a density above the saturation density of GN2 but below the saturated density of LN2 at the assumed temperature for the model were categorized into a third pseudo-state, *transition.* These elements were assumed to contain a mixture of LN2 and GN2, resulting in an average density that was between GN2 and LN2. The procedures shown below were used to resolve the mass of LN2 and mass of GN2 contained within a given transition element at a given time point.

For a given element in the transition pseudo-phase, the element density ($\rho_{element}$) and element volume ($V_{element}$) were obtained as field output from the FE model results. These field output quantities were used to calculate the mass of each transition element according to Equation B1.

Equation B1. Mass of a Transition Element

$$mass_{transition} = \rho_{element} \cdot V_{element}$$

The total mass of each element in the transition pseudo-phase was assumed to comprise a mass of liquid ($mass_{liquid}$) and a mass of vapor ($mass_{vapor}$), as shown in Equation B2.

Equation B2. Mass of Liquid and Vapor within Transition Element

$$mass_{transition} = mass_{vapor} + mass_{liquid}$$

The mass of N2 in the vapor and liquid state within each transition element are assumed to be equal to the volume of each state multiplied by the saturated density of that phase, as shown in Equation B3 and Equation B4.

Equation B3. Mass of Vapor Phase within Transition Element

$$mass_{vapor} = \rho_{vapor}^{sat} \cdot V_{vapor}$$

Equation B4. Mass of Liquid Phase within Transition Element

$$mass_{liquid} = \rho_{liquid}^{sat} \cdot V_{liquid}$$

The total volume of an element ($V_{element}$) in the transition pseudo-phase contains a volume of liquid (V_{liquid}) and a volume of vapor (V_{vapor}) as shown in Equation B5.

Equation B5. Volume of Liquid and Vapor within Transition Element

$$V_{element} = V_{vapor} + V_{liquid}$$

Rearranging Equation B3 and Equation B4 and substituting into Equation B5, the volume of an element containing transition material can be expressed as shown in Equation B6.

Equation B6. Volume of an Element in Terms of Vapor and Liquid Masses and Densities

$$V_{element} = \frac{mass_{vapor}}{\rho_{vapor}^{sat}} + \frac{mass_{liquid}}{\rho_{liquid}^{sat}}$$

Equation B2 can be rearranged and substituted into Equation B6 to eliminate $mass_{vapor}$. The resulting equation is shown in Equation B7.

Equation B7. Volume of an Element with Vapor Mass Eliminated

$$V_{element} = \frac{mass_{element} - mass_{liquid}}{\rho_{vapor}^{sat}} + \frac{mass_{liquid}}{\rho_{liquid}^{sat}}$$

Equation B7 now contains only one unknown, $mass_{liquid}$. This term can be solved for in a series of substitution steps shown in Equation B8.

Equation B8. Mass of Liquid in a Transition Element

$$V_{element} = \frac{mass_{element}}{\rho_{vapor}^{sat}} - \frac{mass_{liquid}}{\rho_{vapor}^{sat}} + \frac{mass_{liquid}}{\rho_{liquid}^{sat}}$$

$$V_{element} - \frac{mass_{element}}{\rho_{vapor}^{sat}} = \frac{mass_{liquid}}{\rho_{liquid}^{sat}} - \frac{mass_{liquid}}{\rho_{vapor}^{sat}}$$

$$V_{element} - \frac{mass_{element}}{\rho_{vapor}^{sat}} = mass_{liquid}\left(\frac{1}{\rho_{liquid}^{sat}} - \frac{1}{\rho_{vapor}^{sat}}\right)$$

$$mass_{liquid} = \frac{V_{element} - \frac{mass_{element}}{\rho_{vapor}^{sat}}}{\frac{1}{\rho_{liquid}^{sat}} - \frac{1}{\rho_{vapor}^{sat}}}$$

Appendix C.
Pneumatic Cavity with Fluid Exchange and Tabulated EOS Model Results Compared

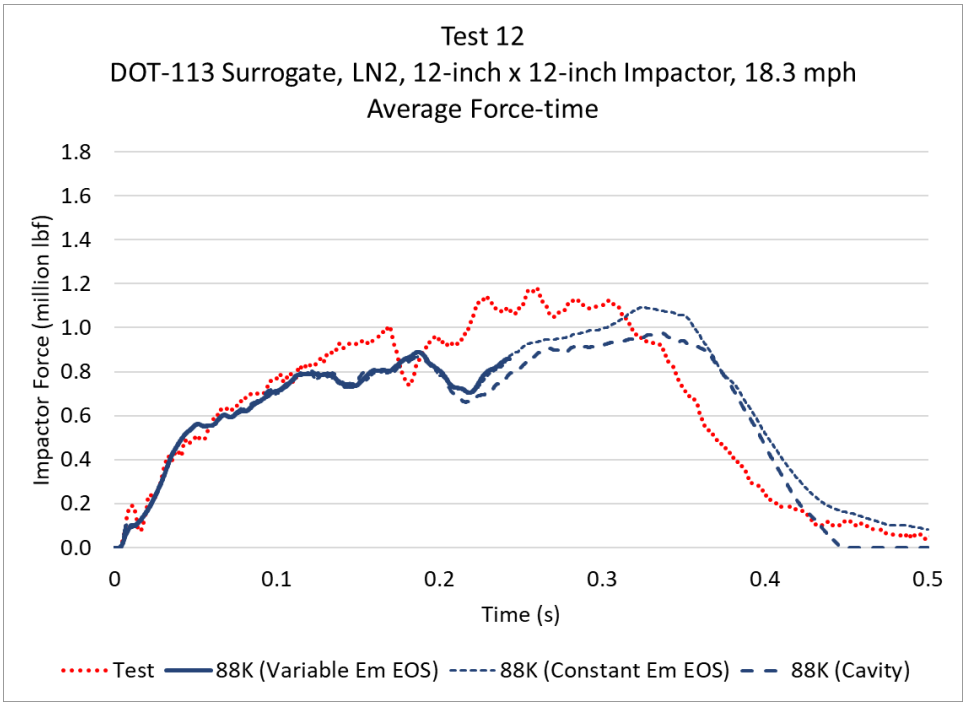

Figure C1. Comparison of Force Versus Time Results, 88 K

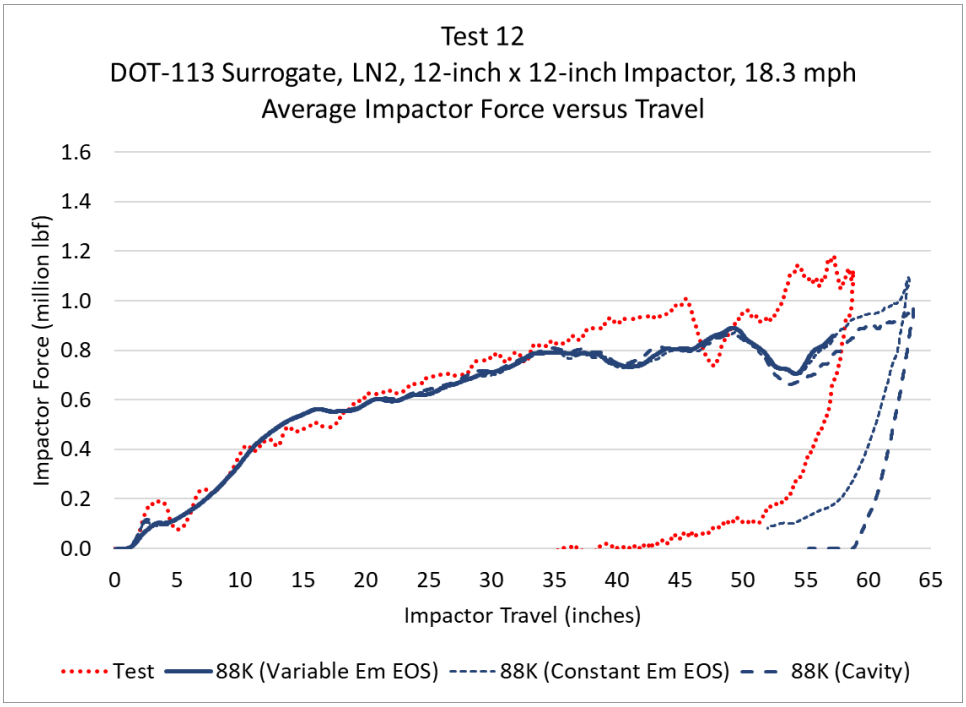

Figure C2. Comparison of Force Versus Impactor Travel Results, 88 K

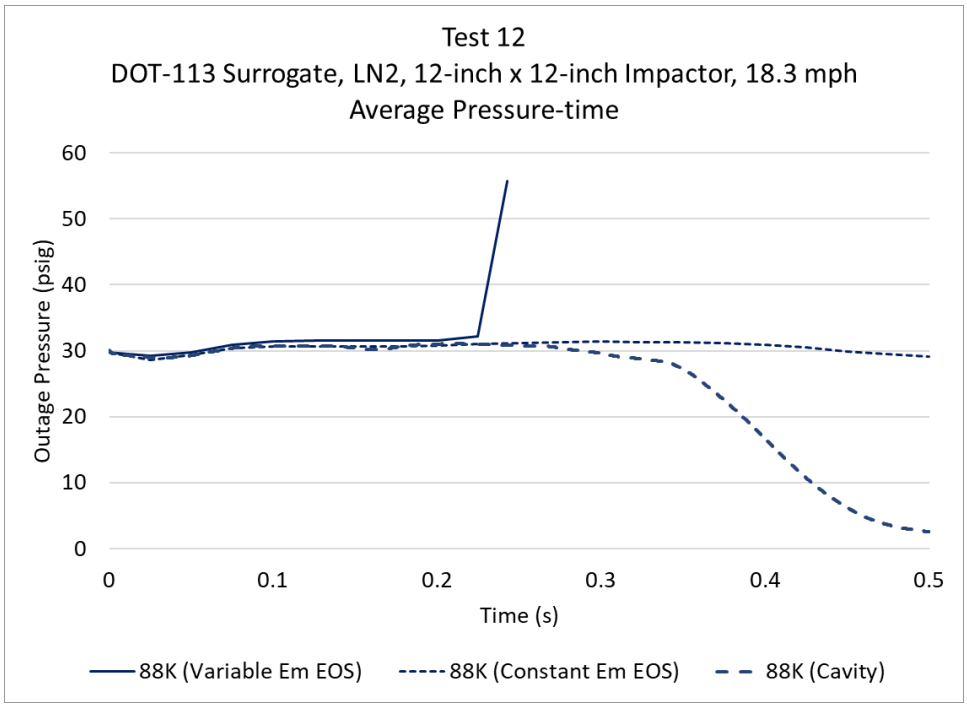

Figure C3. Comparison of Pressure Versus Time Results, 88 K

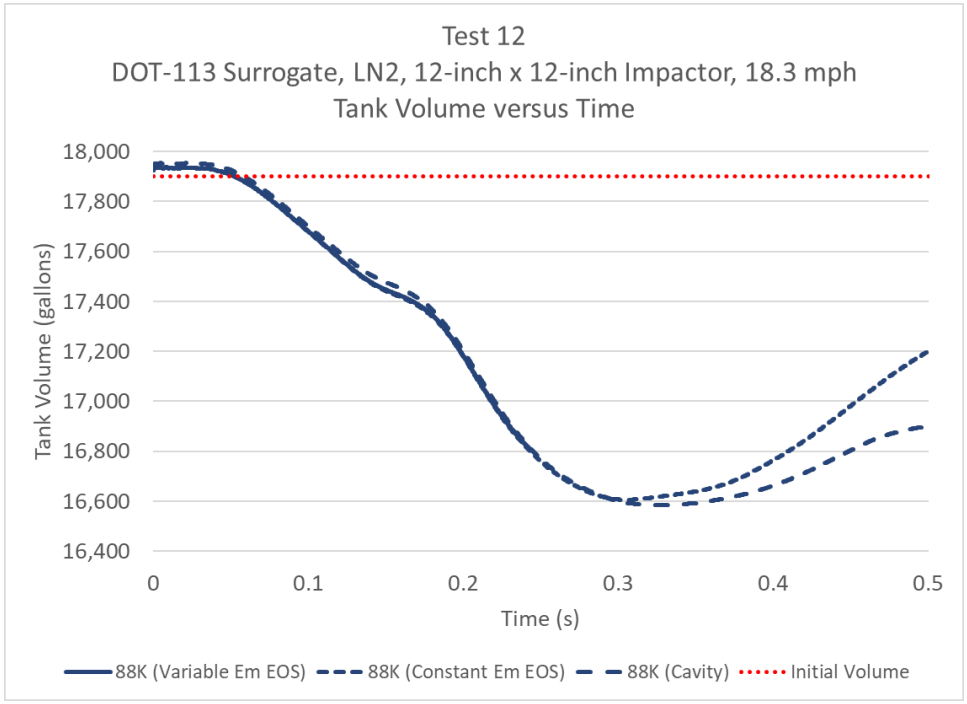

Figure C4. Comparison of Tank Volume Versus Time Results, 88 K

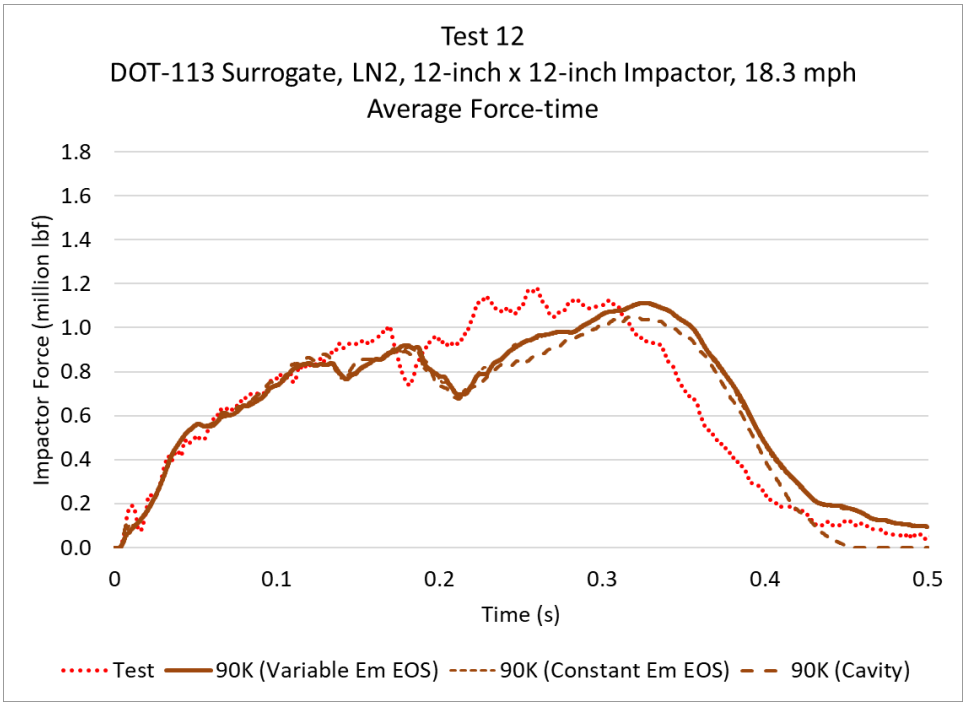

Figure C5. Comparison of Force Versus Time Results, 90 K

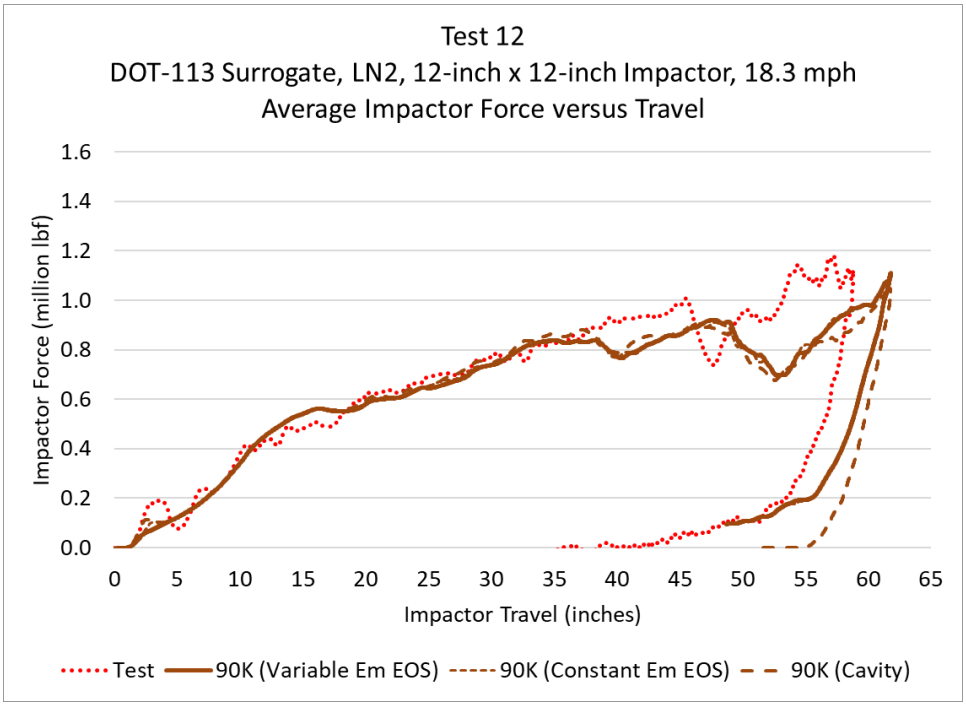

Figure C6. Comparison of Force Versus Impactor Travel Results, 90 K

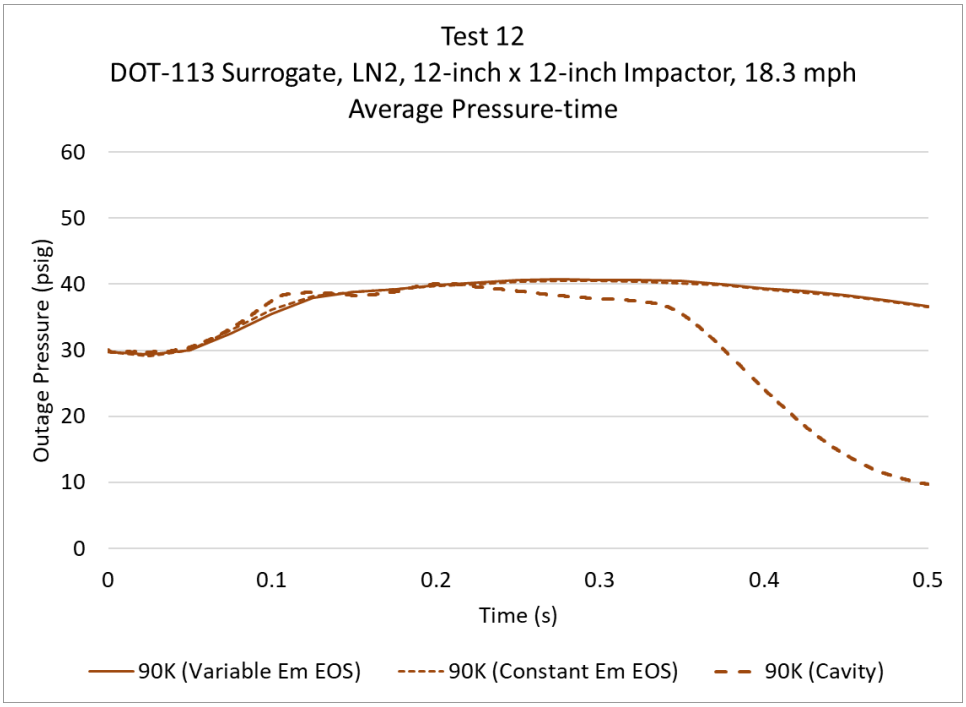

Figure C7. Comparison of Pressure Versus Time Results, 90 K

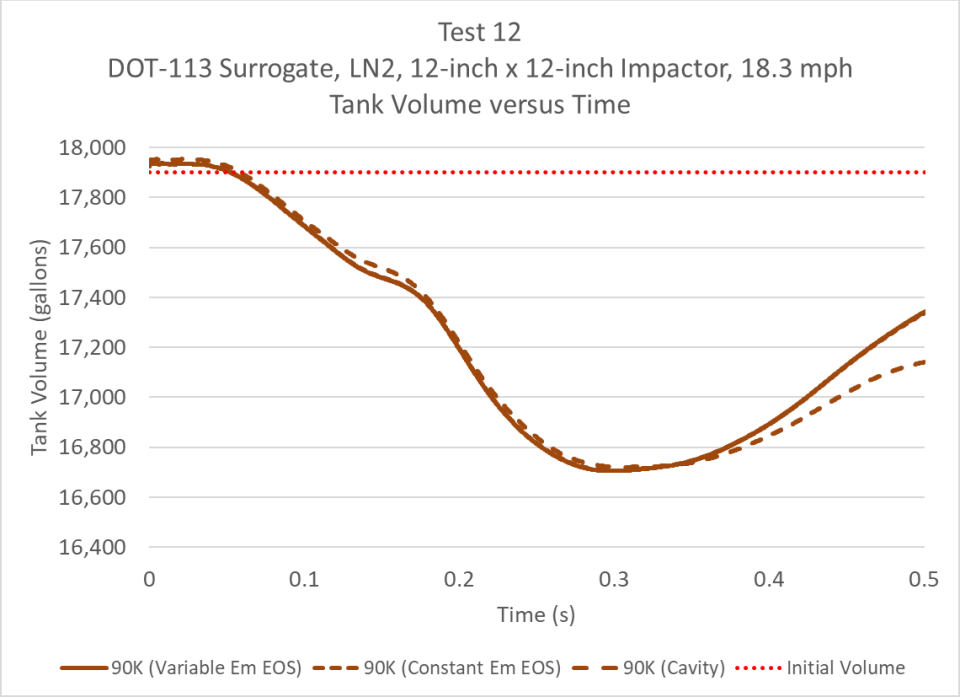

Figure C8. Comparison of Tank Volume Versus Time Results, 90 K

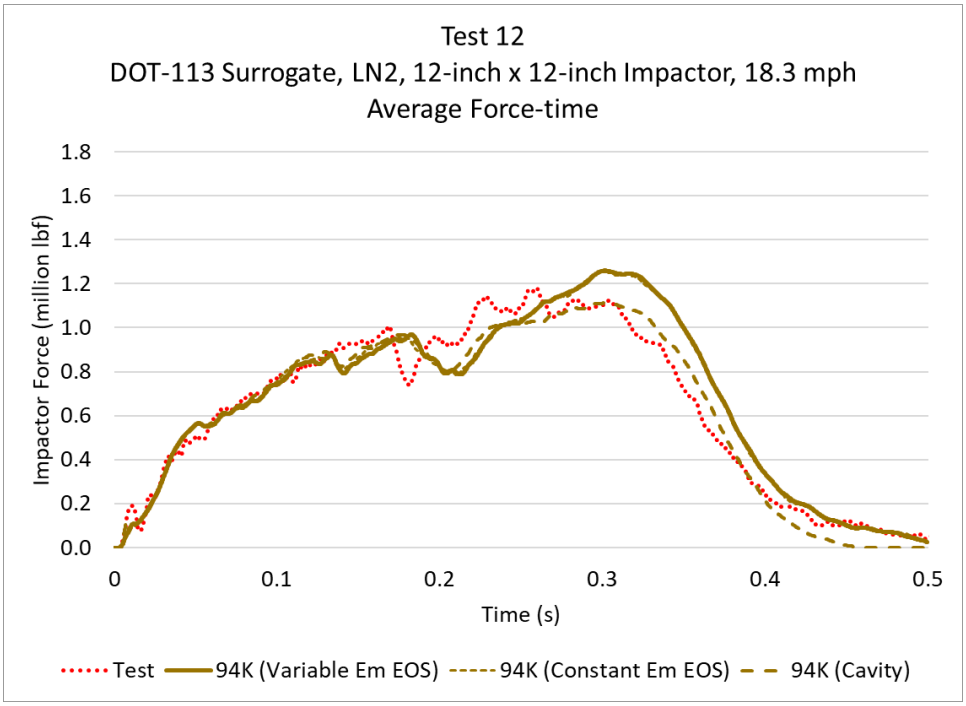

Figure C9. Comparison of Force Versus Time Results, 94 K

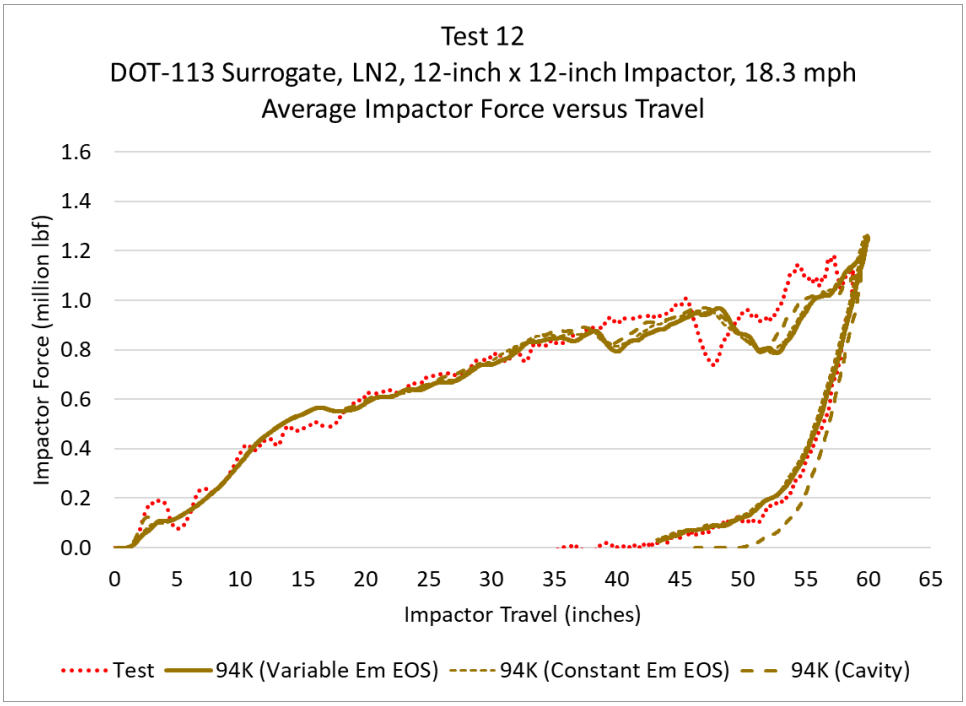

Figure C10. Comparison of Force Versus Impactor Travel Results, 94 K

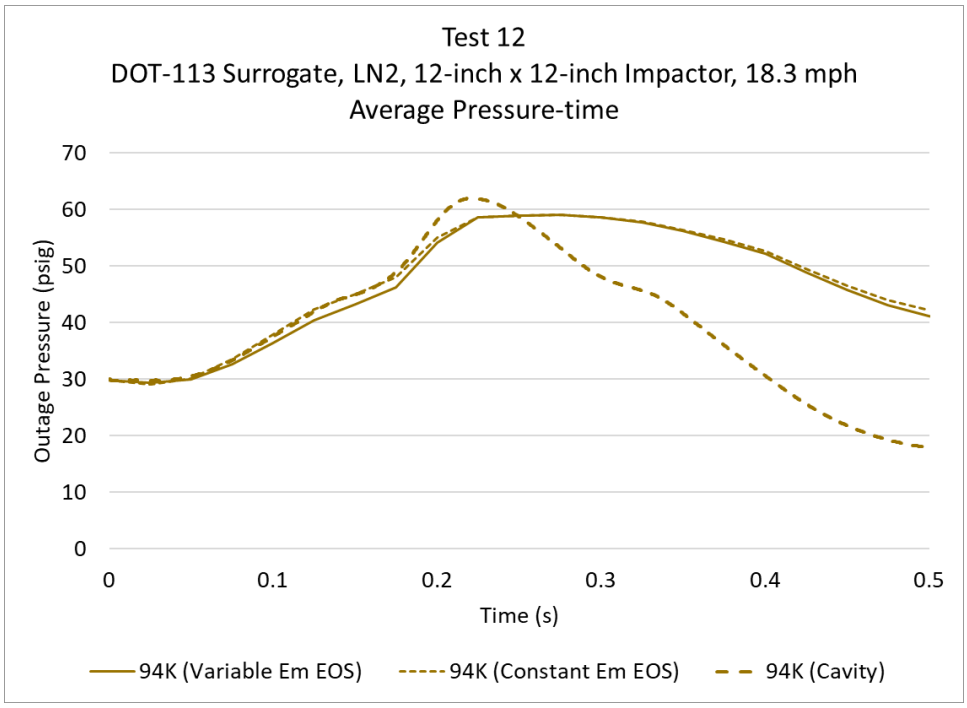

Figure C11. Comparison of Pressure Versus Time Results, 94 K

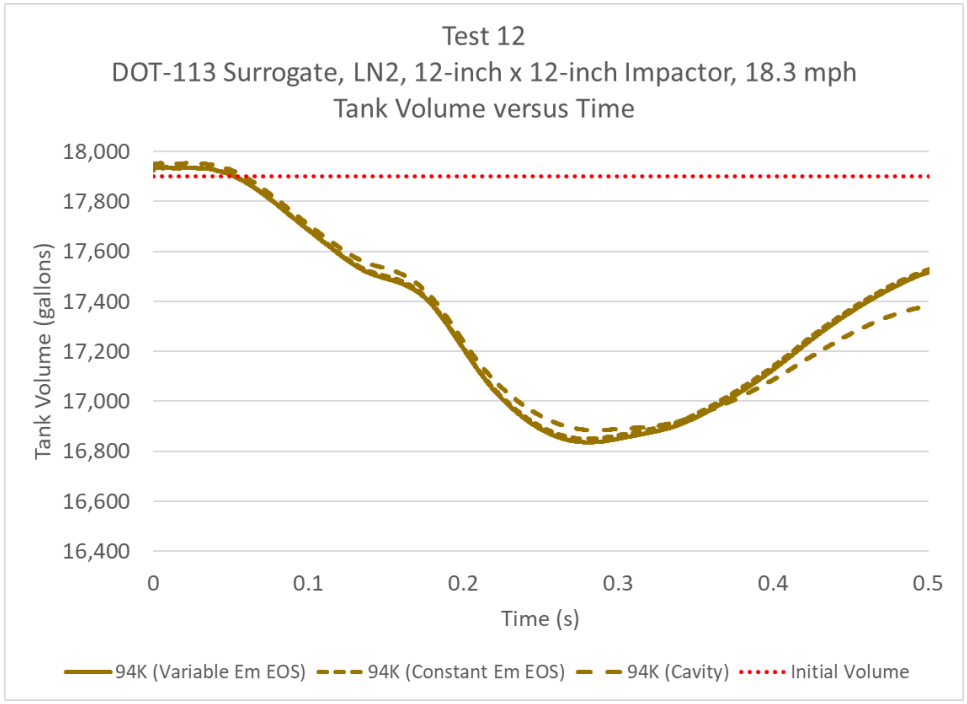

Figure C12. Comparison of Tank Volume Versus Time Results, 94 K

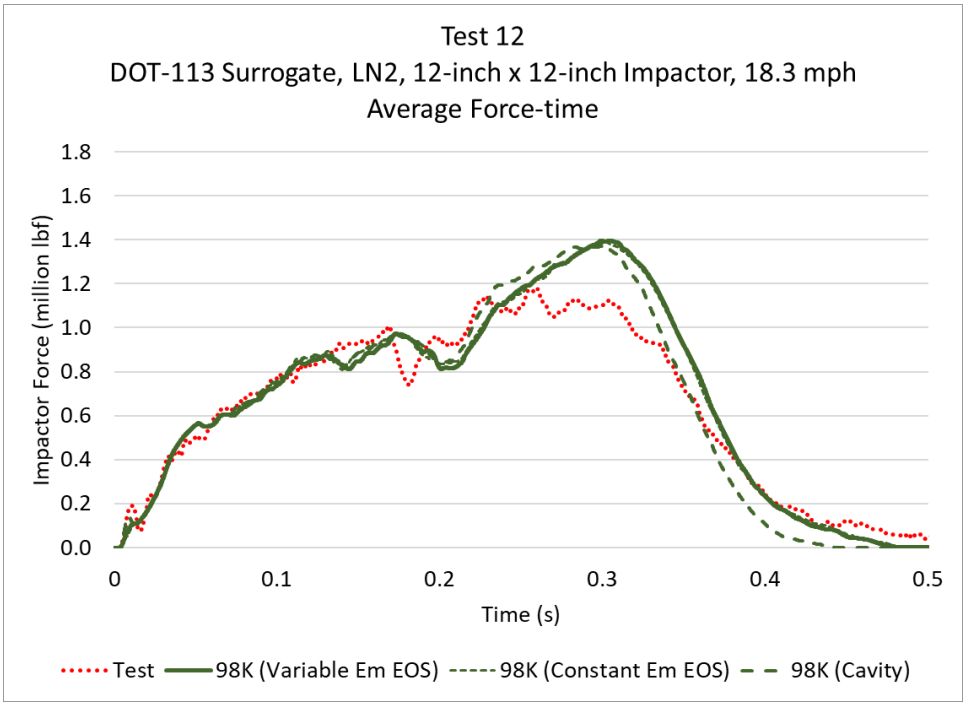

Figure C13. Comparison of Force Versus Time Results, 98 K

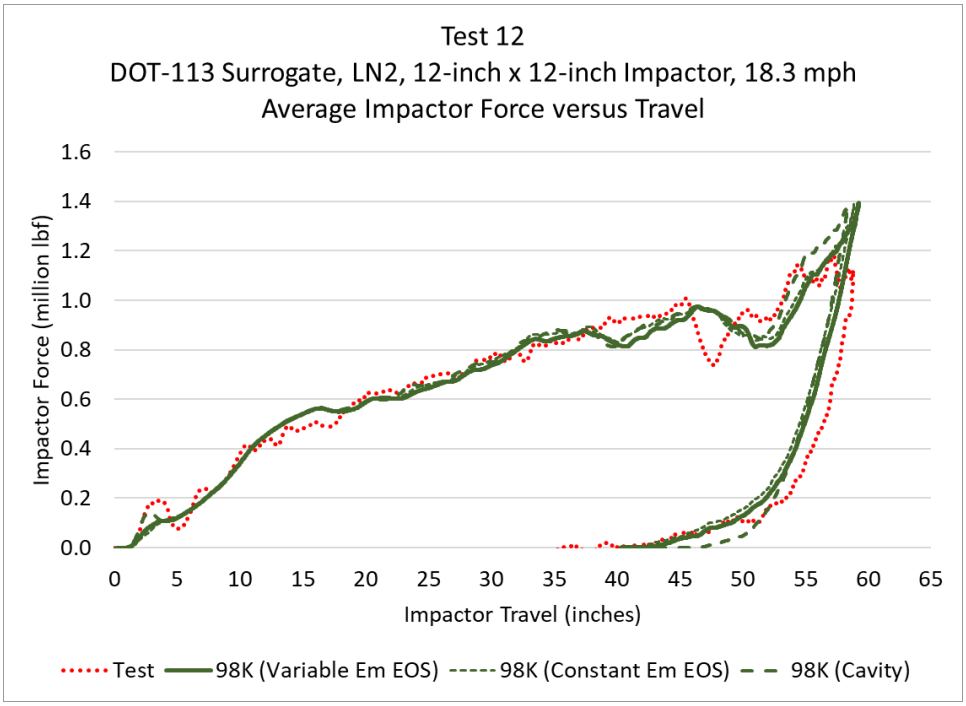

Figure C14. Comparison of Force Versus Impactor Travel Results, 98 K

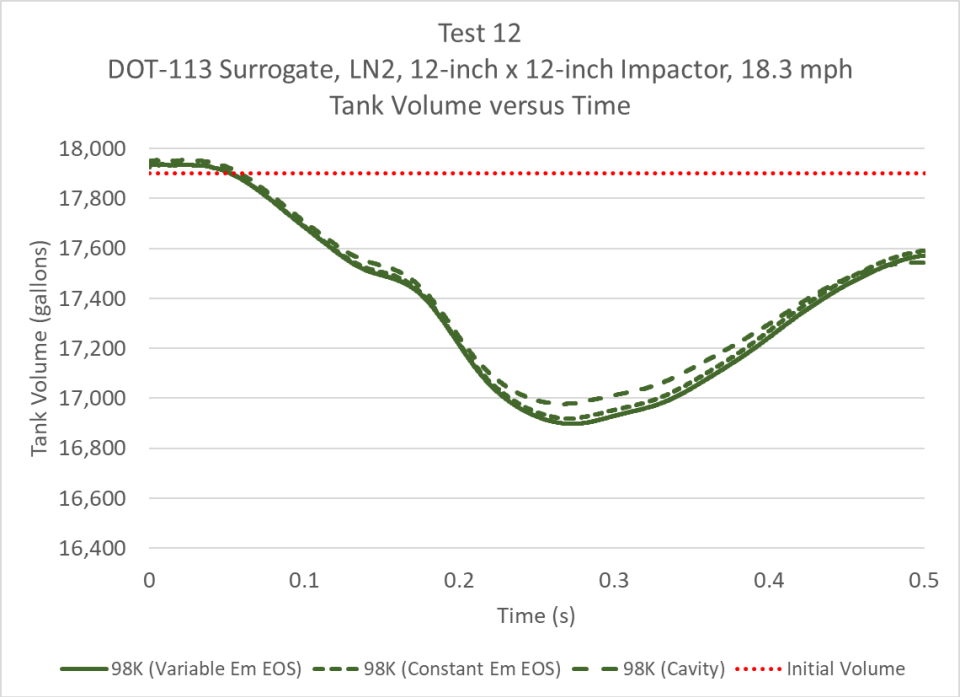

Figure C15. Comparison of Tank Volume Versus Time Results at 98 K

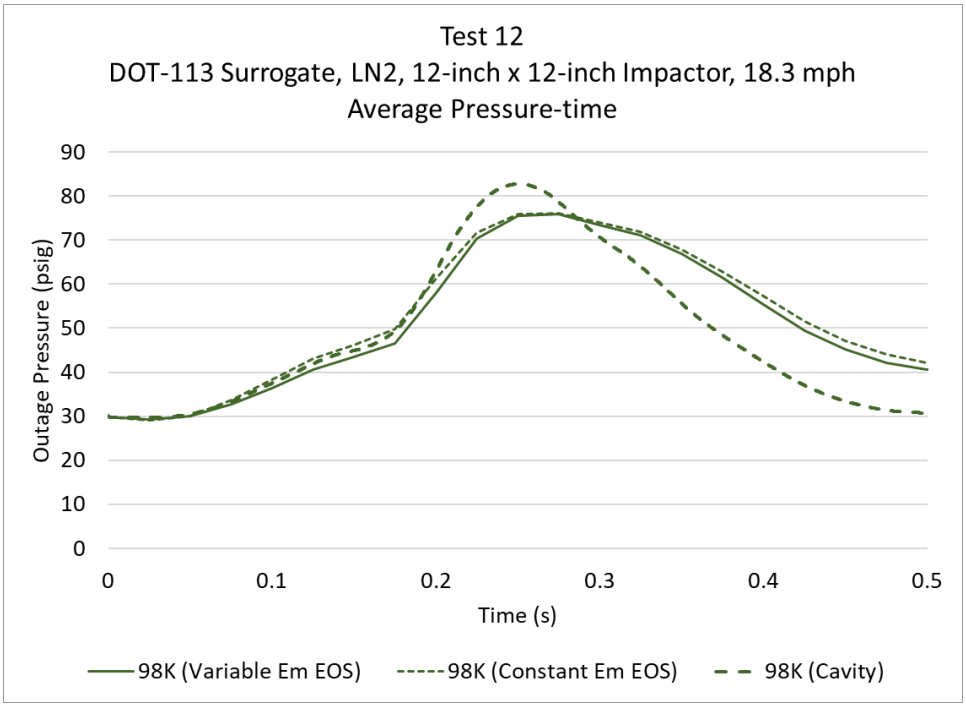

Figure C16. Comparison of Pressure Versus Time Results at 98 K

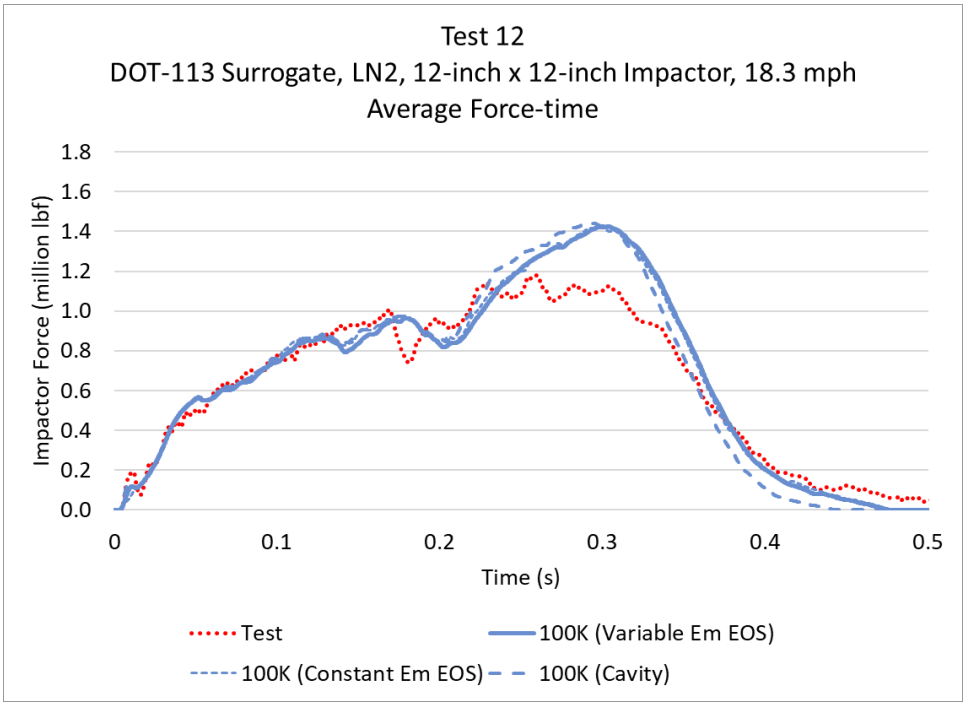

Figure C17. Comparison of Force Versus Time Results, 100 K

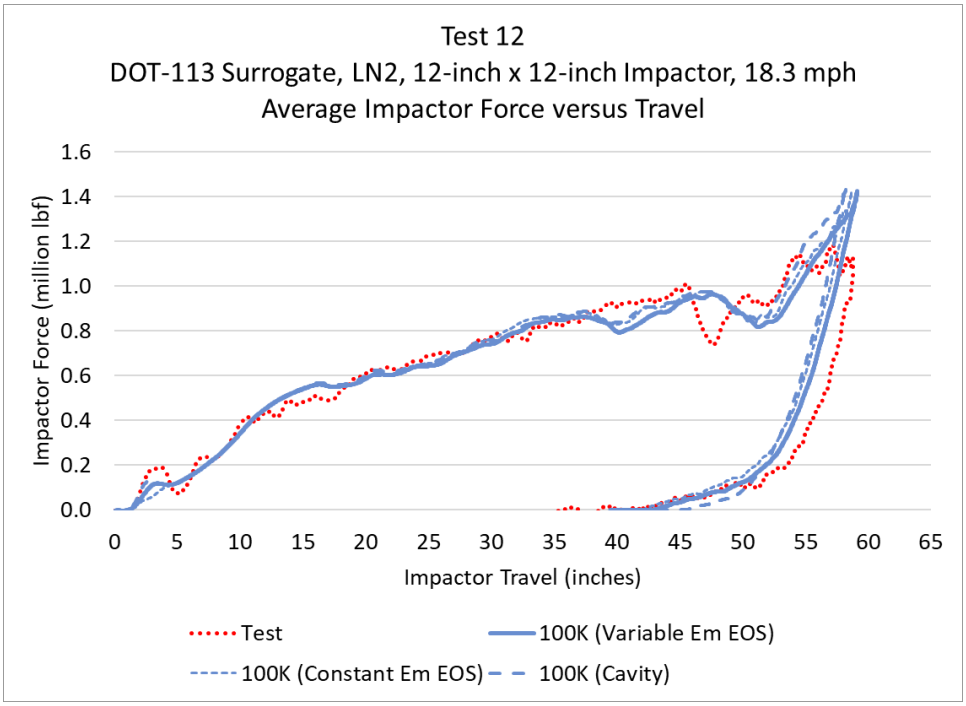

Figure C18. Comparison of Force Versus Impactor Travel Results, 100 K

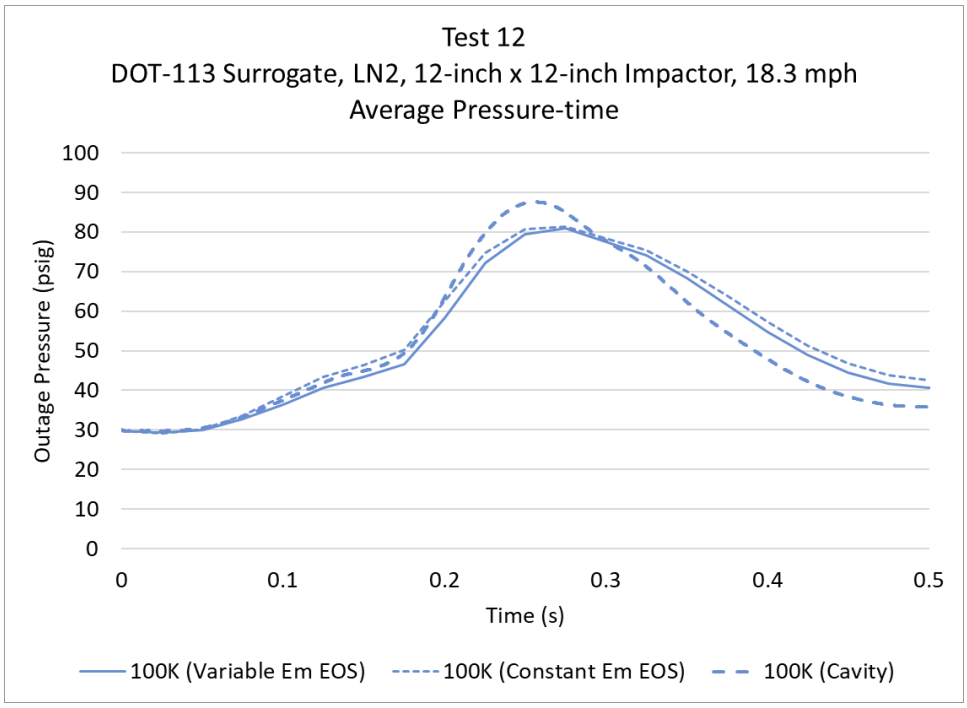

Figure C19. Comparison of Pressure Versus Time Results, 100 K

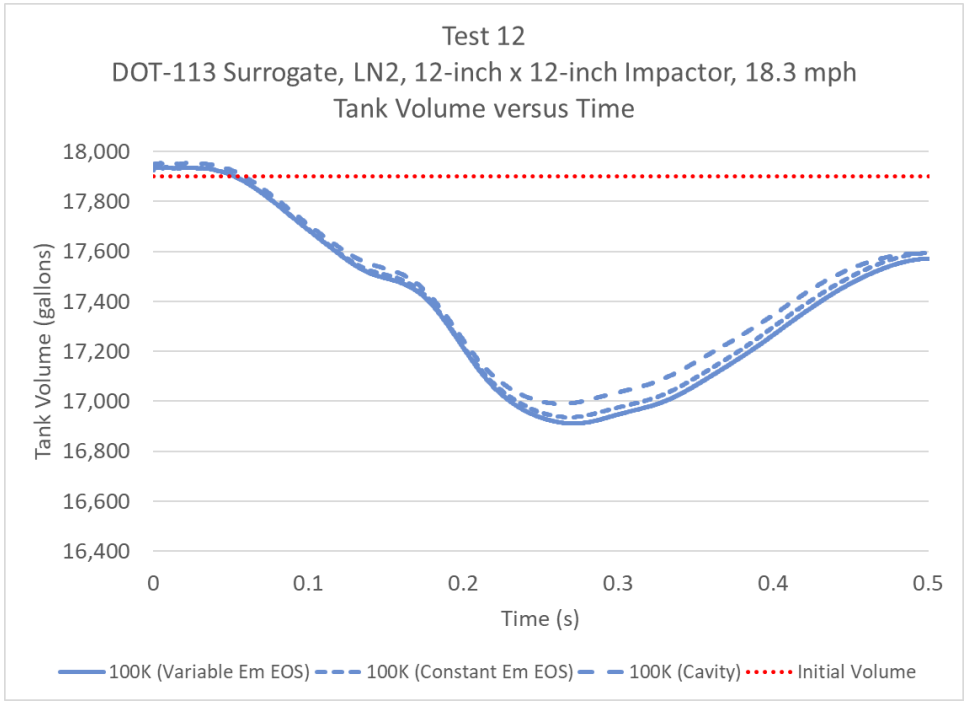

Figure C20. Comparison Tank Volume Versus Time Results at 100 K

Appendix D.
Estimated Post-impact Inner Tank Volume

Following Test 12, the team contracted a third party to perform an internal and external LiDAR scan of the Test 12 surrogate. The resulting point cloud was produced. Using the LS-PrePost Software's "Point Cloud to Mesh" feature, the portion of the point cloud corresponding to the inner tank's surface was meshed using triangular elements [14]. Numerous features, such as the exterior tank, surrounding ground, and interior piping were removed from the point cloud to leave only the surface of the inner tank.

A simplified model approach was used to estimate the volume of the inner tank in its deformed state. The mesh was imported into the Abaqus/2019 CAE FE preprocessor [9] and assigned a rigid element type. The inner tank mesh had all its degrees of freedom constrained. A separate part was modeled as a cloud of particles surrounding the inner tank mesh, as shown in Figure D1. This image shows a top view of the tank and particles with a full section cut normal to the Z plane. These particles were assigned a material having the properties of water as summarized in Table D1.

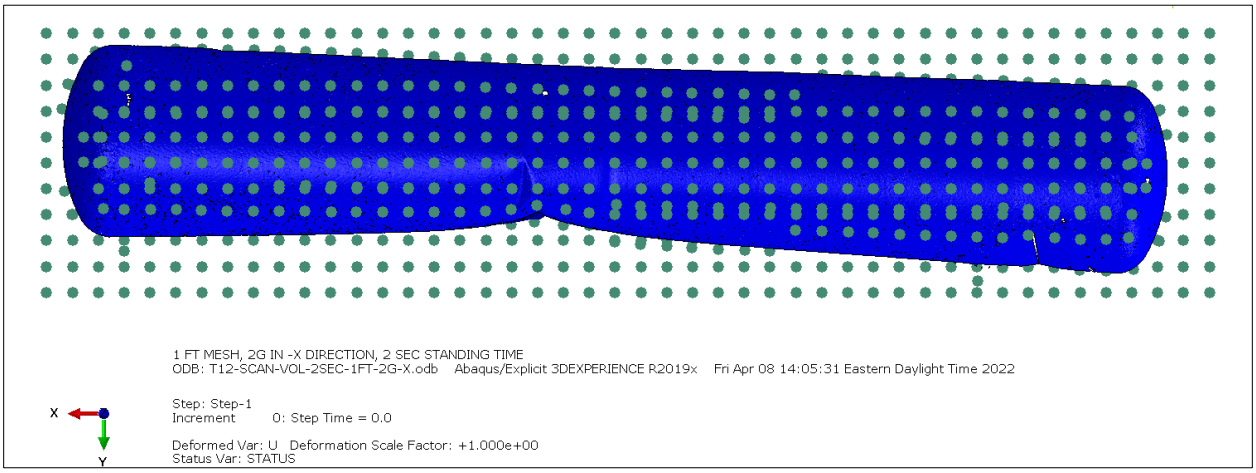

Figure D1. Initial Particle Distribution, 1-inch Spacing (Section Cut)

Table D1. Properties of Water Used in Tank-filling Model

Property	Value	Source
Density	1.9 lbf-s^2/ft/ft^3	[15]
Speed of Sound	4,814 ft/s	[16]

The model used contact between the inner tank surface and the particle cloud. Finally, a gravity load was applied to the model in the -X direction. Increased "G" loads were used to speed up the model. The water particles outside of the tank surface would fall away, but the water within the tank would be contained within the tank through contact. The total weight of water within the tank was obtained through the reaction force acting on the tank. Using the density of water prescribed in the model, the total volume of water in the tank could then be calculated from its total weight. Figure D2 shows the distribution of water within the tank after 2 seconds of settling under 2G.

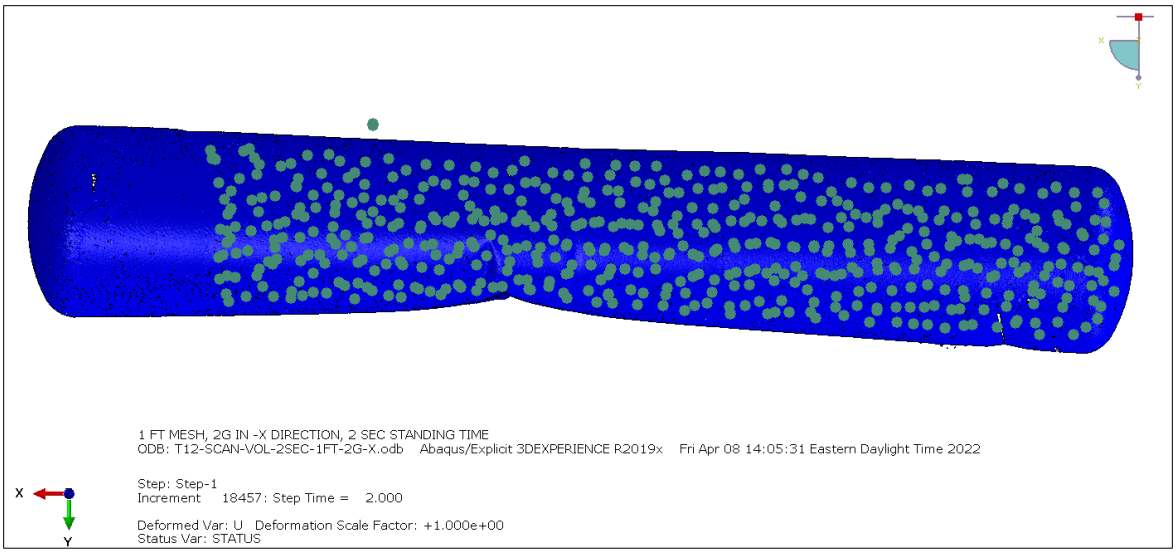

Figure D2. Final Particle Distribution, 1-ft Spacing (Section Cut)

This demonstrated that the approach was viable, but a substantial shortcoming was the obvious empty space toward the +X head of the tank. This "void" space is the result of the initial uniform grid of particles settling under gravity and conforming to the curvature of the tank. The model was re-run using particle spacings of 0.5, 0.25, and 0.125 ft to attempt to fill the tank more completely. The resulting particle distributions after standing in a 2G field are shown in Figure D3 through Figure D5.

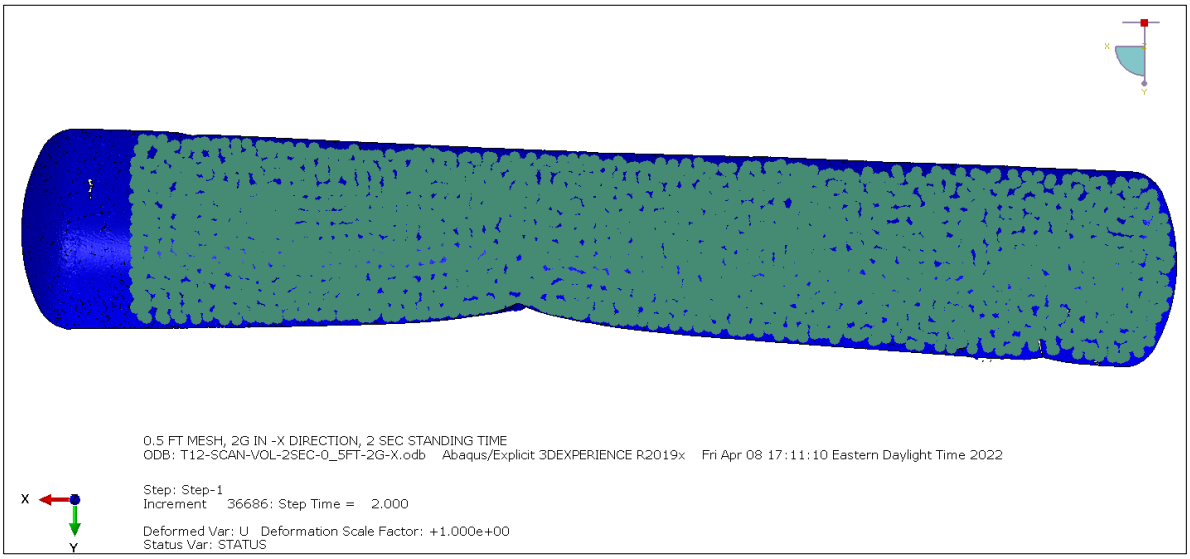

Figure D3. Final Particle Distribution, 0.5-ft Spacing (Section Cut)

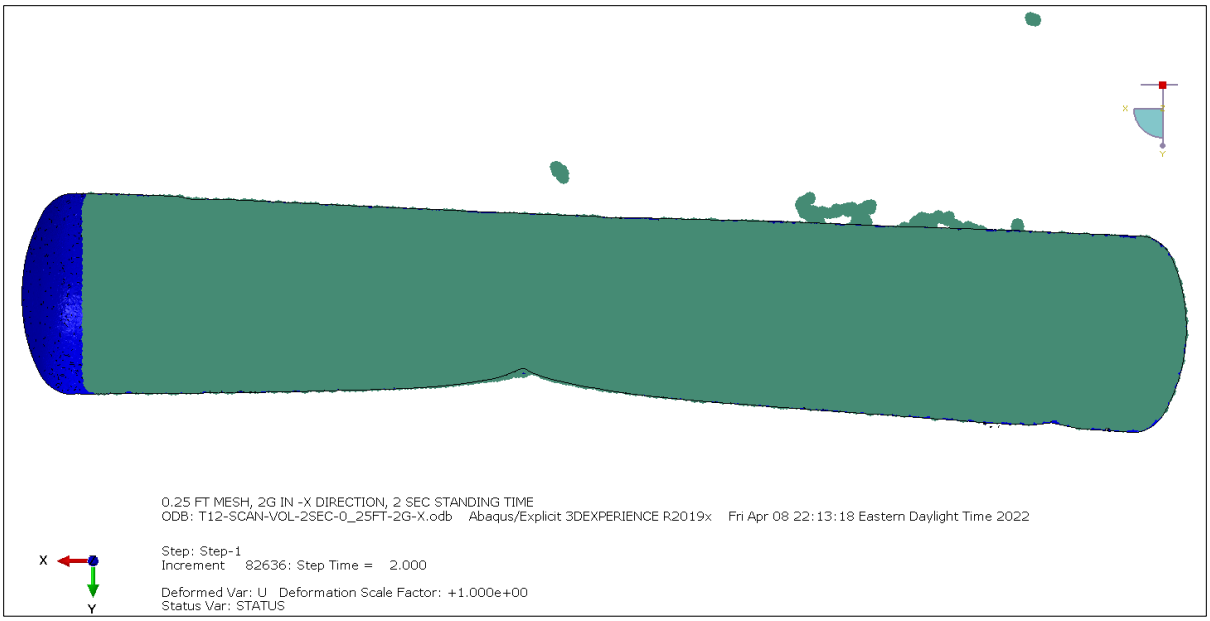

Figure D4. Final Particle Distribution, 0.25-ft Spacing (Section Cut)

Note that the 0.125-ft spacing model shown in Figure D5 was terminated after 1.2 seconds of settling time due to the model's long runtime.

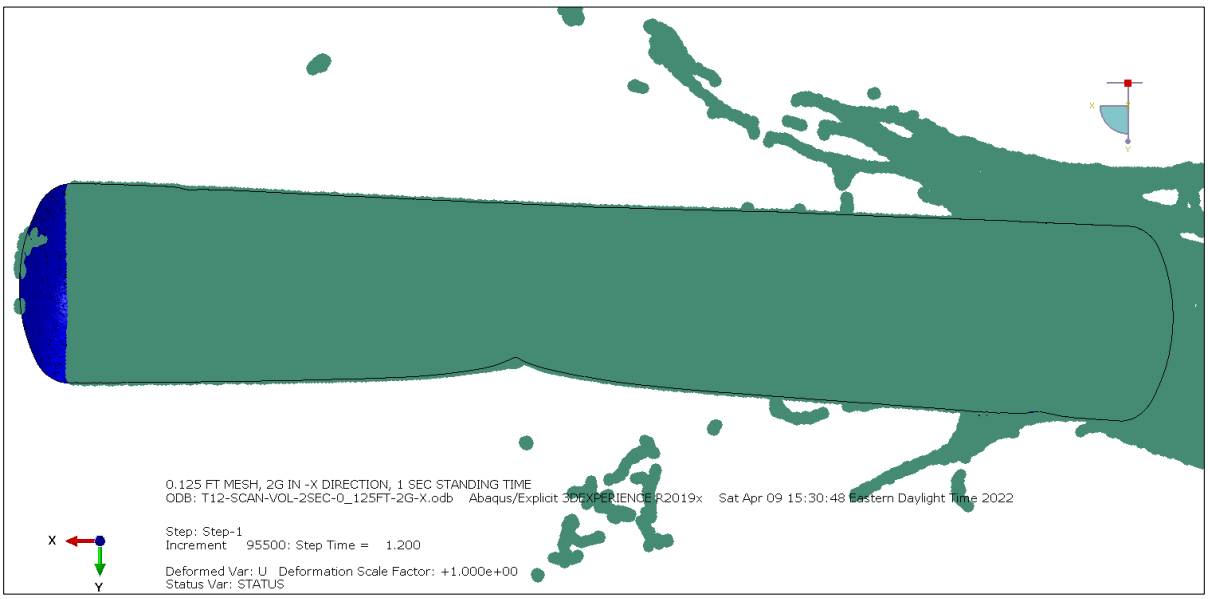

Figure D5. Particle Distribution after 1.2 seconds, 0.125-feet Spacing (Section Cut)

Figure D6 contains a plot of the calculated volume of water within the tank versus time for each of the particle spacings examined. This volume was calculated by dividing the reaction force on the tank by the initial density of water. For each particle spacing, there is an initial overshoot that settles out to a stable value. This initial overshoot is likely due to dynamic forces developing between the water and the tank due to the sudden 2G deceleration. From this figure, it is not

apparent that there is a difference in volume between the different particle spacings, nor between any model and the initial volume of the tank (horizontal dashed line).

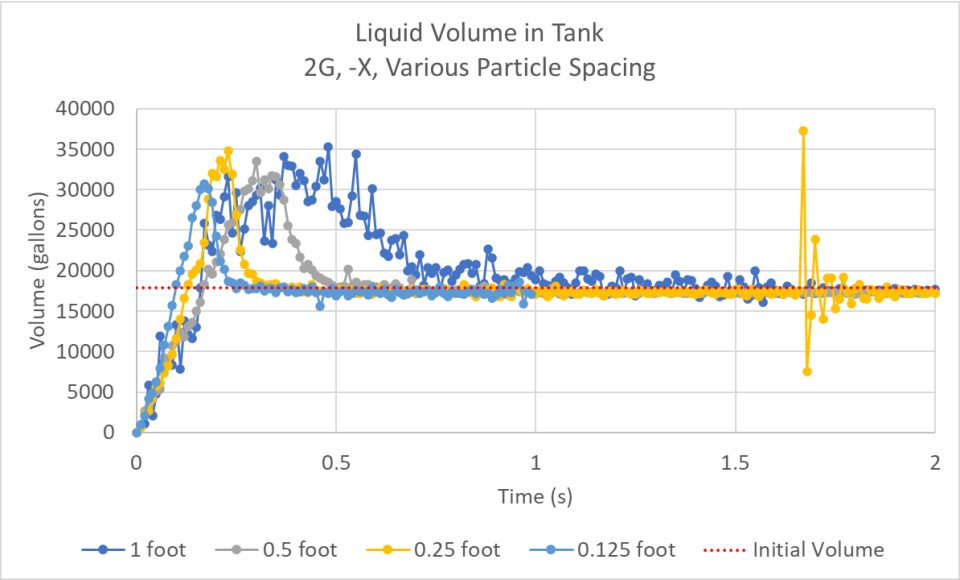

Figure D6. Liquid Volume in Tank Versus Time, 2G Acceleration, Various Particle Mesh Spacings

Figure D1 contains the same data as the previous figure, but with a focused volume scale. It is now apparent that each liquid filling model is settling to a volume that is lower than the initial volume of the tank, as expected. While the data are noisy even at 2 seconds of settling time, the models appear to be converging on a post-impact volume (V_{tank2}) of approximately 17,300 gallons.

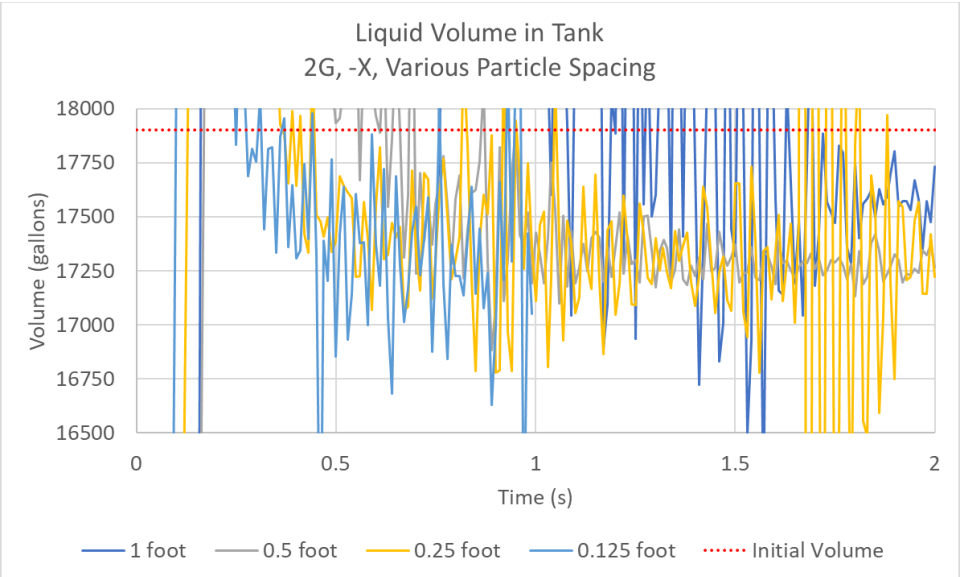

Figure D7. Liquid Volume in Tank Versus Time, 2G Acceleration, Various Particle Mesh Spacings (Focused Y-scale)

Appendix E.
Estimated Amount of Condensation in Test 12[13]

This appendix provides a mathematical model to calculate the rise in pressure in the outage (i.e., vapor) volume space of a cryogenic tank car when the volume of the inner tank is compressed during a side impact. The cryogenic liquid is initially at a pressure above the ambient pressure and is assumed to be in saturated condition corresponding to its pressure.

An equation for the mass fraction of vapor that converts into liquid is presented at the end of this appendix based on the pre- and post-impact (i.e., initial and final) pressure and volume with an assumption of saturated conditions. This equation was applied to the conditions of Test 12; it was estimated that after the test, up to 56 percent of the mass of vapor (GN2) originally present in the outage space had condensed into liquid (LN2). This value may be compared with the estimated mass fractions of GN2 condensation from the FE models described in Section 5.

E.1 Introduction

The physical condition of interest is shown in Figure E1 A and B. Initially, the tank car is partially filled with the cryogenic liquid (generally up to about 85 percent by volume) and the remainder of the volume is occupied by the vapor, which is assumed to be in thermodynamic equilibrium with the liquid (i.e., in saturated condition corresponding to the liquid temperature[14]). This condition is schematically indicated in Figure E1 A, with the initial vapor volume being V1.

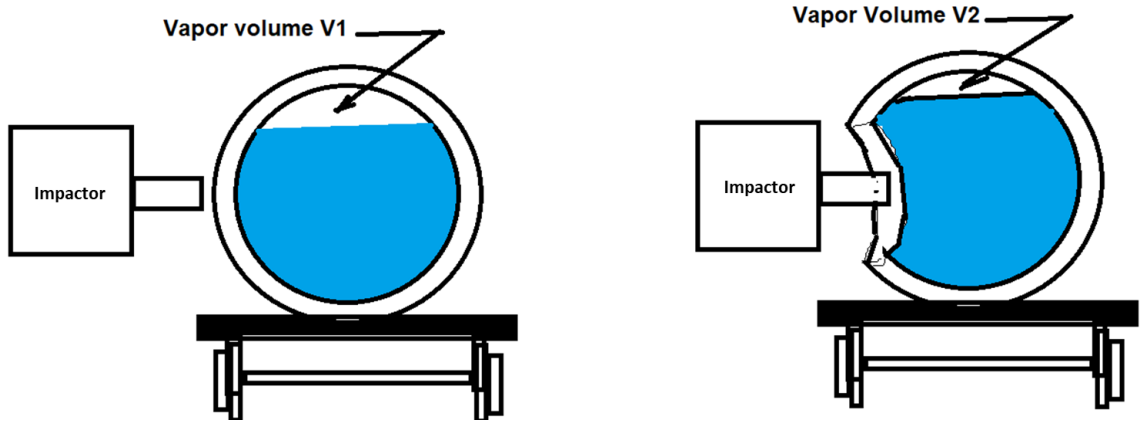

Figure E1. A: Tank Conditions Just Prior to Impact (left) B: Reduced Vapor Volume Due to Deformation of Inner Tank After Impact (right)

In the scenario of interest, the double walled tank car is impacted by an impactor at some point along the length of the tank car and above the truck. It is normally assumed for test purposes that the impactor strikes at the mid-point of the tank car length and at the maximum width (i.e., diameter) of the cylindrical tank. First, the outer shell/tank will be deformed; depending on the initial kinetic energy of the impactor, this outer tank deformation will continue and impact the

[13] This appendix was developed and authored, in part, by Dr. Phani Raj of FRA's Office of Safety.

[14] This assumption differs from the assumption made in the finite element analyses, where the vapor was allowed to exist at a temperature above its saturation temperature.

inner tank and begin to deform it. The inner tank volume will be continuously reduced if the impactor is still moving and the inner tank is not punctured. The inner tank may withstand the impact without puncturing, again depending upon the impactor's initial energy conditions. Figure E1 B shows this situation schematically, without the inner tank being punctured. The final vapor volume, V2, is less than V1.

Since the liquid can be assumed to be an incompressible fluid, the reduction in the tank volume will result in the reduction of the vapor space volume only (i.e., the vapor gets compressed resulting in an increase of its pressure). This also results in the pressure of the liquid being increased by the same value. Generally, moderate compression of a large mass of liquid will not result in any significant (or even measurable) increase in the temperature of the liquid because of the large thermal capacity associated with large liquid mass. The vapor mass in a tank car is relatively low and the specific heat of a gas is also low compared to that of the liquid. Hence, the thermal inertia of the vapor in a tank car is low, resulting in the vapor attaining a higher temperature state (compared to liquid temperature) when compressed. The magnitude of increase in vapor temperature depends upon the rate of compression, the amount of compression (i.e., final volume/initial volume), the heat capacity ratio of the gas, and rate of cooling of the vapor either by the liquid mass or heat loss through the vapor wetted tank wall. In general, compression of a vapor mass will result in a measurable increase in its temperature, except when the rate of compression is very low or the vapor is in contact with a large heat sink.

Two scenarios can be postulated to determine the thermodynamic state (i.e., final pressure and temperature) of vapor in the outage volume of a tank car whose volume is reduced due to impact, assuming that the initial state of vapor is saturated at the tank's initial pressure and corresponding saturation temperature. These two approaches to calculating the final thermodynamic state of the vapor are discussed below.

Two scenarios are considered due to the uncertainty about the magnitude and effect of sloshing and agitation of liquid caused by the impact on the tank car. The sloshing of liquid may result in spraying small droplets of liquid into the vapor volume.

Scenario 1 considers a situation where the rate of heating of the vapor due to compression is equal to the rate of cooling caused by liquid droplets mixing with the vapor. The vapor is assumed to remain at the initial saturation temperature of the vapor-liquid system throughout the impact (i.e., isothermal compression of the vapor).

Scenario 2 considers a situation where the rate of heating of the vapor due to compression is higher than or similar to the rate of cooling due to heat exchange with its surroundings. Scenario 2 examines two different potential thermodynamic paths for the process of heating via compression, cooling due to heat exchange with the surrounding tank and/or liquid nitrogen, and condensation of cooled vapor into liquid.

The research team do not believe the current data from the test will be able to provide direct evidence for one or the other of the above scenarios. The physical phenomena that occur need to be surmised by comparing model results to measured extensive properties of the vapor (such as the pressure in the vapor space).

E.2 Scenario 1

In Scenario 1, it is assumed that the vapor temperature remains constant (at the liquid temperature) due to liquid spray into the vapor space. Many small droplets in the liquid spray are

assumed to mix thoroughly with the vapor. These droplets present a significant surface area for heat transfer, causing part of the vapor mass to condense. In this scenario, the vapor temperature is always equal to the liquid temperature (which is assumed to be the initial liquid temperature). The liquid temperature does not change appreciably from its pre-impact value due to the large mass of liquid, high heat capacity, very low liquid heat of compression, and the fact that the heat generated due to the compression of vapor is small (due to low vapor mass) compared to the sensible heat of the large liquid mass. In this vapor compression scenario, the vapor temperature remains constant and equal to the bulk temperature of the liquid.

E.3 Scenario 2

In Scenario 2, the phenomenon of ideal compression of vapor inside a tank car due to the entry of liquid mass into the vapor volume is discussed. The compression of vapor results in an increase in its pressure and temperature. However, the vapor is convectively and conductively cooled by its contact with the large surface of the vapor-liquid boundary interface. The large mass of liquid acts as a heat sink, essentially maintained at a constant temperature. Thus, the vapor is simultaneously heated by compression and cooled by contact with the liquid mass. After compression, the vapor attains a higher pressure. As the cooling progresses, the pressure decreases along a constant vapor volume (i.e., constant vapor density) line until the vapor thermodynamic condition is the saturation condition corresponding to the then present vapor density. It is entirely possible that further cooling still occurs (i.e., a reduction of pressure at constant density). The vapor now exists in a super saturated condition. When it reaches a thermodynamically unstable condition, a part of the vapor condenses instantaneously, leaving the rest of the uncondensed vapor in a saturated condition corresponding to the new (i.e., lower) vapor density. The mass loss by condensation occurs entirely due to thermodynamic instability at a slightly later but very short time. In this scenario, this cycle is assumed to occur in infinitesimal steps so that at a macro scale, the thermodynamic path of the vapor is along the saturated vapor line with increasing pressure.

Figure E2 shows a simplified temperature-entropy (T-S) diagram for a two-phase system. The figure shows the T-S[15] diagram for the nitrogen system in the region around the initial state, using data from NIST [10]. The possible thermodynamic path of vapor during a short step of the compression (i.e., cooling) condensation cycle is illustrated schematically in Figure E2. The starting point is indicated by 1, the saturated condition of the vapor and liquid before the impact.

A situation in which the vapor is compressed due to the rapid movement of the liquid into the vapor space is considered. In this case, the liquid surface acts very much like the surface of a piston. The entire process is broken into small time steps in which the vapor is compressed slightly and attains a new thermodynamic condition 2, where the pressure and temperature of the vapor are each slightly higher than before the infinitesimal compression. The vapor is cooled by conduction and convection at the same time due to contact with the bulk liquid. This vapor cooling occurs along a constant vapor density line 2-3 (constant density because of the assumption of no vapor mass loss and the fact that after the infinitesimal compression the vapor volume remains constant over the short time step). It is entirely possible that the vapor is subcooled along the line 3-4 until it reaches a thermodynamic limit instability point (shown as

[15] The reference state for the entropy data is S=0 at the normal boiling point for saturated liquid nitrogen, 77.355 K at 1 atmosphere.

Point 4). After this, a part of the vapor instantaneously condenses, and the remaining vapor reaches saturated condition (i.e., pressure and temperature) corresponding to the stability limit at Point 4. This new condition is shown in Figure E2 as point 5. In the next small time step, the above compression-cooling-spontaneous condensation continues (i.e., Point 5 from the first time step becomes Point 1 in the second time step and Point 6 corresponds to Point 2 of the infinitesimal compression step). The result is that the vapor thermodynamic condition traces the saturated vapor line. The pressure in both the vapor and liquid will be the same at the new saturated vapor condition. However, the liquid will be at its original bulk temperature, which will be a subcooled state corresponding to its new pressure.

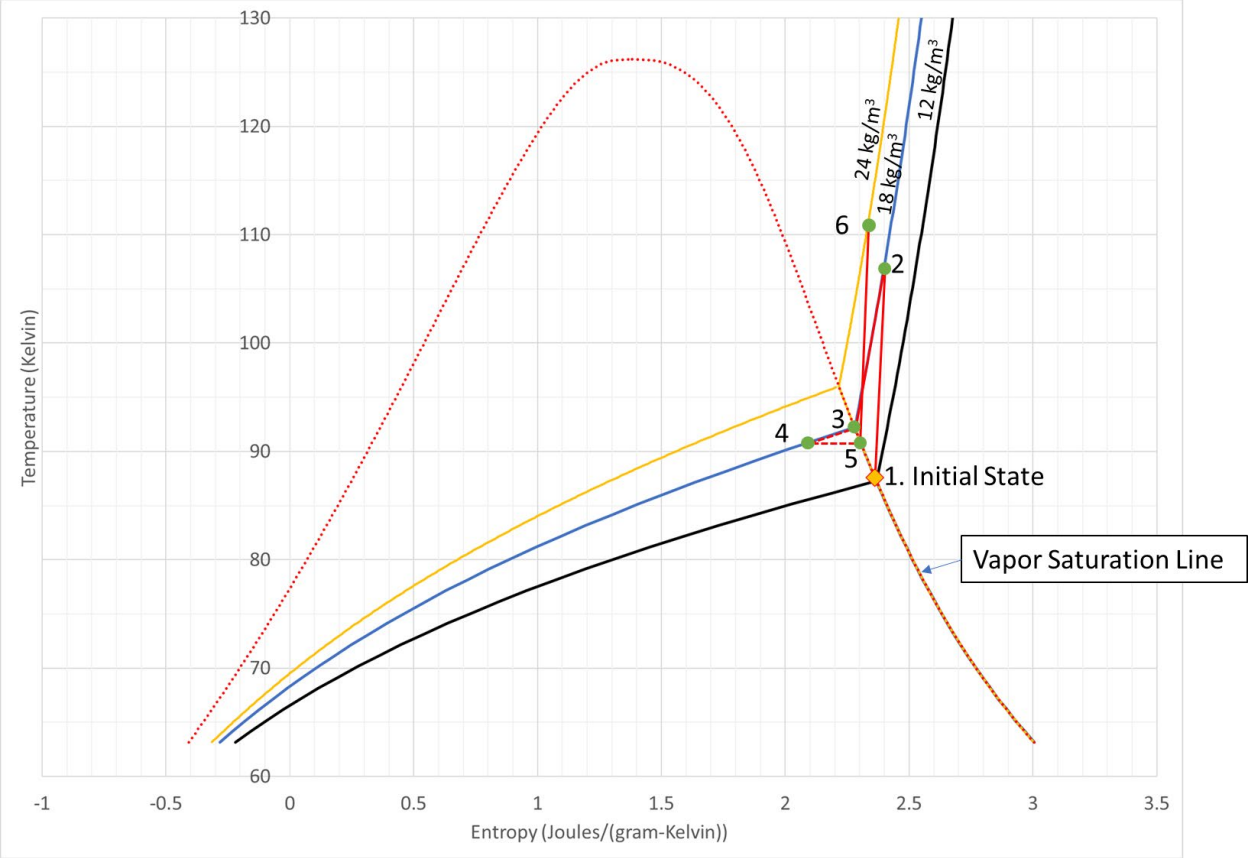

Figure E2. T-S Diagram for Nitrogen with the Vapor Compression Path Shown

In the above description of the vapor compression process (due to the tank car volume reduction) it is assumed that no liquid is sprayed into the vapor volume and therefore no condensation of vapor due to sudden cooling. It can be shown that the bulk liquid temperature does not change appreciably due to its large mass (compared to that of the vapor in the outage volume), its high heat capacity, its extremely low compressibility (i.e., no heat of liquid compression), and the very small amount of latent heat released by the spontaneous condensation (due to thermodynamic instability) of a very small fraction of the vapor.

This entire process may be taking place continuously as the impactor is continuing to “deform” the inner tank. This is because the time scales of equilibration of the vapor to the new “reduced vapor volume” condition will be in the order of milliseconds, whereas the movement of the impactor is in the order of magnitude of seconds. Therefore, one can surmise that there is a

continuous increase in the pressure of the vapor as the impactor is continuing to deform the inner tank. The pressure rise, however, will be lower if the vapor is always in a saturated vapor condition (with or without condensation) compared to the pressure rise were the vapor a non-condensable gas. In the former case (i.e., saturated vapor), the pressure of the vapor will follow the vapor saturation line.

E.4 Thermodynamic Assessment of the Vapor Compression, Scenario 2

A schematic representation of the locus of thermodynamic events that occur in the vapor space of a tank car (containing initially saturated liquid and vapor nitrogen) as the impactor strikes the tank car was shown in Figure E1. As the impactor progresses into the tank car, the outer shell wall deforms inward into the tank. Further movement of the impactor may result in the outer tank wall contacting the wall of the inner tank, which will also deform inward. The result is a progressive reduction in the volume of the inner tank. If the outer wall is punctured and the impactor makes direct contact with the inner tank, the deformation of the inner tank and the rate of reduction of its volume may accelerate. However, the rate of volume reduction is variable during the impact, as the impactor will decelerate, and the rate of tank deformation will also decrease as the impact event occurs. Further, as the tank continues to deform, the reduction in vapor volume with each increment of impactor travel is also variable.

During the time that the inner tank wall is only deforming and not punctured, the reduction in the total volume of the inner tank is entirely compensated by the reduction in the outage (i.e., vapor) volume because the liquid is incompressible at the resulting pressures. The vapor in the outage space is compressed; this compression can be considered adiabatic (and for idealized consideration also isentropic). The assumption is justified because the volume reduction takes place in the order of seconds which is a fast compression, hence an assumed adiabatic compression.[16]

Adiabatic compression of a gas results in an increase in both its pressure and temperature. In this instance, the vapor is initially at a saturated condition and its compression results in a superheated vapor, corresponding to its pressure (see point 2 in Figure E2). Since the vapor is in contact with a large mass (i.e., a large thermal inertia) of liquid whose temperature is essentially constant (because of no heat transfer from outside the tank), the vapor cools. This cooling rate is very high because of the presence of the large constant temperature liquid acting as a heat sink. The cooling occurs along the constant vapor density curve because the mass of vapor in the compressed space is constant and the volume after compression is also constant.

The overall compression of vapor due to continuous reduction in volume can be considered as a series of small steps in volume reduction, resulting in the above-described compression and cooling phenomena. The initial (i.e., prior to impact) condition of the vapor in the outage space is represented by Point 1 on Figure E2, which is on the vapor saturation line and at a point corresponding to the saturation temperature (T^{sat}) of the liquid. In this analysis, the liquid is assumed to remain at this T_i temperature throughout the ram-caused compression of the vapor. Point 2 is the final point of the adiabatic and isentropic compression of the vapor, due to a small volume reduction dV. Before the next compression step due to impactor movement, this

[16] In previous FE modeling of impact tests using air and water (rather than cryogenic liquid nitrogen), an *isothermal* assumption was found to provide better agreement with test measurements compared to adiabatic conditions.

adiabatically compressed gas rapidly loses heat to the liquid, its temperature decreasing along the constant vapor density line. This line intersects the vapor saturation line at Point 3.

After the first cycle of the thermodynamic process, there are two potential scenarios that should be considered:

(1) If the vapor does not condense, one can assume that the next dV compression step starts at Point 3 and results in reaching Point 6 isentropically and adiabatically. This cycle then repeats in small dV steps until the impactor comes to rest and no breach of inner tank has occurred. This scenario of physical and thermodynamic events could occur due to the assumption that the time constant for compression is of the same order of magnitude (i.e., seconds) as the movement of the impactor, whereas the cooling of the compressed gas occurs at a faster (i.e., millisecond) time frame due to the very large heat sink (in the form of a cold liquid) with which the vapor is in contact but not necessarily at temperature equilibrium. In this scenario the vapor is always assumed to have the same initial mass and saturated condition corresponding to the new pressure at each step and occupying smaller volumes as the tank deformation continues.

(2) It is entirely possible that the vapor, in cooling from Point 2 along the constant density line, is subcooled below Point 3 due to paucity of nucleation sites for initiating condensation. This process is shown by dotted line 3-4. However, the vapor condenses at some supercooled condition 4, and the mass fraction of vapor that is condensed is *f*. In this case, the initial vapor loses a mass that is *f* multiplied by its original mass and attains a saturated vapor condition shown schematically in Figure E2 as Point 5. The compression cycle with each dV incremental reduction in volume is repeated (i.e., Point 5 from the first increment becomes Point 1 in the second increment and Point 6 becomes the condition after the second infinitesimal step compression), and at every step a mass fraction *f* is removed by condensation of the vapor into a liquid. The final pressure reached when the impactor stops moving is less than that attained in Scenario 1.

It can be shown that if the compression is reversible (i.e., the meaning of isentropic compression) and that cooling along the constant density line is reversible (which is also true because it is a constant volume process), then irrespective of the infinitesimal steps described above, the final pressure in the vapor (for a specified change of the volume from its original volume) can be computed in a single step. This is illustrated in the mathematical analysis of the above thermodynamic phenomena.

E.5 Correlation for the Saturated Properties of Nitrogen

Figure E3 shows the plot of the saturated vapor pressure vs. saturated vapor temperature for nitrogen using data from Strobridge [18].

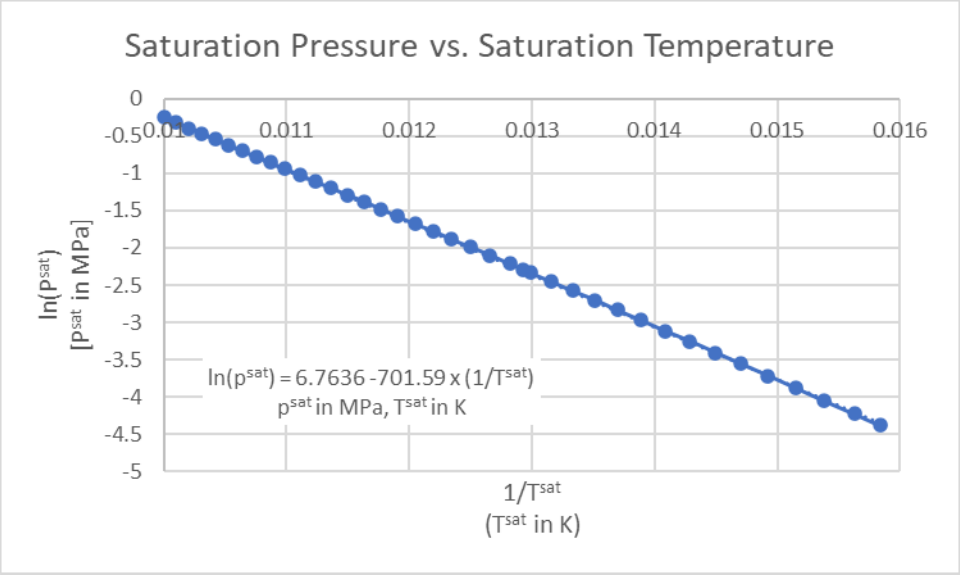

Figure E3. Saturation Pressure vs. Temperature for Nitrogen

The P vs. T correlation obtained from this graph is shown by Equation E1.

Equation E1. Correlation Between Saturation Pressure and Temperature for Nitrogen

$$\ln(p^{sat}) = 6.7636 - \frac{701.59}{T^{sat}}$$

p^{sat} in MPa, T^{sat} in K

Figure E4 shows the correlation between the saturated vapor pressure and saturated vapor density for nitrogen using data from Strobridge [18].

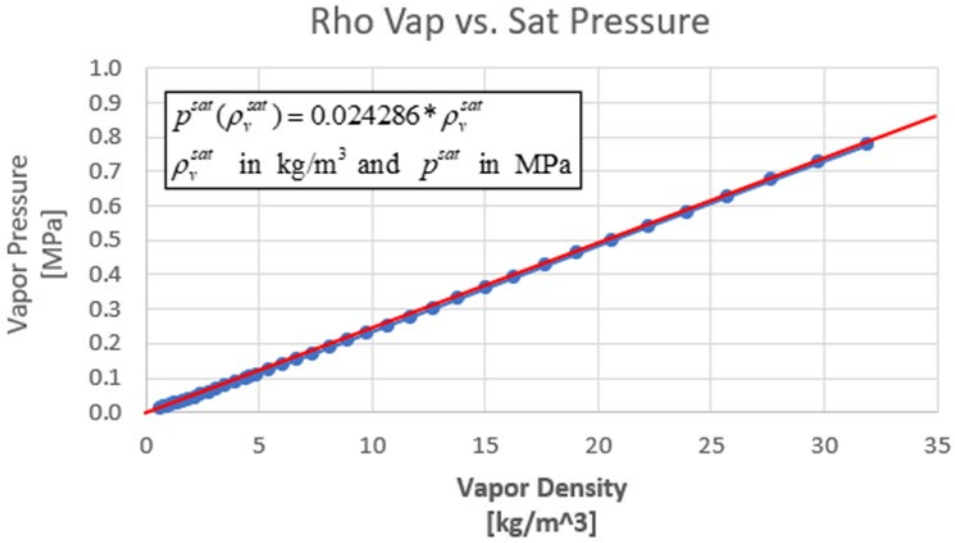

Figure E4. Saturation Pressure vs. Saturation Vapor Density for Nitrogen

The correlation generated from the graph is shown in Equation E2.

Equation E2. Correlation Between Saturation Pressure and Saturated Vapor Density for Nitrogen

$$p^{sat}(\rho_v^{sat}) = 0.024286 * \rho_v^{sat}$$
$$\rho_v^{sat} \text{ in kg/m}^3 \text{ and } p^{sat} \text{ in MPa}$$

E.6 Mathematical Model for the Thermodynamic Phenomenon of Scenario 1

The following assumptions are made in this analysis:

1 The saturation vapor pressure and saturated vapor density are uniquely related for a given cryogenic substance (e.g., nitrogen).
2 The saturated vapor pressure and saturation temperature are uniquely related for the substance under consideration.
3 Vapor compression by the reduction in the volume can be considered as adiabatic and isentropic.
4 The cooling of the vapor heated by compression is "fast" and results in its saturated vapor pressure corresponding to the new vapor density.
5 If vapor condensation is considered, an assumption is made that a fraction f of the mass of the vapor present at the beginning of the compression step condenses. This condensation fraction f is assumed to be the same for all steps in the compression cycle. The value of f is not known *a priori.*

The symbols used in the calculations in this section are defined in Table E1.

Table E1. Symbols Used in This Section

Symbol	Definition
V_1	Volume of the vapor space before the impactor makes contact
V_2	Final vapor volume after the side impact and "springback" of the inner tank
f	Fraction of vapor mass that is condensed due to vapor subcooling effect, which is assumed to be a constant for all saturated pressure condition
p_1	Initial pressure of the vapor measured prior to side impact
p_2	Final vapor pressure measured when the volume is V_2
T_1	Initial temperature of vapor
T_2	Final temperature of vapor assumed to saturated at p_2
ρ_1	Initial density of vapor in the outage volume
ρ_2	Density in the final volume (after accounting for any condensation of vapor) assumed to be saturated
p^{sat}	Saturation pressure
ρ_v^{sat}	Saturated vapor density
b	Coefficient in saturated vapor pressure-density relationship
m_v	Vapor mass
V_v	Vapor volume

The pressure-vapor density saturated relationship for vapor shown in Figure E4 can be generally expressed according to Equation E3.

Equation E3. General Form of Pressure-Density Relationship for Saturated Vapor

$$p^{sat} \stackrel{\text{def}}{=} p(\rho_v^{sat}) = b \cdot \rho_v^{sat}$$

The density of the vapor is the ratio of the vapor's mass to its volume, as shown in Equation E4.

Equation E4. Vapor Density

$$\rho_v = \frac{m_v}{V_v}$$

An incremental change in vapor density can be expressed according to Equation E5.

Equation E5. Incremental Change in Vapor Density

$$\frac{d\rho_v}{\rho_v} = \frac{dm_v}{m_v} - \frac{dV_v}{V_v}$$

The incremental change in vapor mass (dm_v) due to condensation can be expressed as a fraction (f) of the initial vapor mass (m_v) according to Equation E6.

Equation E6. Incremental Change in Vapor Mass Due to Condensation

$$dm_v = -f \cdot m_v$$

Substituting Equation E3 and Equation E6 into Equation E5 and rearranging yields Equation E7 for saturated vapor.

Equation E7. Fraction of Vapor Mass Condensing for Saturated Vapor

$$\frac{dp_v}{p_v} + \frac{dV_v}{V_v} = -f$$

Equation E7 can be rewritten as Equation E8, assuming the vapor remains saturated.

Equation E8. Fraction of Vapor Mass Condensing for Saturated Vapor as a Function of Pressure and Volume

$$d\left[\ln\left(p^{sat}V^{sat}\right)\right] = -f$$

By raising e to the power of both sides of Equation E8 and inserting terms for the initial and final pressure and volume of the vapor becomes Equation E9.

Equation E9. Relationship between Initial and Final Pressures and Volumes and Fraction of Saturated Vapor Mass Condensing to Liquid

$$\left[p_2^{sat}\ V_2^{sat}\right] = \left[p_1^{sat}\ V_1^{sat}\right] x \exp(-f)$$

Equation E9 provides a recipe for determining the final saturation pressure at any vapor volume V_2 starting with vapor volume V_1 and initial saturation pressure p_1. If f=0, there is no condensation of vapor and pV is conserved. In ideal gas situations, the conservation of pV implies an isothermal behavior of the gas. This constancy of temperature is not the case in a

vapor that is in saturated equilibrium at all pressures with its saturation temperature. In the case of vapor condition indicated by Equation E9, the final temperature of the vapor is T_2, which is the saturation temperature corresponding to p_2.

Several assumptions made in these calculations differ from the assumptions used to develop the Tabulated EOS used in the FE models. In the case of the Tabulated EOS, the GN2 was initially assumed to be in an unsaturated condition, requiring a pressure increase to reach saturation. The Tabulated EOS was assumed to apply to an isothermal phase change, where $T_2 = T_1$.

E.7 Application to Test 12 Results

Assuming Vapor Initially at Saturation Temperature

The mass fraction of the initial vapor that condenses can be calculated using the rearranged form of Equation E9 shown in Equation E10 if the initial and final pressures and volumes of the vapor are known and the initial and final temperature of the vapor is assumed to be constant.

Equation E10. Fraction of Vapor Mass to Condense as a Function of Initial and Final Pressures and Volumes

$$f = -\ln\left(\frac{p_2 \cdot V_2}{p_1 \cdot V_1}\right)$$

For Test 12, the initial pressure and vapor volume were known quantities as described in the Test 12 report [3]. The initial pressure (p_1) was approximately 30 psig (42.3 psia) based on measurements made with pressure transducers and a mechanical pressure gauge. The outage level of the tank was estimated to be approximately 9 percent at the time of the test. Since the tank had a nominal capacity before the impact (V_{ltank}) of 17,900 gallons, the initial outage volume (V_1) was therefore approximately 1,611 gallons. The initial volume of liquid ($V_{lliquid}$) was the remaining volume within the tank, or 16,289 gallons.

The instrumentation measured data for 30 seconds post-impact. Between 29 and 30 seconds after impact the pressures (p_2) measured by the six pressure transducers stabilized at approximately 26 psig (38.3 psia). No venting occurred during the test, as confirmed by pressure transducers installed in the pipe between the tank and PRV and by review of the test videos[17].

The last quantity to be determined is the post-test volume of the vapor (V_2). The post-test volume of the now-deformed inner tank was not directly measured. This volume could be estimated from a LiDAR scan made of the inner tank. The mesh resulting from the LiDAR scan is shown in Figure E5. The post-impact volume was estimated to be 17,300 gallons. The process of estimating the volume of the inner tank from the LiDAR scan is discussed in Appendix D.

[17]Release of GN2 to atmosphere at cryogenic temperatures would produce an easily observable white cloud of condensed water vapor.

(Top Image: Top View, Bottom Image: Front View)

Figure E5. Post-test 12 LiDAR Scan of Inner Tank

Equation E10 requires the post-impact volume of vapor, not of the entire tank. Assuming that the LN2 was incompressible and that the increase in LN2 volume associated with any vapor condensation was negligible, the post-impact vapor volume can be calculated as the difference between the post-impact tank volume (V_{2tank}) and the initial volume of LN2 in the tank ($V_{1liquid}$), as shown in Equation E11.

Equation E11. Post-impact Vapor Volume

$$V_2 = V_{2tank} - V_{1liquid}$$

$$V_2 = 17{,}300gal - 16{,}289gal = \ 1{,}011\ gal$$

Finally, inserting the post-test vapor volume calculated in Equation E11 into Equation E10 the mass fraction of vapor that condensed (f) in Test 12 is estimated according to Equation E12.

Equation E12. Mass Fraction of Vapor to Condense in Test 12

$$f = -\ln\left(\frac{38.3\ psia \cdot 1{,}011gal}{42.3\ psia \cdot 1{,}611gal}\right)$$

$$f = 56.5\%$$

While a rough approximation due to the simplifications and assumptions discussed above (e.g., the vapor remained saturated at all pressures between initial and final states), these calculations make physical sense. Slightly more than half of the initial vapor, by mass, condensed into a liquid because of the impact. This is a logical explanation for why the post-impact pressure within the tank was less than the pre-impact pressure when the volume of the tank was clearly reduced during the test.

Assuming Vapor Initially Above Saturation Temperature

The above equations assume that the initial and final temperatures of the vapor are at the corresponding saturation temperature for the measured initial and final pressure. The approach used in the FE modeling described in the main body of the report assumed that the vapor was initially at a temperature above its saturation temperature at the measured initial pressure. A second approach to estimating the mass fraction of vapor to condense was made assuming the vapor initially existed at a temperature above its saturation temperature. In this second approach, the vapor was assumed to be fully saturated after the impact, as the liquid and vapor were violently mixed via sloshing during and after the side impact. Therefore, the team used a public database [10] to compute initial densities for the vapor at the known pre-test pressure of 42.3 psia and a range of temperatures, consistent with the temperature range used in the FE models (88 K to 100 K). The initial densities as a function of initial temperature (T_1) are shown in Table E2.

Table E2. Density of GN2 at 42.3 psia as a Function of Temperature

T_1 (K)	ρ_1 (mol/gal)
88	1.66
90	1.61
92	1.56
94	1.52
96	1.48
98	1.45
100	1.41

The final density of the saturated vapor was calculated as 1.52 mol/gal at the measured post-test pressure of 38.3 psia and the assumed corresponding saturation temperature of 86.5 K. Using these densities and the measured initial and final volumes of the outage, the team calculated the mass fraction of vapor to condense. Without the assumption of saturation, Equation E3 cannot be substituted into Equation E6 to yield Equation E7, which relates mass fraction to condense to change in pressure and volume. Instead, the mass fraction to condense was calculated using change in density and volume with a similar approach shown below.

Equation E6 can be rewritten as Equation E13 by substituting the product of vapor density and volume ($\rho\ V$) for vapor mass (m).

Equation E13. Fraction of Vapor Mass Condensing for Unsaturated Vapor

$$\frac{d(\rho_v \cdot V_v)}{\rho_v \cdot V_v} = -f$$

Equation E13 can be rewritten as a function of density and volume yielding Equation E14.

Equation E14. Fraction of Vapor Mass Condensing for Unsaturated Vapor as a Function of Vapor Density and Volume

$$d\ln(\rho_v \cdot V_v) = -f$$

Substituting in the initial and final vapor mass yields Equation E15.

Equation E15. Fraction of Vapor Mass to Condense as a Function of Initial and Final Vapor Density and Volume

$$\boldsymbol{f = -\ln\left(\frac{\rho_2 \cdot V_2}{\rho_1 \cdot V_1}\right)}$$

Applying Equation E15 to the initial and final volumes of vapor from Test 12, and assuming an initial vapor temperature at saturation (87.6 K), produces Equation E16.

Equation E16. Fraction of Vapor Mass to Condense assuming Vapor at Saturation Temperature

$$f_{87.6K} = -\ln\left(\frac{1.52\frac{mol}{gal} \cdot 1{,}011 gal}{1.67\frac{mol}{gal} \cdot 1{,}611 gal}\right)$$

$$f_{87.6K} = 55.9\%$$

Using the values of T_1 and ρ_1 shown in Table E2 produces corresponding values of f_{T1} shown in Table E3.

Table E3. Fraction of Vapor Mass to Condense as a Function of Assumed Initial Vapor Temperatures

Assumed Initial Vapor Temperature (T_1) (K)	Fraction of Vapor Mass to Condense f_{T1}
87.6	55.9%
88	55%
90	52%
92	50%
94	47%
96	44%
98	42%
100	39%

Figure E6 shows relationship between initial vapor temperature and the mass fraction of vapor to condense. As expected, the computed mass fraction of 55.9 percent at the saturation temperature of 87.6 K is in approximate agreement with the result obtained using Equation E12 (56.5 percent). As the initial temperature of the vapor is assumed to increase above the saturation temperature, the estimated fraction of the original mass of vapor that condenses decreases.

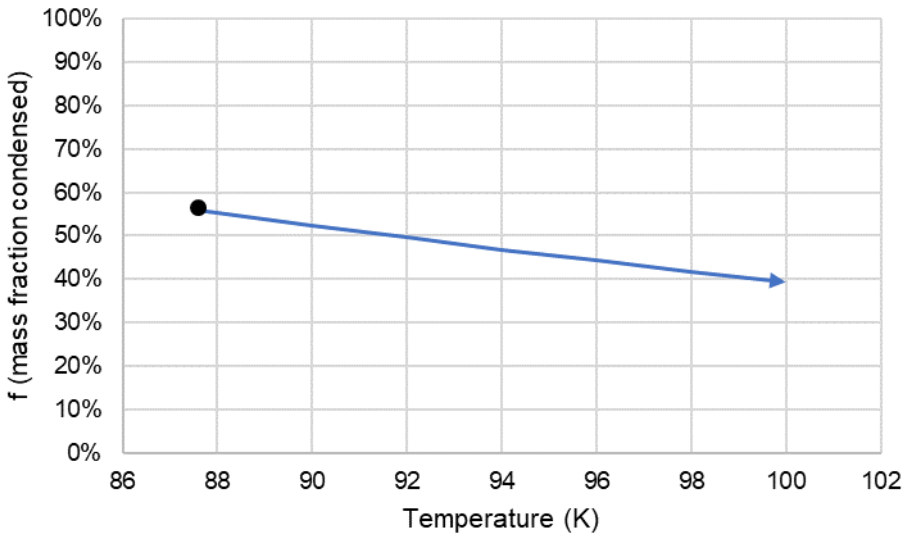

Figure E6. Vapor Mass Fraction to Condense vs Initial Vapor Temperature

It should be noted that the results from Figure E6 cannot be directly compared with the results from the FE models presented in Section 5 because the FE models used an isothermal condition for the vapor and the models were not run until the inner tank was fully allowed to "springback" after the impact. However, it is encouraging that both the FE models and the calculations presented in this appendix indicated that there was a significant amount of vapor condensation during the side impact.

Abbreviations and Acronyms

ACRONYM	DEFINITION
AAR	Association of American Railroads
ASTM	American Society for Testing and Materials
DOF	Degrees-of-Freedom
DOT	Department of Transportation
EOS	Equations of State
FE	Finite Element
FEA	Finite Element Analysis
FRA	Federal Railroad Administration
kip	kilopound (1000 lbf)
LN2	Liquid nitrogen
LNG	Liquefied Natural Gas
MLI	Multi-layer Insulation
N2	Nitrogen
NIST	National Institute of Standards and Technology
PEEQ	Plastic Equivalent Strain
PHMSA	Pipeline and Hazardous Materials Safety Administration
PRV	Pressure Relief Valve
SPH	Smoothed Particle Hydrodynamic
SRB	Smooth Round Bar
STDP	Start to discharge pressure
T304	ASTM A240 Type 304 Stainless Steel
TC128	AAR TC128, Grade B Carbon Steel
TTC	Transportation Technology Center (the site)
TTCI	Transportation Technology Center, Inc. (now called MxV Rail)
Volpe	Volpe National Transportation Systems Center